62 72037 Copy 537

[redacted]

NASA TM X-213

NASA TM X-213

TECHNICAL MEMORANDUM

X-213

INVESTIGATION OF THE AERODYNAMIC CHARACTERISTICS OF A SUPERSONIC HORIZONTAL-ATTITUDE VTOL AIRPLANE MODEL AT MACH NUMBERS OF 1.57, 2.14, 2.54, AND 2.87

By Arthur E. Franklin and Robert M. Lust

Langley Research Center
Langley Field, Va.

N67-31732
(ACCESSION NUMBER)
(THRU)
155
(PAGES)
1
(CODE)
TMX-213
(NASA CR OR TMX OR AD NUMBER)
02
(CATEGORY)
FACILITY FORM 602

[redacted] prohibited by law.

NATIONAL AERONAUTICS AND SPACE ADMINISTRATION

WASHINGTON October 1960

[redacted]

[redacted]

NATIONAL AERONAUTICS AND SPACE ADMINISTRATION

TECHNICAL MEMORANDUM X-213

INVESTIGATION OF THE AERODYNAMIC CHARACTERISTICS OF A SUPERSONIC HORIZONTAL-ATTITUDE VTOL AIRPLANE MODEL AT MACH NUMBERS OF 1.57, 2.14, 2.54, AND 2.87*

By Arthur E. Franklin and Robert M. Lust

SUMMARY

An investigation was made in the Langley Unitary Plan wind tunnel to determine the drag and the static longitudinal and lateral stability characteristics, horizontal-tail hinge-moment characteristics, and wing-tip-nacelle pressure-distribution characteristics of a model of a supersonic horizontal-attitude VTOL airplane at Mach numbers of 1.57, 2.14, 2.34, and 2.87 and a Reynolds number of about 3.52×10^6 per foot. The results of the investigation are presented without analysis.

INTRODUCTION

An investigation of the aerodynamic characteristics of a model of a supersonic horizontal-attitude VTOL airplane was conducted in the Langley Unitary Plan wind tunnel. The tests were conducted at Mach numbers of 1.57, 2.14, 2.34, and 2.87. Various horizontal-tail and fuselage inlet configurations were investigated. In addition, the horizontal-tail hinge-moment characteristics and the wing-tip-nacelle pressure-distribution characteristics of the model were also determined. The results of this investigation are presented herein without analysis and are supplemented with summaries of the aerodynamic parameters.

SYMBOLS

The longitudinal stability characteristics of the model are referred to the stability system of axes. The lateral stability characteristics

* Title, Unclassified.

C[redacted]

[redacted]

of the model are referred to the body system of axes. The systems of axes used and the positive directions of forces, moments, and angles are shown in figure 1. The moment6 of the model are presented about a point located at the 0.330-chord point of the wing mean aerodynamic chord and 0.29 inch above the fuselage reference line. The horizontal-tail hinge moments are presented about a point located at the 0.385-chord point of the horizontal-tail mean aerodynamic chord. The symbols used in this paper are defined as follows:

b span of wing or of exposed-panel surface, in.

c chord, in. L 3 5 5

$\bar{c}$ wing mean aerodynamic chord, in.

$\bar{c}_H$ horizontal-tail mean aerodynamic chord of exposed panel, in.

$\bar{c}_V$ vertical-tail mean aerodynamic chord of exposed panel, in.

C_D drag coefficient, $\frac{\text{Drag}}{qS}$

$C_{D,i}$ internal drag coefficient

$C_{D,b}$ base drag Coefficient, $\frac{\text{Base drag}}{qS}$

C_p pressure coefficient

C_L lift coefficient, $\frac{\text{Lift}}{qS}$

C_m pitching-moment coefficient, $\frac{\text{Pitching moment}}{qS\bar{c}}$

C_l rolling-moment coefficient, $\frac{\text{Rolling moment}}{qSb}$

C_n yawing-moment coefficient, $\frac{\text{Yawing moment}}{qSb}$

C_Y side-force coefficient, $\frac{\text{Side force}}{qS}$

C_{L_α} lift-curve slope $(\alpha \approx 0^\circ)$, $\frac{\partial C_L}{\partial \alpha}$

[redacted]

$C_{m_{C_L}}$	pitching-moment-curve slope (C_L at $a \approx 0^\circ$), $\frac{\partial C_m}{\partial C_L}$
C_{l_β}	effective-dihedral parameter ($\beta \approx 0^\circ$), $\frac{\partial C_l}{\partial \beta}$ per degree
C_{n_β}	directional stability parameter ($\beta \approx 0^\circ$), $\frac{\partial C_n}{\partial \beta}$ per degree
C_{Y_β}	side-force parameter ($\beta \approx 0^\circ$), $\frac{\partial C_Y}{\partial \beta}$ per degree
$C_{l_{\delta_V}}$	vertical-tail rolling-moment parameter due to yaw-control deflection ($\delta_V \approx 0^\circ$), $\frac{\partial C_l}{}$
$C_{n_{\delta_V}}$	yaw-control effectiveness parameter ($\delta_V \approx 0^\circ$), $\frac{\partial C_n}{\partial \delta_V}$
$C_{D,min}$	minimum drag coefficient
$\frac{\Delta C_D}{C_L^2}$	drag-due-to-lift factor, $\frac{C_D - C_{D,min}}{C_L^2}$
L/D	lift-drag ratio, C_L/C_D
C_B	vertical-tail bending-moment coefficient, $\frac{\text{Bending moment}}{q(Sb)_{\text{surface}}}$
$C_{H,L}$ and $C_{H,R}$	hinge-moment coefficients of left and right exposed panels of horizontal tail about its axes of rotation, $\frac{\text{Hinge moment}}{q(S\bar{c})_{\text{surface}}}$
S	total area of wing or exposed-panel surface area of vertical and horizontal tails, sq ft
M	free-stream Mach number
R	Reynolds number

L
3
5
5

q free-stream dynamic pressure, lb/sq ft

α angle of attack referred to fuselage reference line, deg

β angle of sideslip referred to model plane of symmetry, deg

δ_V yaw-control angle, positive as shown in figure 1(c), deg

δ_H pitch-control angle, positive as shown in figure 1(c), deg

Subscripts: L355

0 value taken at zero lift coefficient

S stability axis

Configuration component designations:

W_1 wing with wing-tip nacelle in normal position

W_2 wing with wing-tip nacelle in forward position

W_3 wing with wing-tip nacelle off

B fuselage

H_0 horizontal tail with 0° dihedral

H_{30} horizontal tail with -30° dihedral

V_2 vertical tail

v_2 ventral fin

I fuselage inlet open

I_f fuselage inlet faired

APPARATUS AND MODELS

The tests were conducted in the low Mach number test section of the Langley Unitary Plan wind tunnel. This tunnel is a variable-pressure, continuous return-flow type. The test section is 4 feet square and approximately 7 feet in length. The nozzle leading to the test section is of the asymmetric sliding-block type. Mach numbers may be varied continuously through a Mach number range from approximately 1.57 to 2.87 without tunnel shutdown.

L
3
5
5

The basic model has a wing with 9.3° sweepback of the quarter chard, an aspect ratio of 2.42, a taper ratio of 0.43, 0° dihedral, and a modified NACA 65A005 airfoil section with a blunt trailing edge. Photographs of the model are presented in figure 2. Details of the model are shown in figure 3 and the geometric characteristics are given in table I. The horizontal tail with 0° dihedral shown in figure 4 has a 30.0° sweepback of the quarter chord, an aspect ratio of 2.90, a taper ratio of 0.49, and a modified NACA 65A004 airfoil section. The horizontal tail with -30° dihedral shown in figure 4 has a 34.0° sweepback of the quarter chord, an aspect ratio of 2.46, a taper ratio of 0.49, and a modified NACA 65A004 airfoil section. The vertical tail shown in figure 5 has an angle of sweepback of 47.5° at the quarter chord, an aspect ratio of 1.27, a taper ratio of 0.39, and a modified NACA 65A004 airfoil section. The ventral fin, shown in figure 6 has an angle of sweepback of 40.5° at the quarter chord, an aspect ratio of 0.35, a taper ratio of 0.62, and a modified NACA 65A004 airfoil section. The nacelle, shown in figure 7, was mounted on each wing tip. Each nacelle had a fineness ratio of 4.47 based on nacelle length and the diameter of a circle whose area is equal to the frontal area of the nacelle, 0.018 square foot. Two inlets shown in figures 3 and 8 were mounted on the side of the fuselage beneath the wing. The air taken into these inlets was ducted through the fuselage and discharged at the base of the model through a single exit.

Forces and moments for the complete model were measured by means of a six-component, electrical strain-gage balance. This balance was attached, by means of a sting, to the tunnel central support system. The moments were measured at a point located at 33 percent of the wing mean aerodynamic chord and 14.15 percent of the mean aerodynamic chord below the wing chord line.

An additional component of the model system was a remotely operated adjustable coupling with which tests can be performed at variable sideslip angles concurrently with variable angles of attack. This coupling was placed between the model sting and the tunnel central support system. The vertical tail and horizontal tails were independently and manually positioned. Control-surface deflections were preset and measured with an inclinometer. Duct losses were determined by measuring a static pressure on the inner wall of the nacelle near the exit and a total pressure in the same longitudinal plane and on the center line of the nacelle duct. A similar method was used to determine fuselage duct losses. Base pressures were obtained by pressure measurement at the base of the right nacelle and fuselage.

TESTS

L355

Tests were made through an angle-of-attack range from approximately -6° to 15° at angles of sideslip of about 0° and 4°. Tests were also made through an angle-of-sideslip range from approximately -6° to 8° at angles of attack of about 0°, 5°, and 10°. All basic model tests were made with a stabilizer deflection of 0°.

The test conditions of Mach number, stagnation and dynamic pressure, and Reynolds number are listed in the following table:

M	Stagnation pressure, lb/sq in. abs	Dynamic pressure, lb/sq ft	Reynolds number, per foot
1.57	12.9	788	3.52×10^6
2.14	16.0	758	3.52
2.54	19.8	710	3.52
2.87	23.6	650	3.52

The Reynolds number based on the mean aerodynamic chord of the wing is 1.6×10^6. The dewpoint for all tests was maintained below -30° F to prevent adverse condensation effects. The stagnation temperature was maintained at 125° F for all Mach numbers except 2.54 and 2.87 where it was 150° F.

CORRECTIONS AND ACCURACY

The calibration of the flow has shown that there is a small upflow in the test section. The results presented herein have been corrected for this flow misalinement. The maximum deviation of local Mach number in the portion of the tunnel occupied by the model was ± 0.015 from the average values listed in the preceding section.

[redacted]

The angles of attack and sideslip of the model have been corrected for the deflection of the model sting and balance under load. The control-surface angles were prepositioned to the desired angle of deflection. The loading effect on the control surfaces was ascertained to be small and is listed in the table of accuracies.

The internal duct losses for flow through the nacelles and inlets were determined by measurement of static and total pressures near the duct exit. Once determined these losses were translated into internal drag coefficients which are presented in figure 9. Base drag coefficients were computed from the measured base pressures. These coefficients are presented in figure 10. The drag coefficients presented in this paper have not been corrected for either base drag or internal drag. Pressure measurements were also made over the upper surface of the right wing-tip nacelle. These pressures were recorded on manometer boards and reduced to coefficients.

The estimated accuracy of the force and moment coefficients and angles based on calibration and repeatability of the data is as follows:

C_L	±0.0020
C_D	±0.0010
C_m	±0.0050
C_l	±0.0002
C_n	±0.002
C_Y	±0.0050
α, deg	±0.100
β, deg	±0.100
δ_H, deg	±0.100
δ_V, deg	±0.100

PRESENTATION OF RESULTS

The results of an investigation of the aerodynamic characteristics of a model of a supersonic horizontal-attitude VTOL airplane are presented in figures that are organized as follows:

	Figures
Schlieren photographs of model	11 and 12
Longitudinal stability characteristics:	
Effect of various model components	13
Effect of various inlet conditions	14

[redacted]

Figures

Langley Research Center,
National Aeronautics and Space Administration,
Langley Field, Va., October 2, 1959.

TABLE I.- GEOMETRIC CHARACTERISTICS OF A MODEL OF A SUPERSONIC HORIZONTAL-ATTITUDE VTOL AIRPLANE

Location of center of moments:	
Longitudinal distance from the nose. in.	16.66
Vertical distance above fuselage reference line. in.	0.29
Wing:	
Airfoil section	NACA 65A005 (modified)
Total area (measured between nacelle center lines). sq ft	0.45
Span (measured between nacelle center lines). in.	12.48
Mean aerodynamic chord. in.	5.42
Aspect ratio	2.42
Taper ratio	0.43
Sweep of quarter-chord line. deg	9.3
Incidence. deg	0
Dihedral. deg	0
Distance of $\bar{c}$ above fuselage reference line. in.	1.05
Horizontal tail:	
Airfoil section	NACA 65A004 (modified)
Exposed area. sq ft:	
H_0	0.10
H_{30}	0.12
Exposed span. in.	6.54
Mean aerodynamic chord of exposed panel. $\bar{c}_H$, in.:	
H_0	2.40
H_{30}	2.77
Aspect ratio:	
H_0	2.90
H_{30}	2.46
raper ratio	0.49
Sweep of quarter-chord line. deg:	
H_0	30.0
H_{30}	34.0
Incidence. deg	0
Dihedral. deg:	
H_0	0
H_{30}	-30.0
Tail length. in.	12.37
Distance $\bar{c}_H$ below body reference line. in.:	
H_0	0.16
H_{30}	0.99
Vertical tail:	
Airfoil section	NACA 65A004 (modified)
Exposed area. sq ft	0.08
Exposed span. in.	3.82
Mean aerodynamic chord of exposed panel. in.	3.40
Aspect ratio	1.27
Taper ratio	0.39
Sweepback of quarter-chord line. deg	47.5
Ventral fin:	
Airfoil section	NACA 65A004 (modified)
Area. sq ft	0.03
Span. in.	1.68
Mean aerodynamic chord. in.	3.54
Aspect ratio	0.35
Taper ratio	0.62
Sweepback of quarter-chord line. deg	40.5

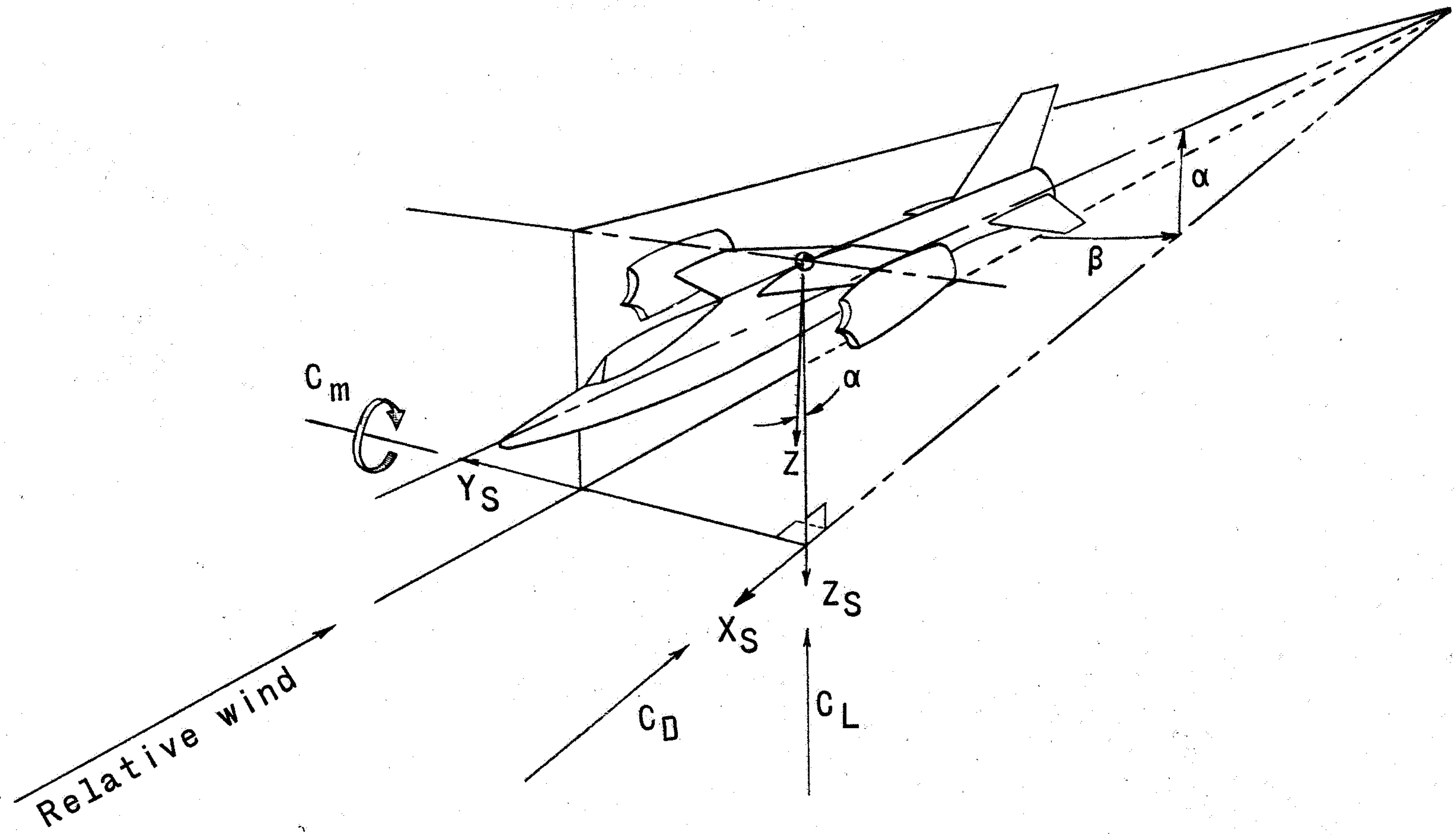

(a) Stability axes.

Figure 1.- Axes systems. Positive values of forces, moments, and angles are indicated by arrows.

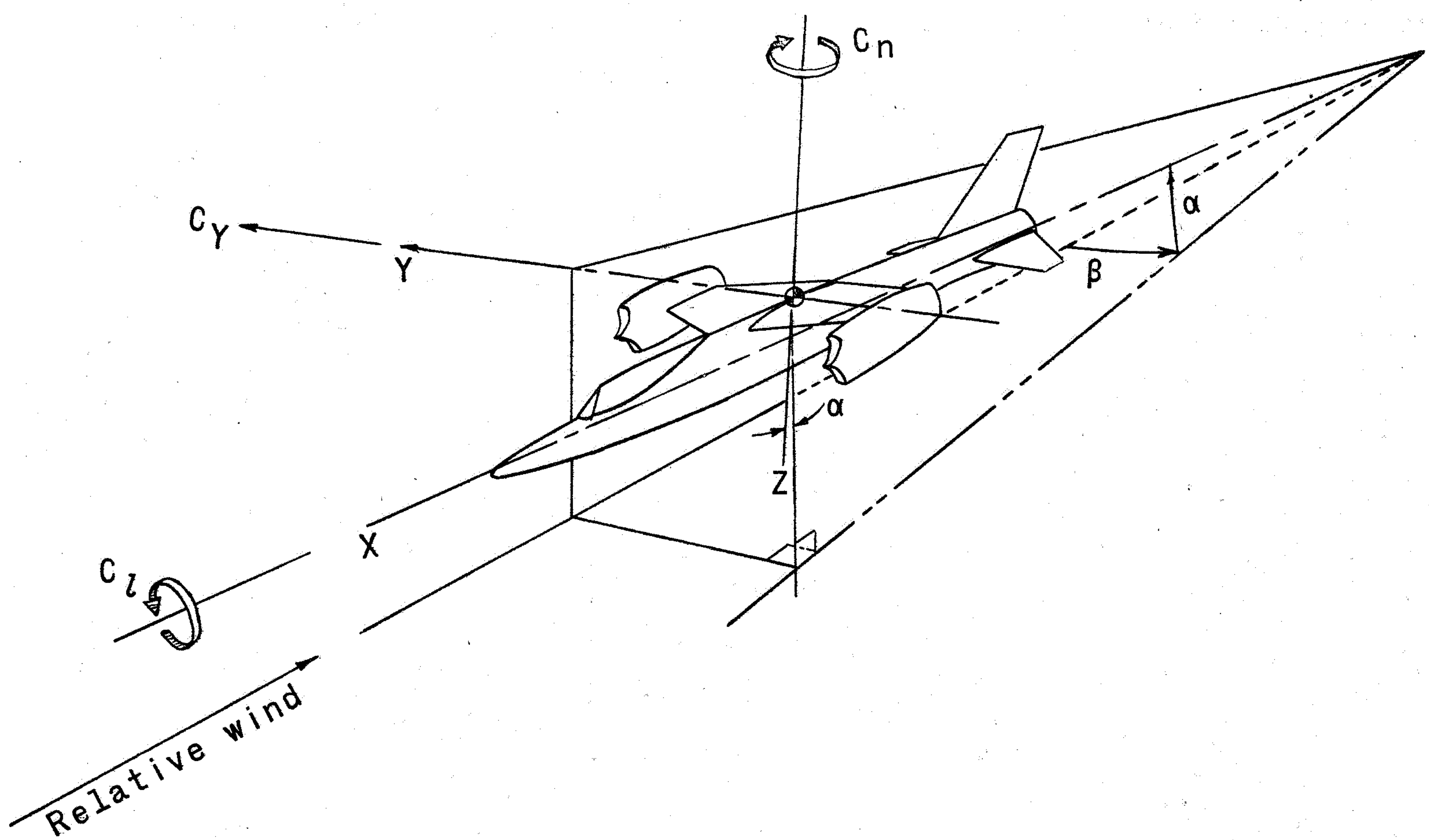

(b) Body axes.

Figure 1.- Continued.

[redacted]

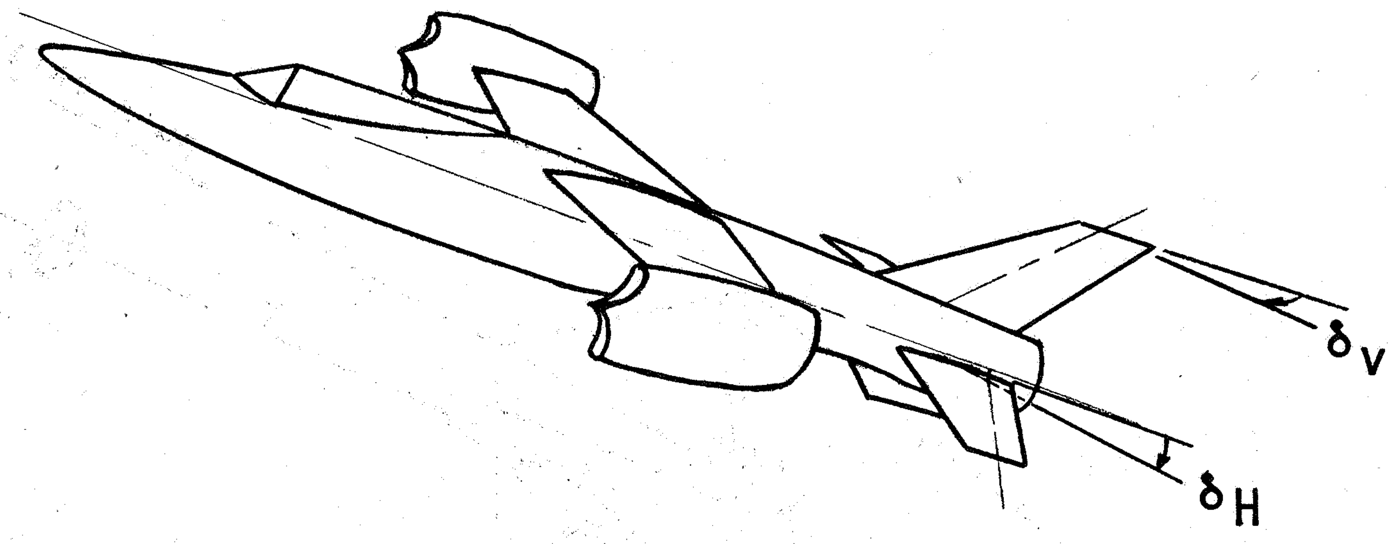

(c) Control-surface deflections.

Figure 1.- Concluded.

[redacted]

[redacted]

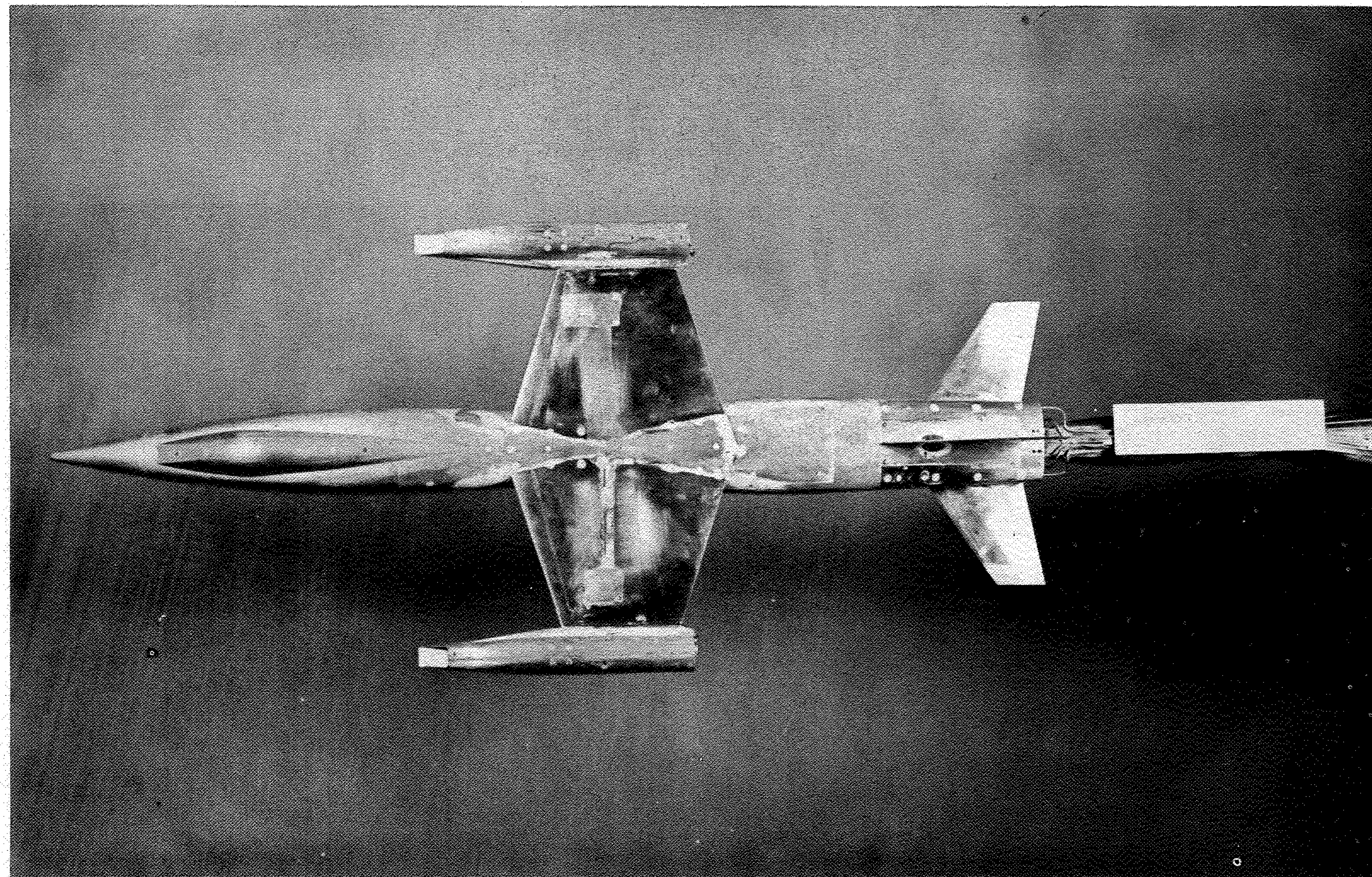

(a) Top view of $W_1BH_0V_2v_2$ configuration. L-58-2120

Figure 2 - Supersonic horizontal-attitude VTOL airplane models used in this investigation.

[redacted]

[redacted]

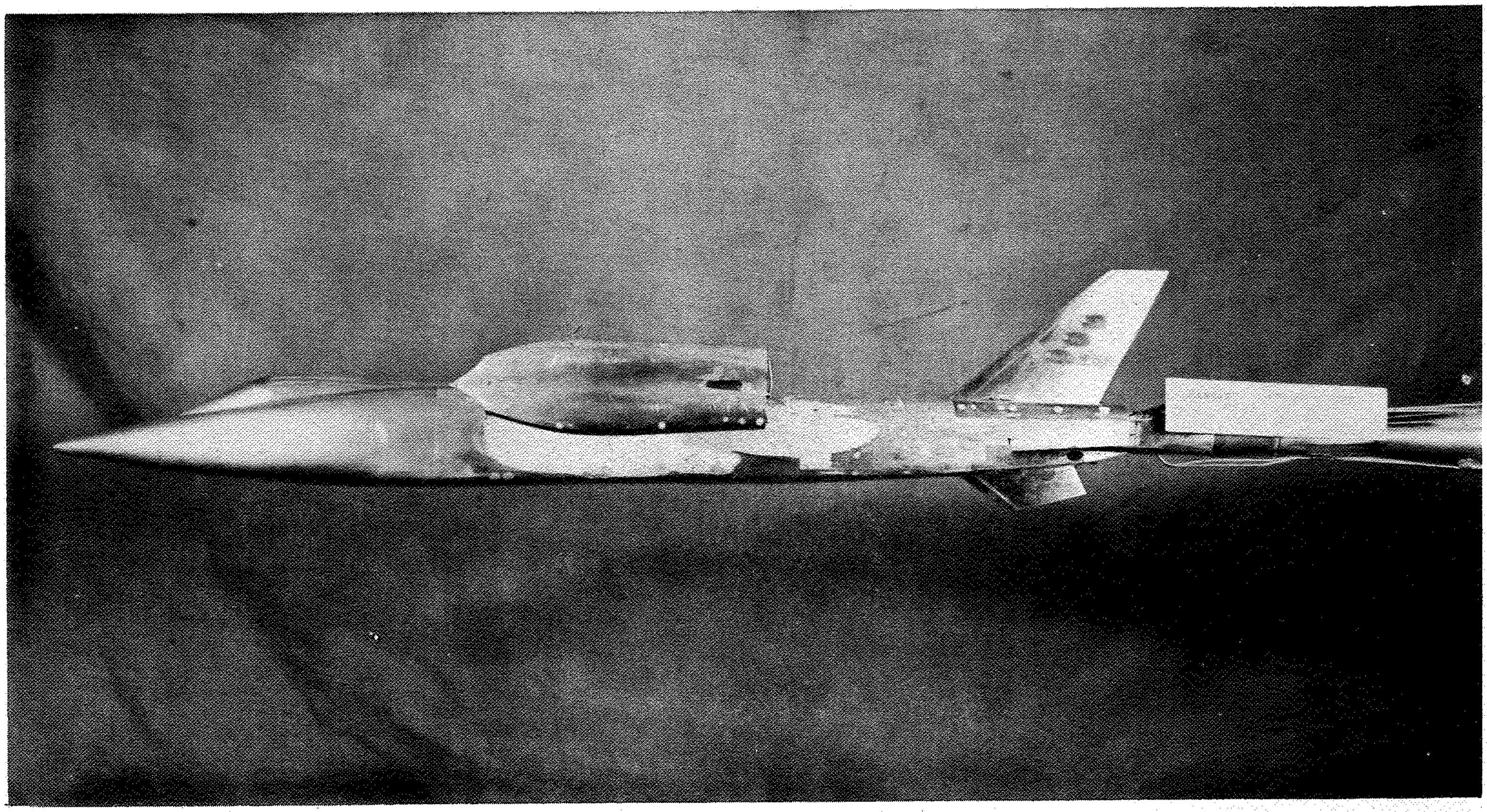

(b) Side view of $W_1BH_0V_2v_2$ configuration. L-58-2121

Figure 2 - Continued.

[redacted]

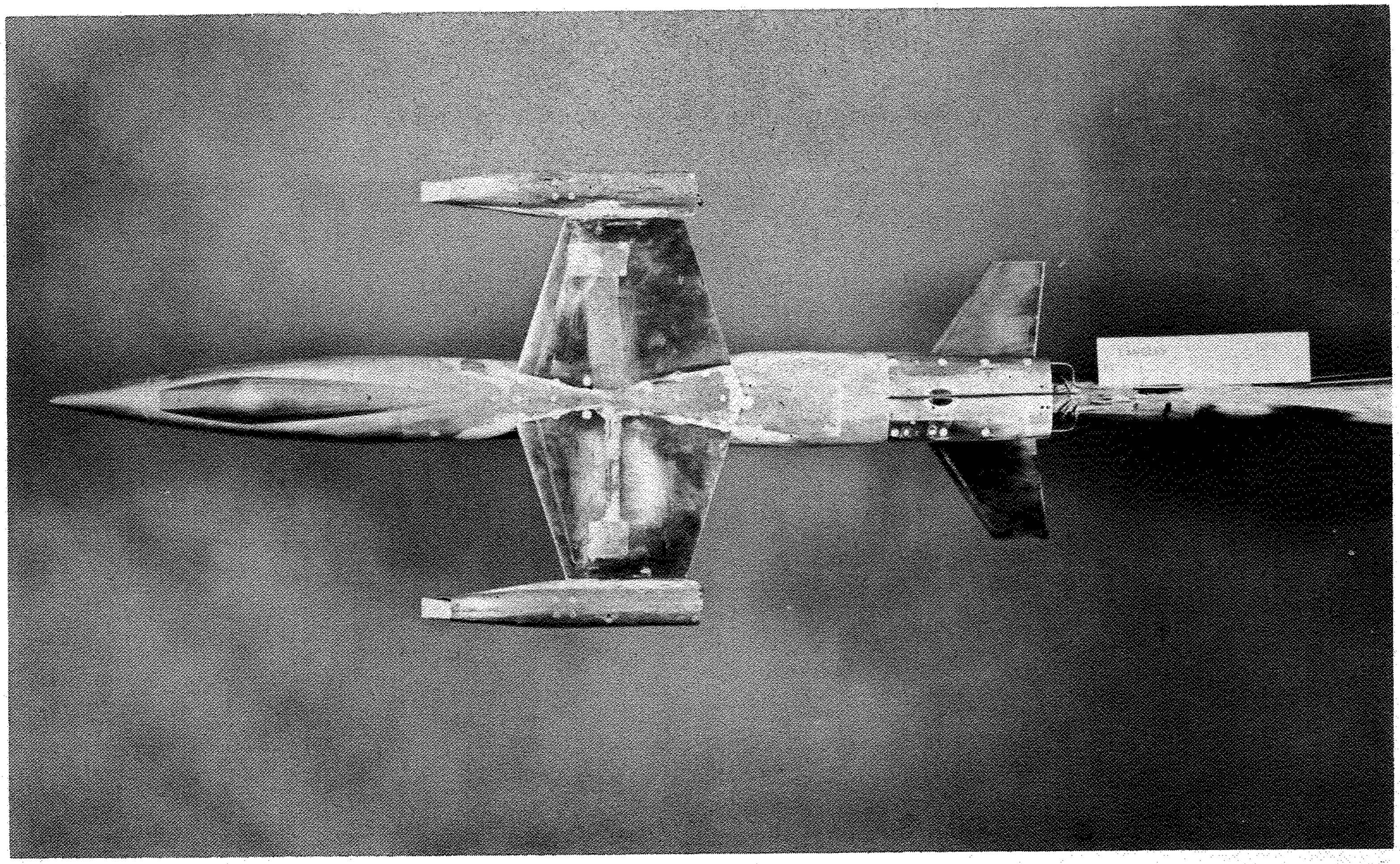

(c) Top view of $W_1BH_{30}V_2v_2$ configuration. L-58-2122

Figure 2.- Continued.

[redacted]

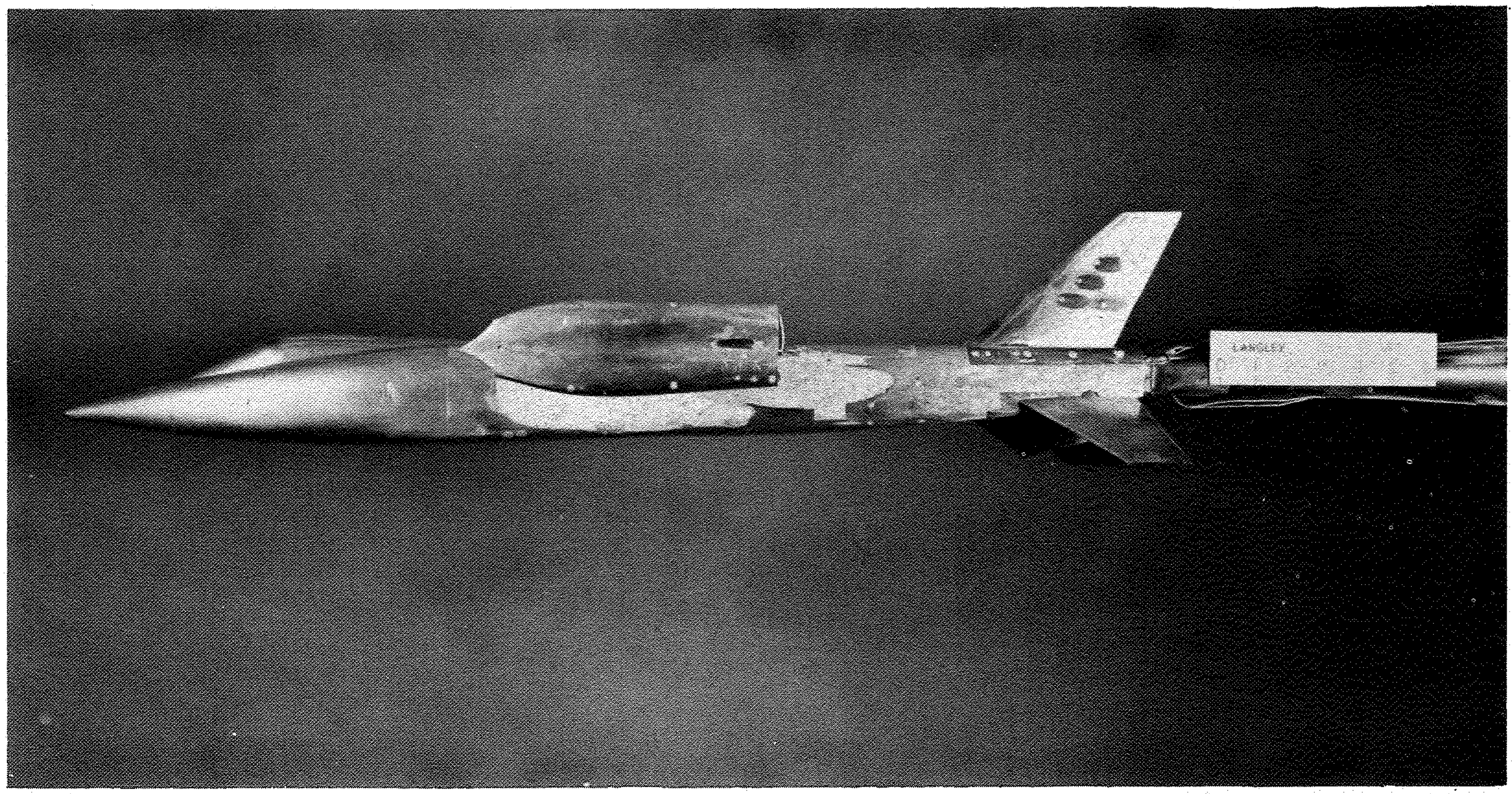

(d) Side view of $W_1BH_{30}V_2v_2$ configuration. L-58-2123

Figure 2.- Continued.

L-355

[redacted]

[redacted]

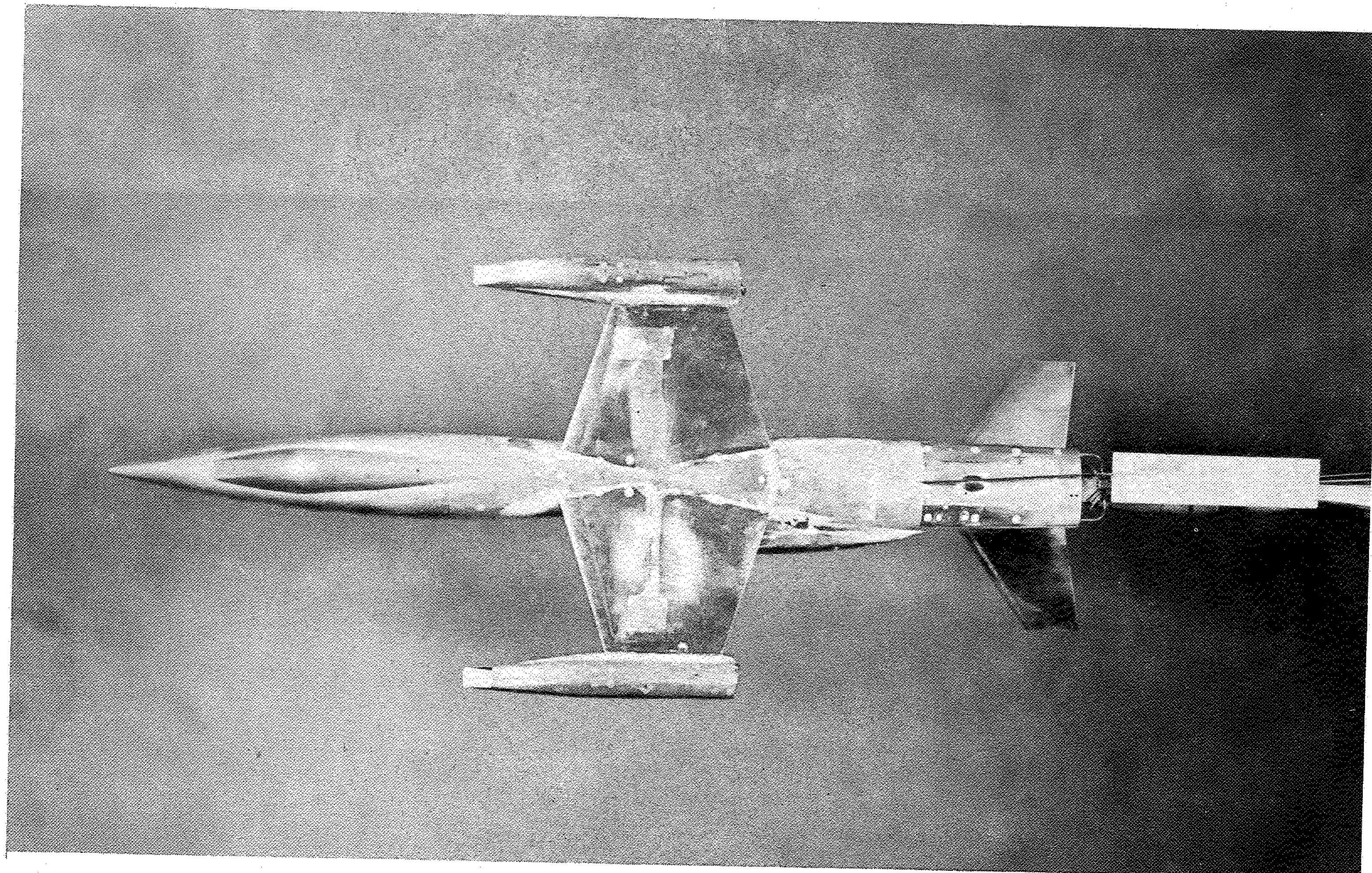

(e) Top view of $W_1BH_{30}V_2v_2I$ configuration. L-58-2124

Figure 2.- Continued.

[redacted]

[redacted]

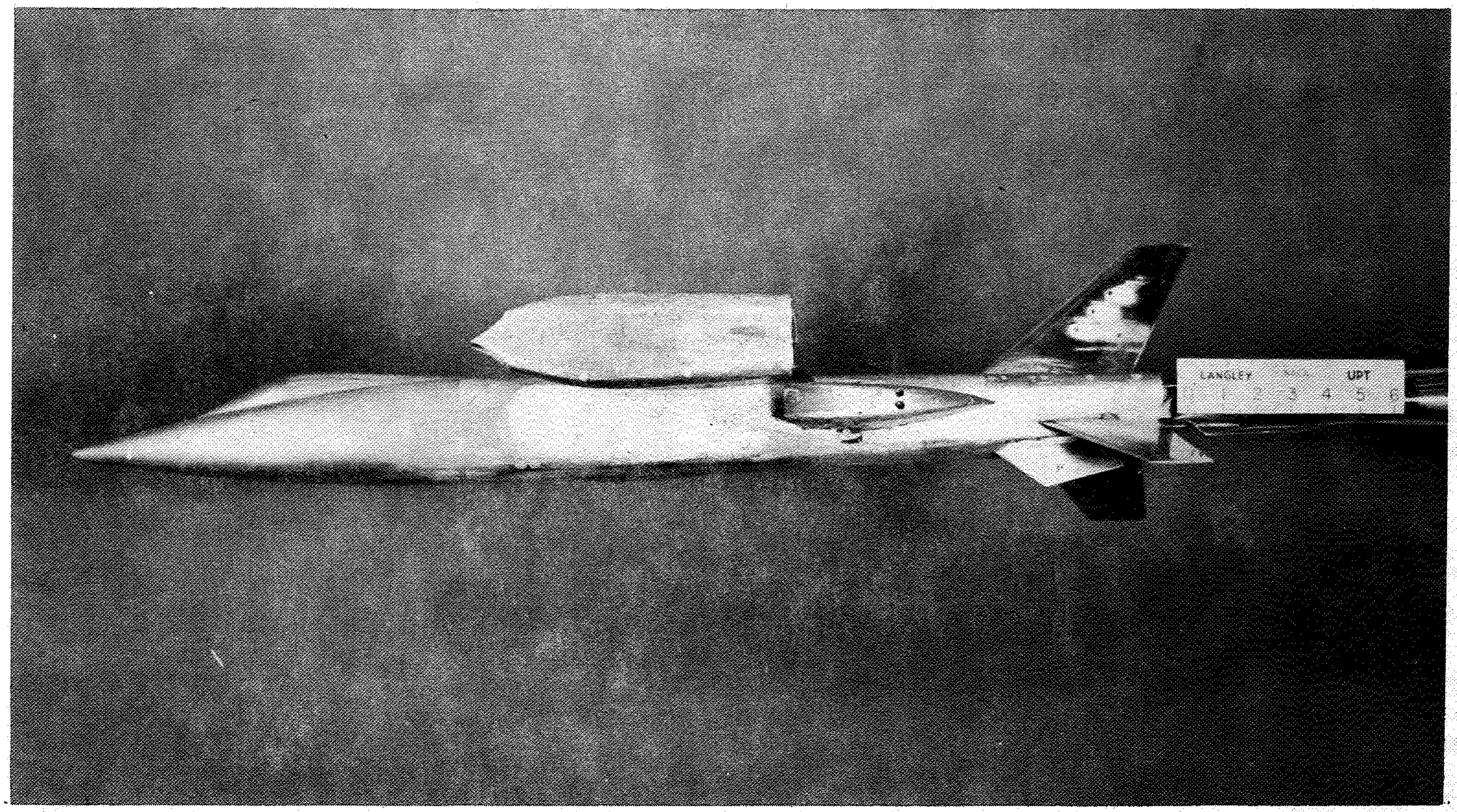

(f) Side view of $W_1BH_{30}V_2v_2I$ configuration. L-58-2125

Figure 2 - Continued.

[redacted]

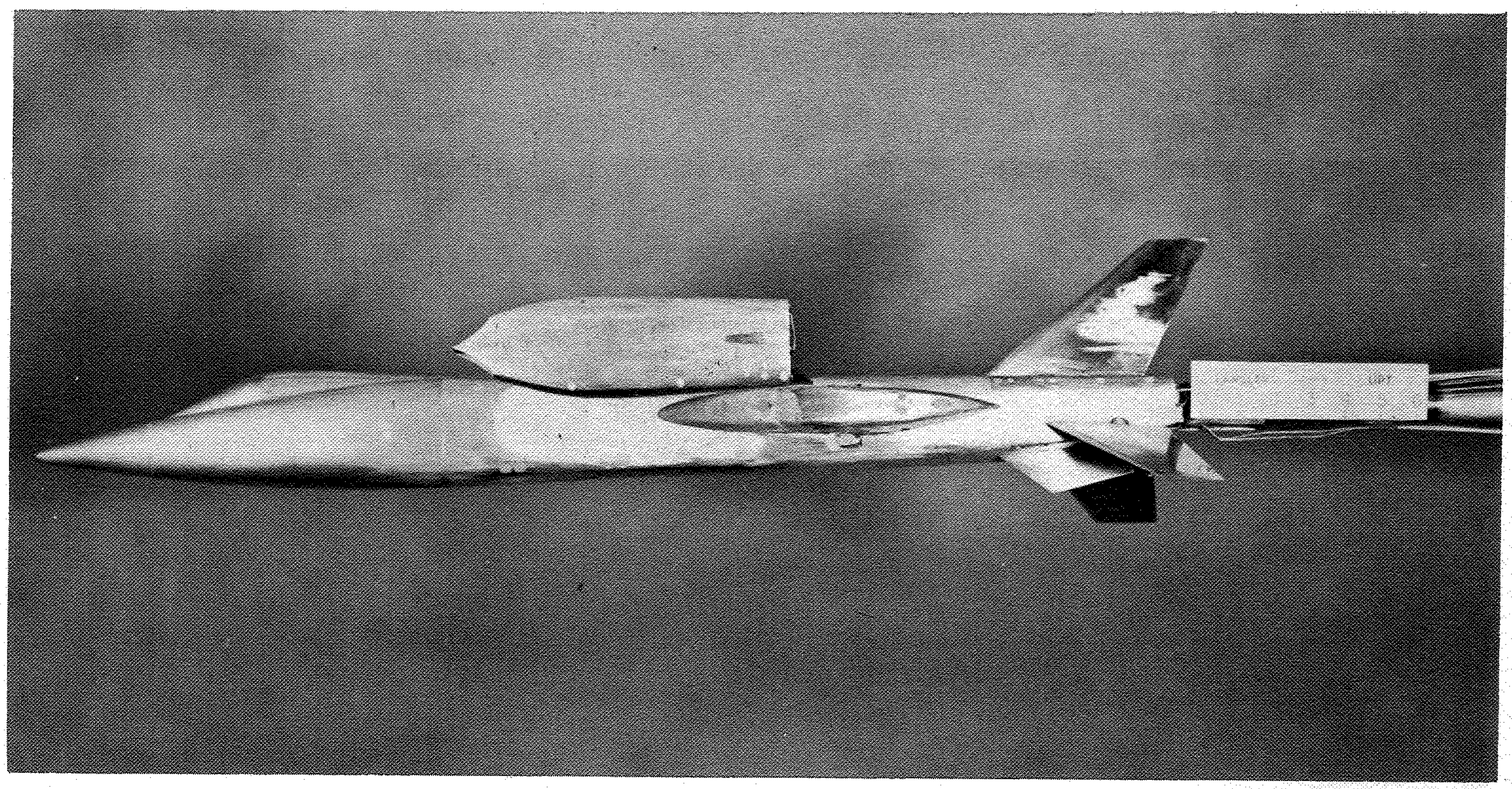

(g) Side view of $W_1BH_{30}V_2v_2I_f$ configuration. L-58-2126

Figure 2 - Continued.

[redacted]

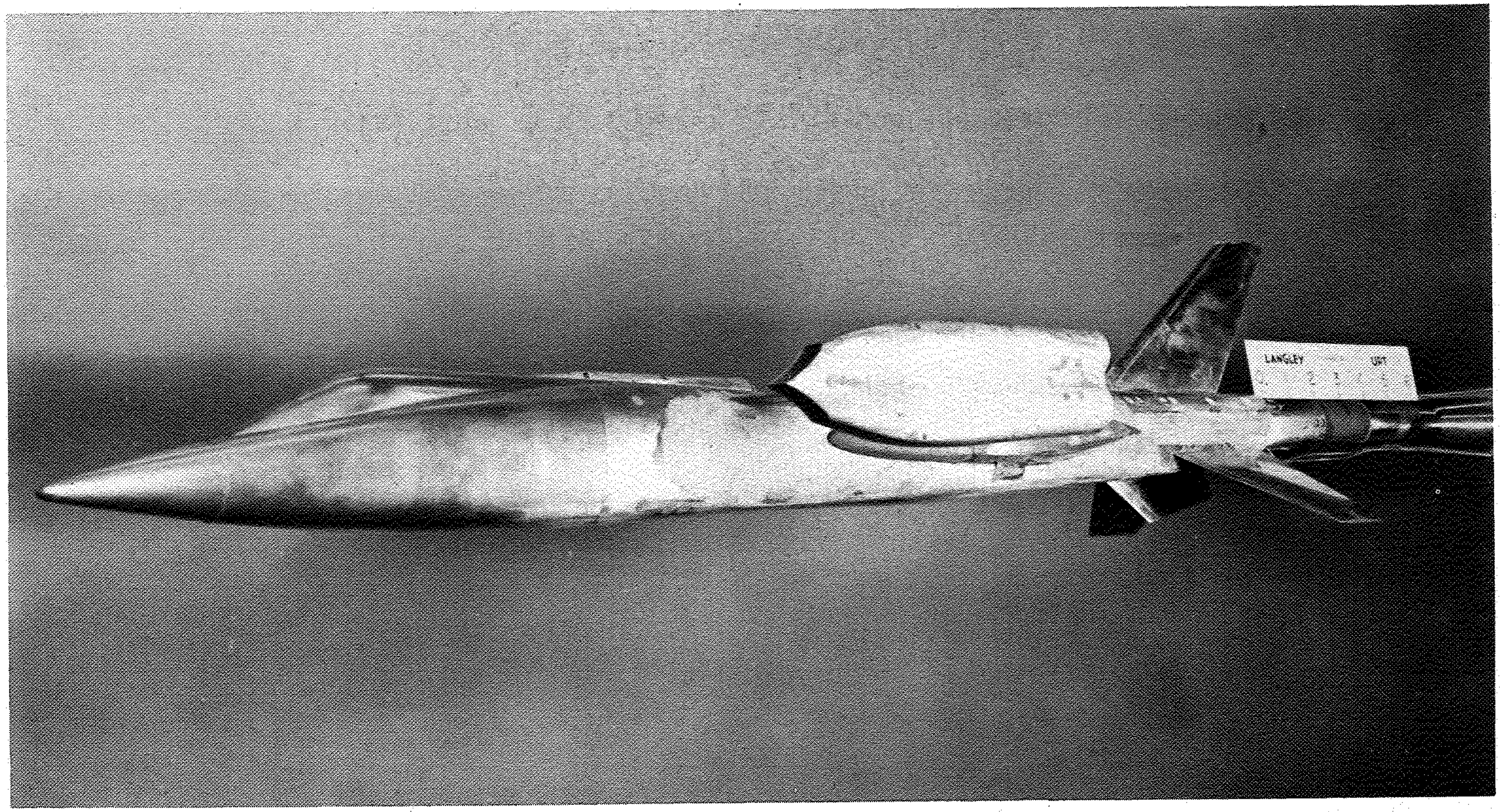

L-58-2127

(h) Three-quarter side view of $W_1BH_{30}V_2v_2I_f$ configuration.

Figure 2 - C clu[illegible]d

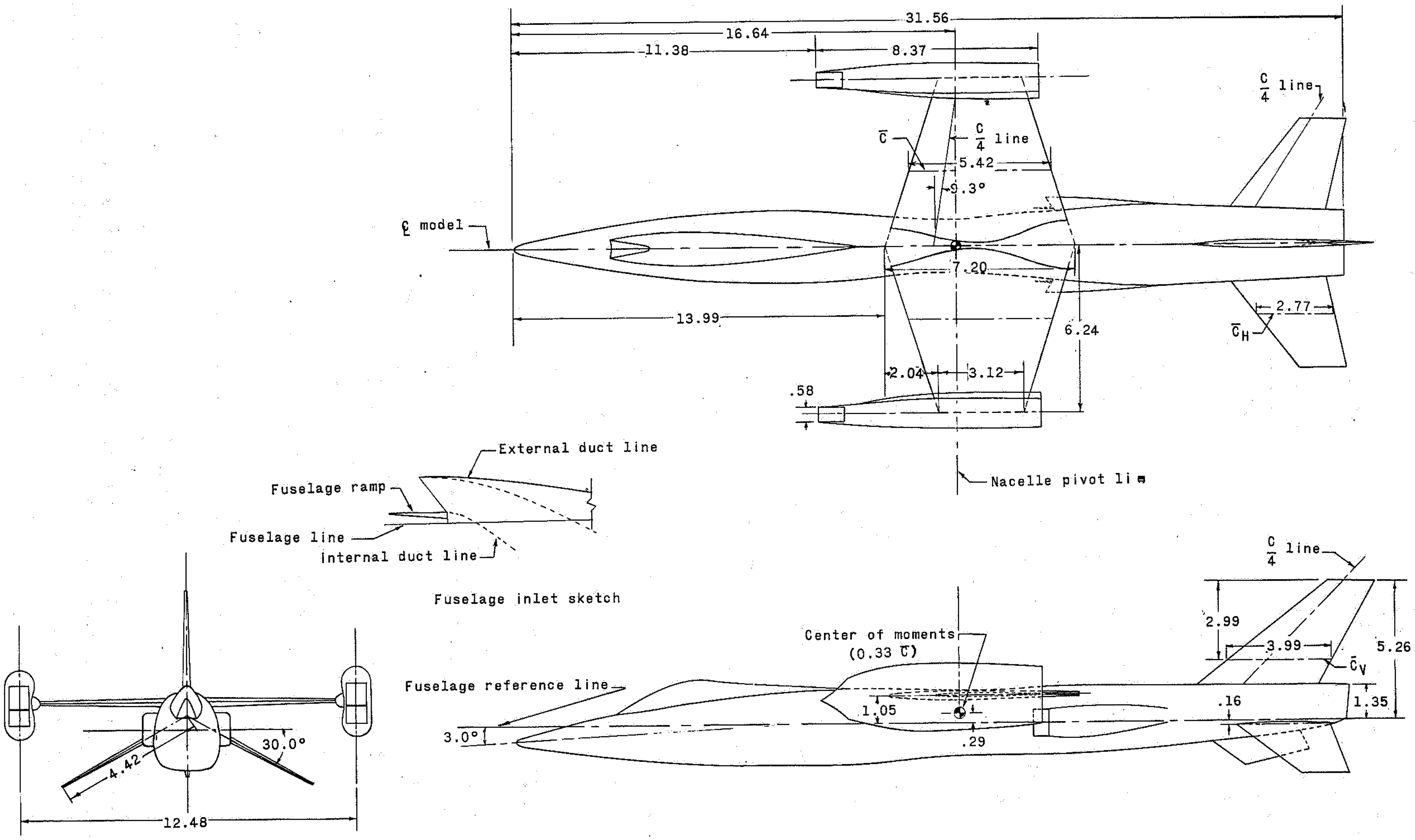

Figure 3.- Details of a model of a supersonic horizontal-attitude VTOL airplane. Dimensions are in inches unless otherwise noted.

[redacted]

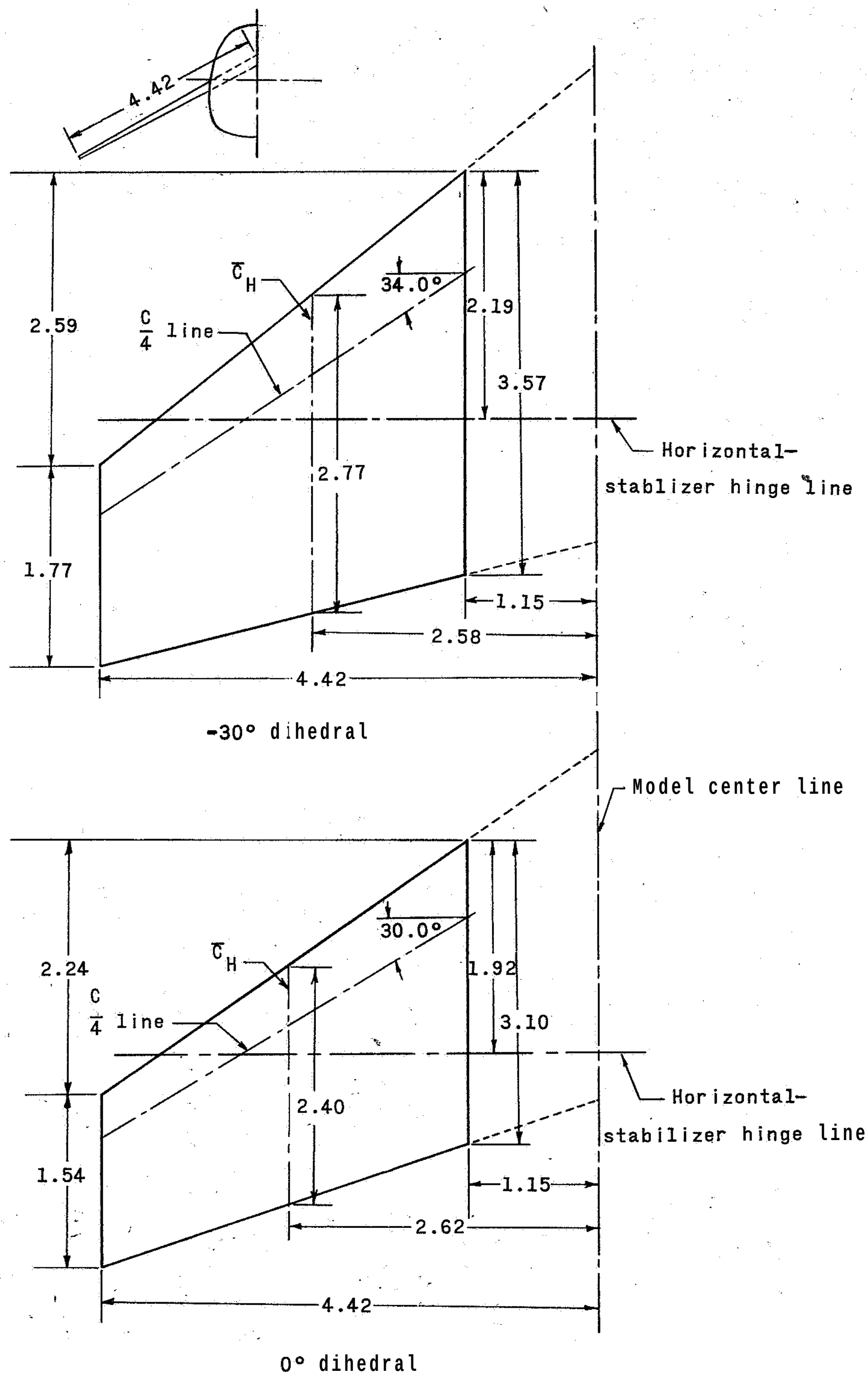

Figure 4.- Drawings of the horizontal stabilizer of a supersonic horizontal-attitude VTOL airplane model. Dimensions are in inches unless otherwise noted.

[redacted]

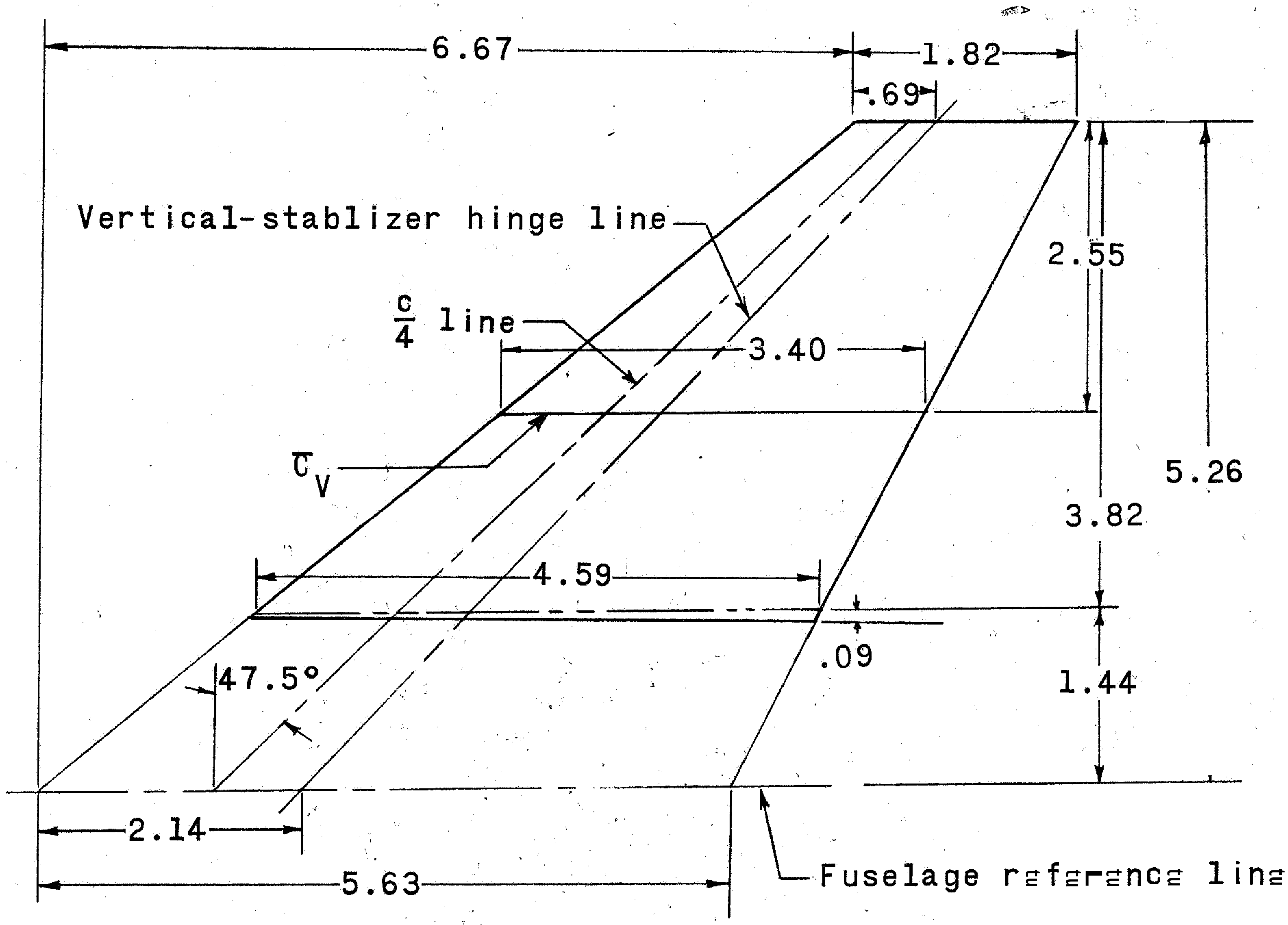

Figure 5.- Drawing of the vertical stabilizer of a supersonic horizontal-attitude VTOL airplane model. Dimensions are in inches unless otherwise indicated.

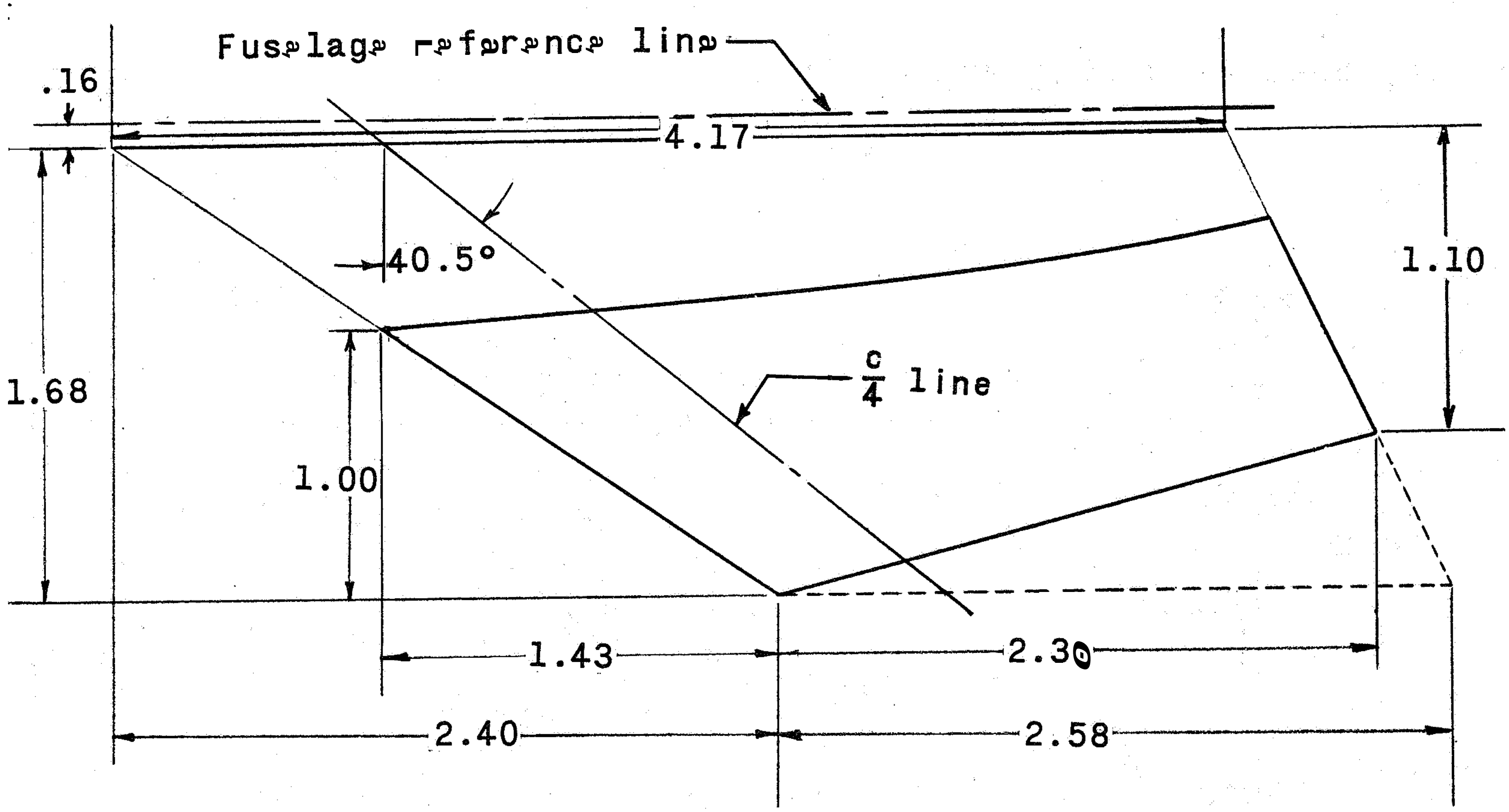

Figure 6.- Drawing of the ventral fin of a supersonic horizontal-attitude VTOL airplane model.
Dimensions are in inches unless otherwise indicated.

Nacelle surface pressure orifices		
orifice	nacelle station, x, in.	x/l
1	1.460	.174
2	2.200	.262
3	3.140	.375
4	4.360	.520
5	5.400	.645
6	6.640	.793
7	8.068	.962
l = 8.37 inches		

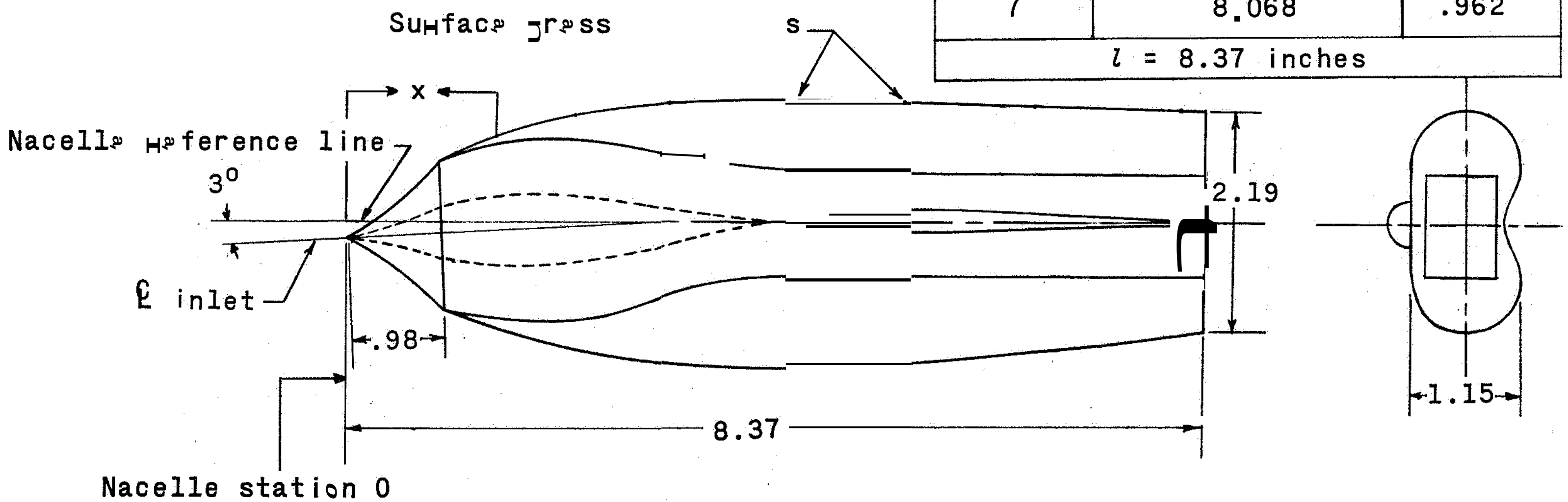

Figure 7.- Drawing of the wing-tip nacelle. Dimensions are in inches unless otherwise noted.

[redacted]

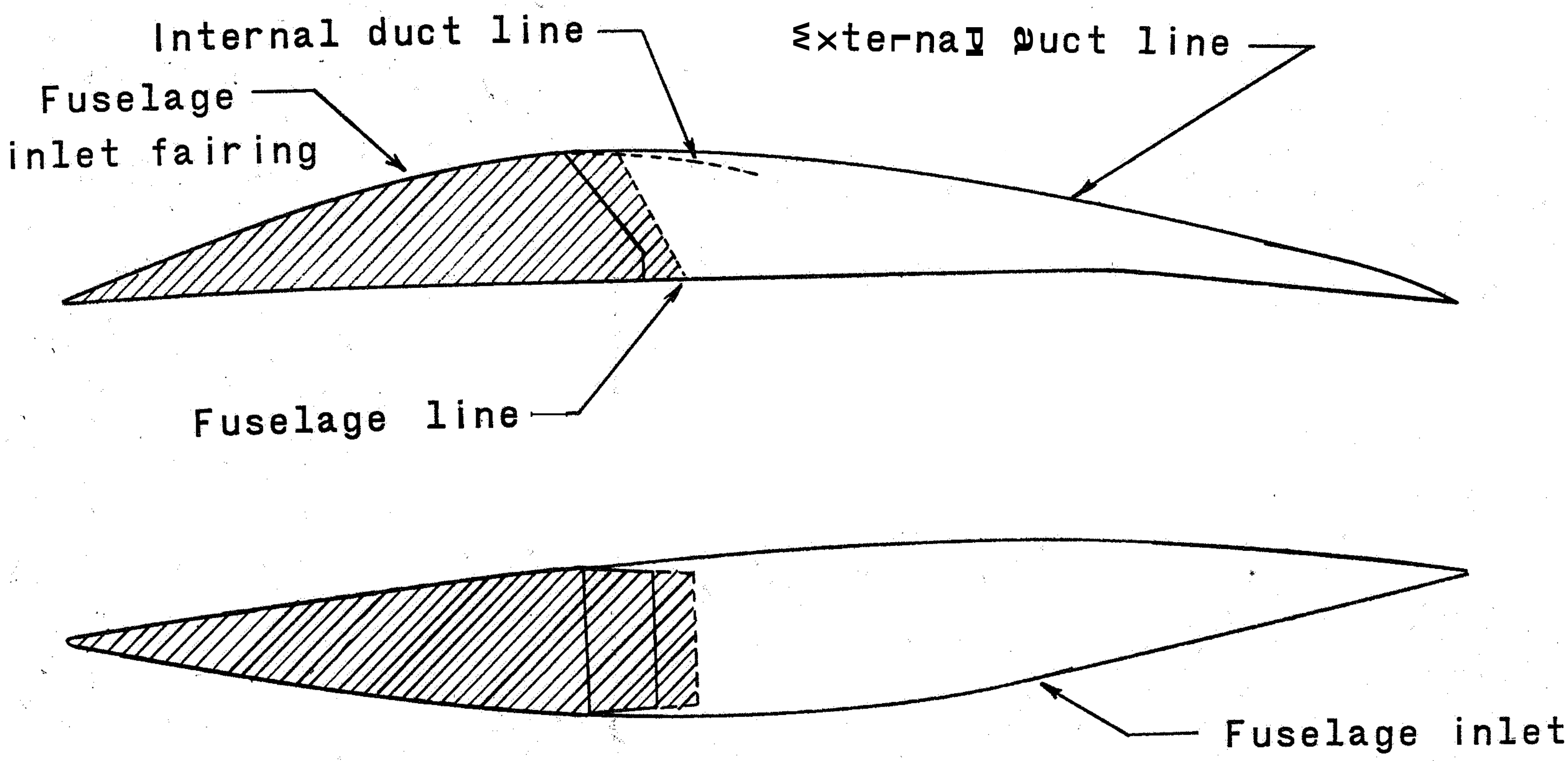

Figure 8 - Sketch of inlet fairing.

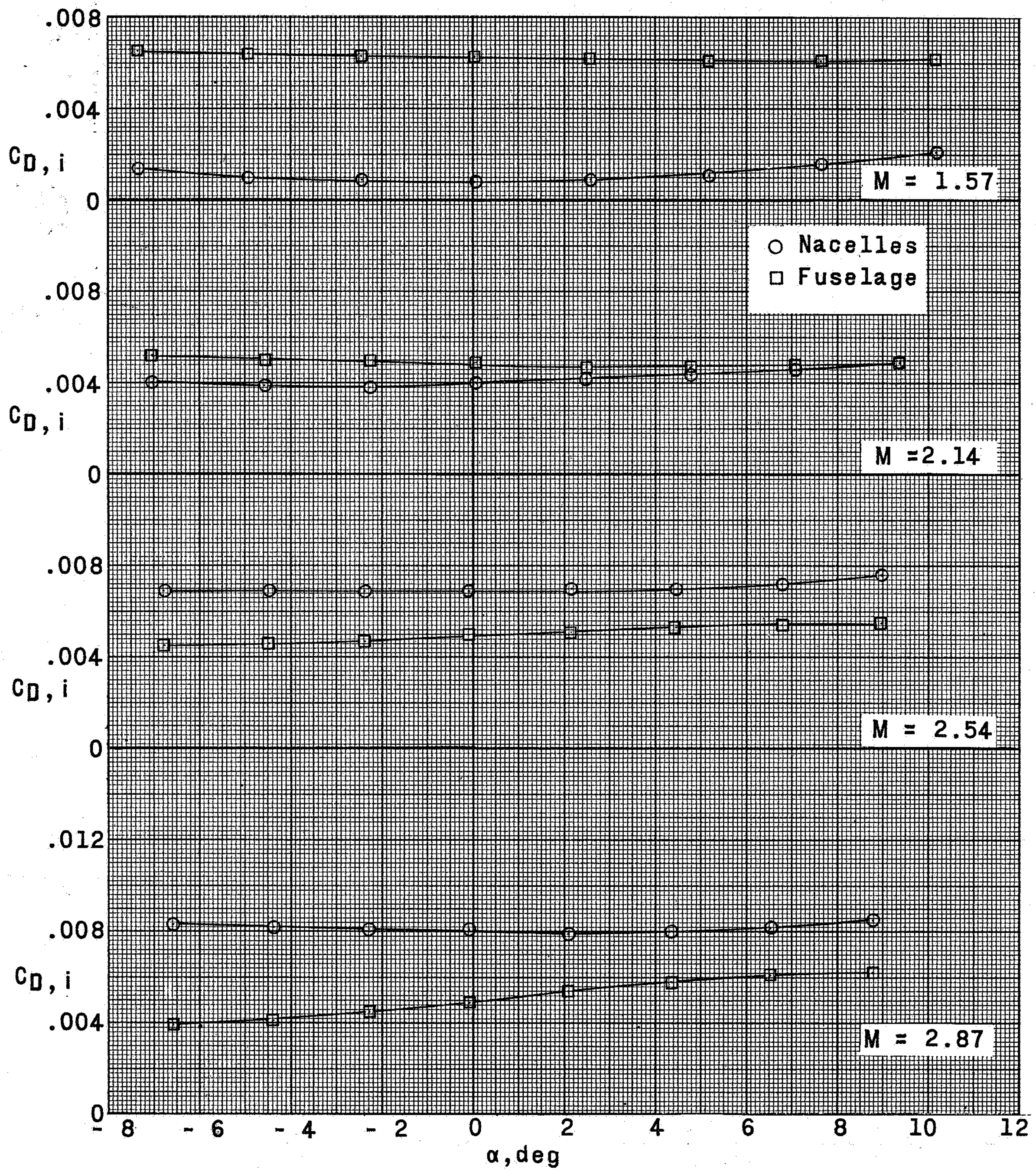

Figure 9.- Variation of internal drag coefficient of a supersonic horizontal-attitude VTOL airplane model at a nominal Reynolds number of 3.52×10^6 per foot.

[redacted]

[redacted]

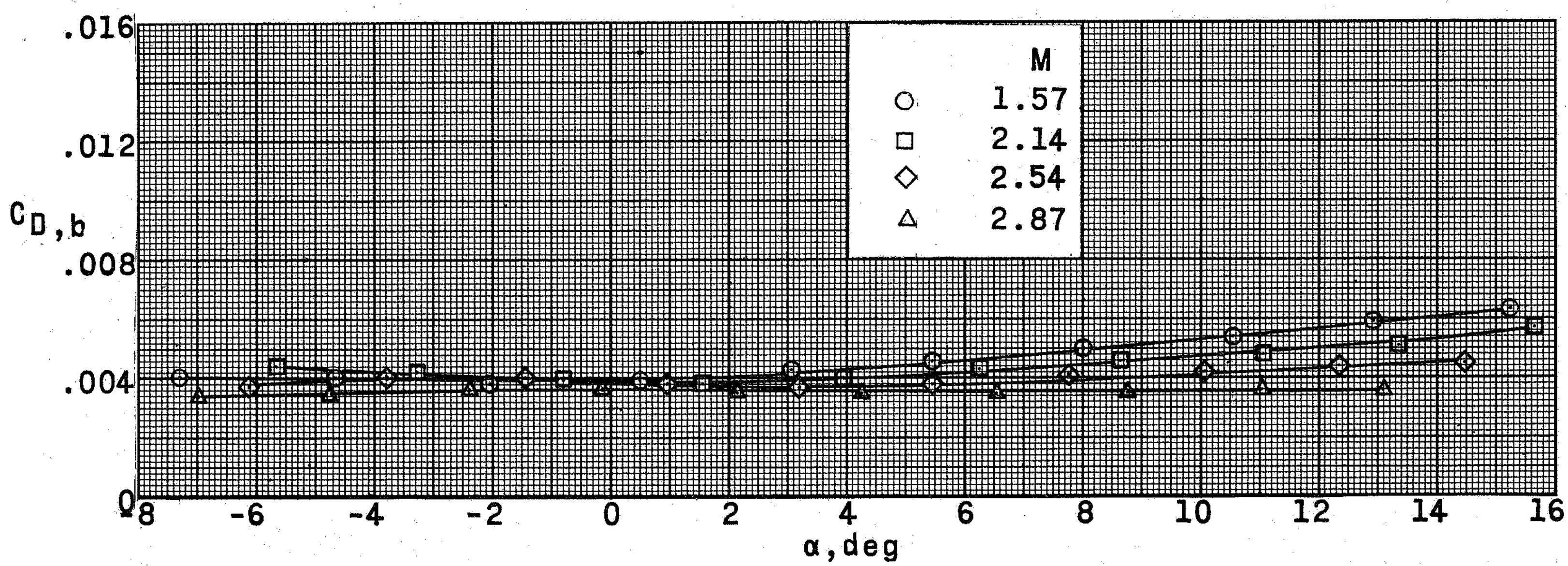

Figure 10 - Variation of base drag coefficient of a supersonic horizontal-attitude VTOL airplane model at a nominal Reynolds number of 3.52×10^6 per foot.

[redacted]

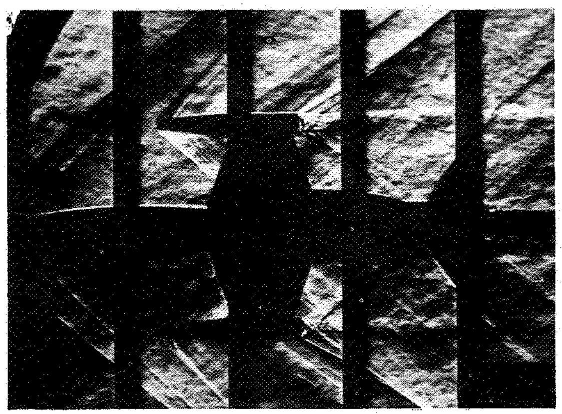

$\alpha \approx 0°; \beta \approx 0°$

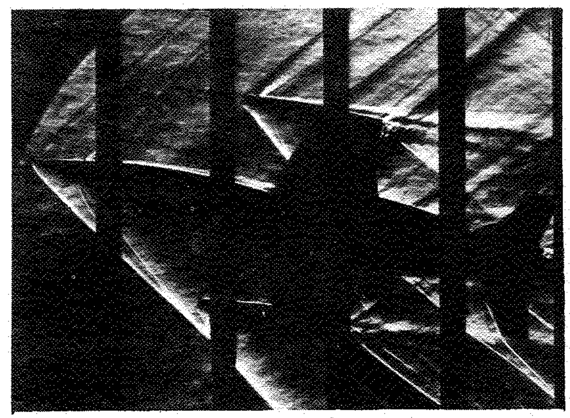

$\alpha \approx 0°; \beta \approx 12°$

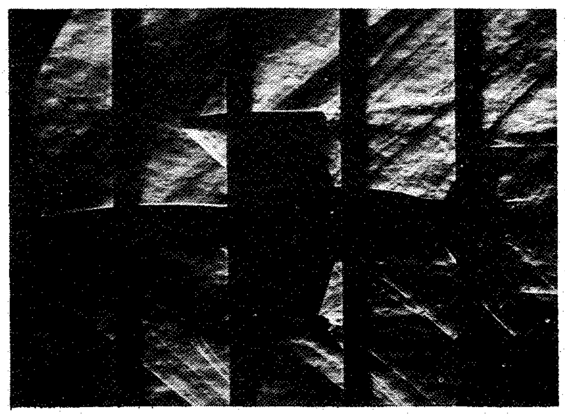

$\alpha \approx 8°; \beta \approx 0°$

(a) M = 1.57.

L-59-6089

Figure 11 - Schlieren photographs of the plan form of a supersonic horizontal-attitude VTOL airplane model in the Langley Unitary Plan wind tunnel. Reynolds number, 3.52×10^6.

[redacted]

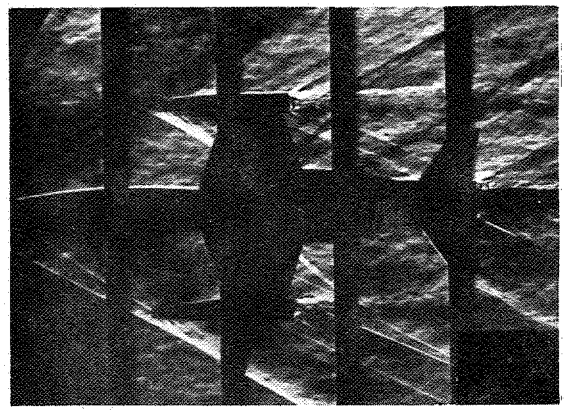

α≈0°; β≈0°

α≈10°; β≈4°

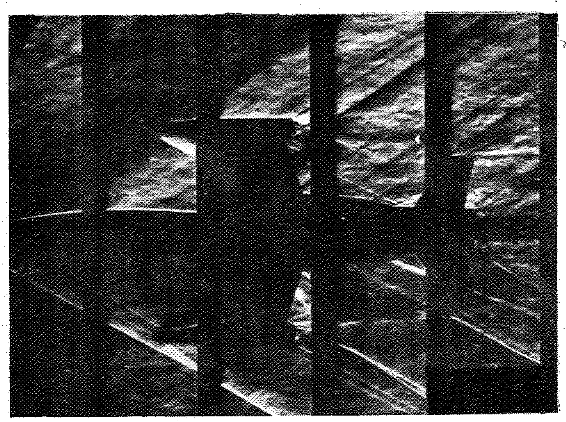

α≈8°; β≈0°

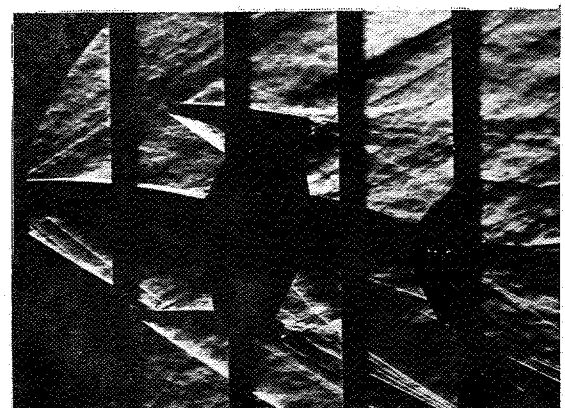

α≈7°; β≈8°

(b) $M = 2.14$. L-59-6090

Figure 11 - Continued.

[redacted]

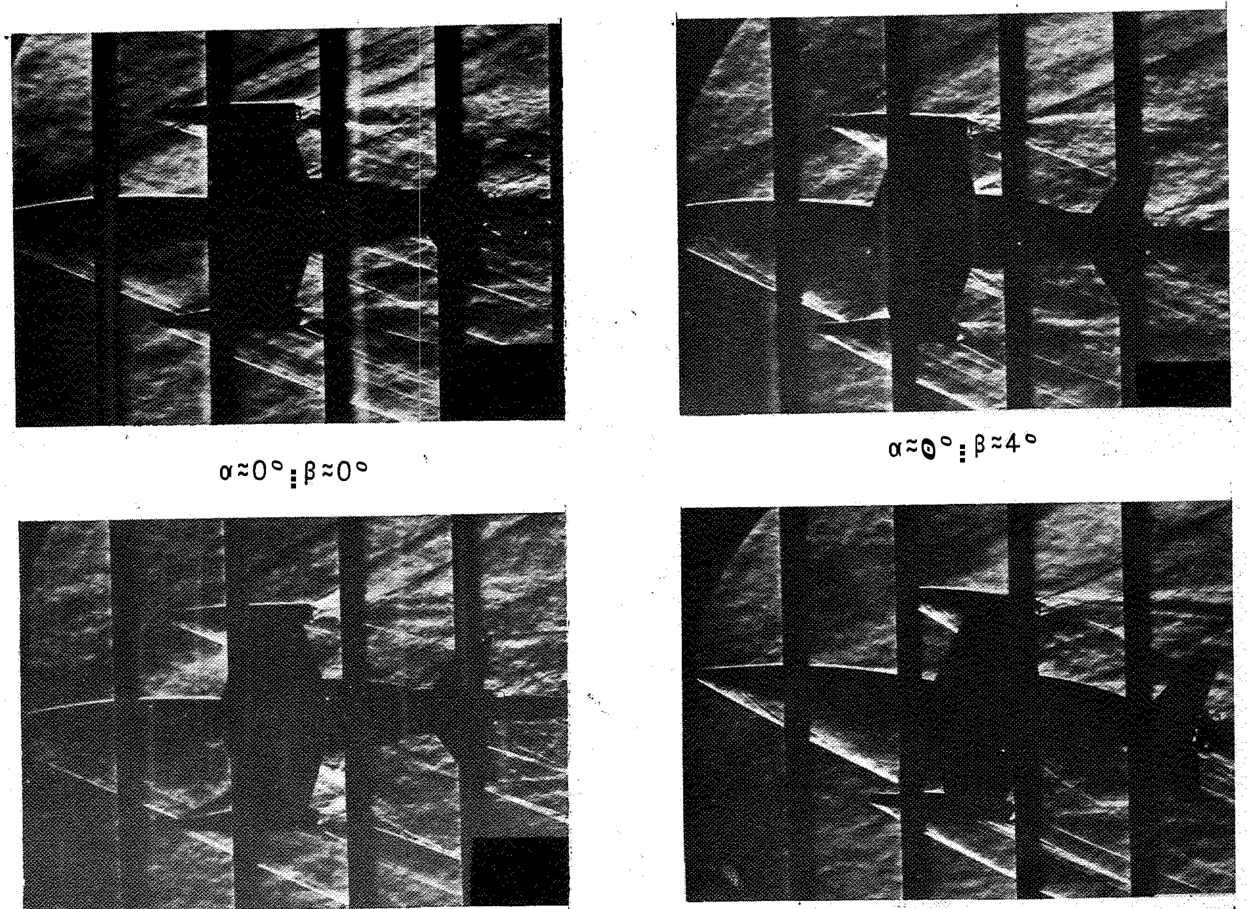

$\alpha \approx 0^\circ ; \beta \approx 0^\circ$ $\alpha \approx 0^\circ ; \beta \approx 4^\circ$

$\alpha \approx 8^\circ ; \beta \approx 0^\circ$ $\alpha \approx 0^\circ ; \beta \approx 3^\circ$

(c) M = 2.87. L-59-6091

Figure 11.- Concluded.

[redacted]

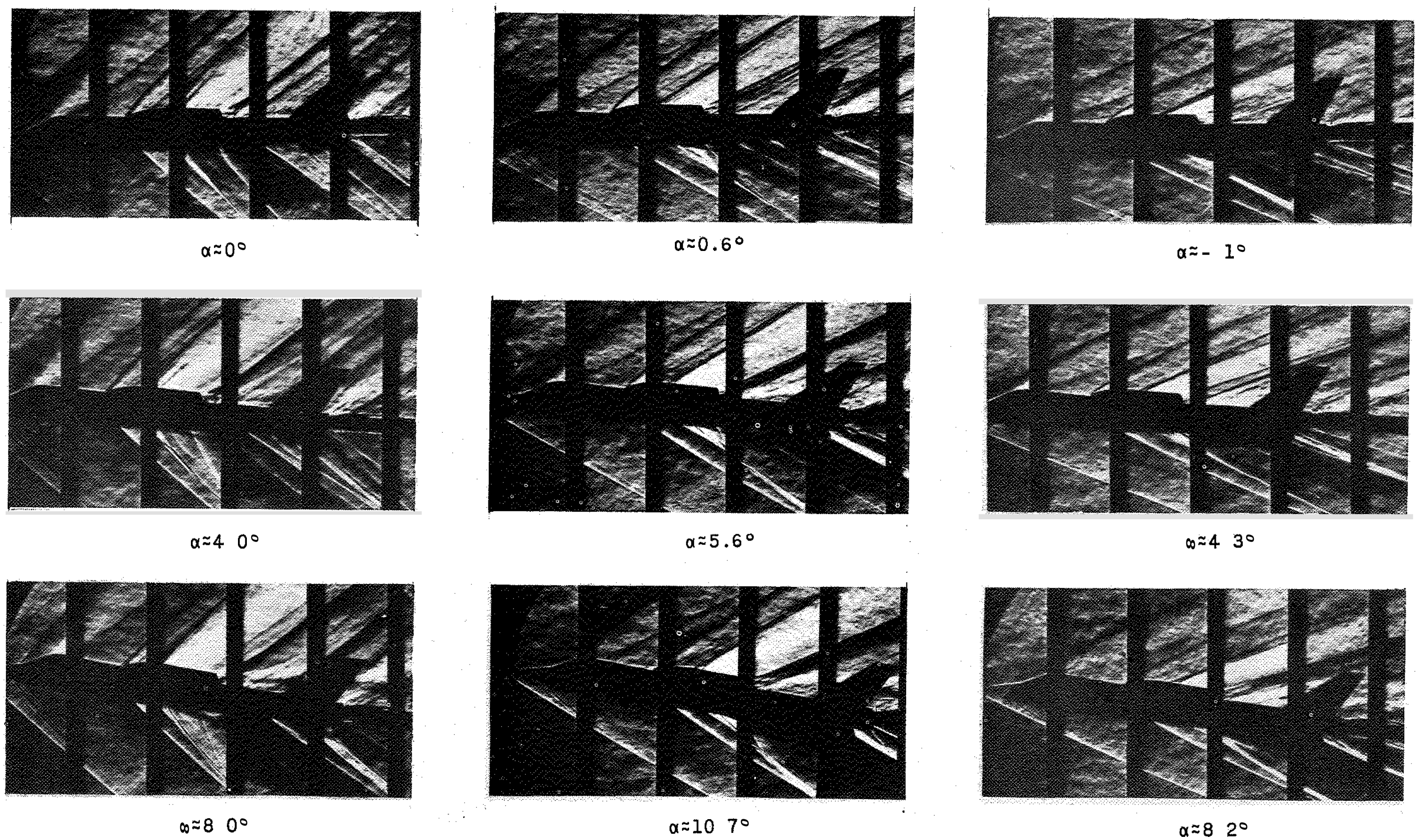

(a) $M = 1.57$. (b) $M = 2.14$. (c) $M = 2.87$. L-59-6092

Figure 12.- Schlieren photographs of the side view of a supersonic horizontal-attitude VTOL airplane model in the Langley Unitary Plan wind tunnel. Reynolds number, 3.52×10^6.

[redacted]

[redacted]

L-35

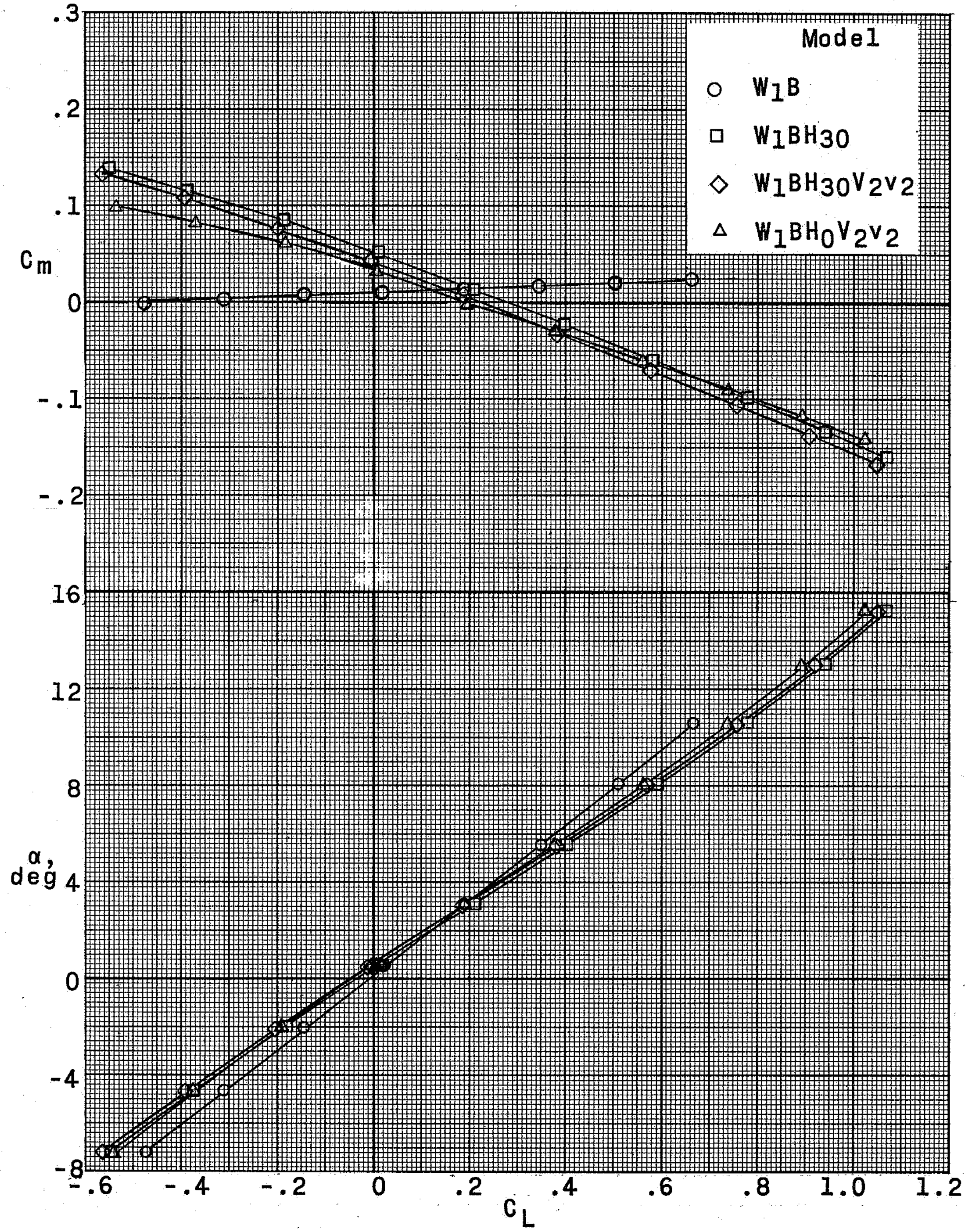

(a) M = 1.57.

Figure 13.- Longitudinal stability characteristics of a supersonic horizontal-attitude VTOL airplane model with various combinations of model components.

[redacted]

[redacted]

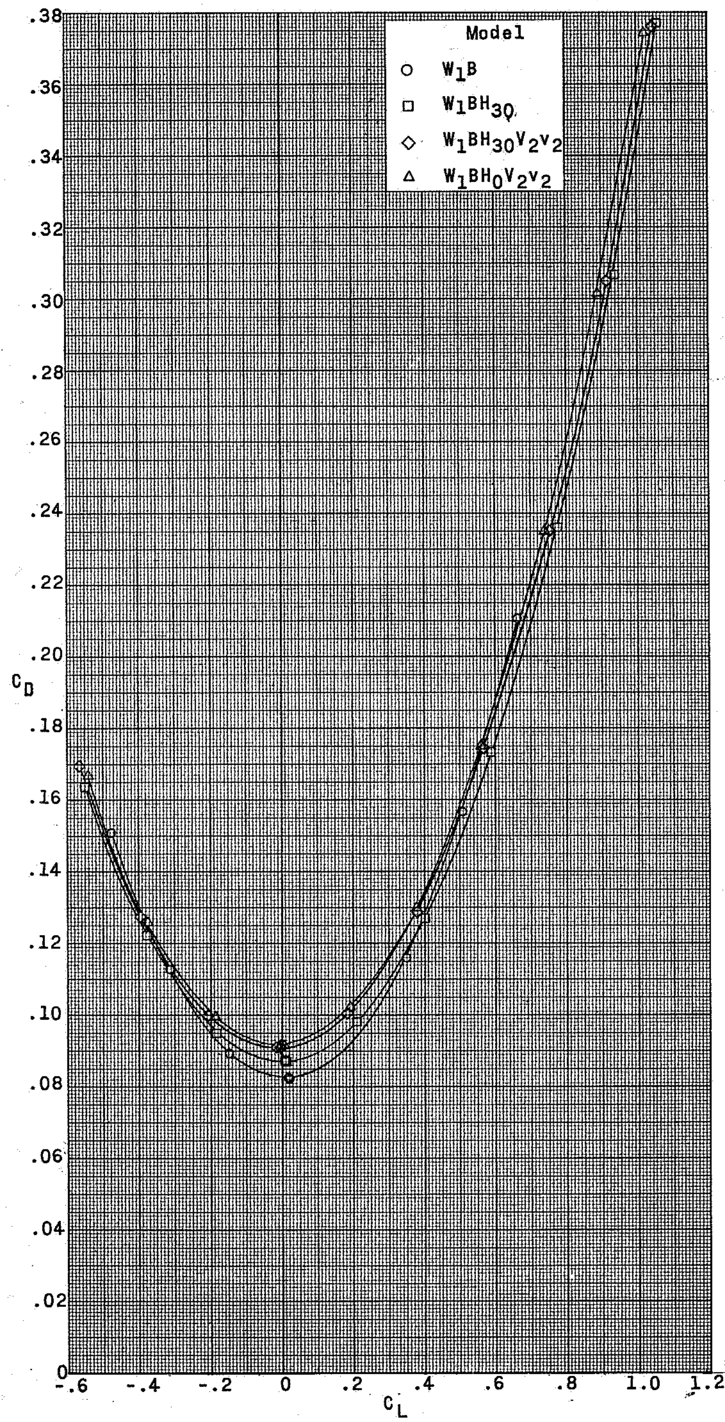

(a) Concluded.

Figure 13.- Continued.

L-355

[redacted]

L-355

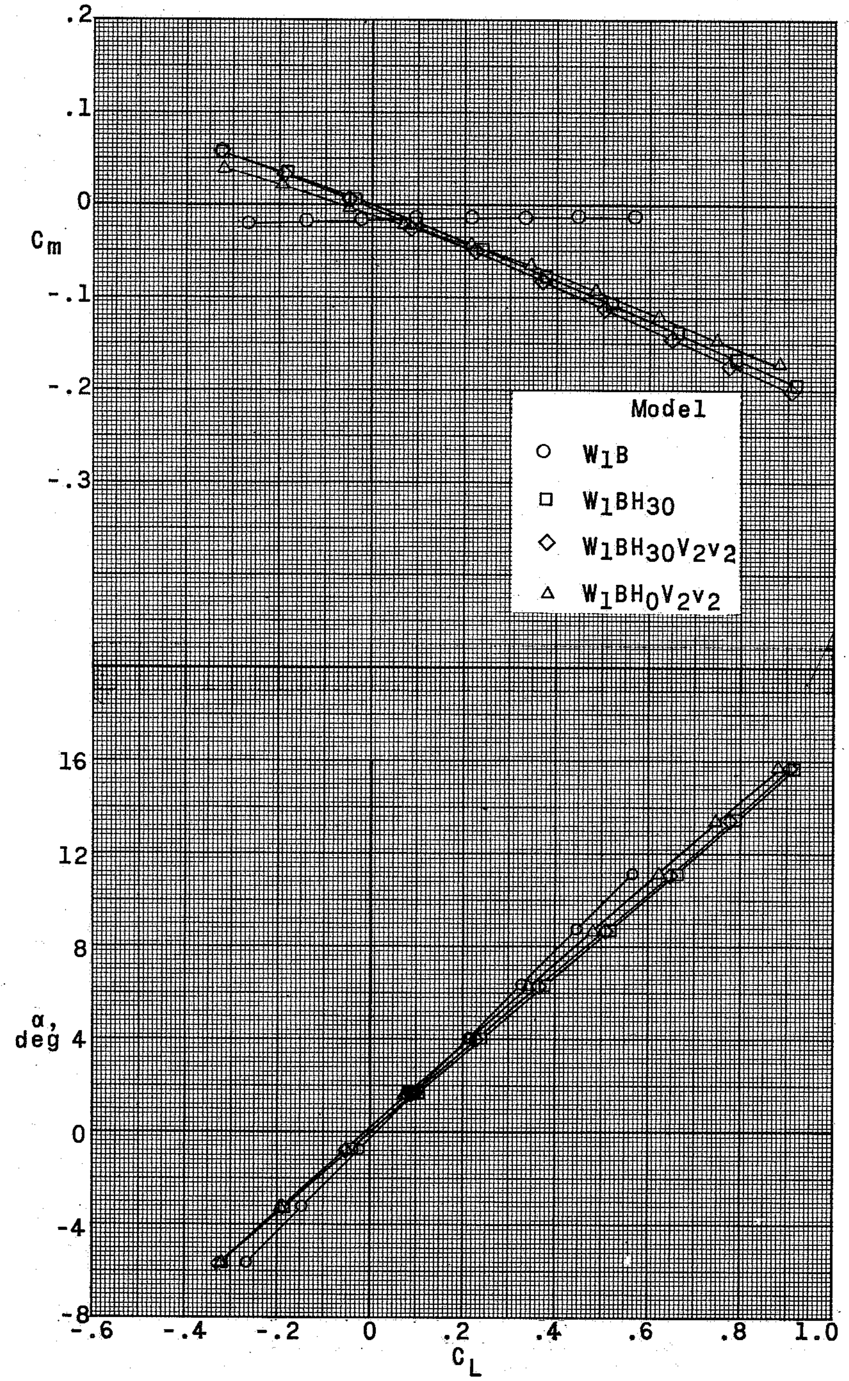

(b) M = 2.14.

Figure 13.- Continued.

[redacted]

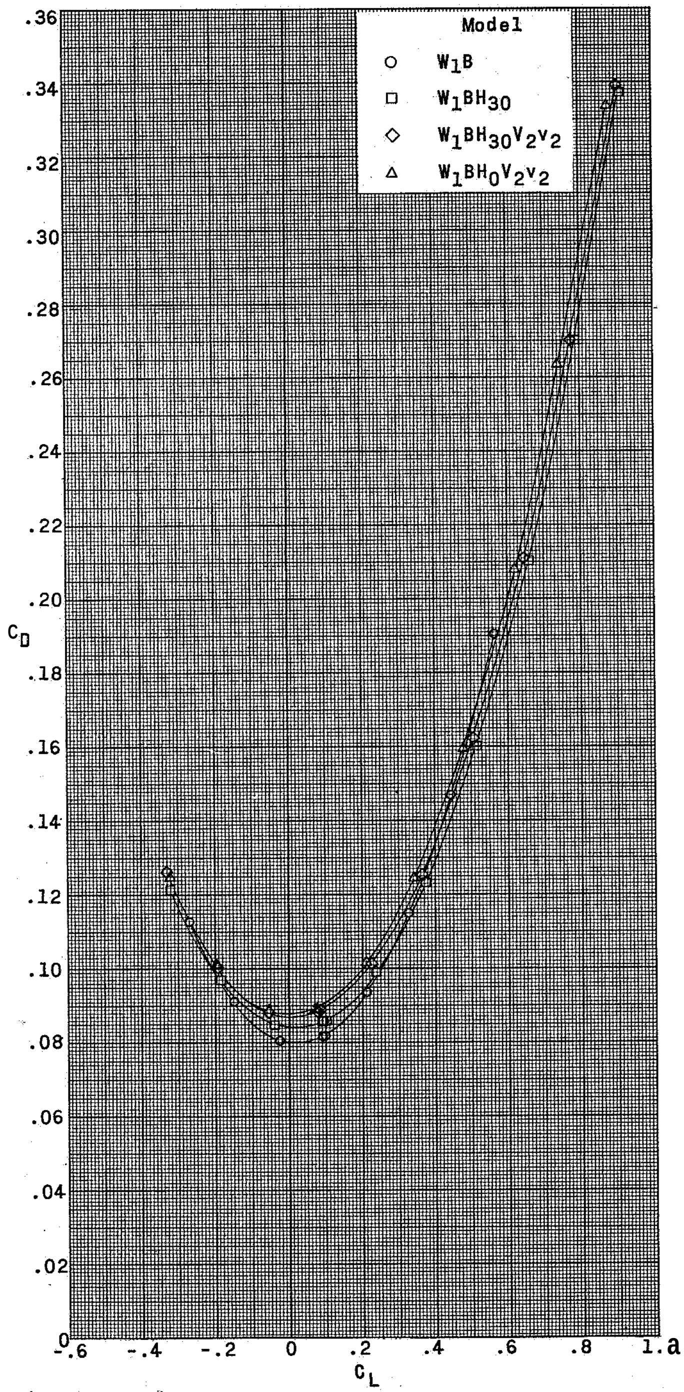

(b) Concluded.

Figure 13.- Continued.

L-355

[redacted]

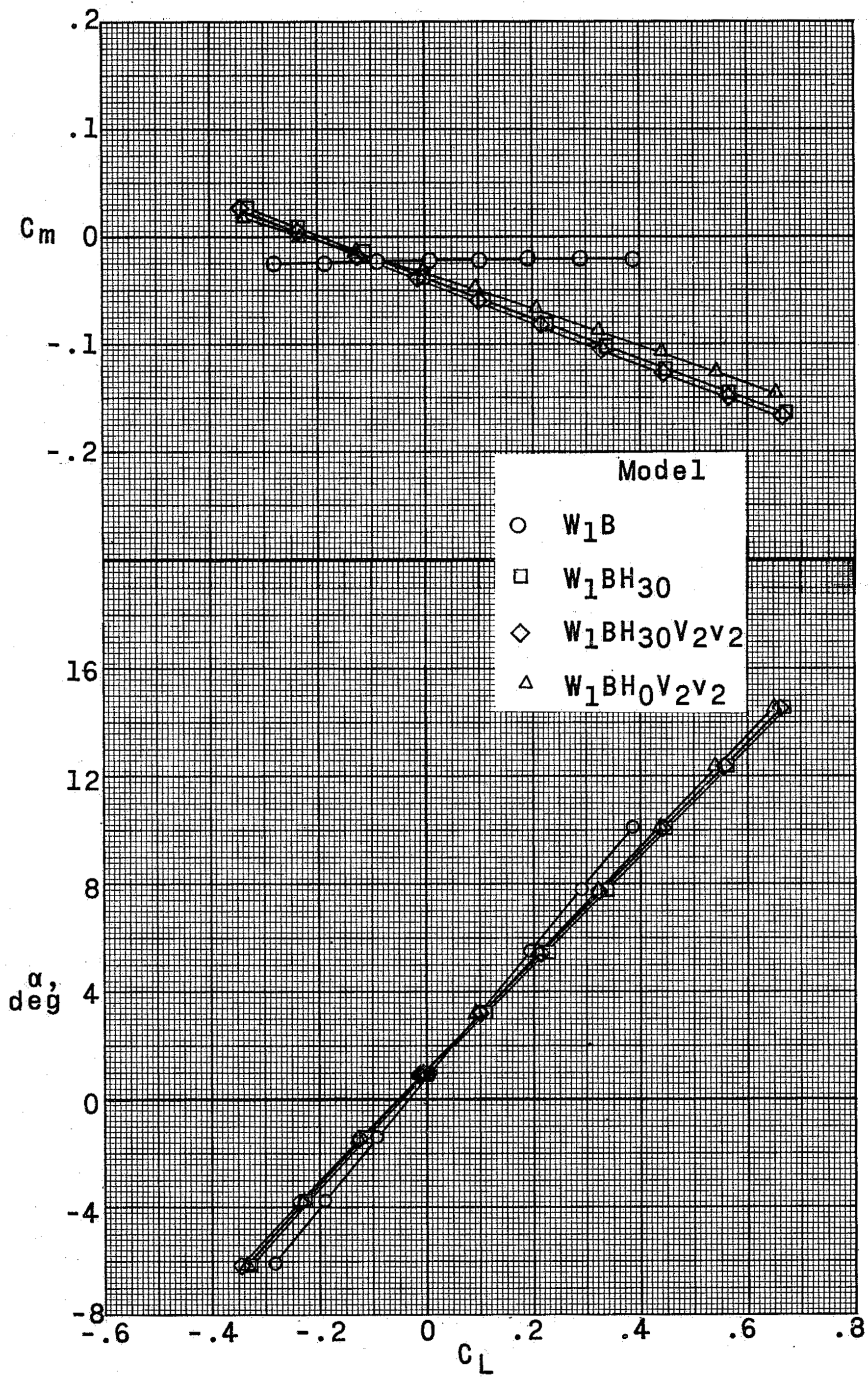

(c) M = 2.54.

Figure 13.- Continued.

[redacted]

[redacted]

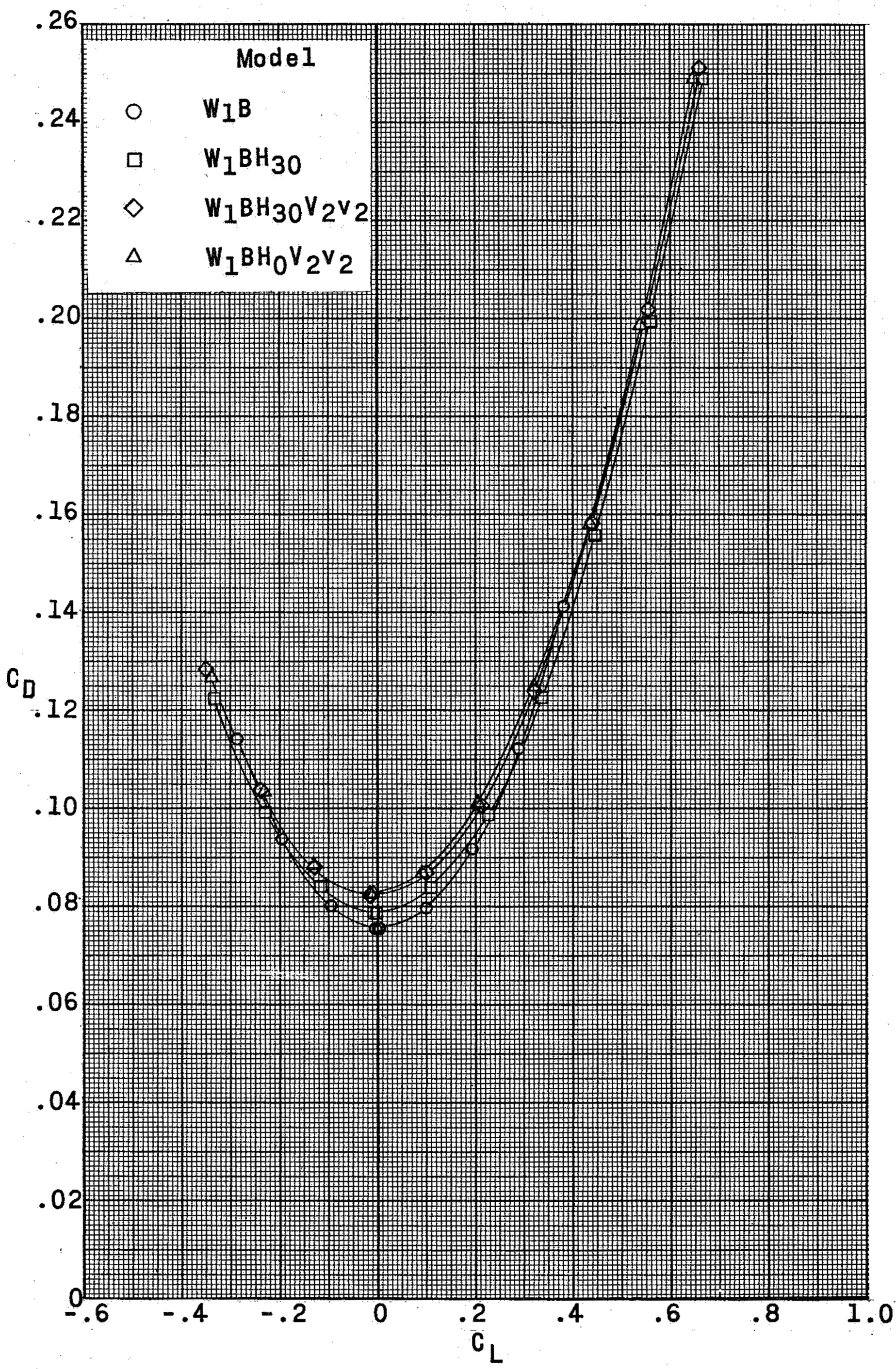

(c) Concluded.

Figure 13.- Continued.

[redacted]

[redacted]

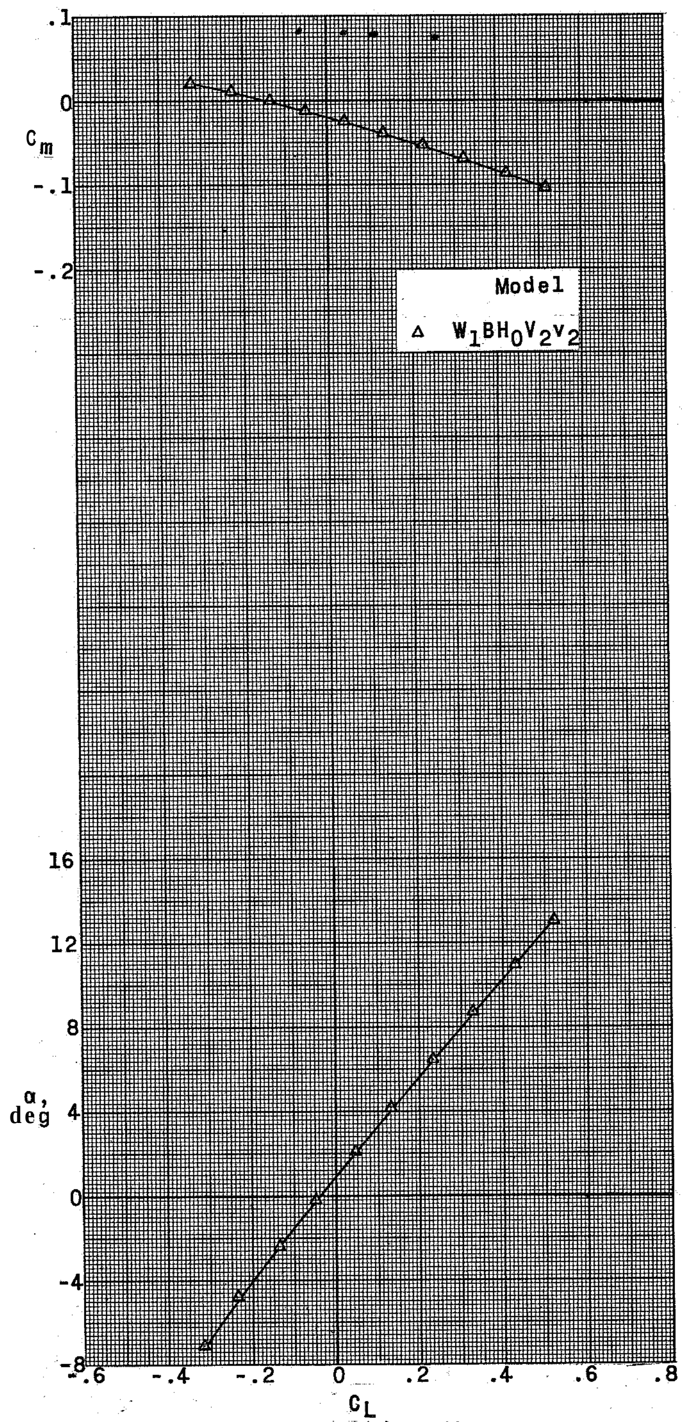

(d) M = 2.87.

Figure 13.- Continued.

[redacted]

[redacted]

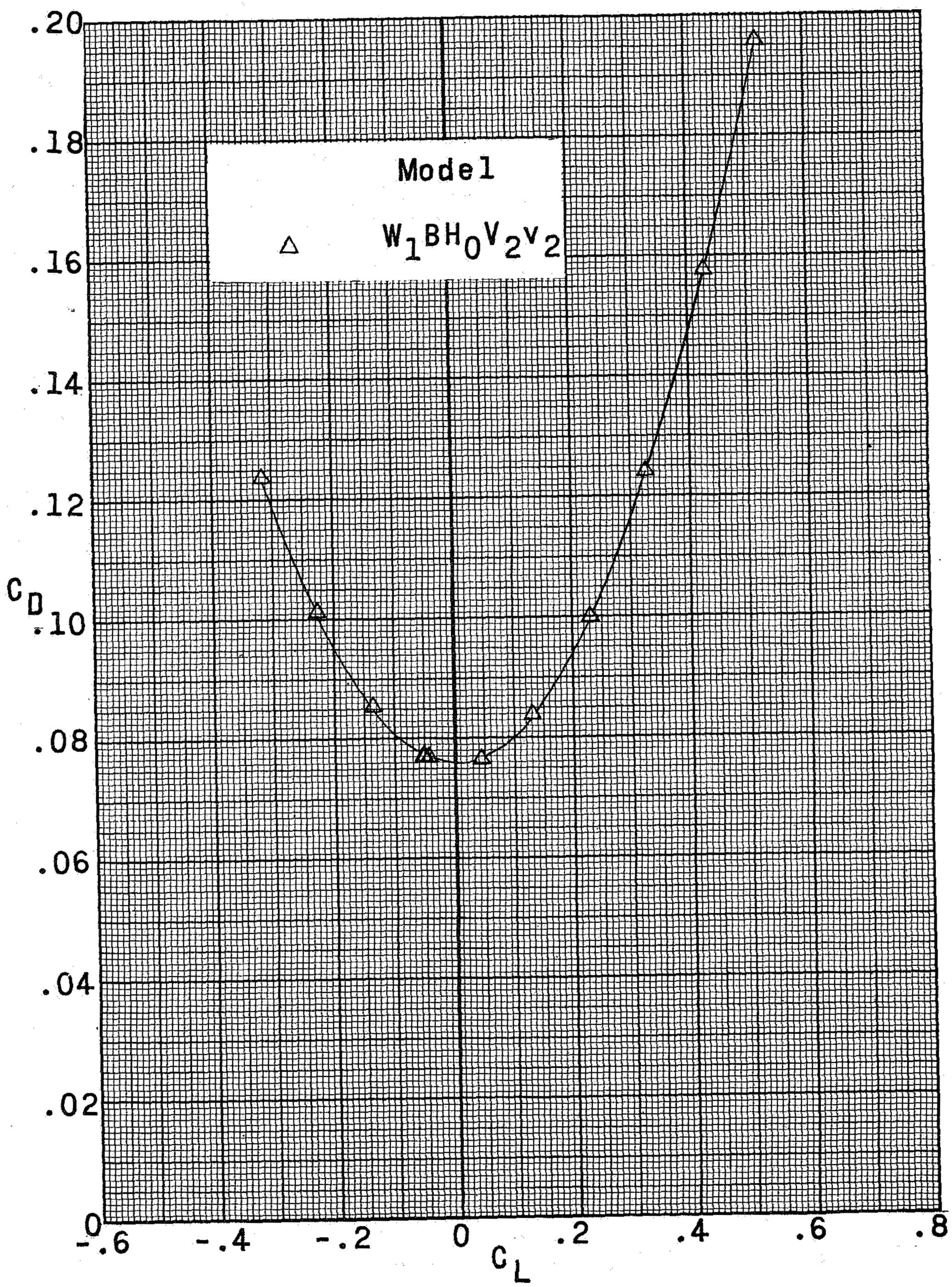

(d) **Concluded.**

Figure 13.- **Concluded.**

[redacted]

[redacted]

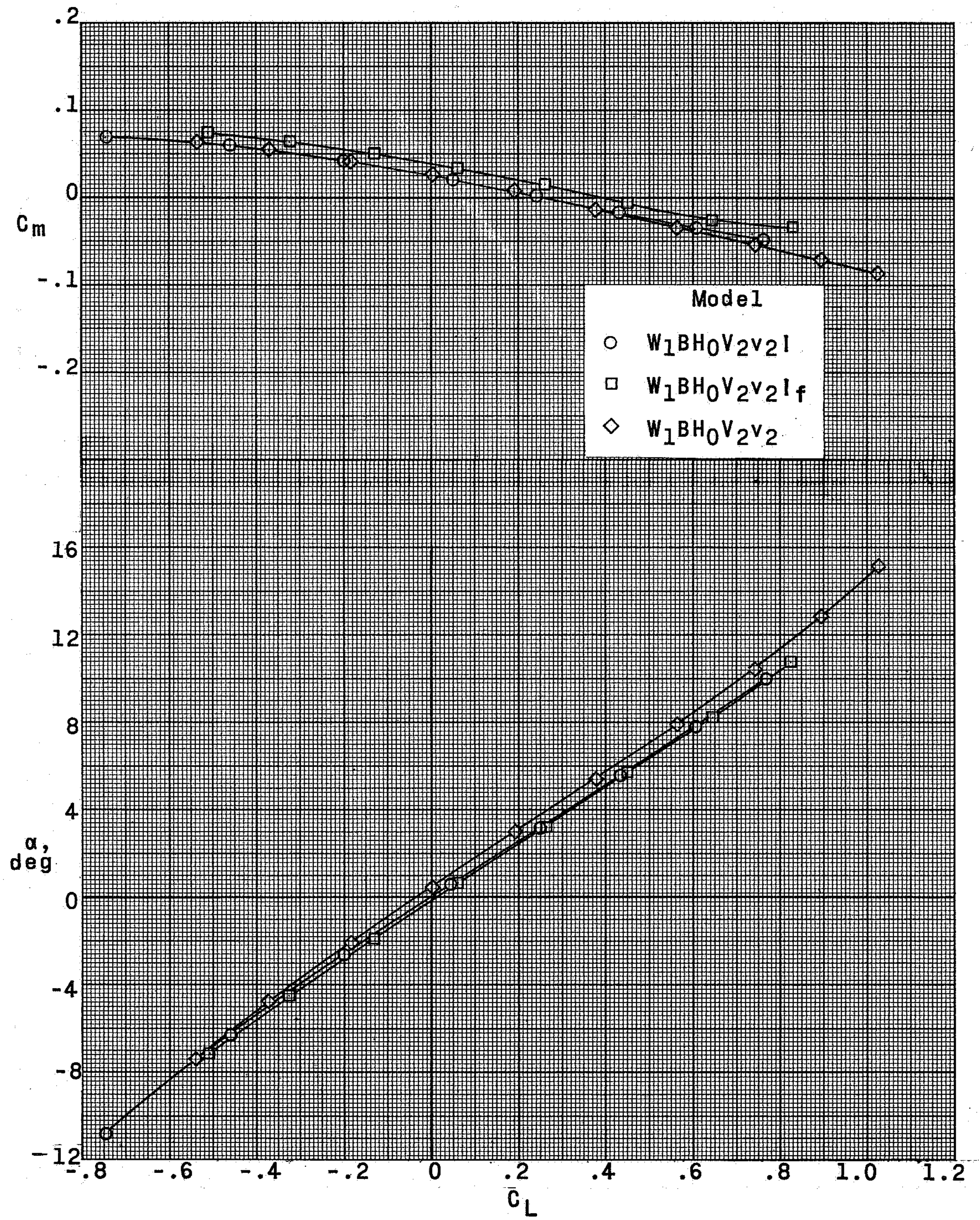

(a) M = 1.57.

Figure 14.- Longitudinal stability characteristics of a supersonic horizontal-attitude VTOL airplane model as affected by inlets.

[redacted]

[redacted]

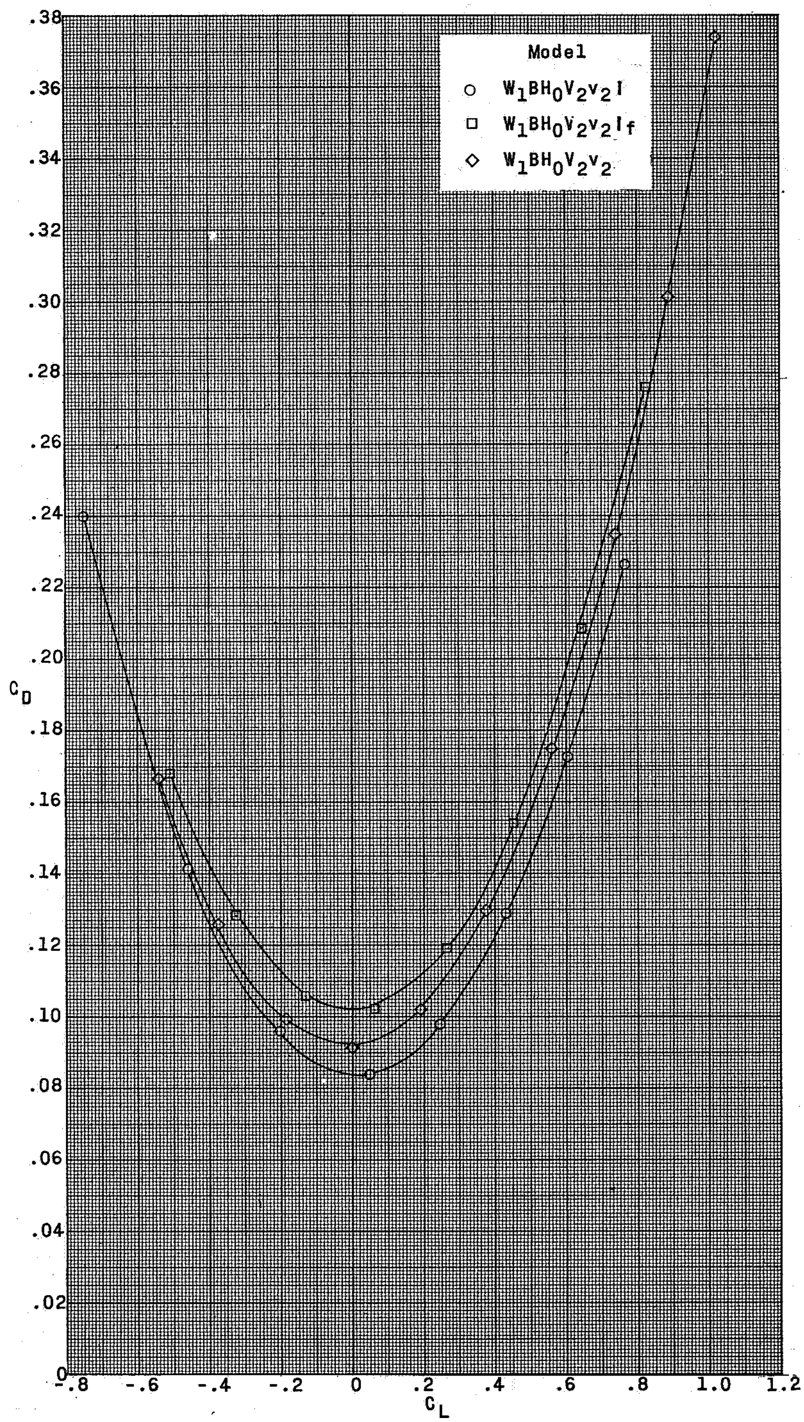

(a) Concluded.

Figure 14.- Continued.

[redacted]

[redacted]

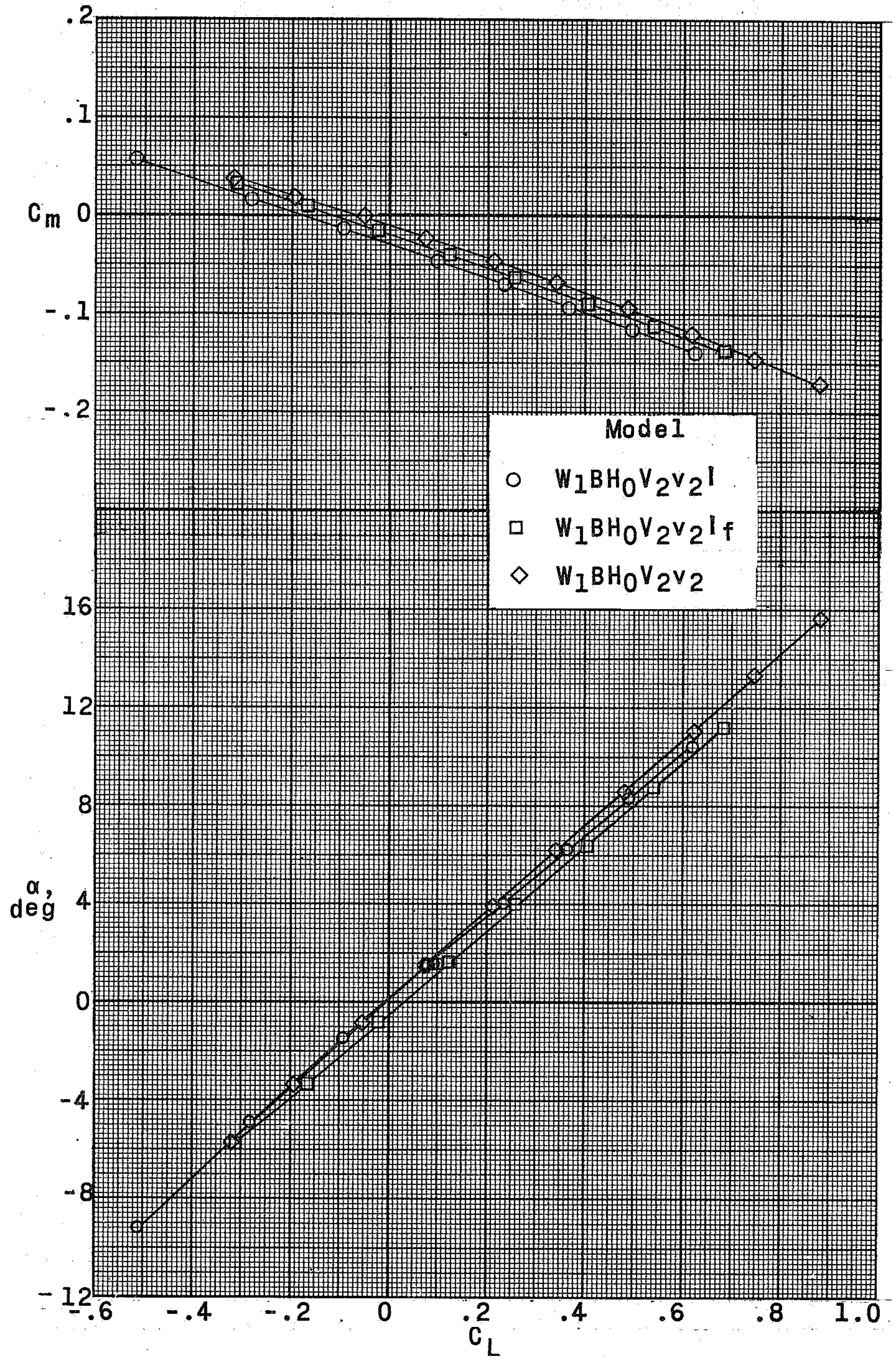

(b) $M = 2.14$.

Figure 14.- Continued.

[redacted]

[redacted]

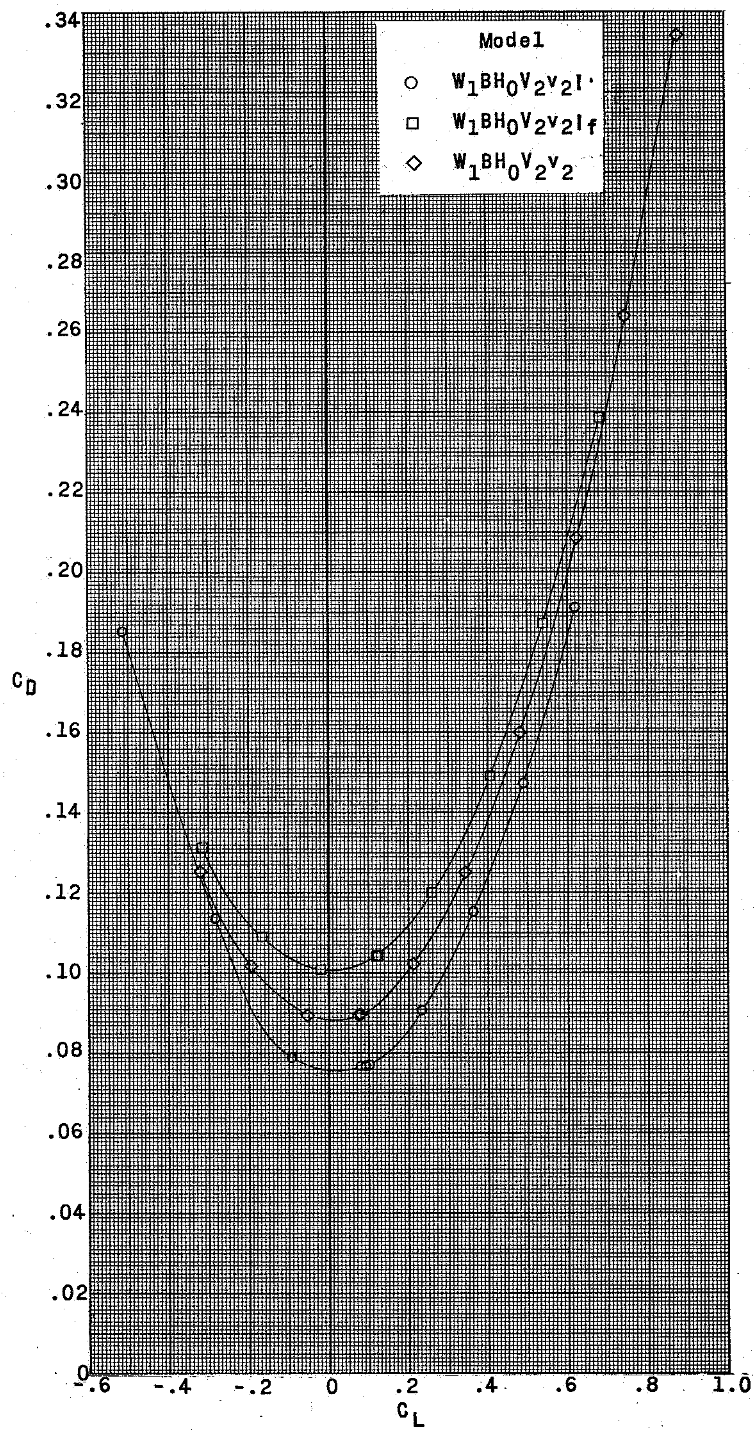

(b) Concluded.

Figure 14.- Continued.

[redacted]

L-355

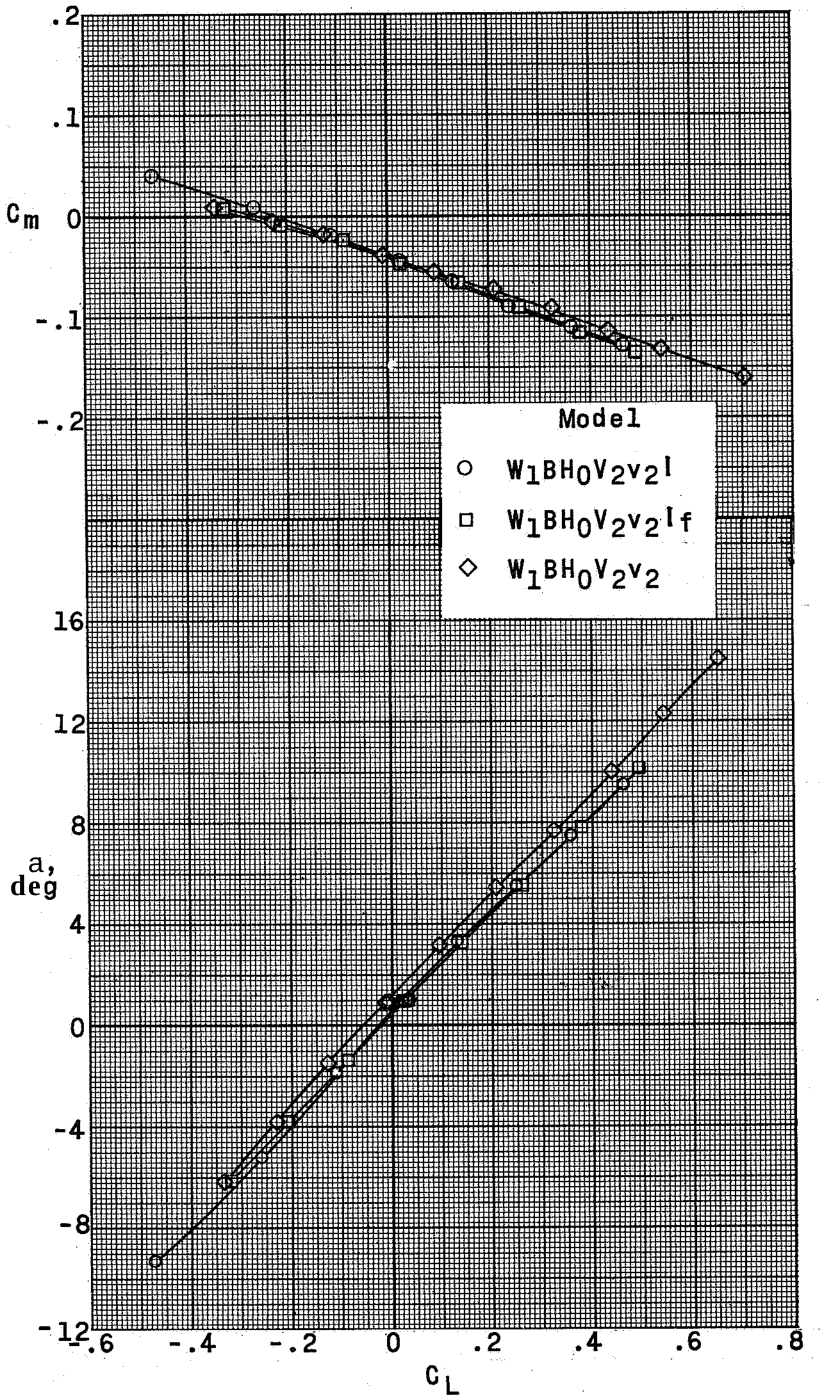

(c) M = 2.54.

Figure 14.- Continued.

[redacted]

[redacted]

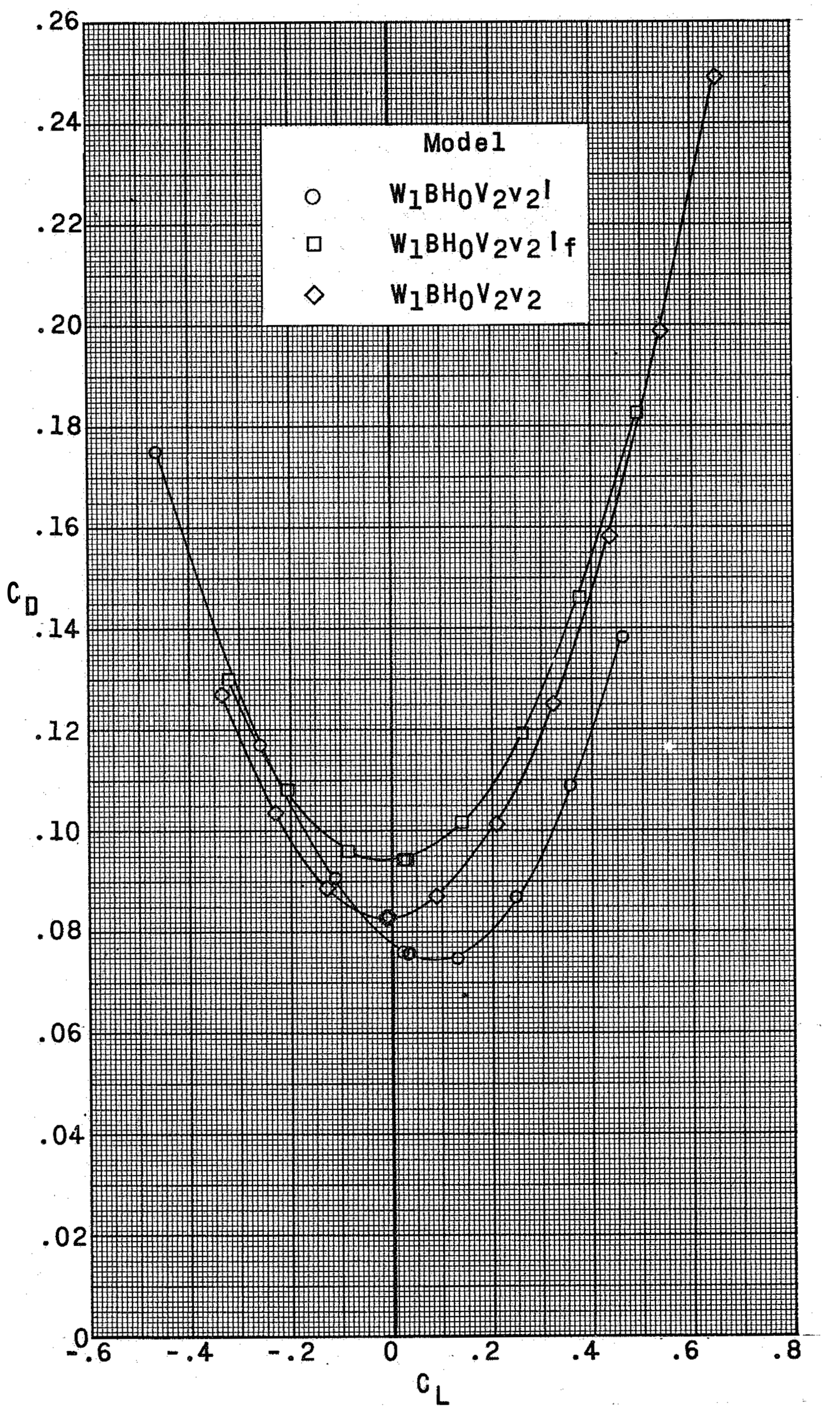

(c) Concluded.

Figure 14.- Continued.

L-355

[redacted]

[redacted]

L-355

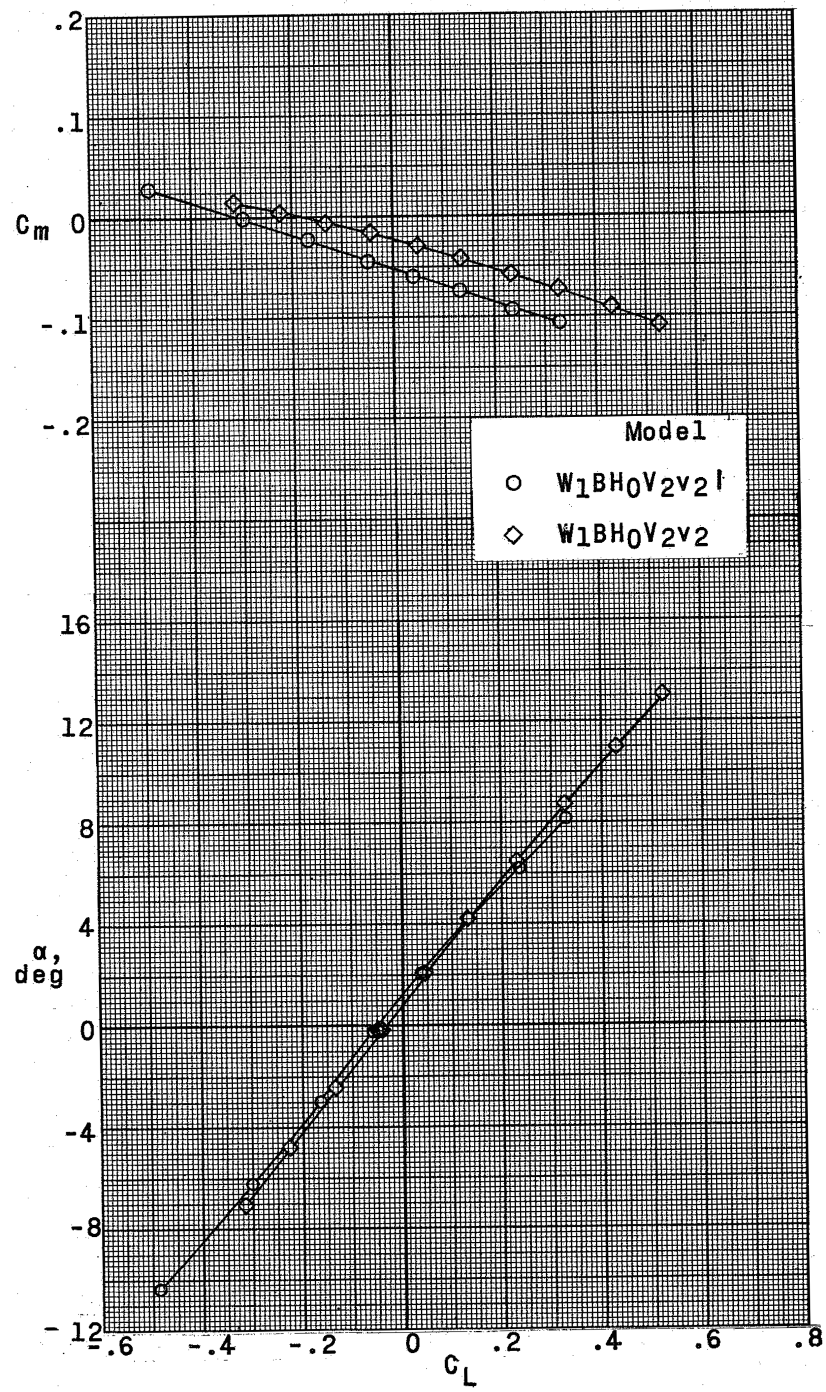

(d) M = 2.87.

Figure 14.- Continued.

[redacted]

[redacted]

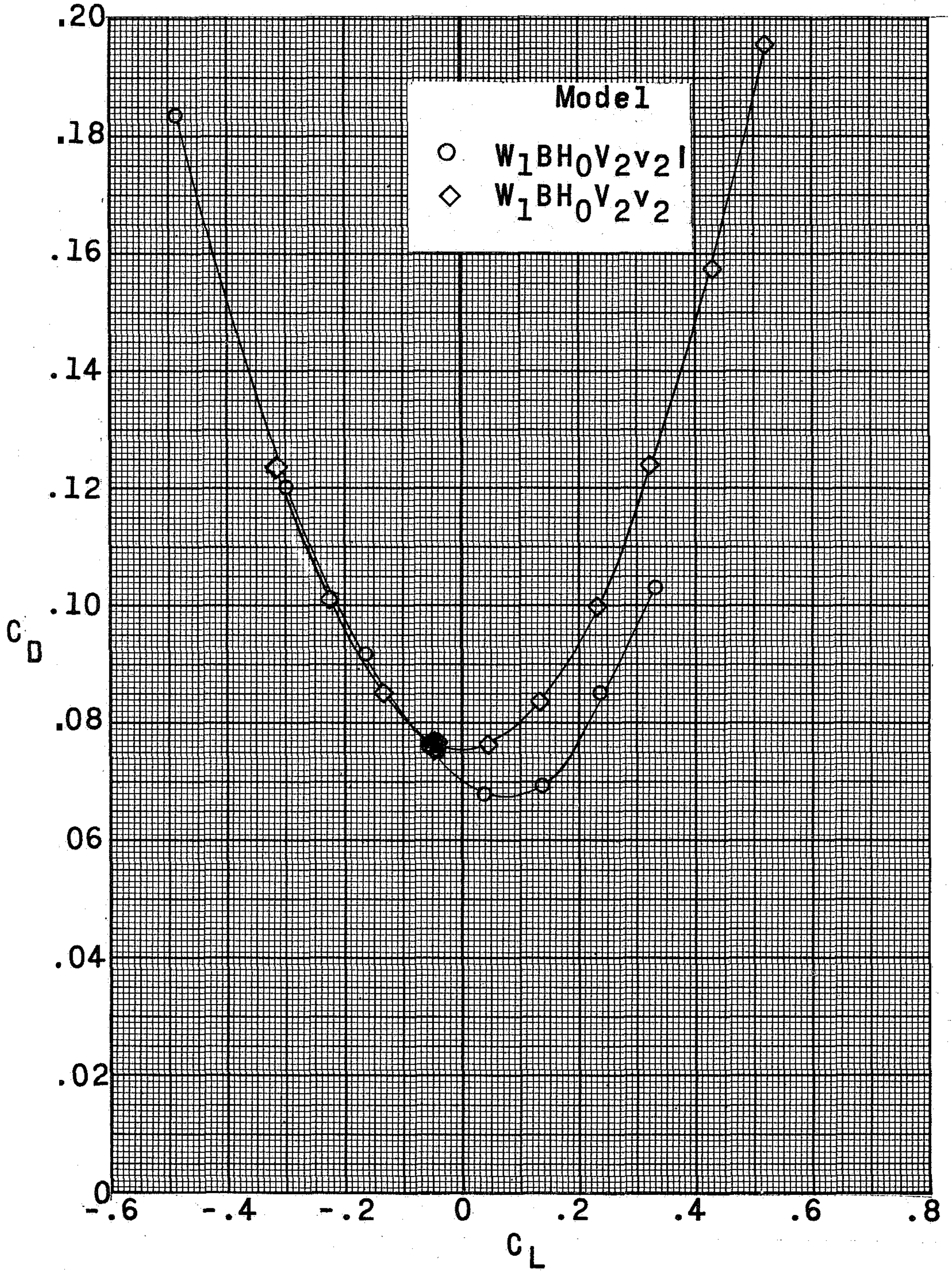

(d) Concluded.

Figure 14.- Concluded.

L-355

[redacted]

[redacted]

L-355

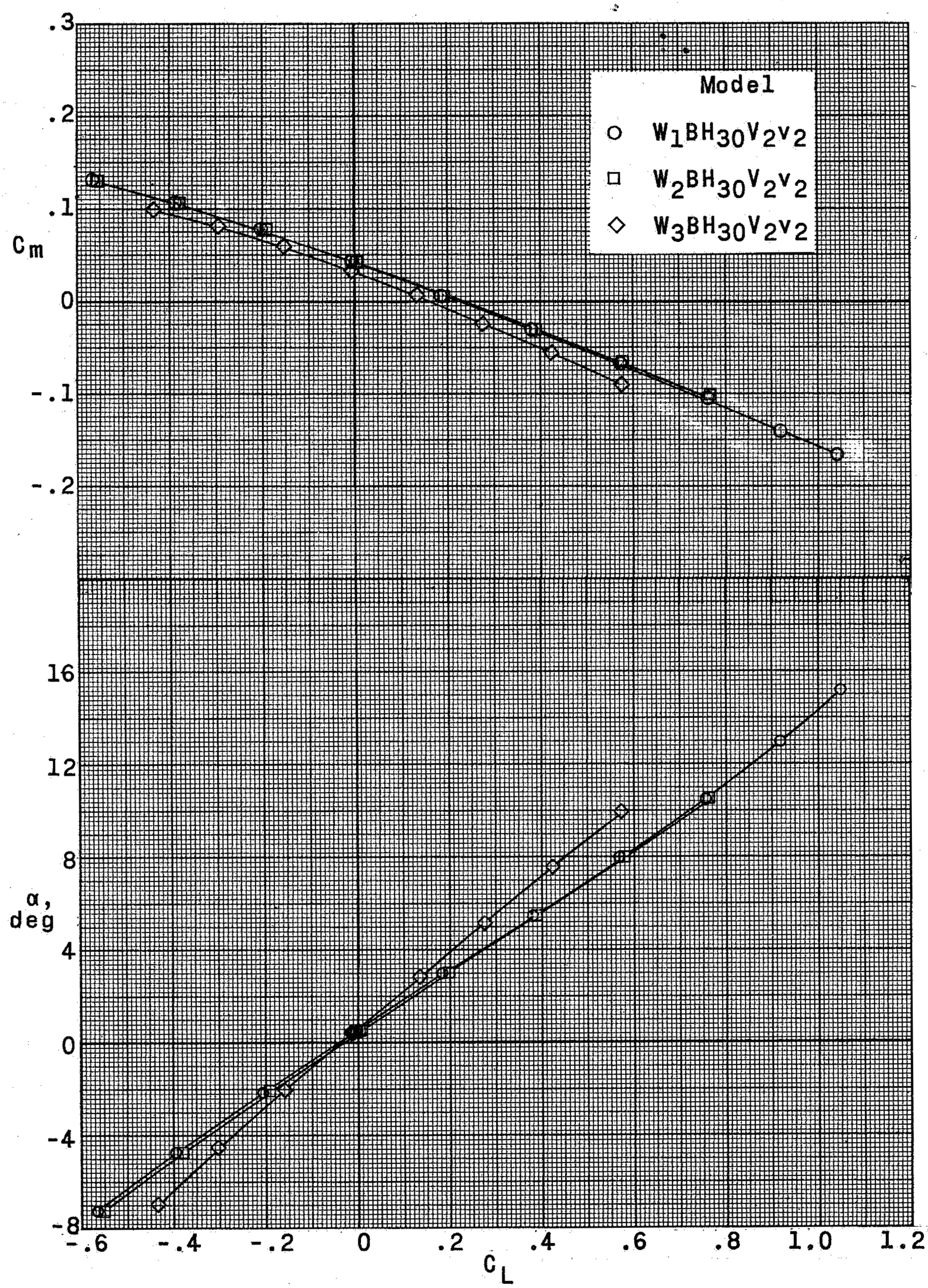

(a) M = 1.57.

Figure 15.- Longitudinal stability characteristics of a supersonic horizontal-attitude VTOL airplane model with various nacelle positions.

[redacted]

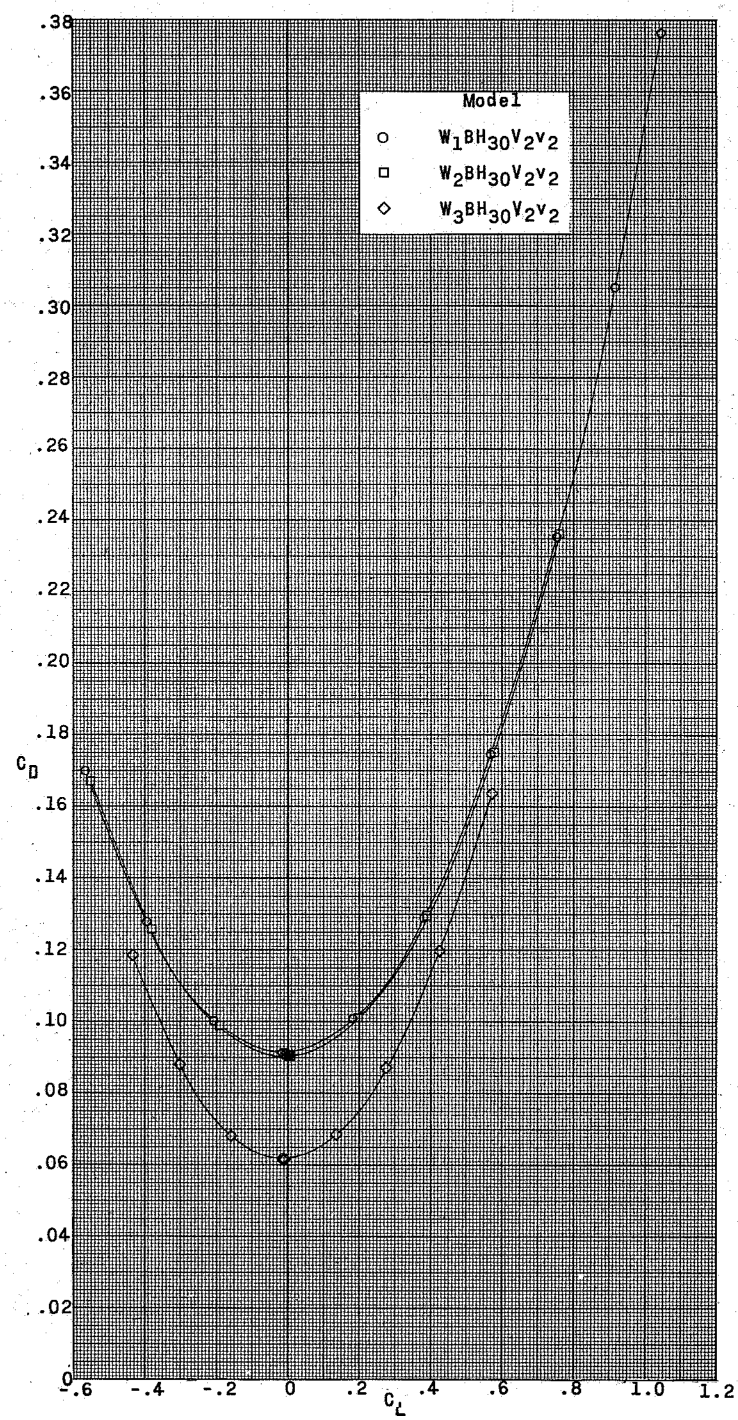

L-355

(a) Concluded.

Figure 15.- Continued.

[redacted]

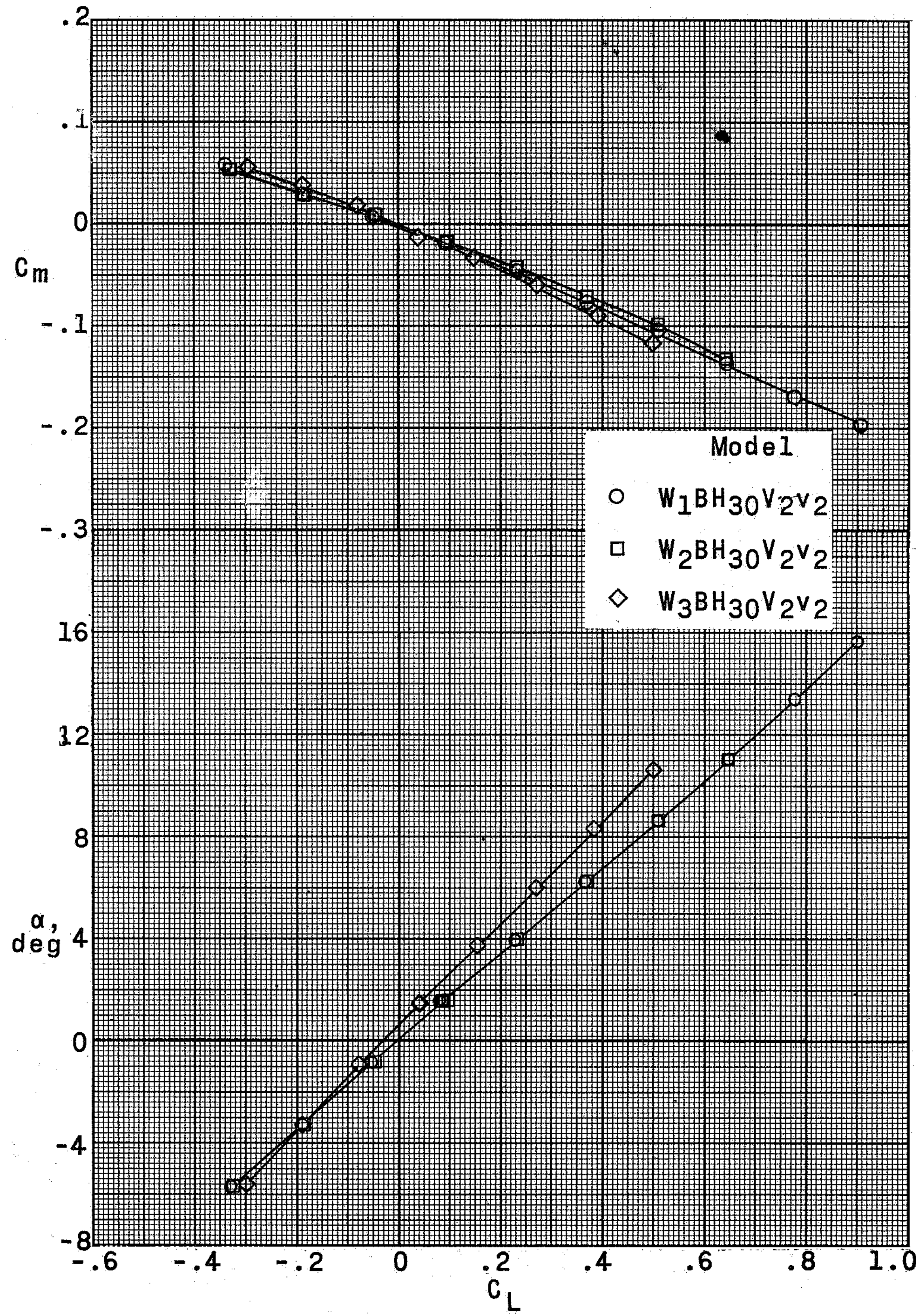

(b) M = 2.14.

Figure 15.- Continued.

[redacted]

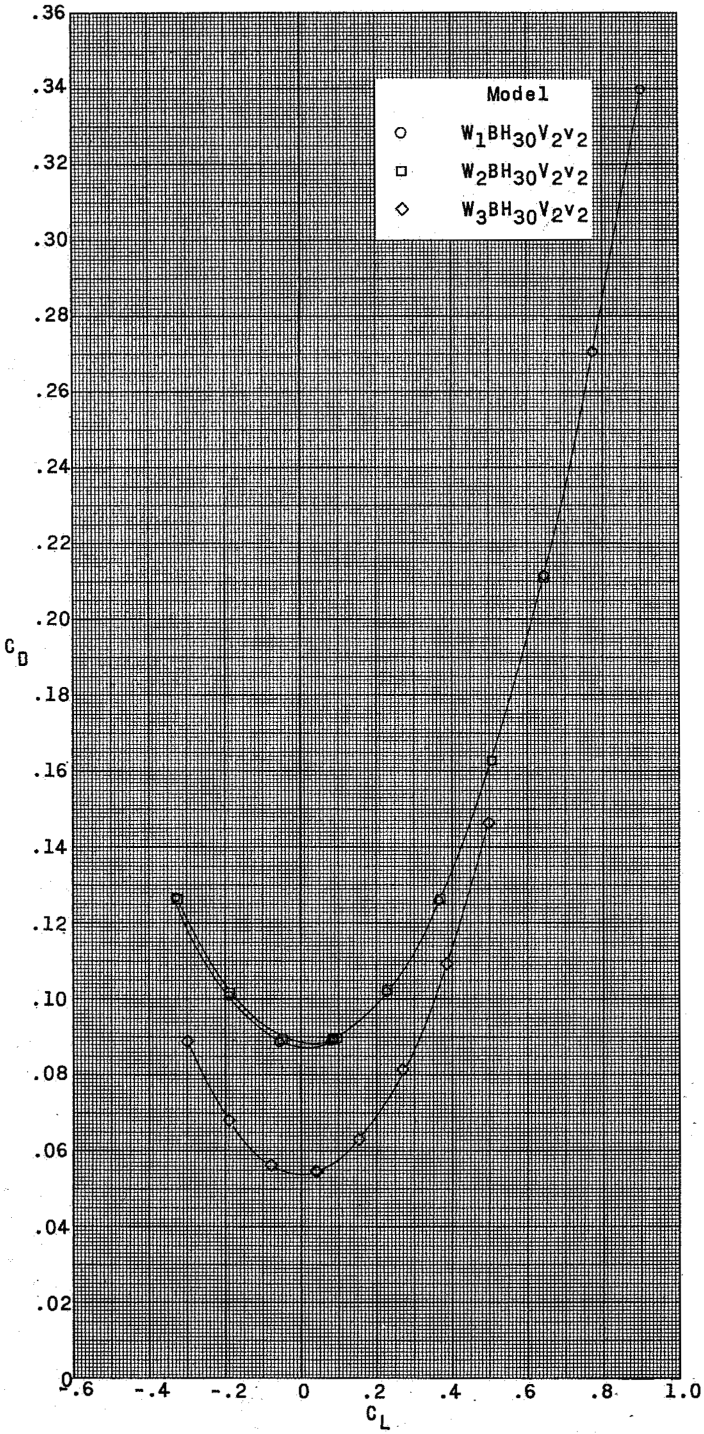

(b) Concluded.

Figure 15.- Continued.

L-355

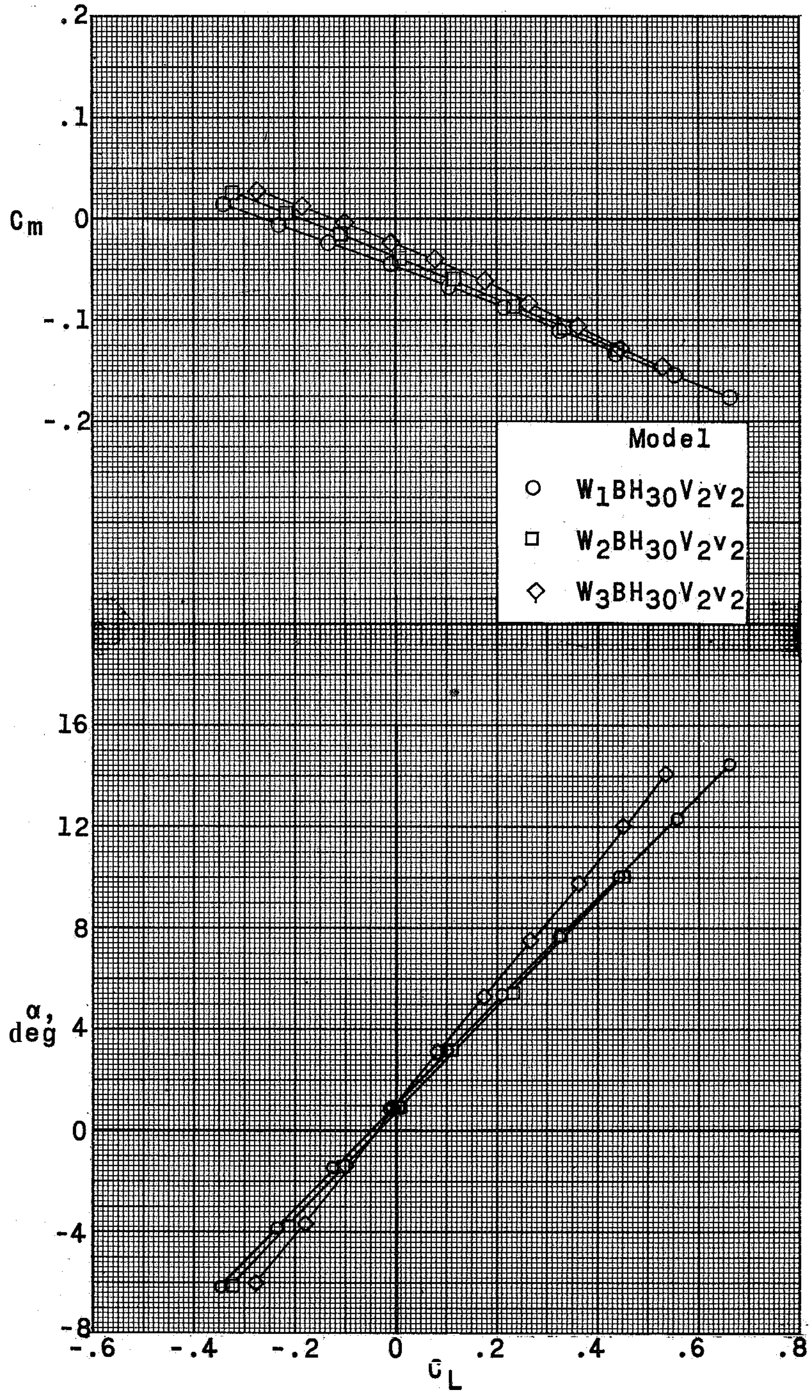

(c) M = 2.54.

Figure 15.- Continued.

[redacted]

[redacted]

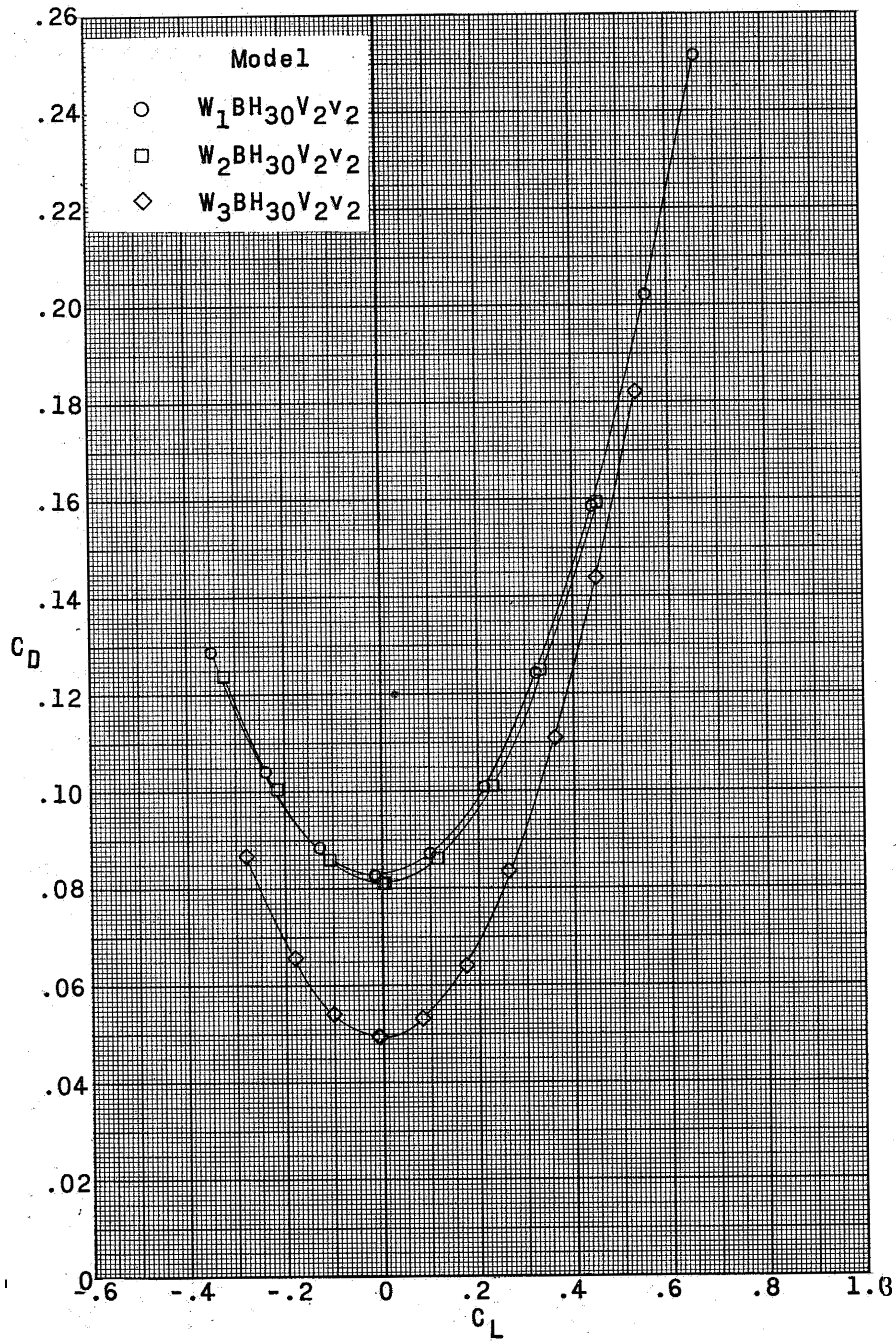

(c) Concluded.

Figure 15.- Concluded.

L-355

[redacted]

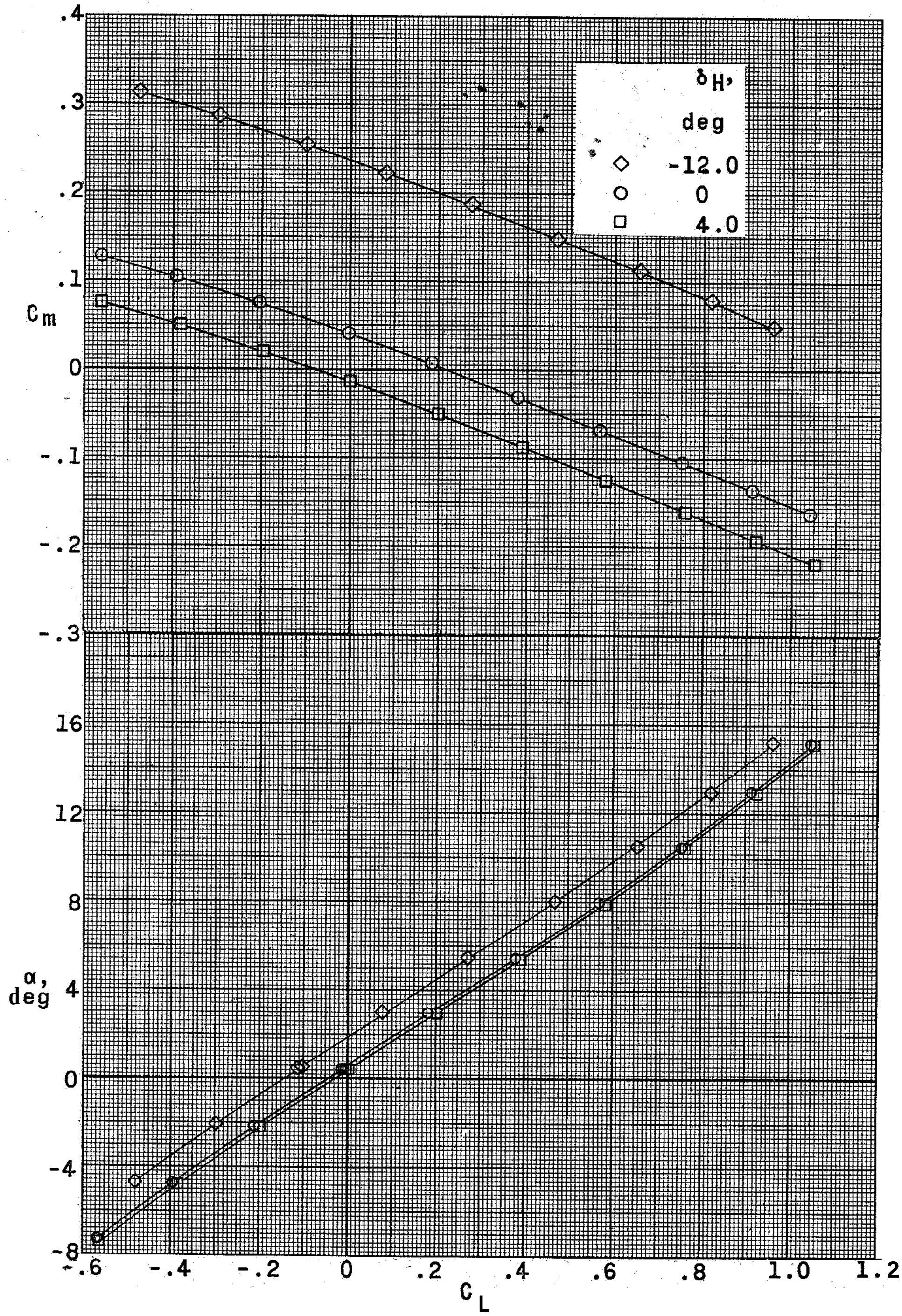

(a) M = 1.57.

Figure 16.- Longitudinal stability characteristics of a supersonic horizontal-attitude VTOL airplane model with various deflections of the horizontal tail. $W_1BH_{30}V_2v_2$ configuration.

[redacted]

[redacted]

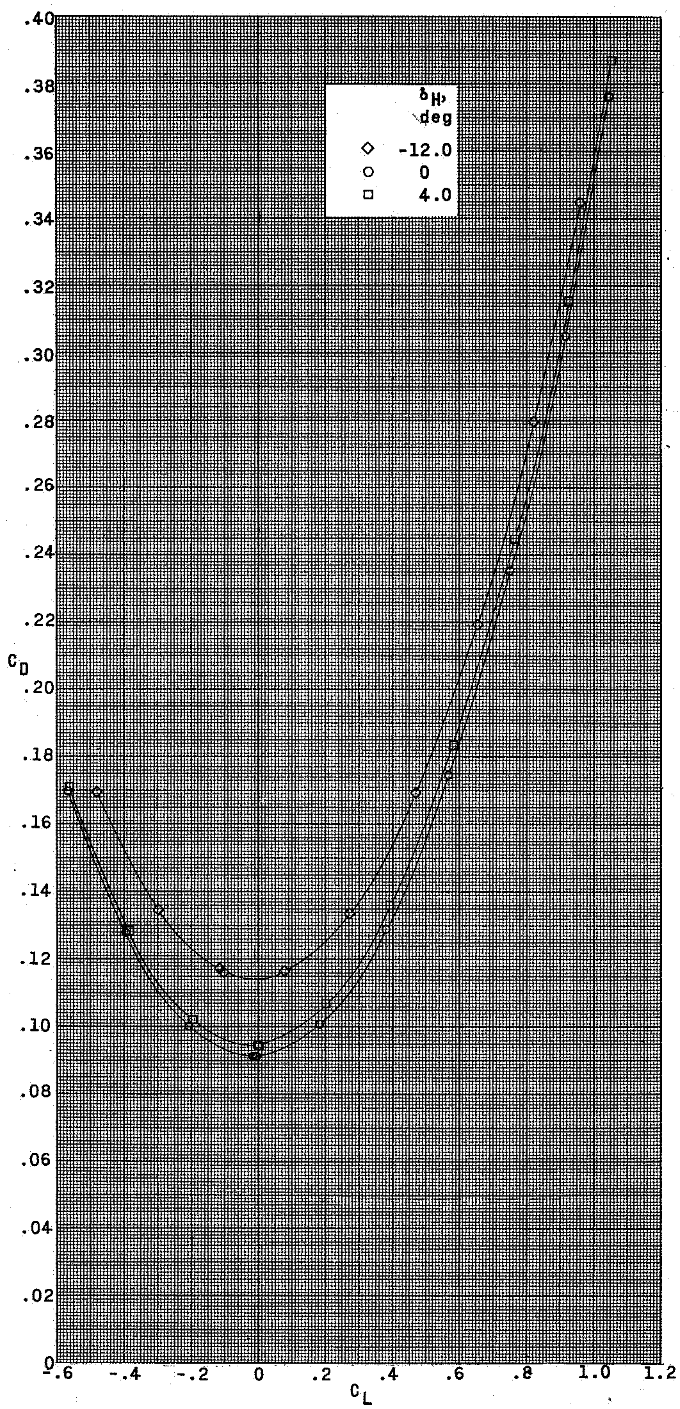

(a) Concluded.

Figure 16.- Continued.

[redacted]

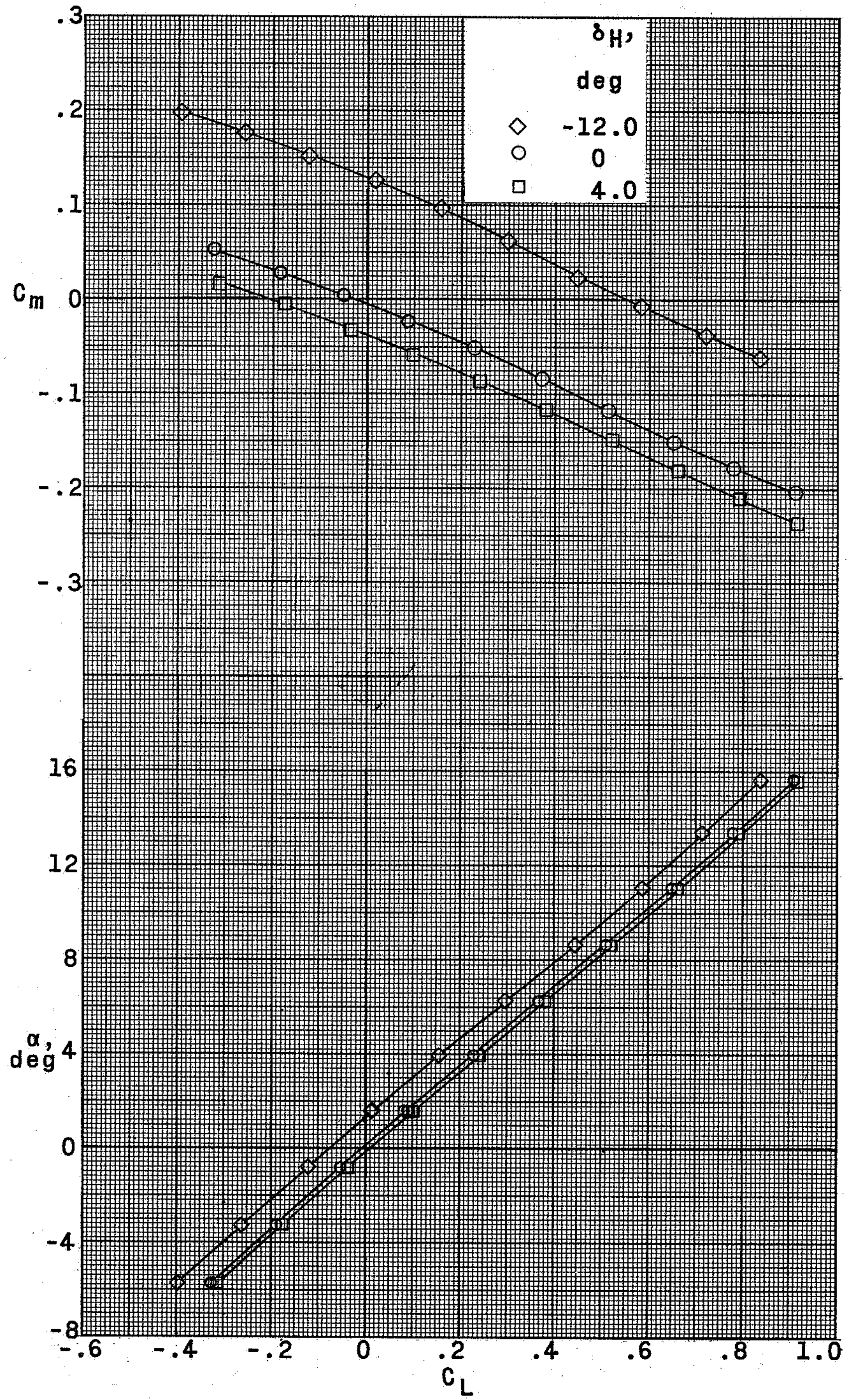

(b) M = 2.14.

Figure 16.- Continued.

[redacted]

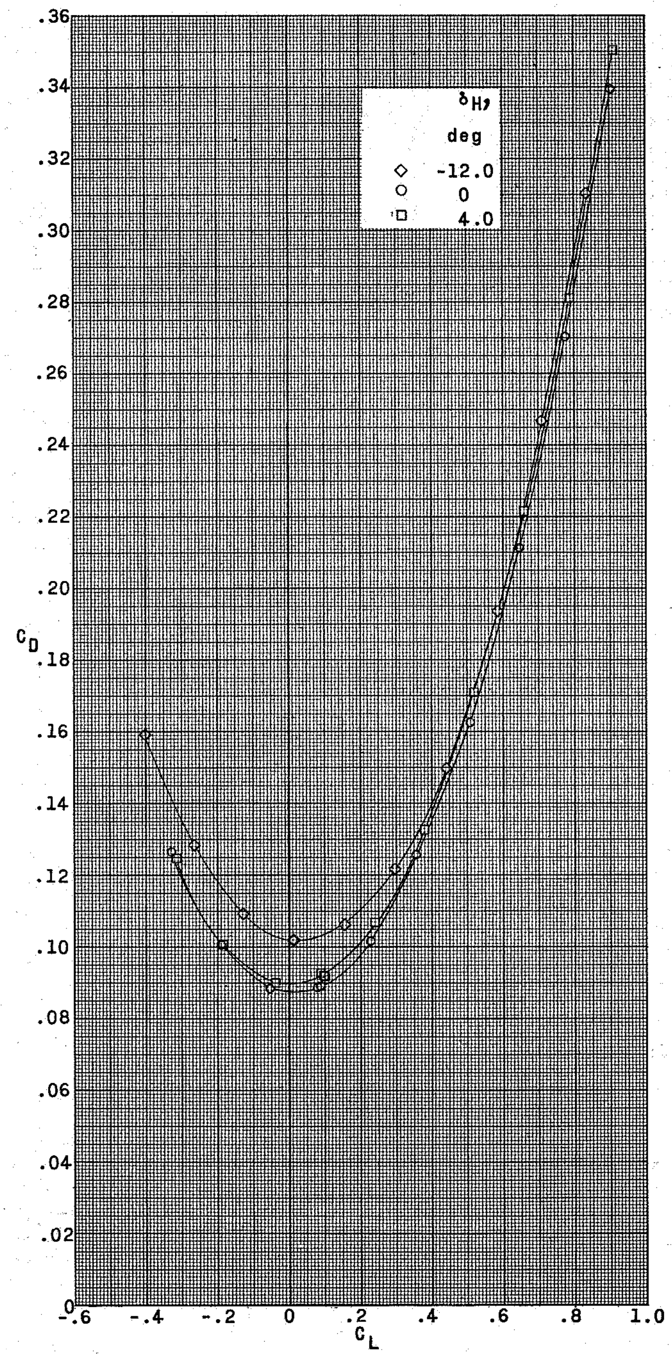

(b) Concluded.

Figure 16.- Continued.

[redacted]

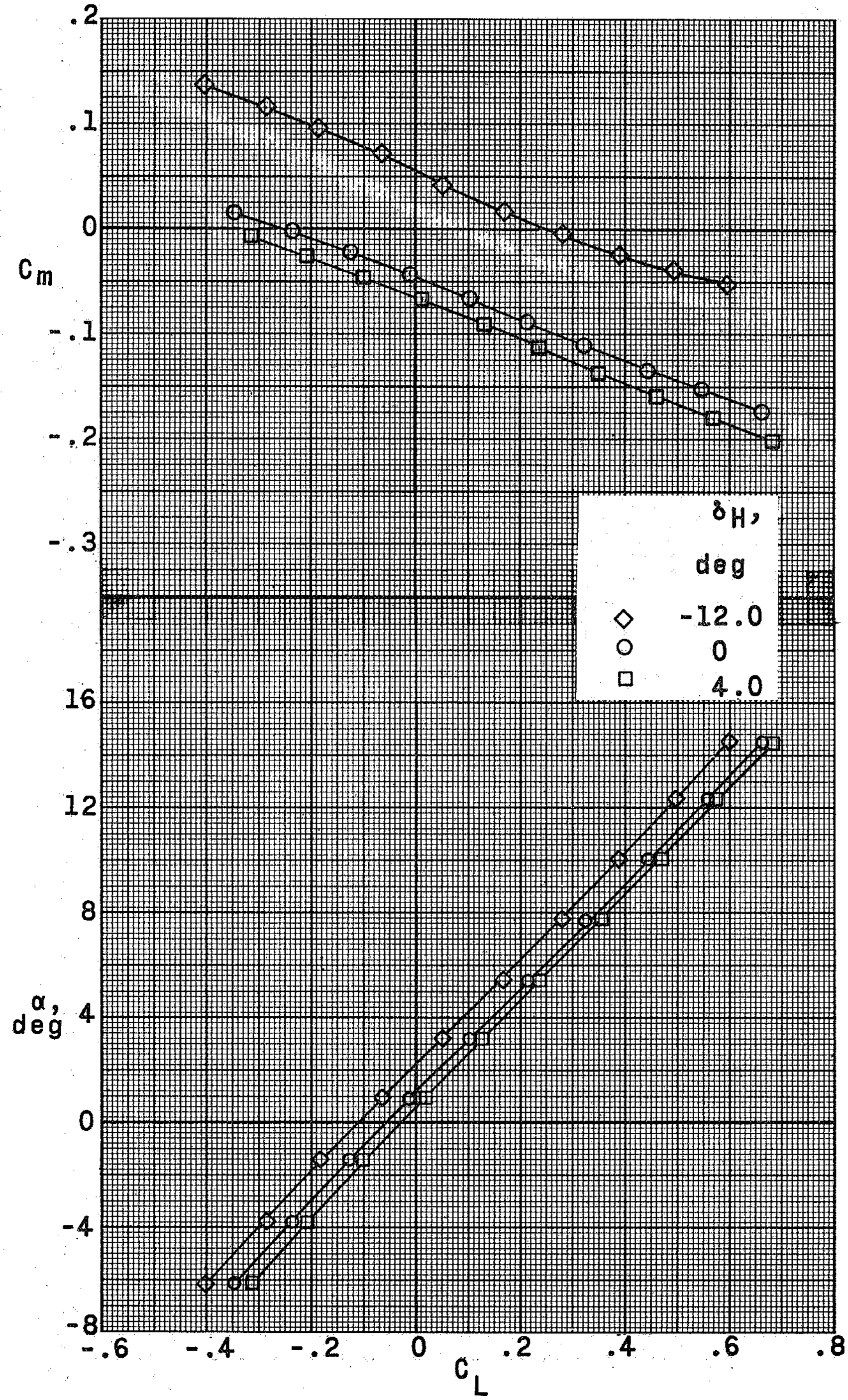

(c) M = 2.54.

Figure 16.- Continued.

[redacted]

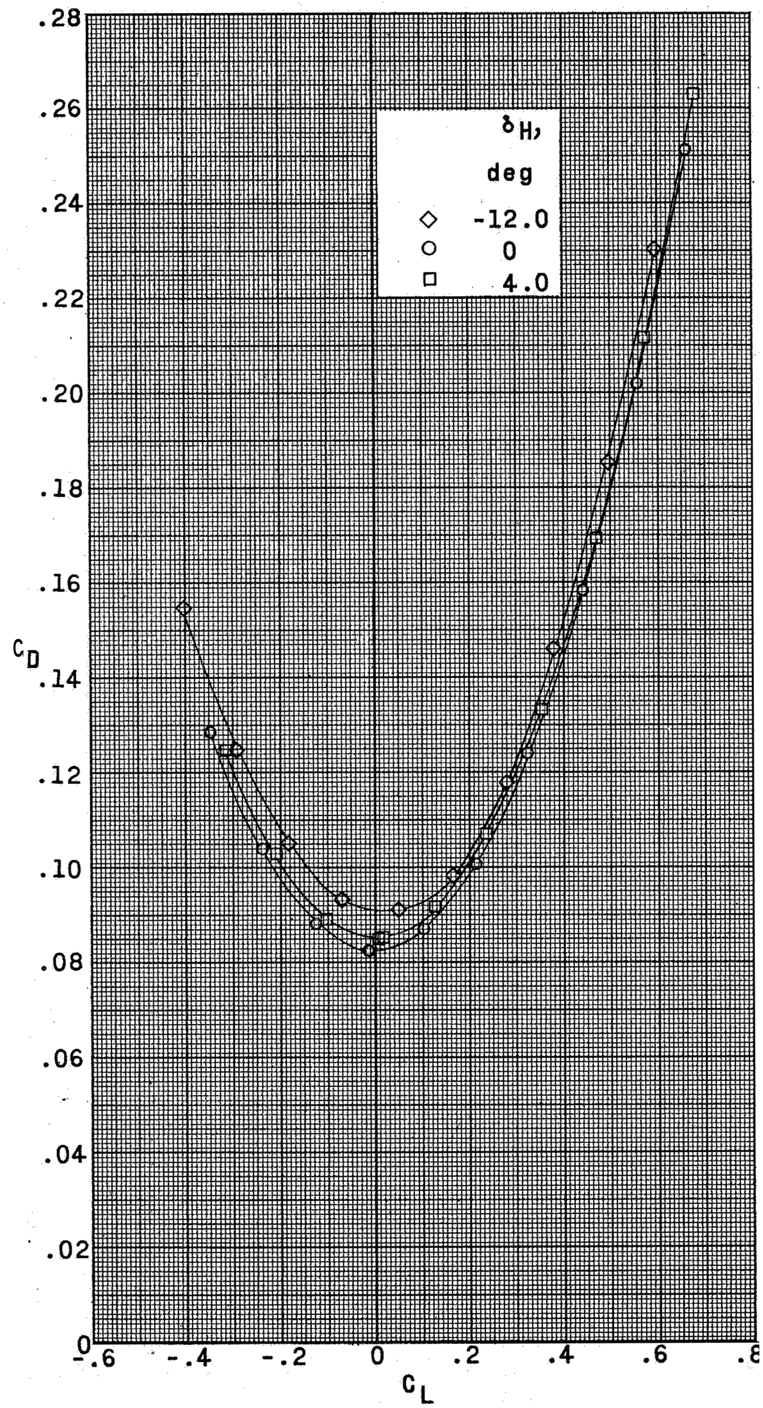

(c) Concluded.

Figure 16.- Concluded.

[redacted]

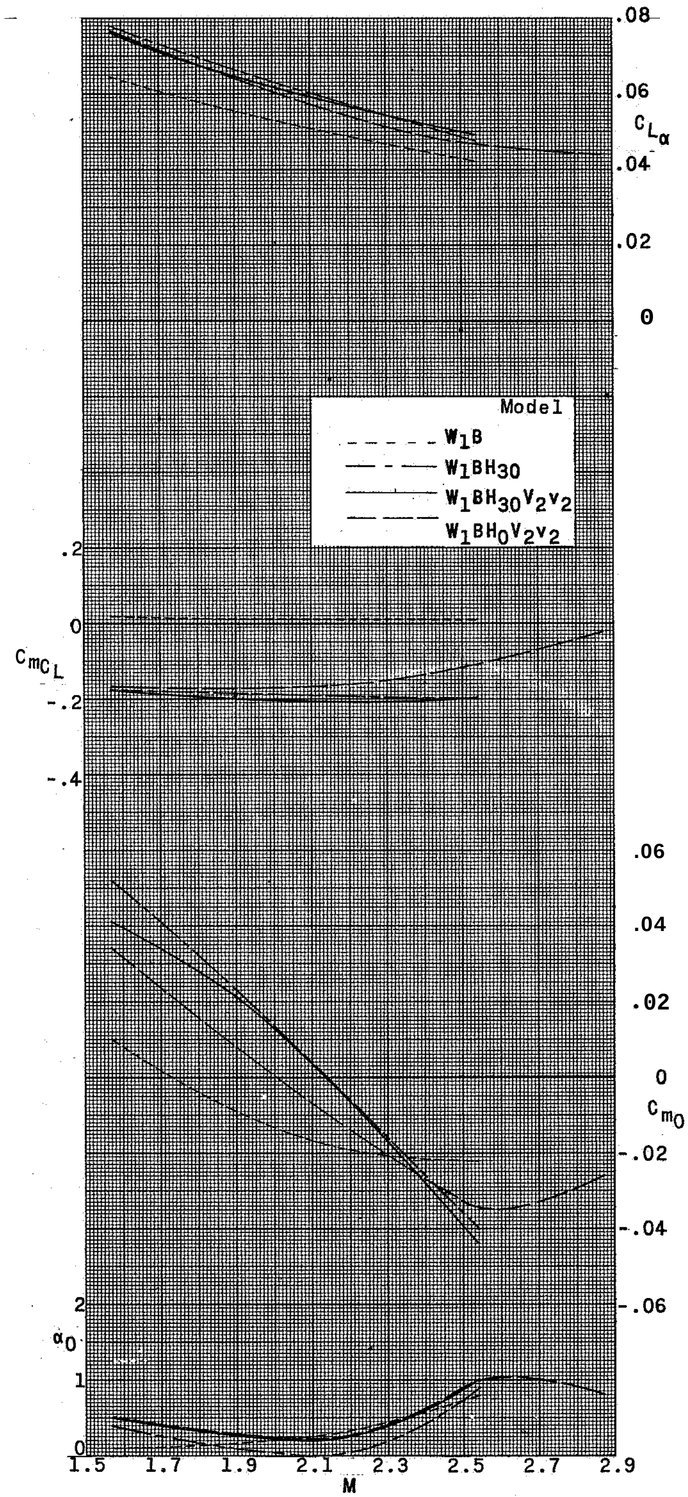

Figure 17.- Summary of longitudinal stability characteristics of a supersonic horizontal-attitude VTOL airplane model.

L-355

[redacted]

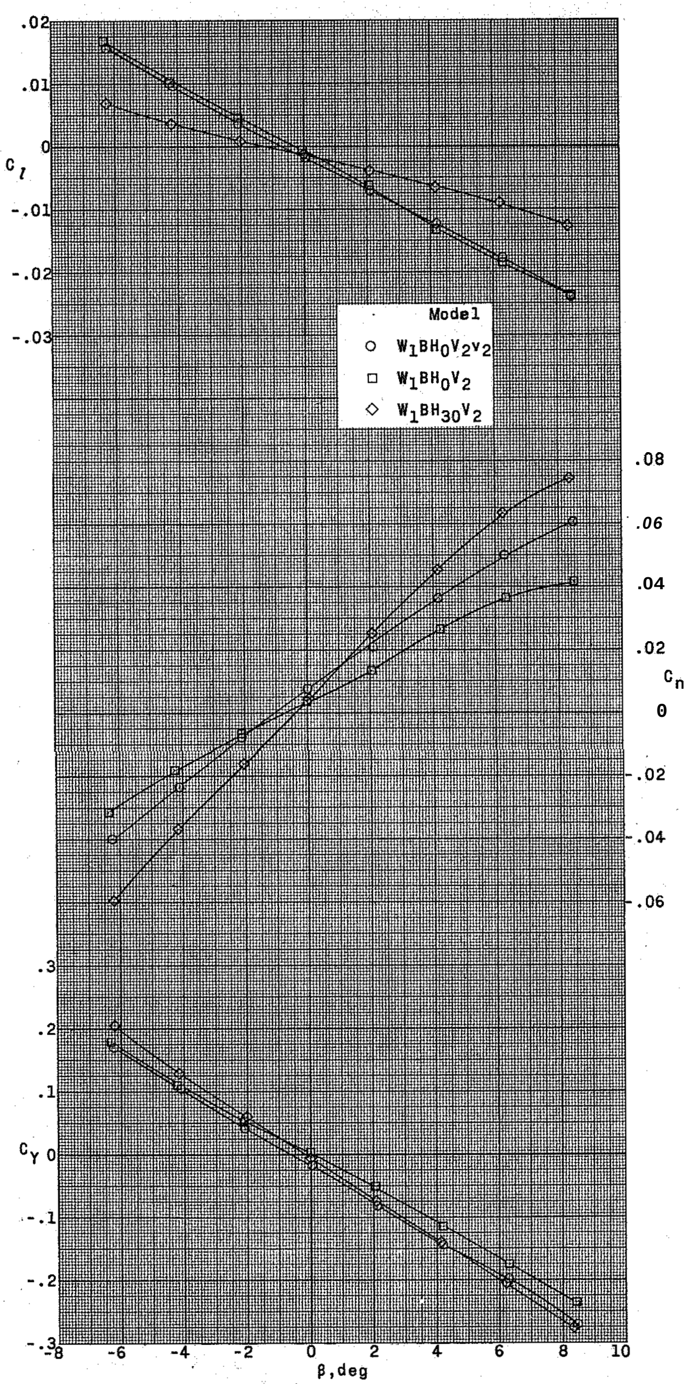

(a) $\alpha = 0.5^{\circ}$.

Figure 18.- Lateral stability characteristics of a supersonic horizontal-attitude VTOL airplane model with various tail configurations at M = 1.57.

L-355

L-355

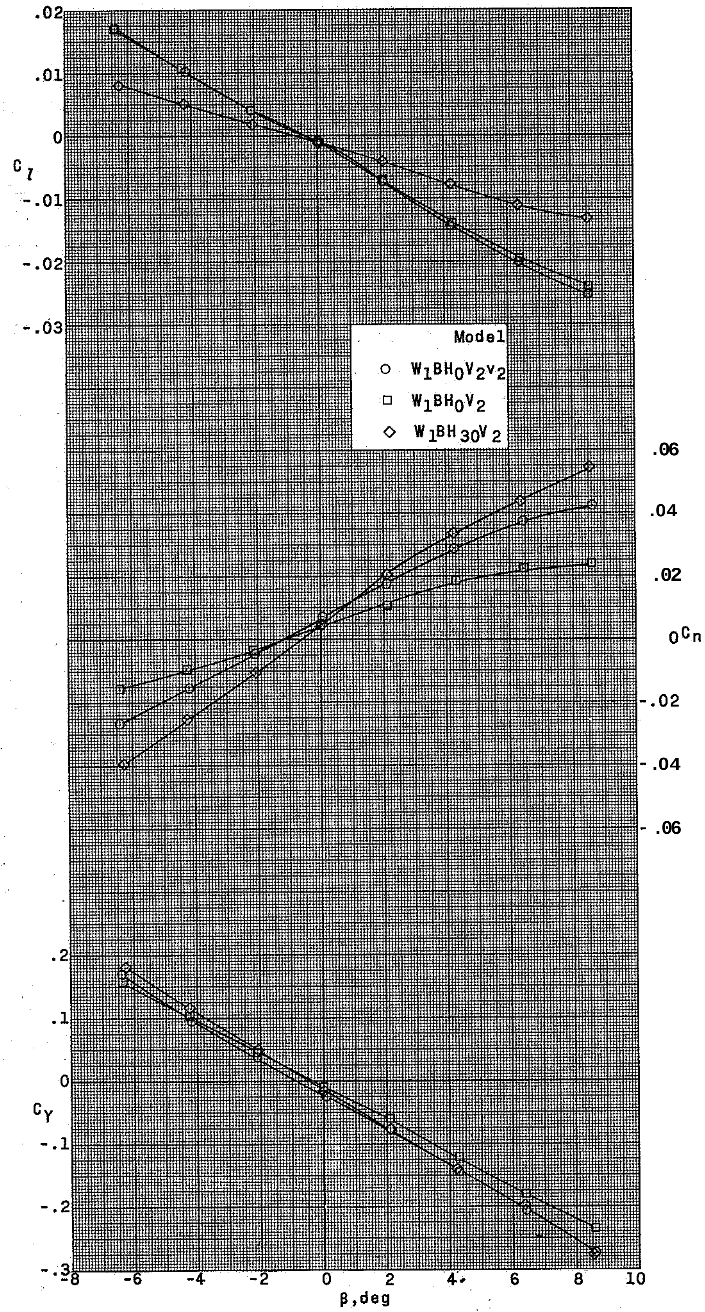

(b) $\alpha = 5.5^{\circ}$.

Figure 18.- Continued.

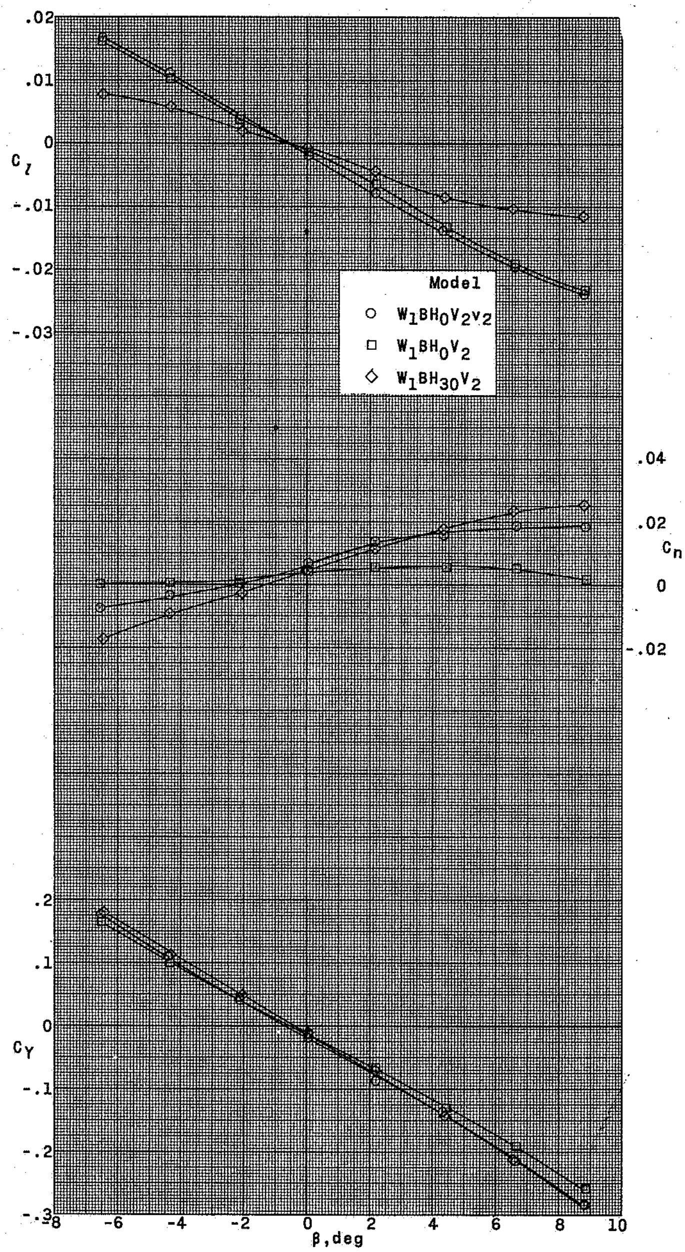

(c) $\alpha = 10.5^{\circ}$.

Figure 18.- Concluded.

L-355

L-355

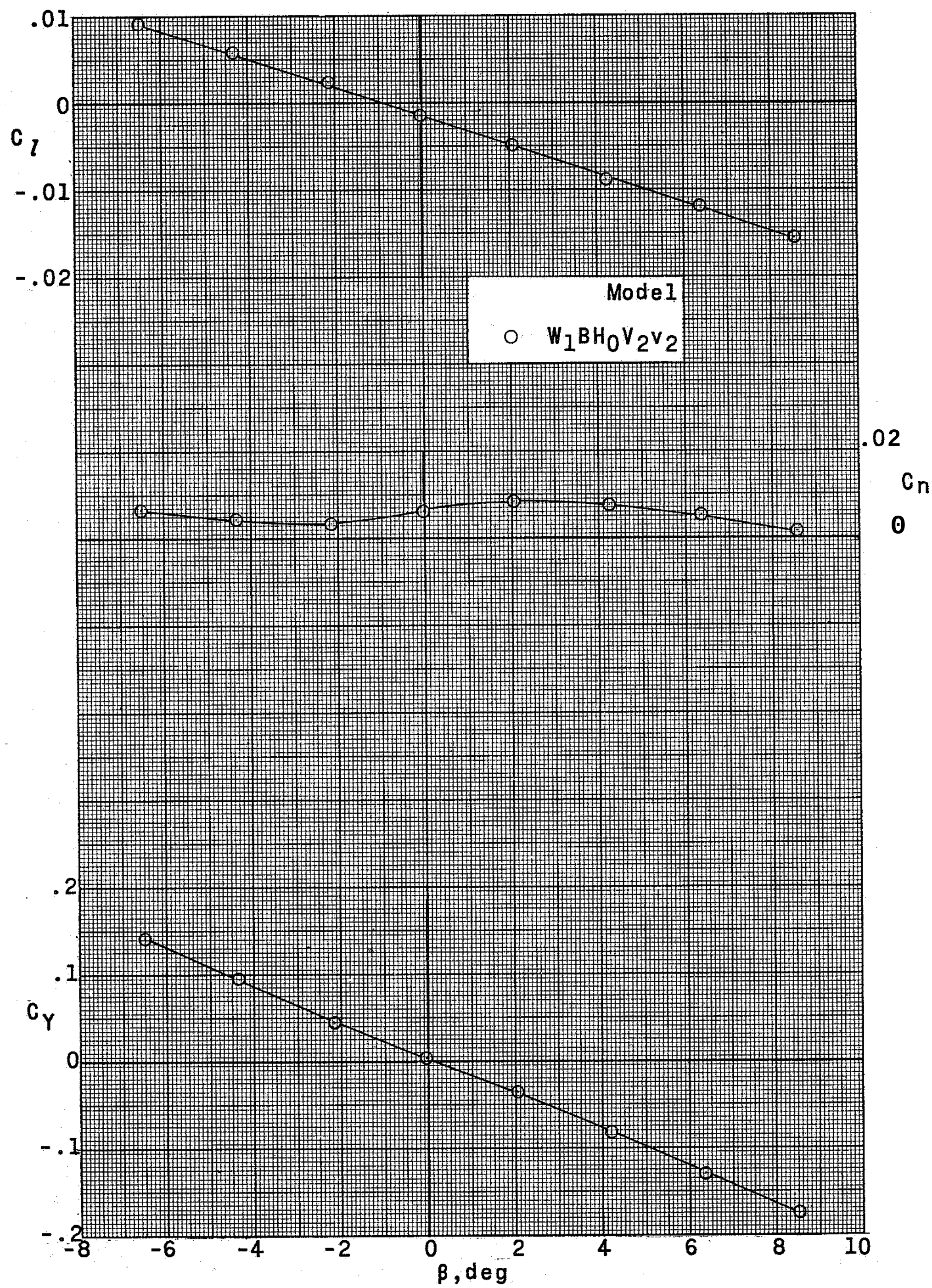

(a) a = 1.6°.

Figure 19.- Lateral stability characteristics of a supersonic horizontal-attitude VTOL airplane model at M = 2.14.

[redacted]

[redacted]

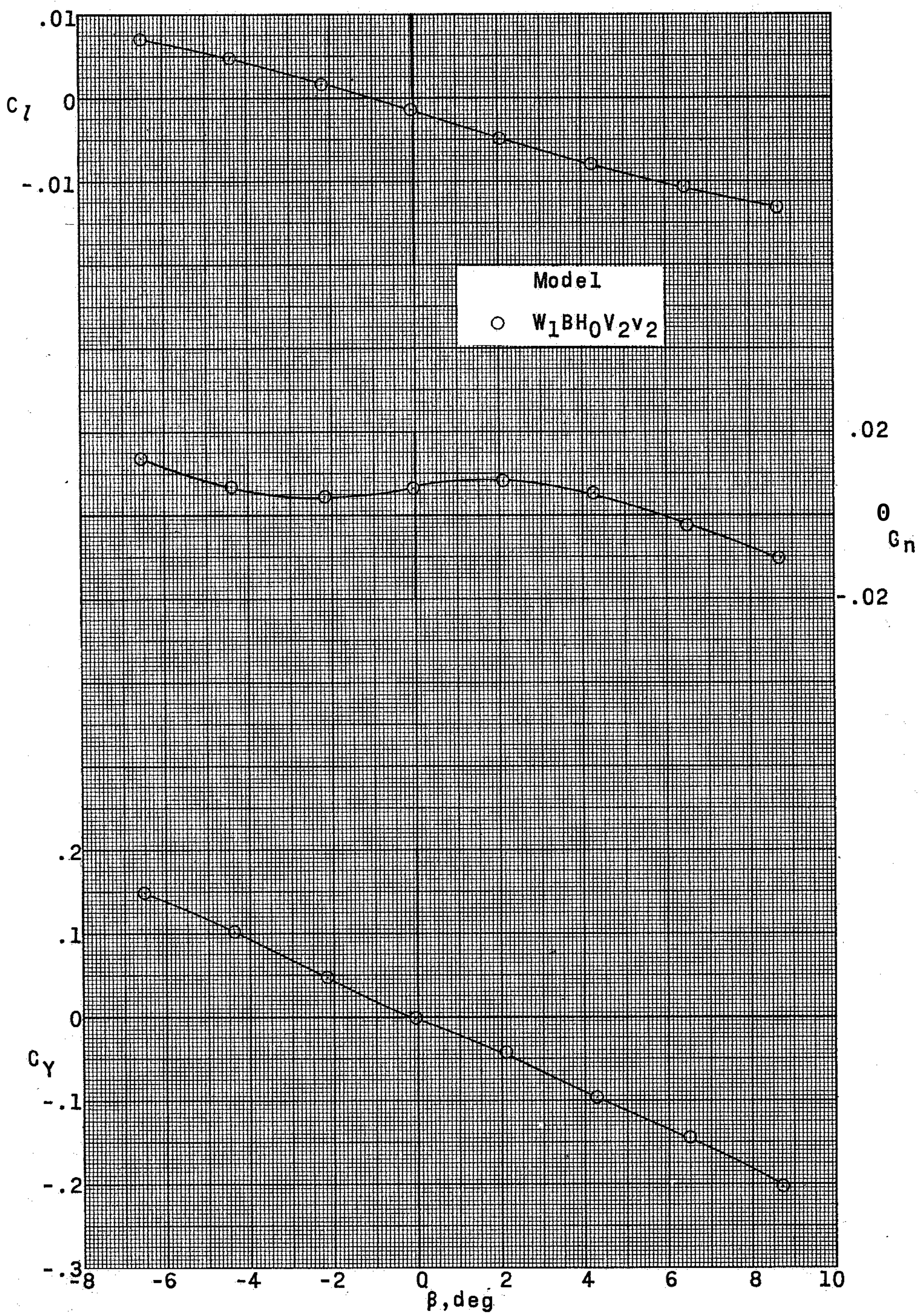

(b) $\alpha = 6.2^{\circ}$.

Figure 19.- Continued.

I-355

[redacted]

L-355

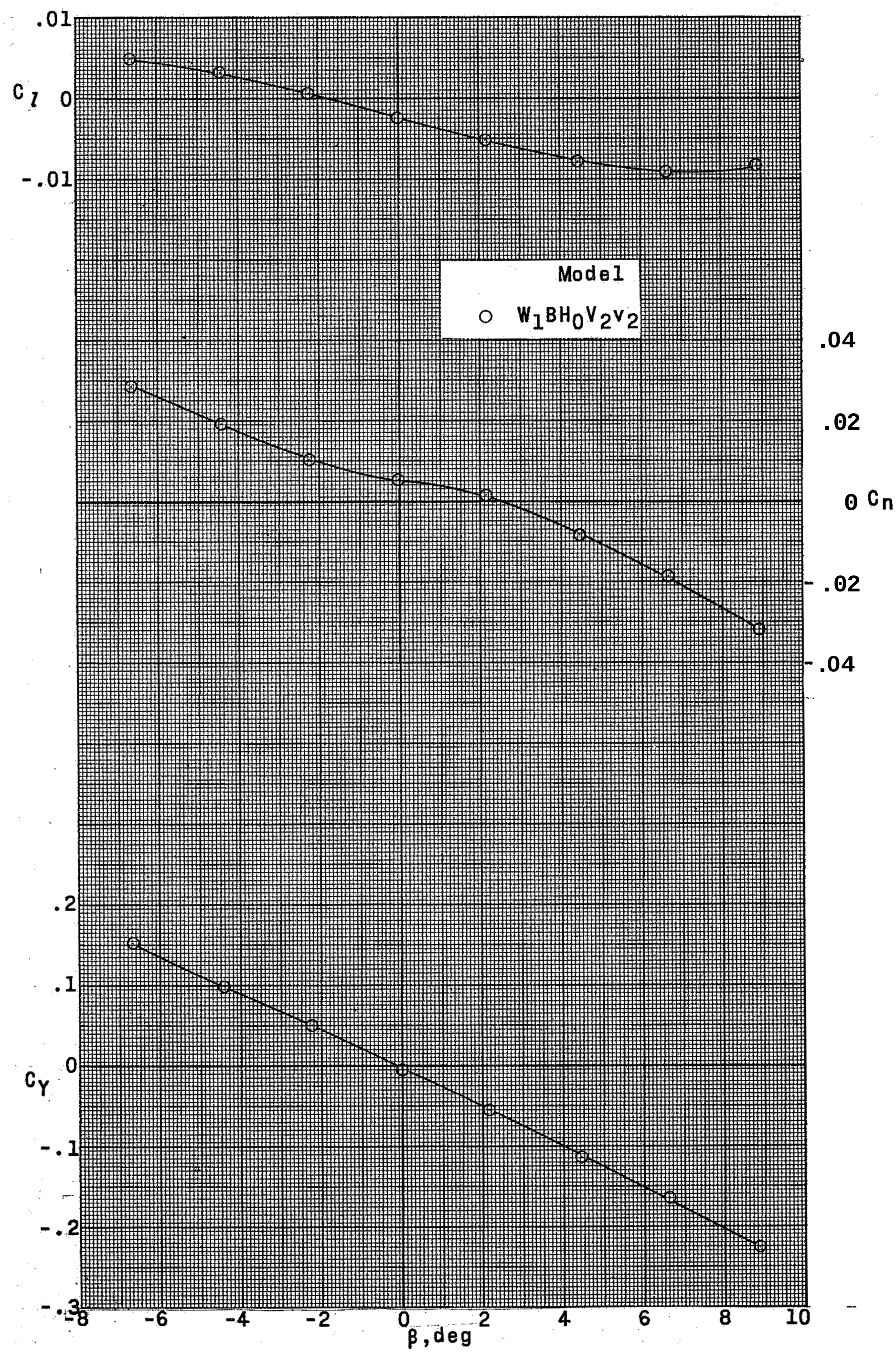

(c) $\alpha = 11.0^\circ$.

Figure 19.- Concluded.

[redacted]

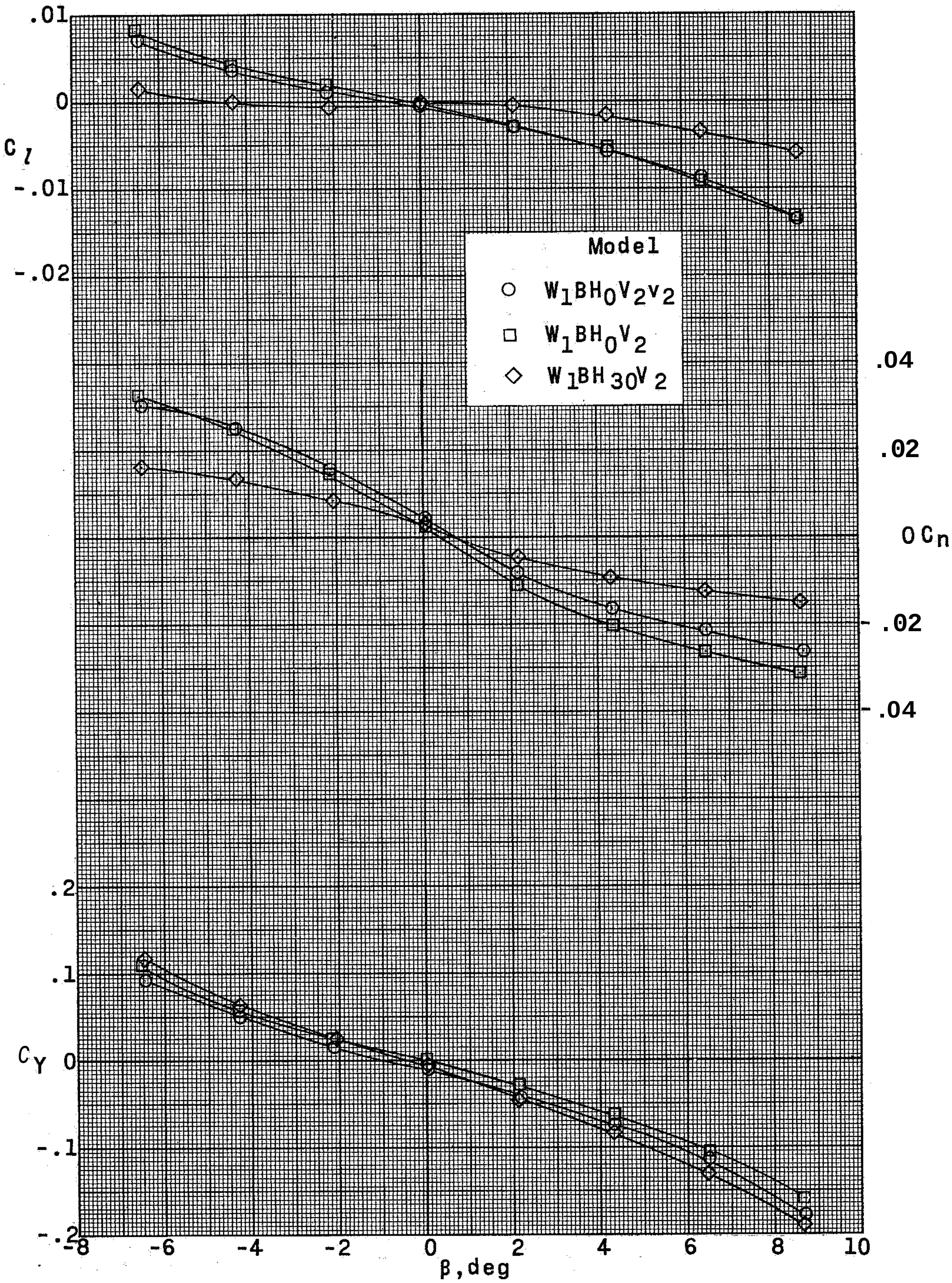

(a) $\alpha = 1.0^{\circ}$.

Figure 20.- Lateral stability characteristics of a supersonic horizontal-attitude **VTOL** airplane model with various tail configurations at **M** = 2.54.

L-355

[redacted]

L-355

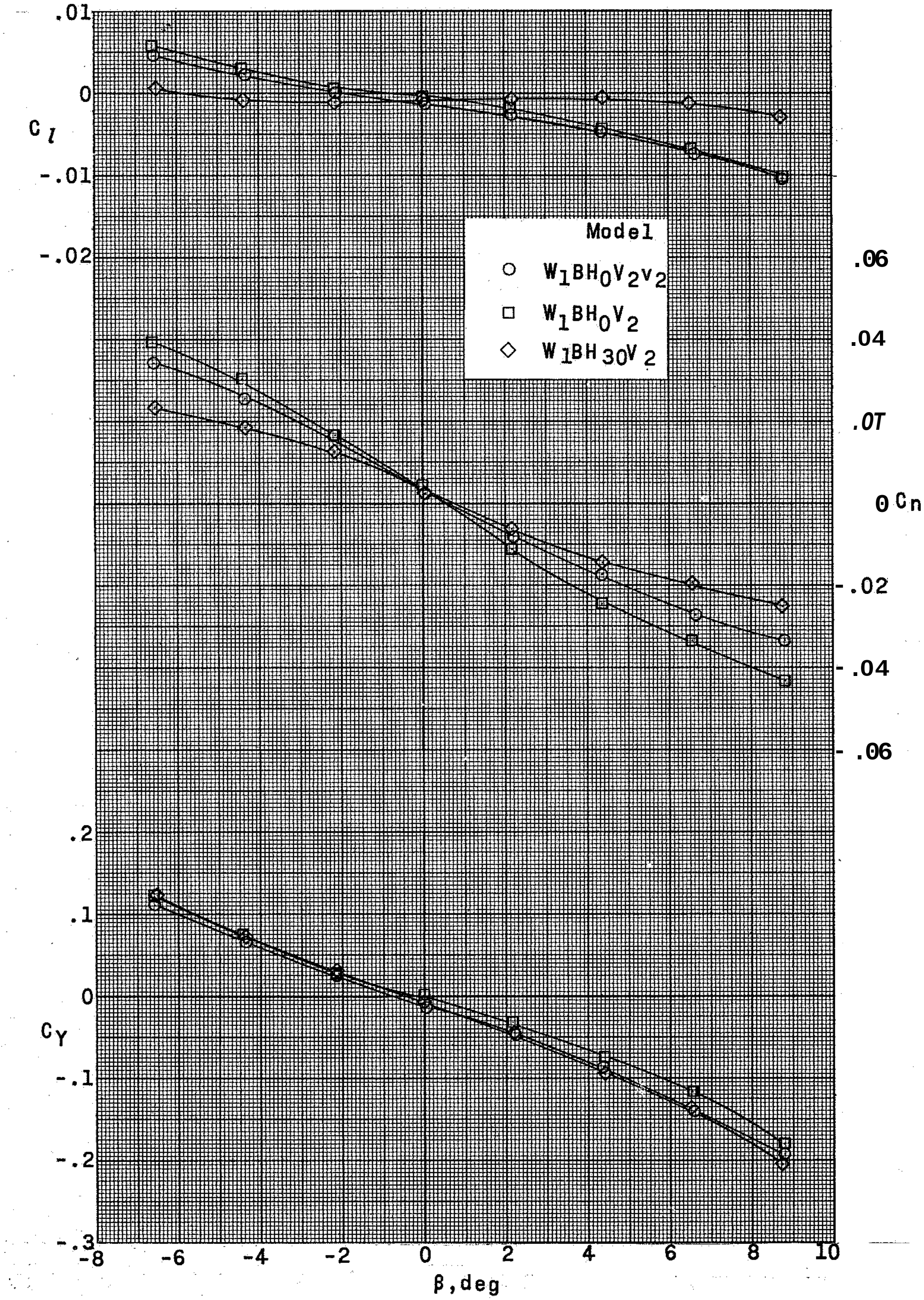

(b) $\alpha = 5.5^{\circ}$.

Figure 20.- Continued.

[redacted]

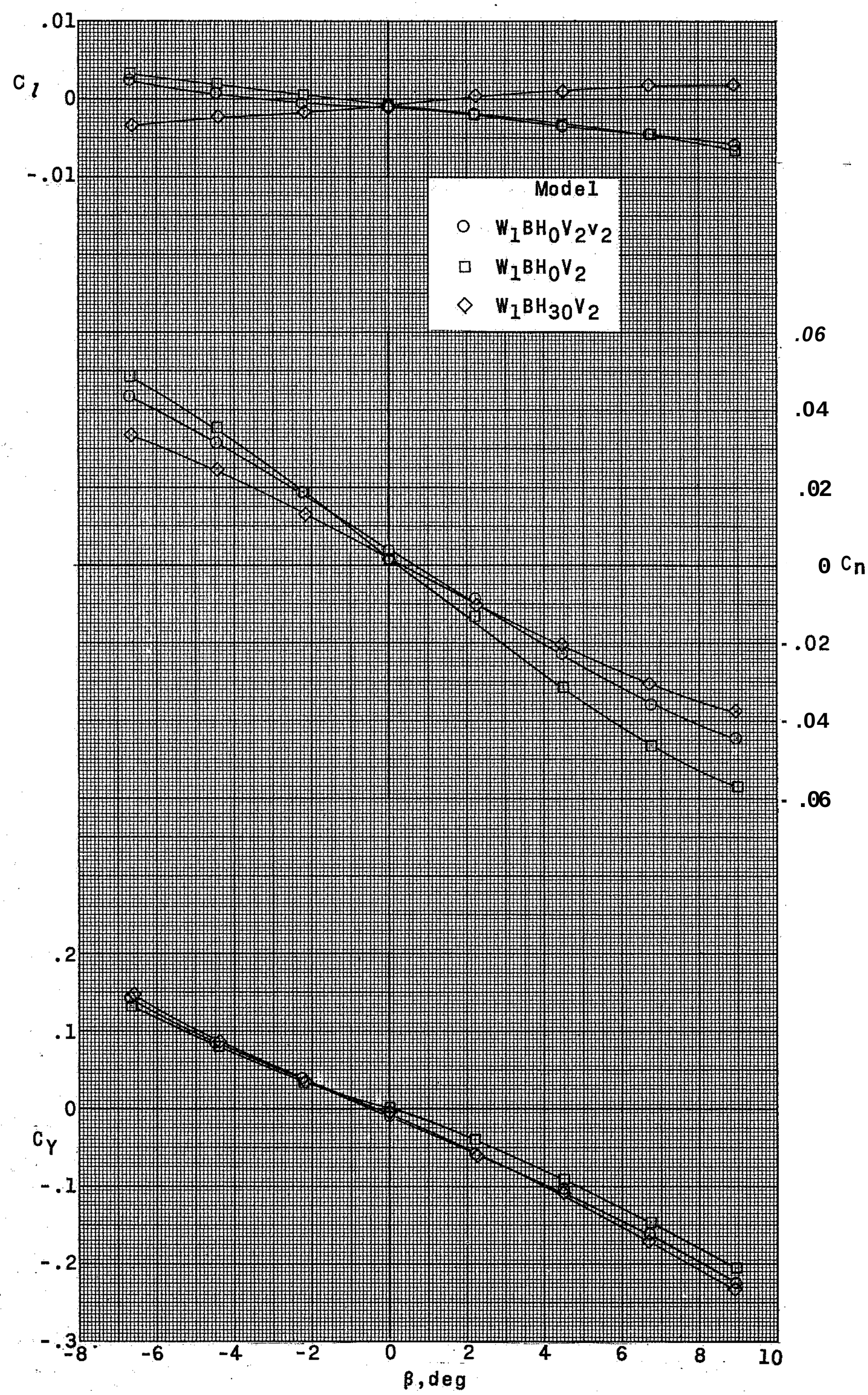

(c) a = 10.10.

Figure 20.- Concluded.

L-355

[redacted]

[redacted]

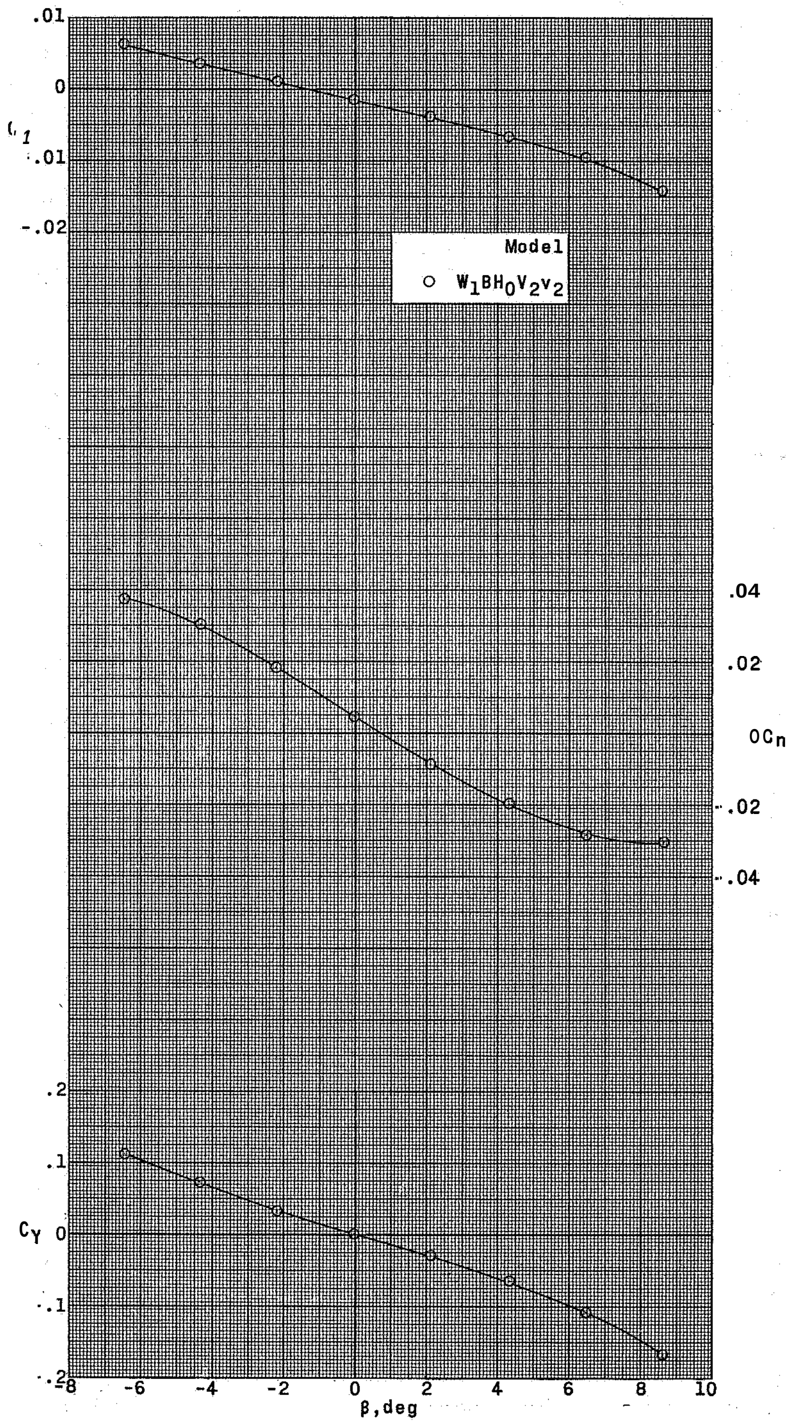

(a) $\alpha = 0.1^\circ$.

Figure 21.- Lateral stability characteristics of a supersonic horizontal-attitude VTOL airplane model at $M = 2.87$.

[redacted]

[redacted]

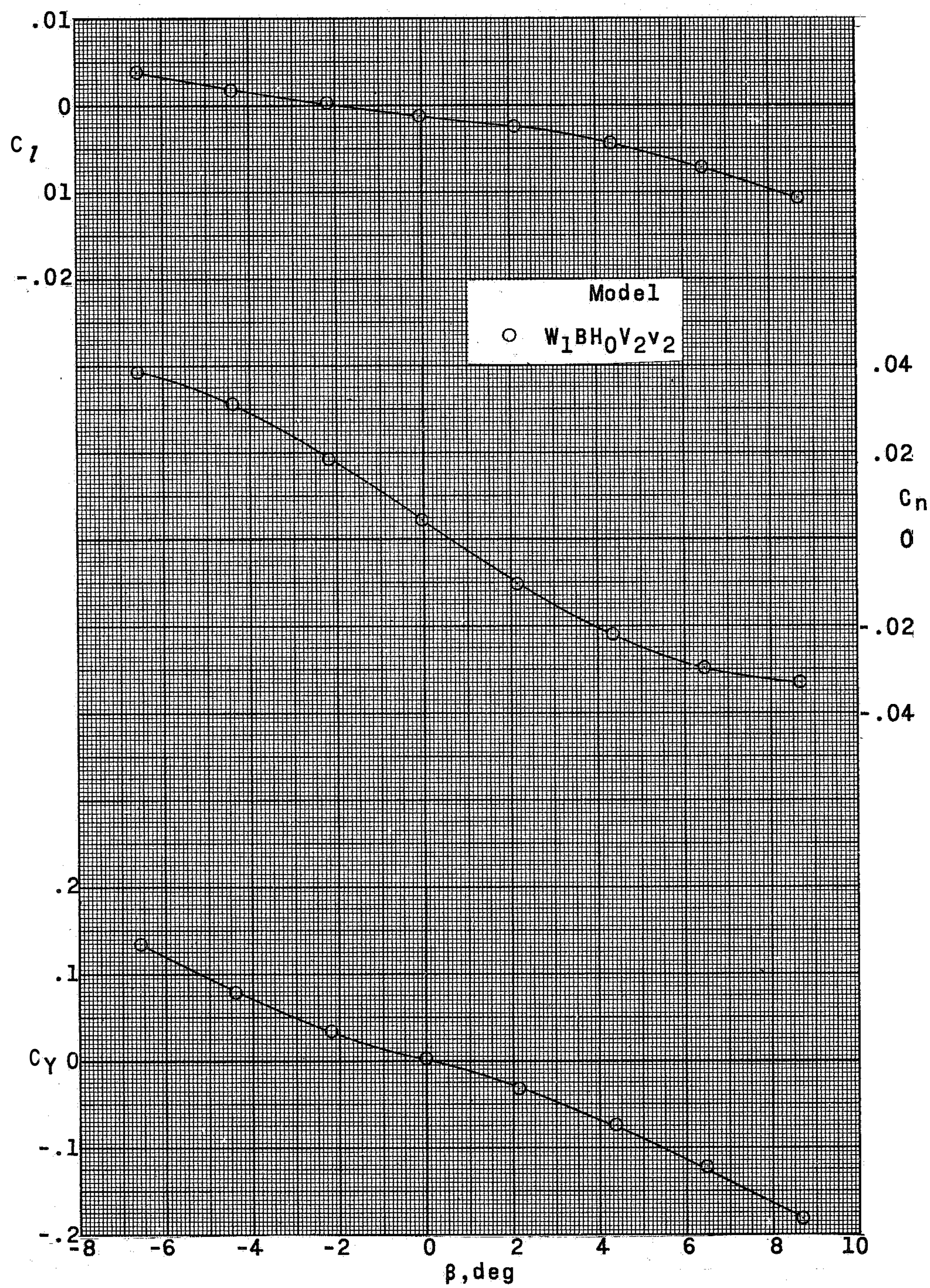

(b) $\alpha = 4.3^{\circ}$.

Figure 21.- Continued.

L-3[redacted]

[redacted]

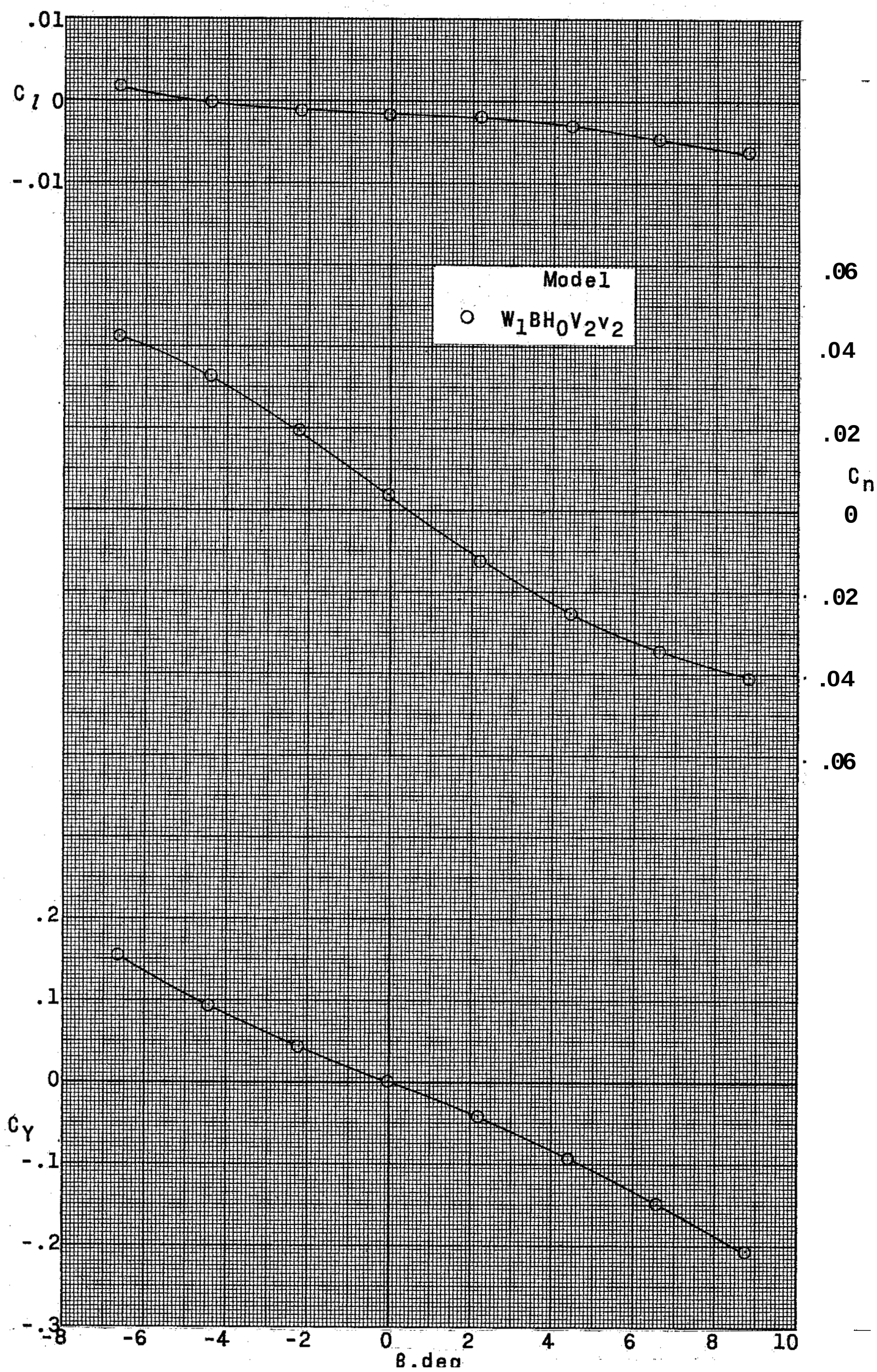

(c) $\alpha = 8.8^{o}$.

Figure 21.- Concluded.

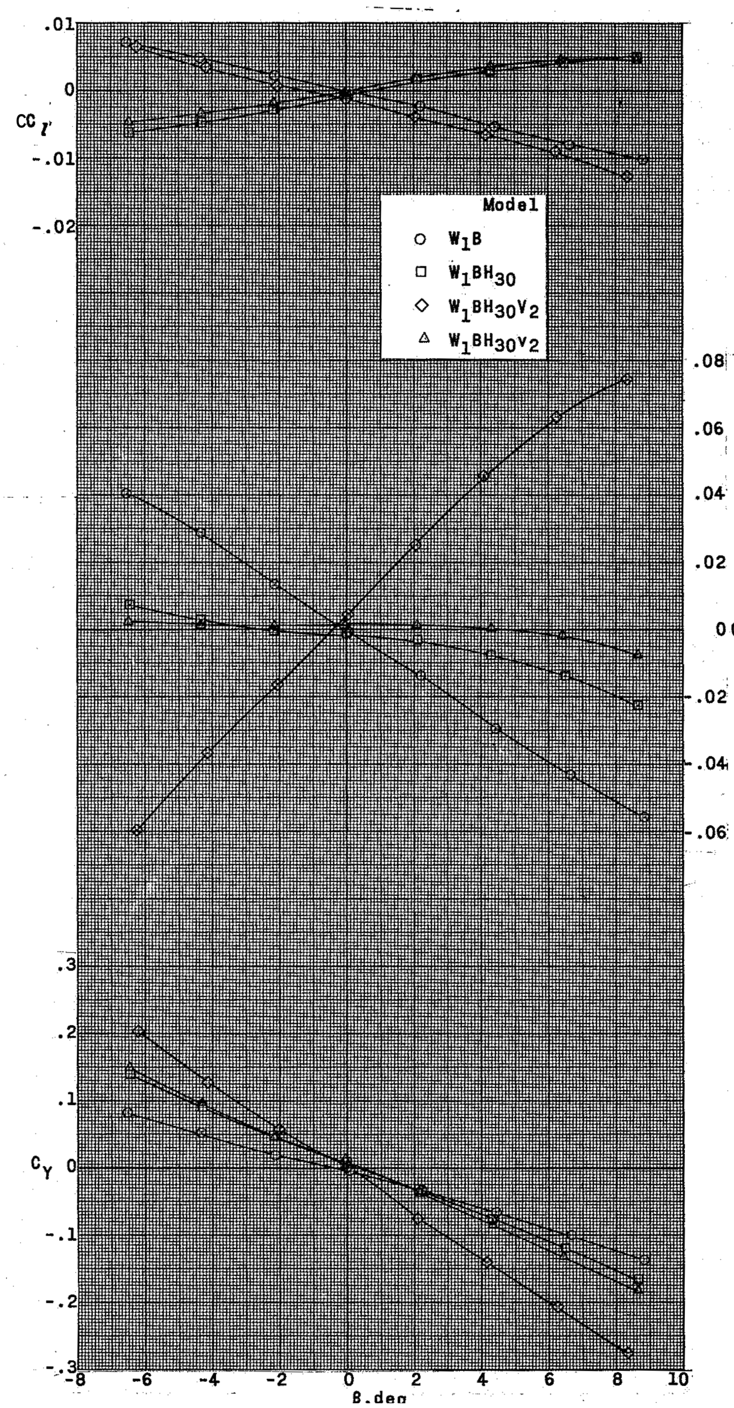

(a) $\alpha = 0.5^{o}$.

Figure 22.- Lateral stability characteristics of a supersonic horizontal-attitude VTOL airplane model with various model components at $M = 1.57$.

[redacted]

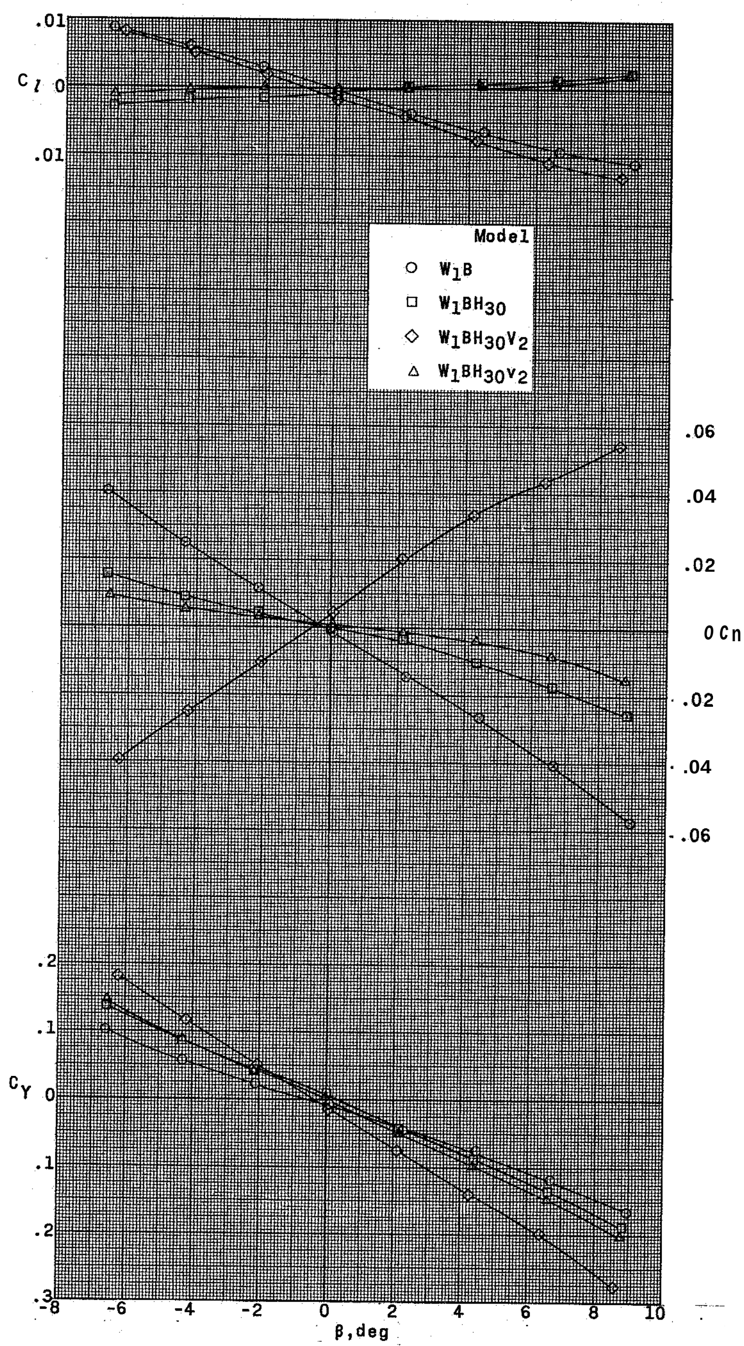

(b) $\alpha = 5.5^{\circ}$.

Figure 22.- **Continued.**

[redacted]

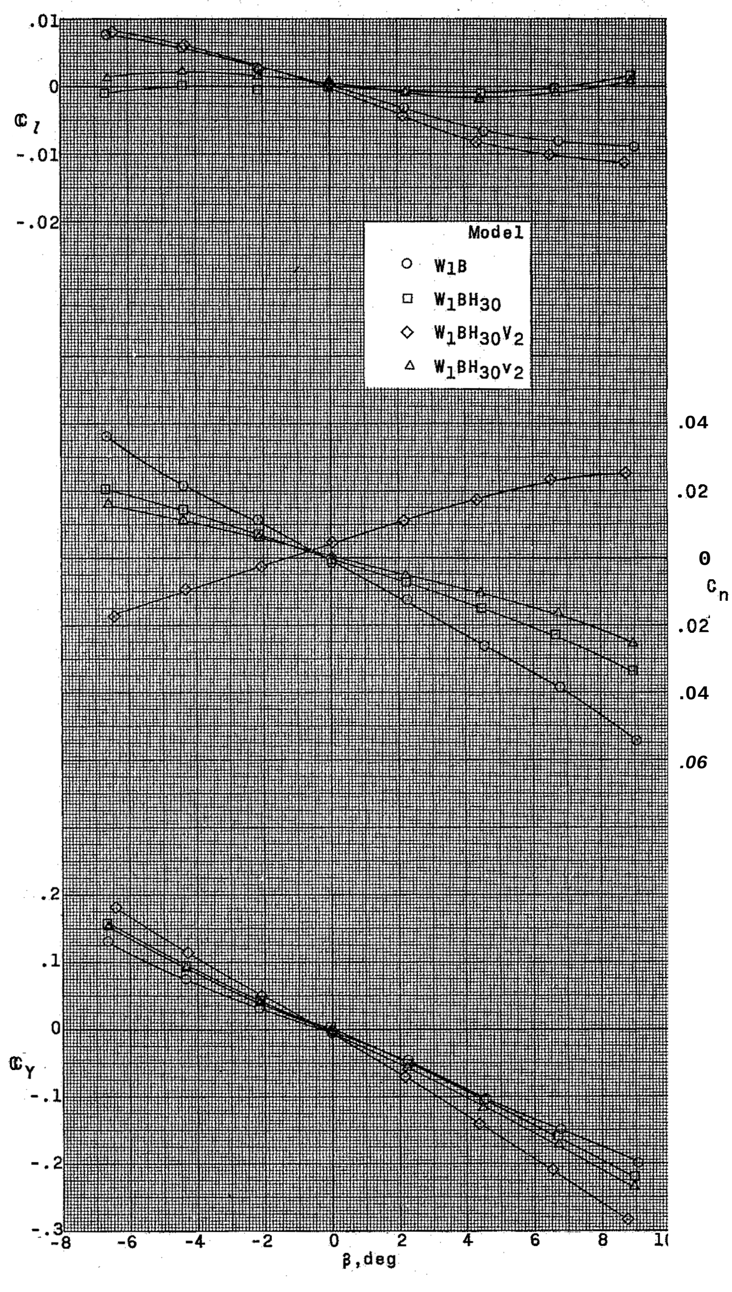

(c) $\alpha = 10.5^{\circ}$.

Figure 22.- Concluded.

[redacted]

L-355

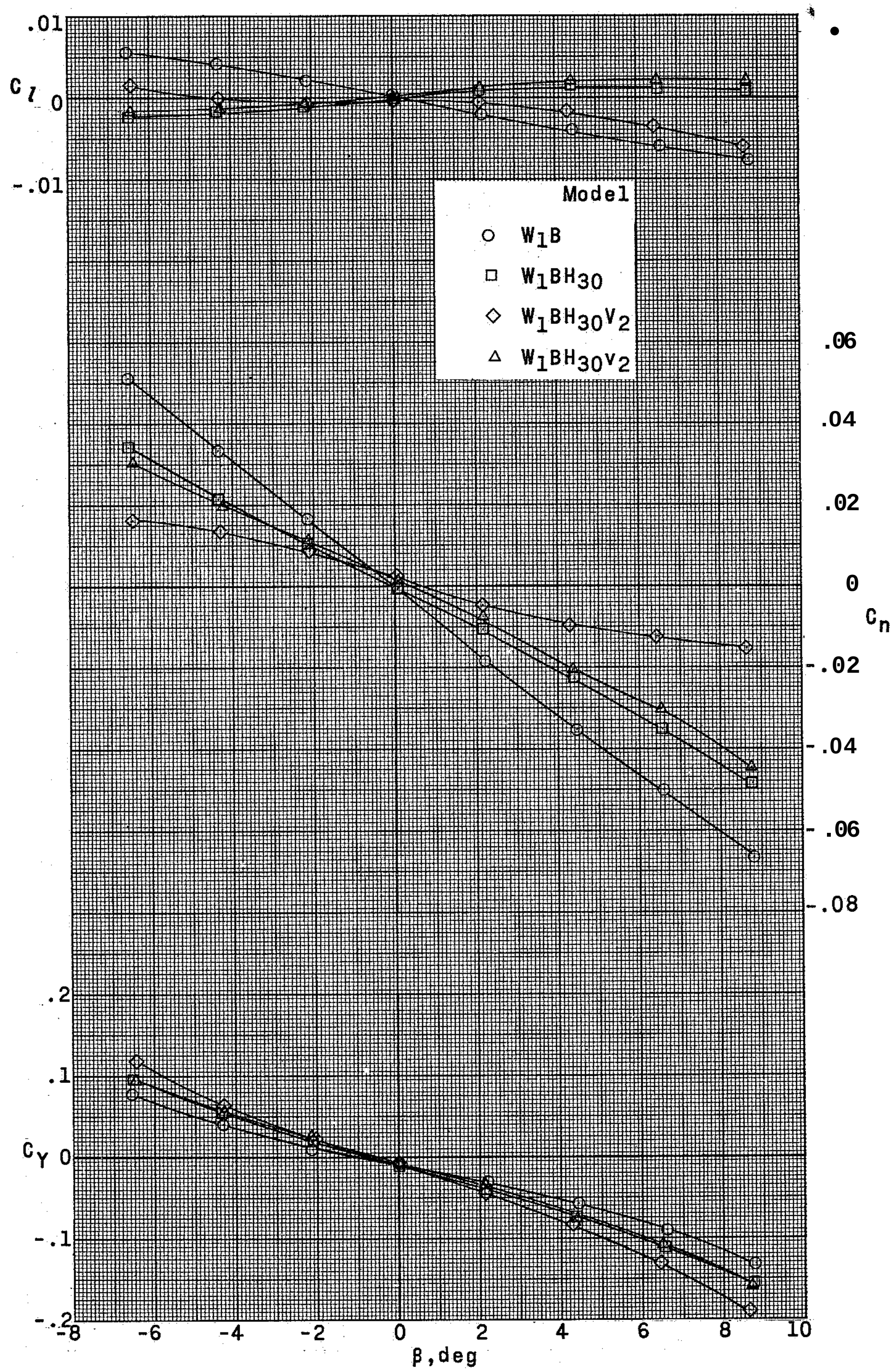

(a) $\alpha = 1.0^{\circ}$.

Figure 23.- Lateral stability characteristics of a supersonic horizontal-attitude VTOL airplane model with various model components at $M = 2.54$.

[redacted]

[redacted]

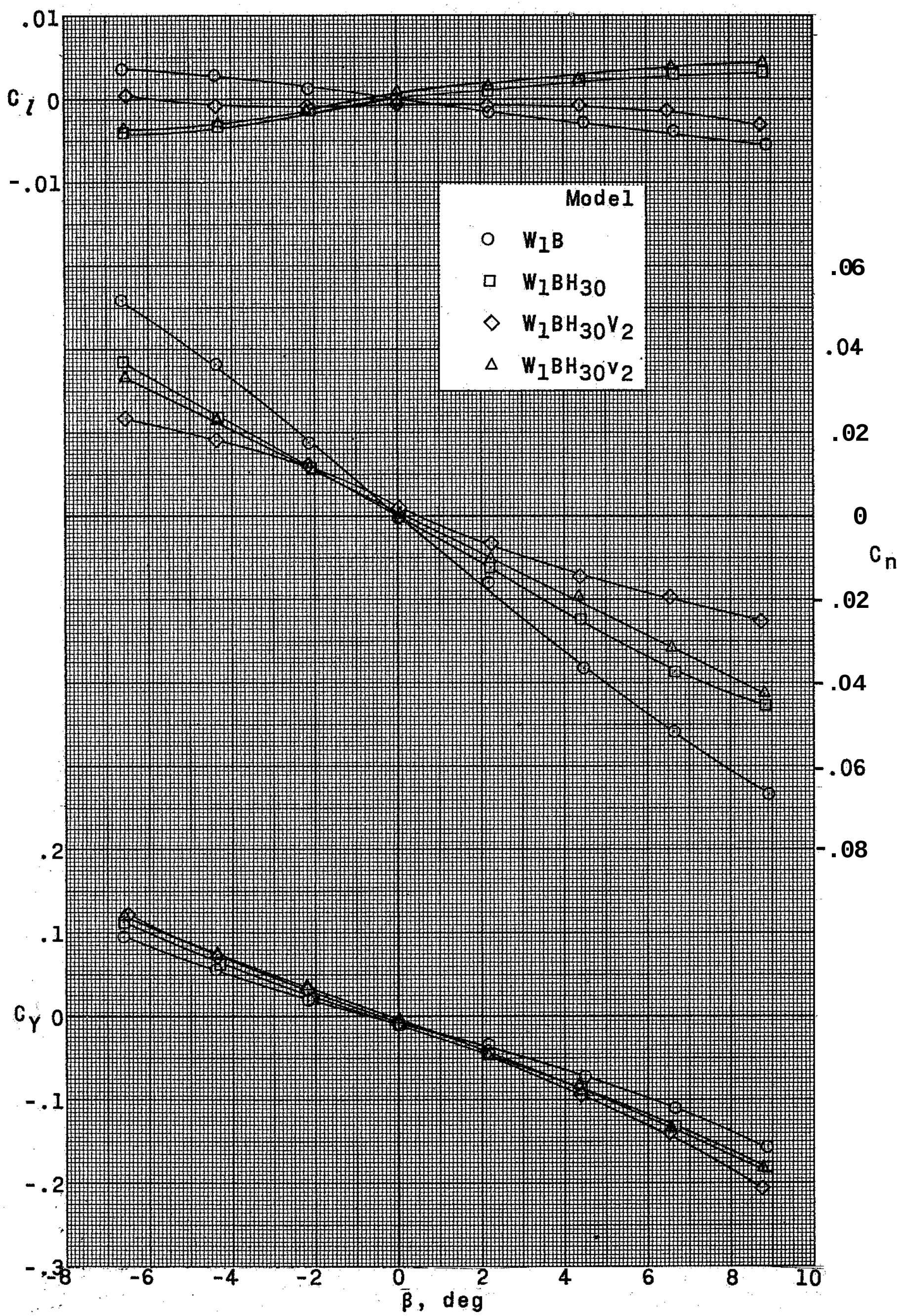

L-355

(b) $\alpha = 5.5^{\circ}$.

Figure 23.- Continued.

[redacted]

[redacted]

L-355

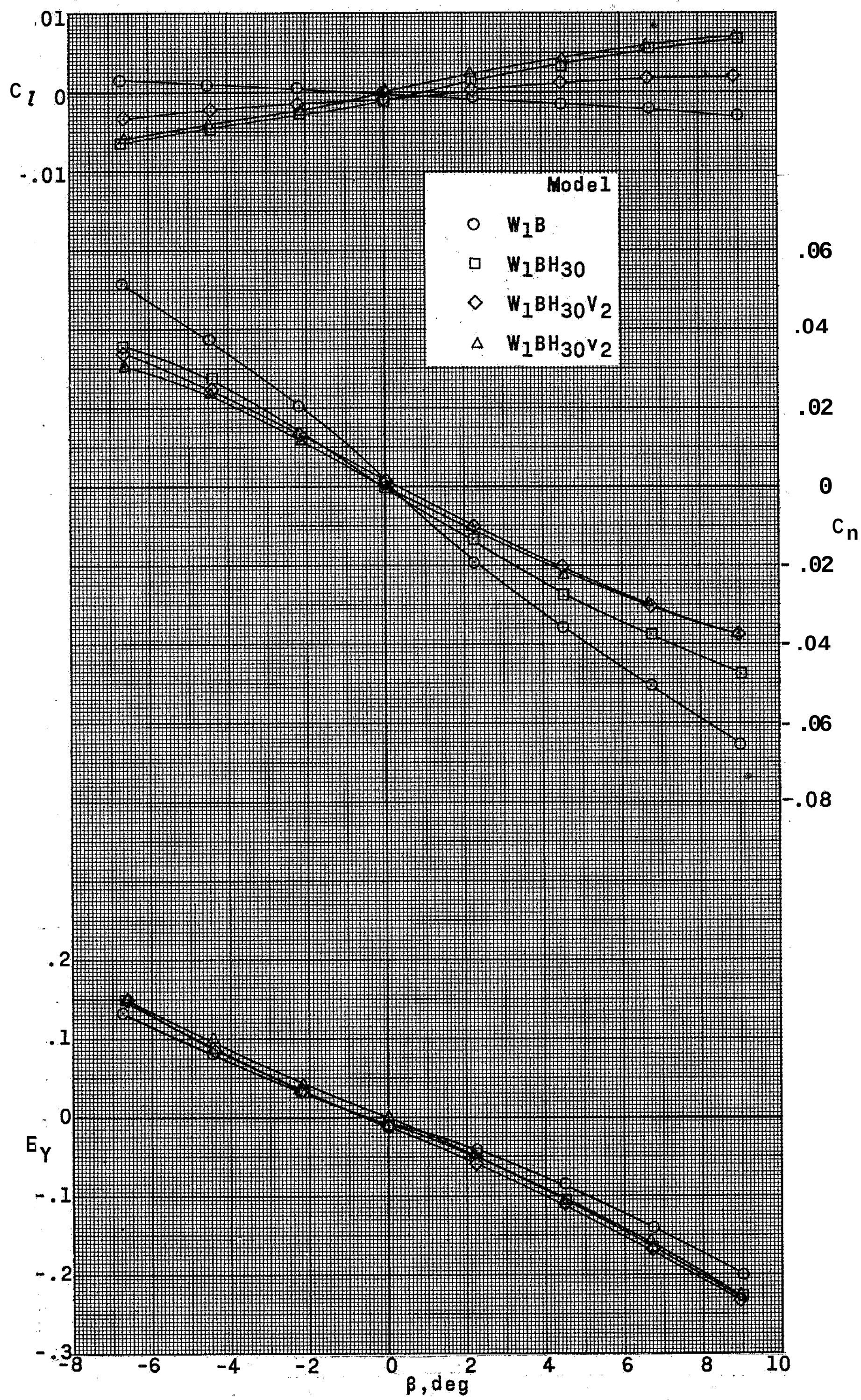

(c) a = 10.1°.

Figure 23.- Concluded.

[redacted]

[redacted]

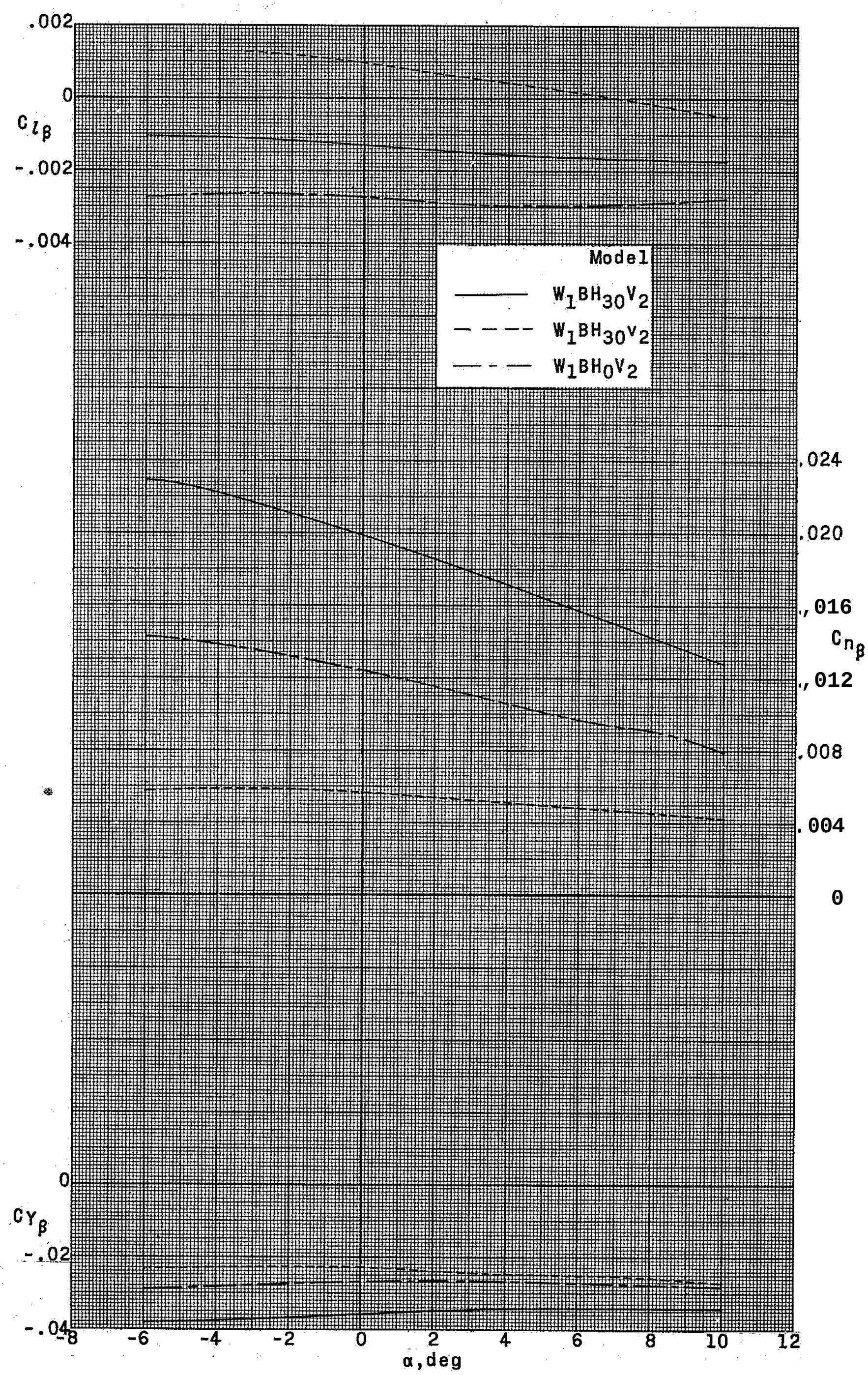

(a) M = 1.57.

Figure 24.- Summary of lateral stability characteristics of a supersonic horizontal-attitude VTOL airplane model as affected by various tail configurations.

[redacted]

[redacted]

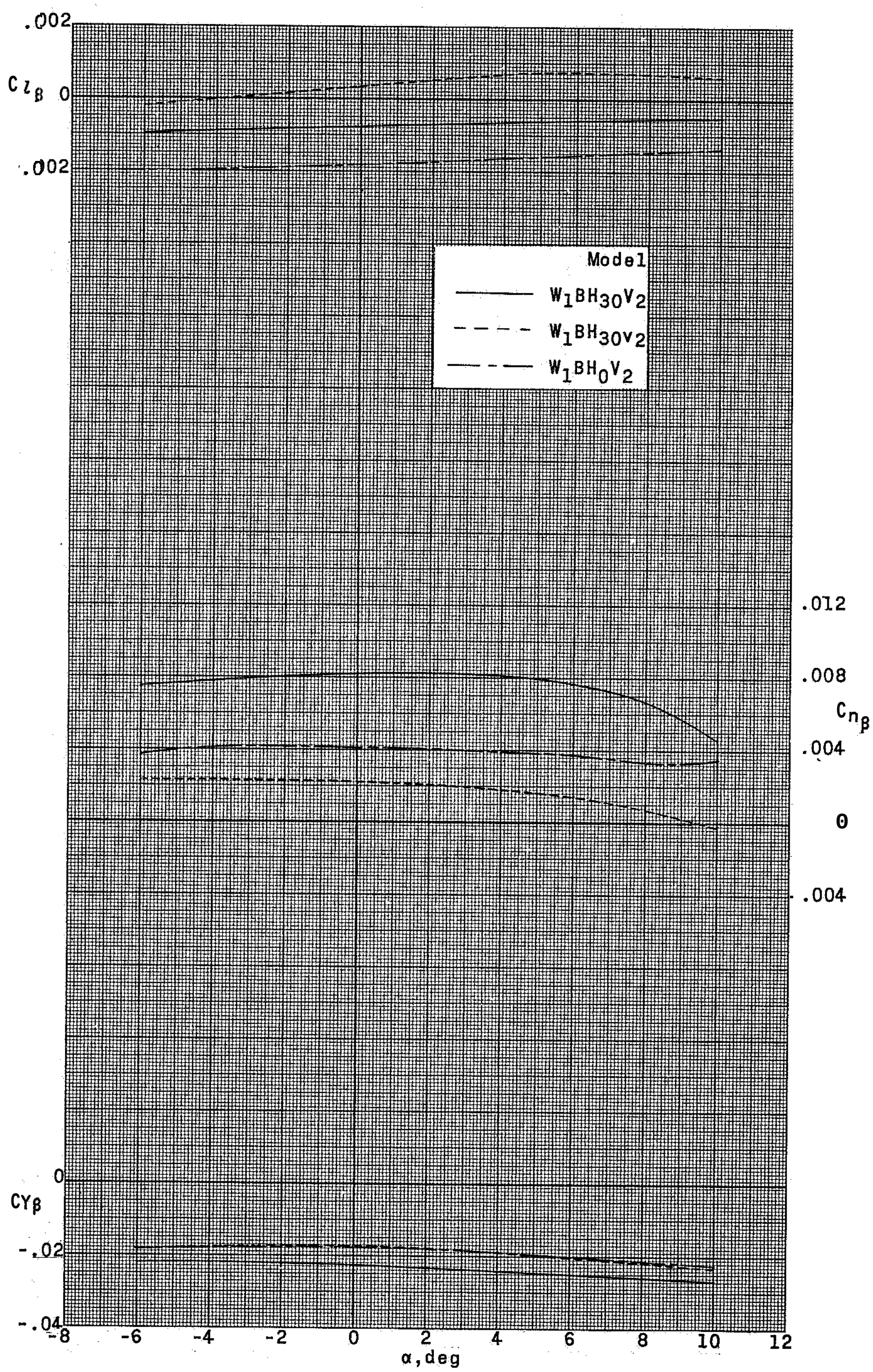

(b) M = 2.14.

Figure 24.- Continued.

[redacted]

[redacted]

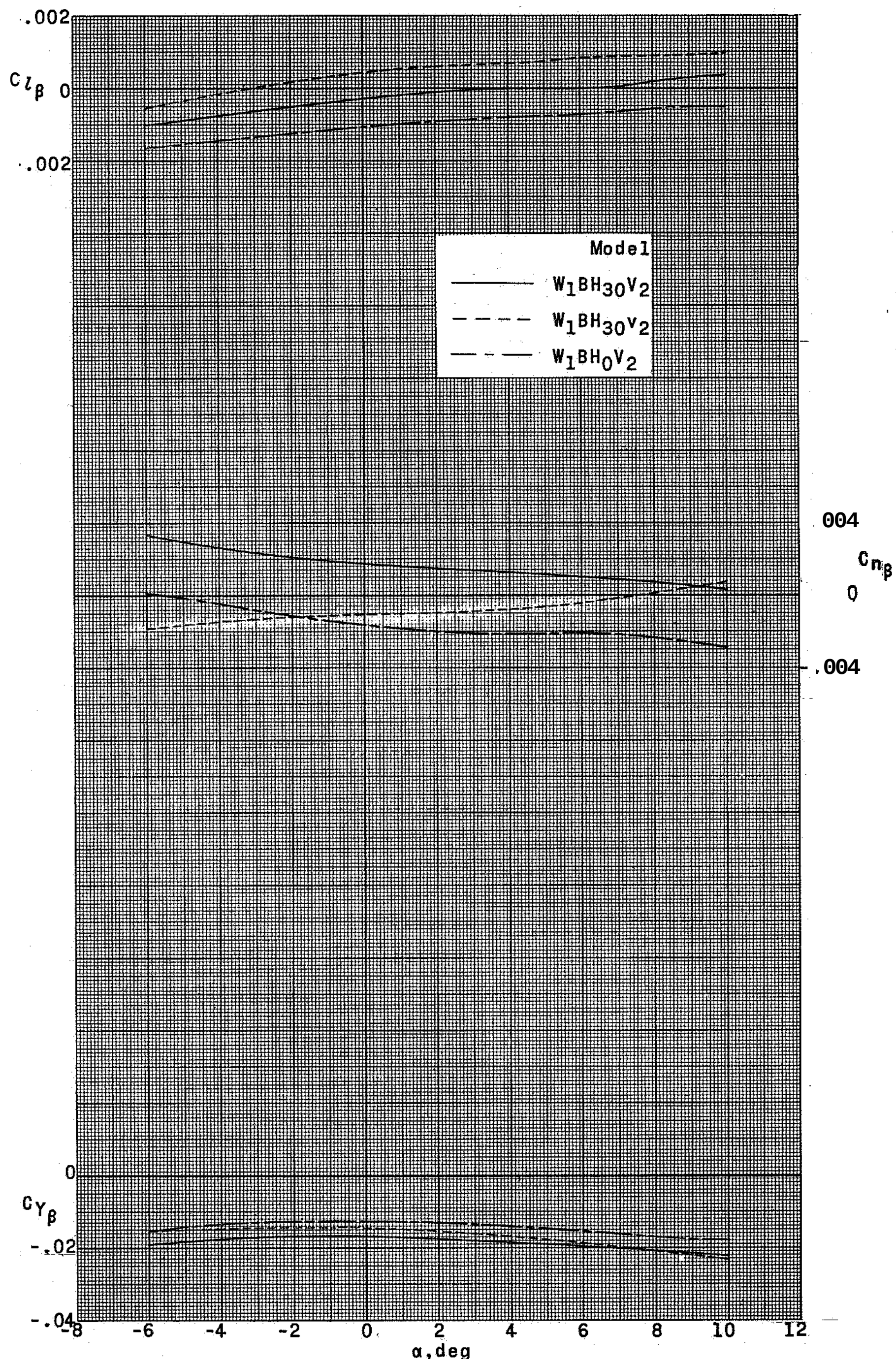

(c) M = 2.54.

Figure 24.- Concluded.

L-355

[redacted]

L-355

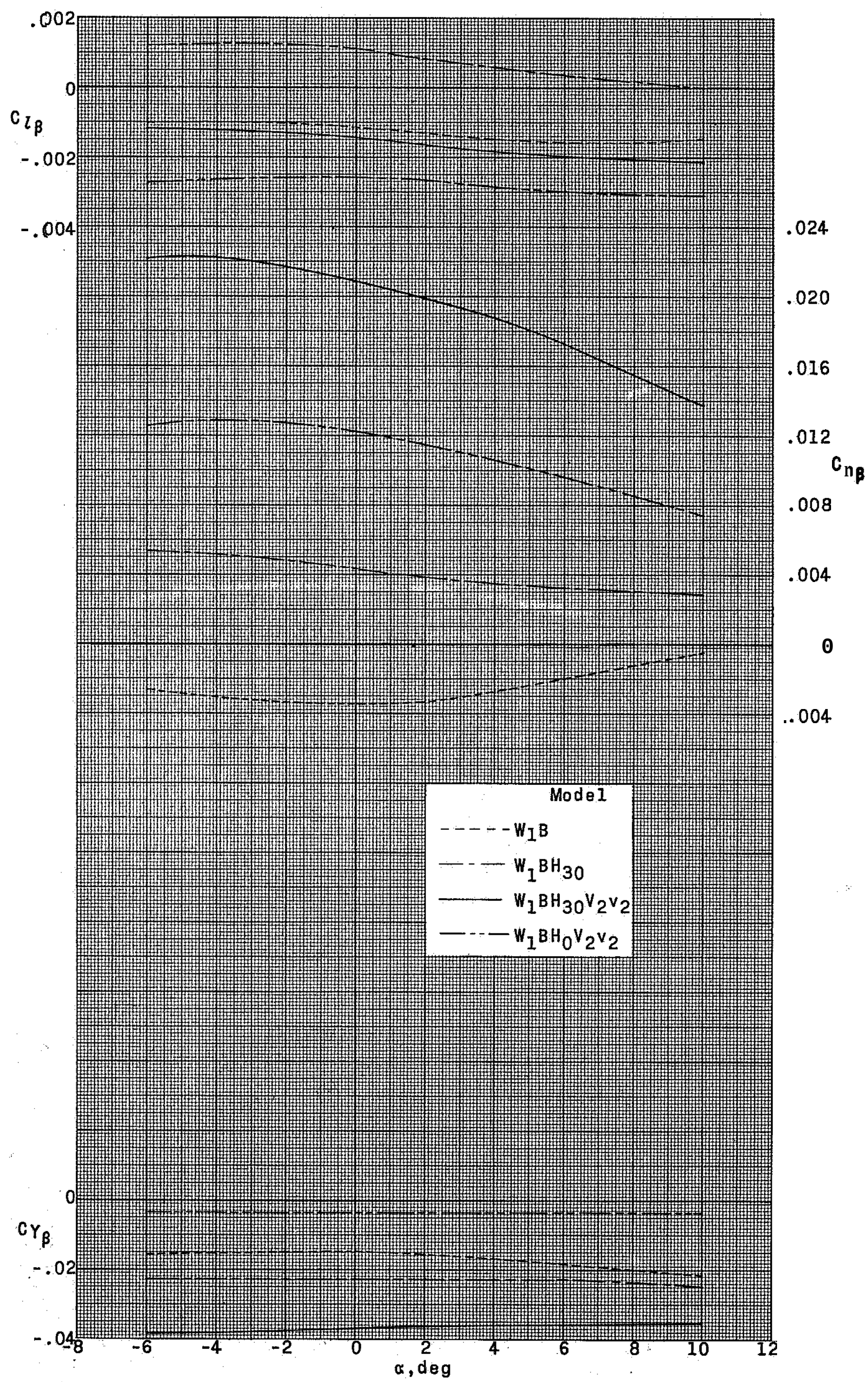

(a) M = 1.57.

Figure 25.- Summary of lateral stability characteristics of a supersonic horizontal-attitude VTOL airplane model as affected by various model components.

[redacted]

[redacted]

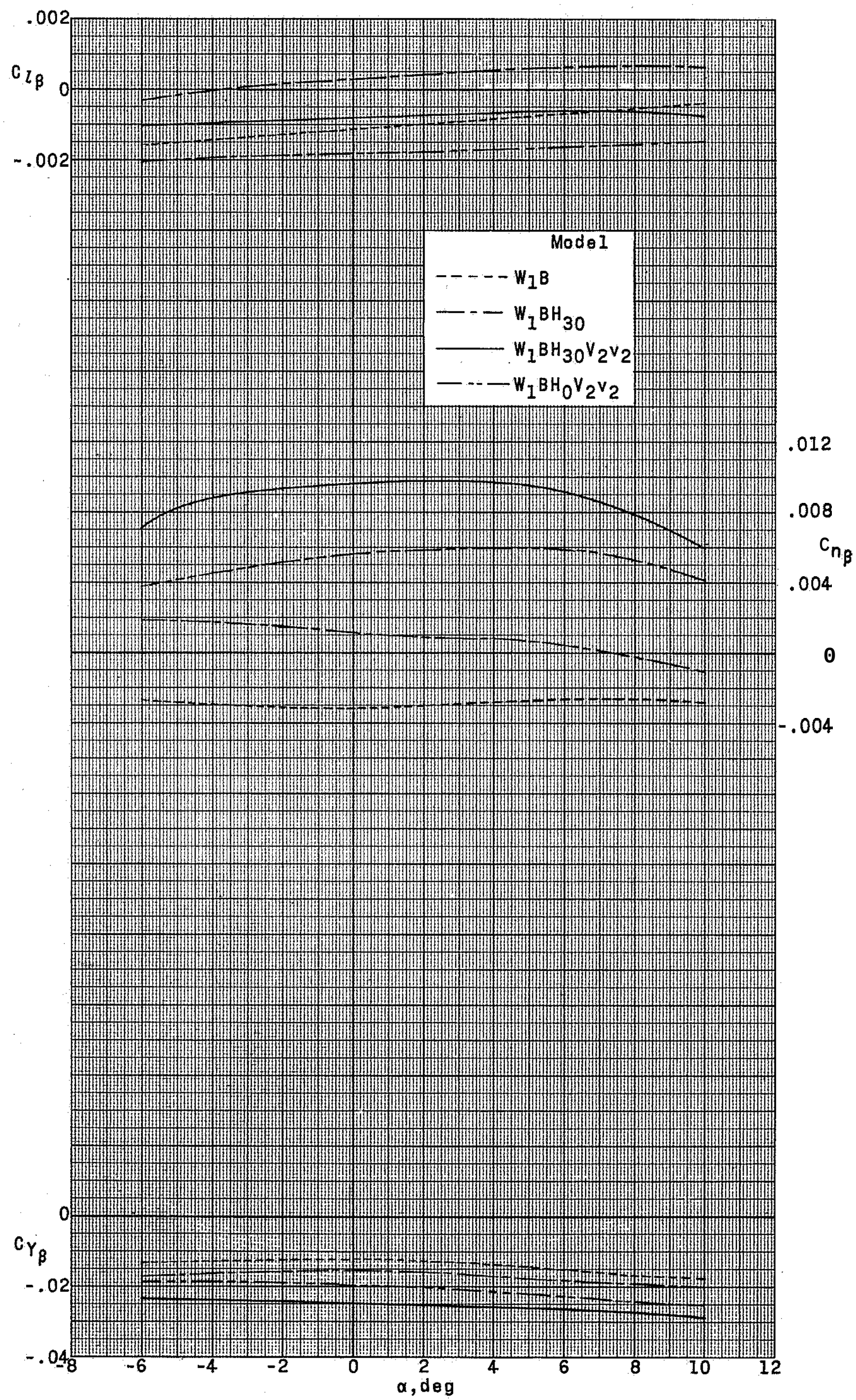

(b) M = 2.14.

Figure 25.- Continued.

L-355

[redacted]

L-355

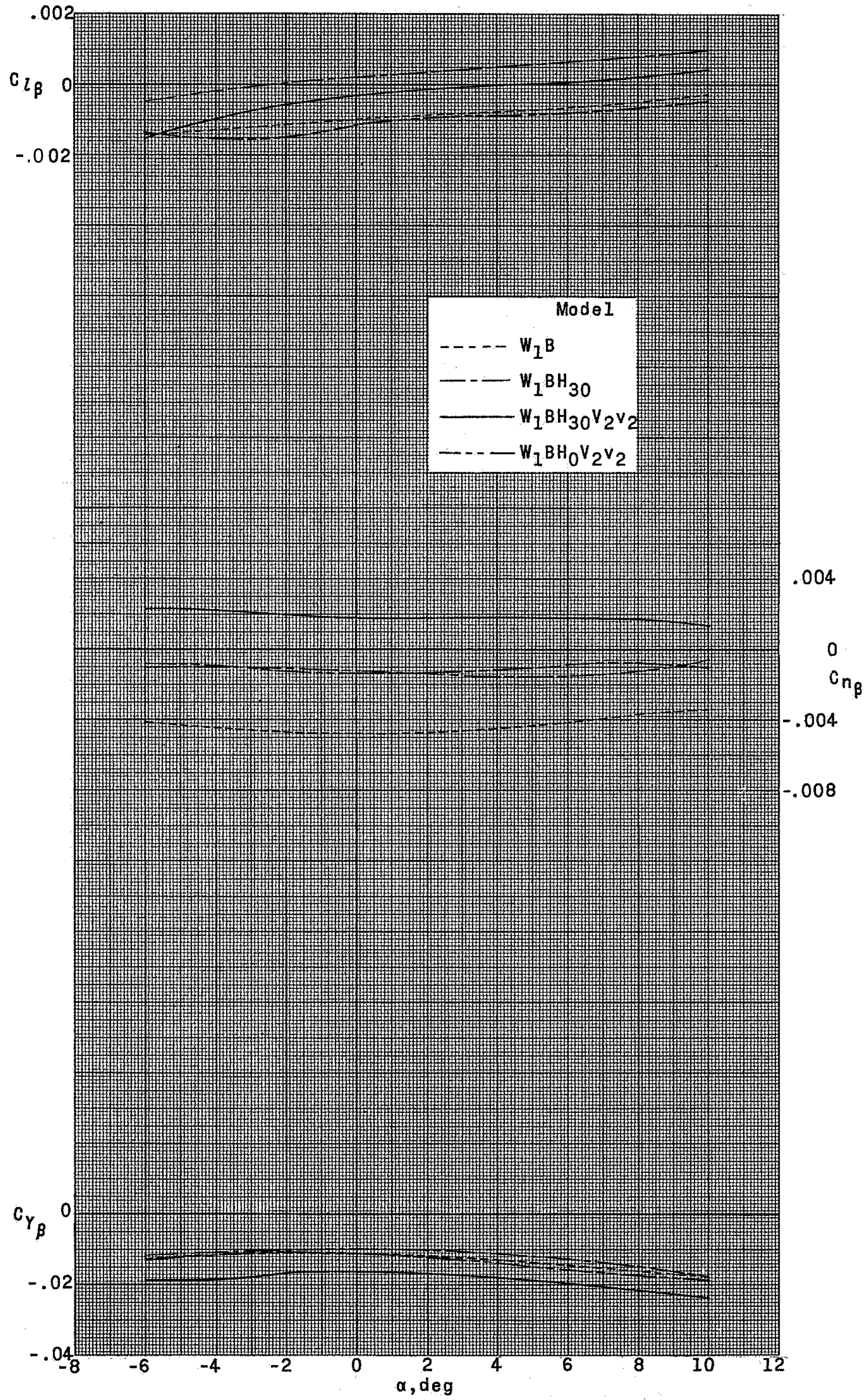

(c) $M = 2.54$.

Figure 25.- Continued.

[redacted]

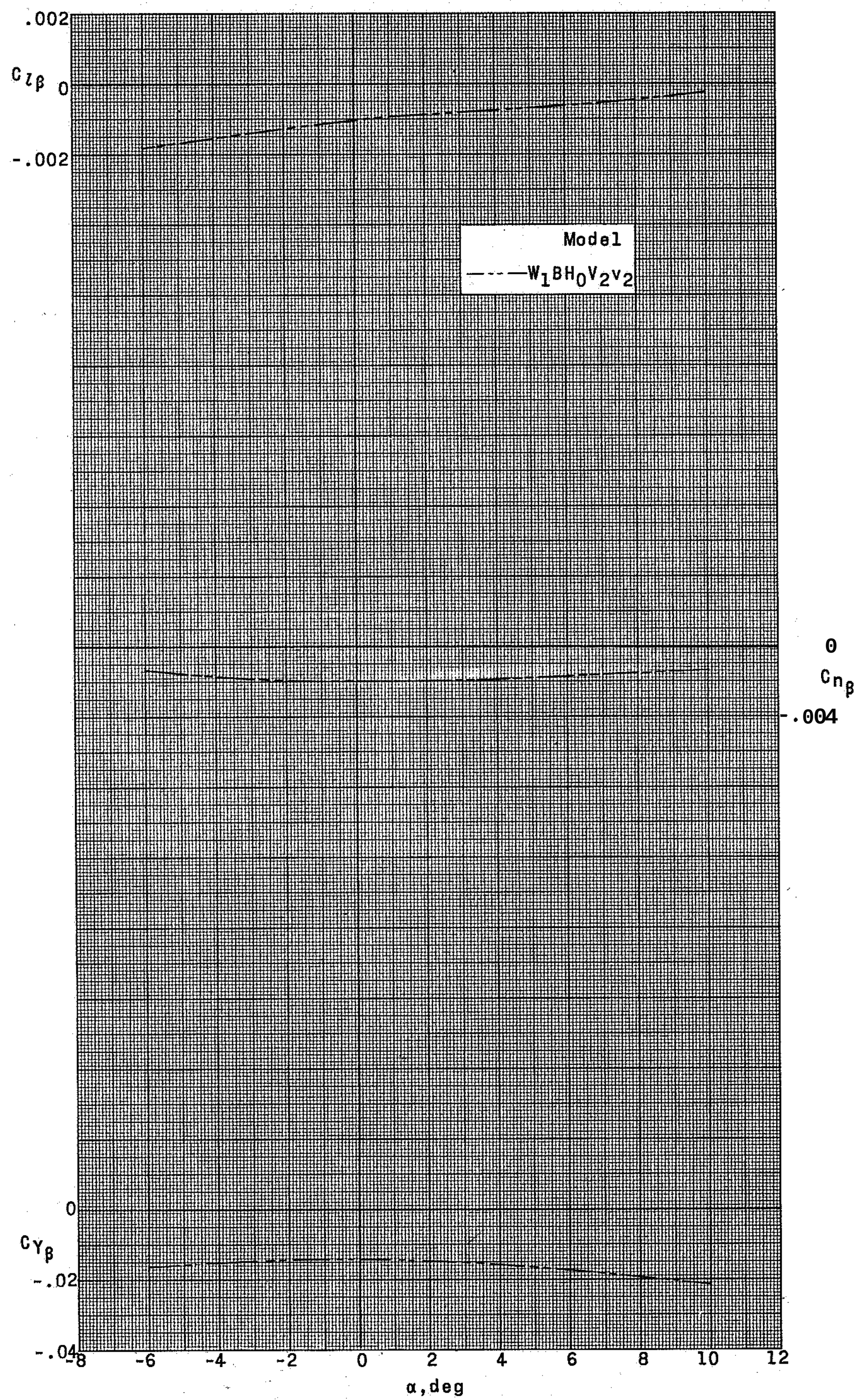

(d) M = 2.87.

Figure 25.- Concluded.

L-355

L-355

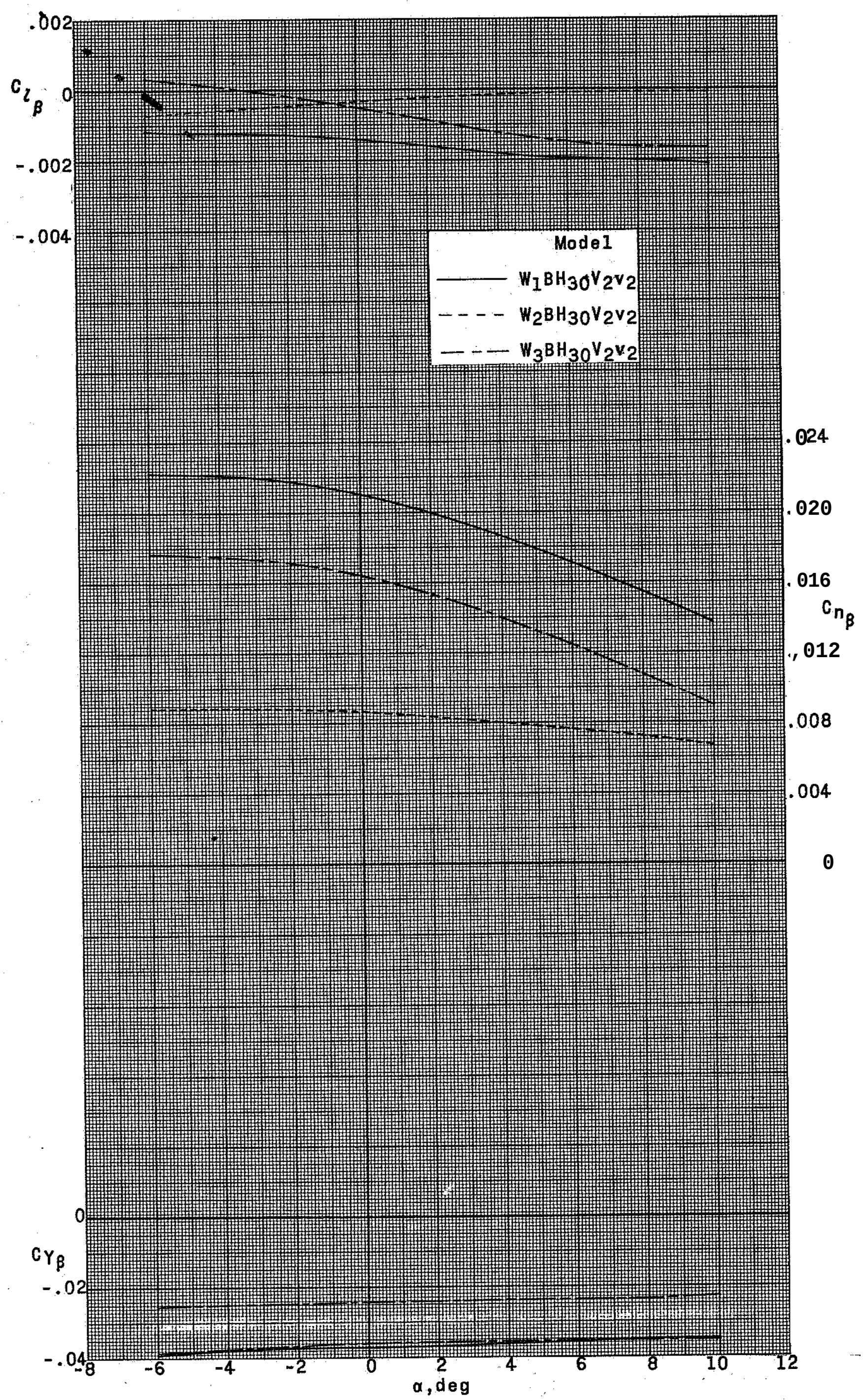

(a) M = 1.57.

Figure 26.- Summary of lateral stability characteristics of a supersonic horizontal-attitude VTOL airplane model as affected by various positions of nacelle.

[redacted]

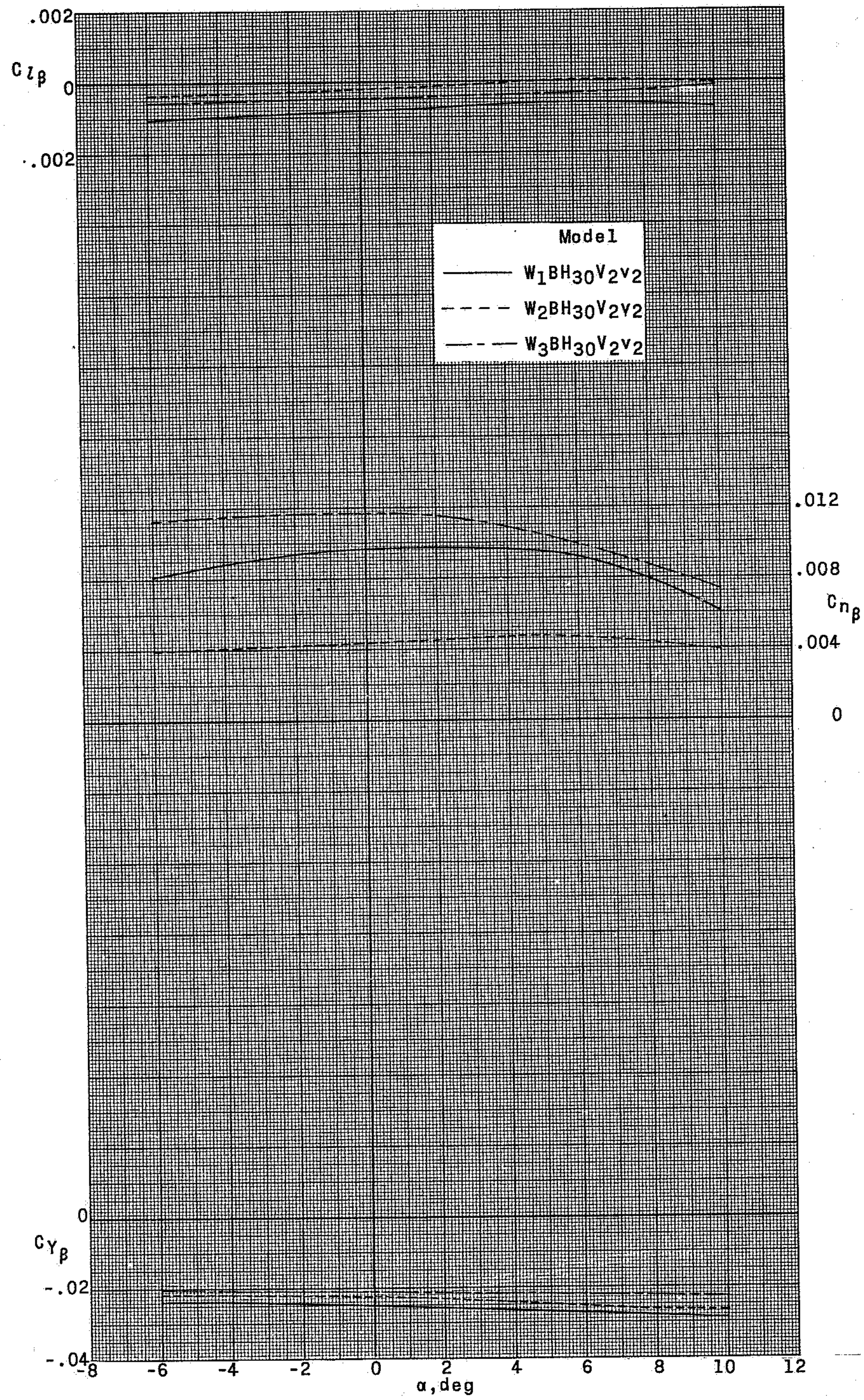

(b) M = 2.14.

Figure 26.- Continued.

[redacted]

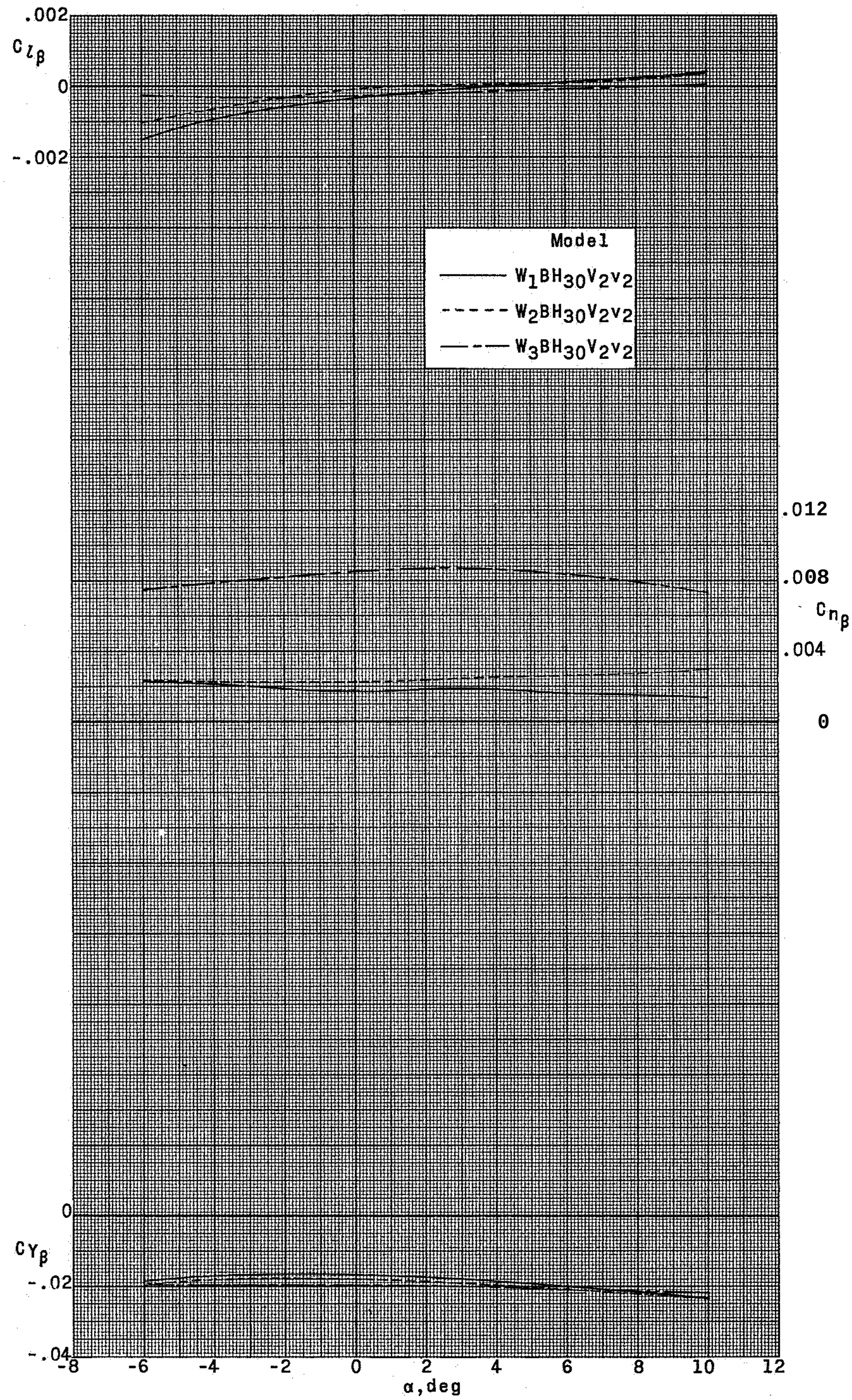

(c) M = 2.54.

Figure 26. - Concluded.

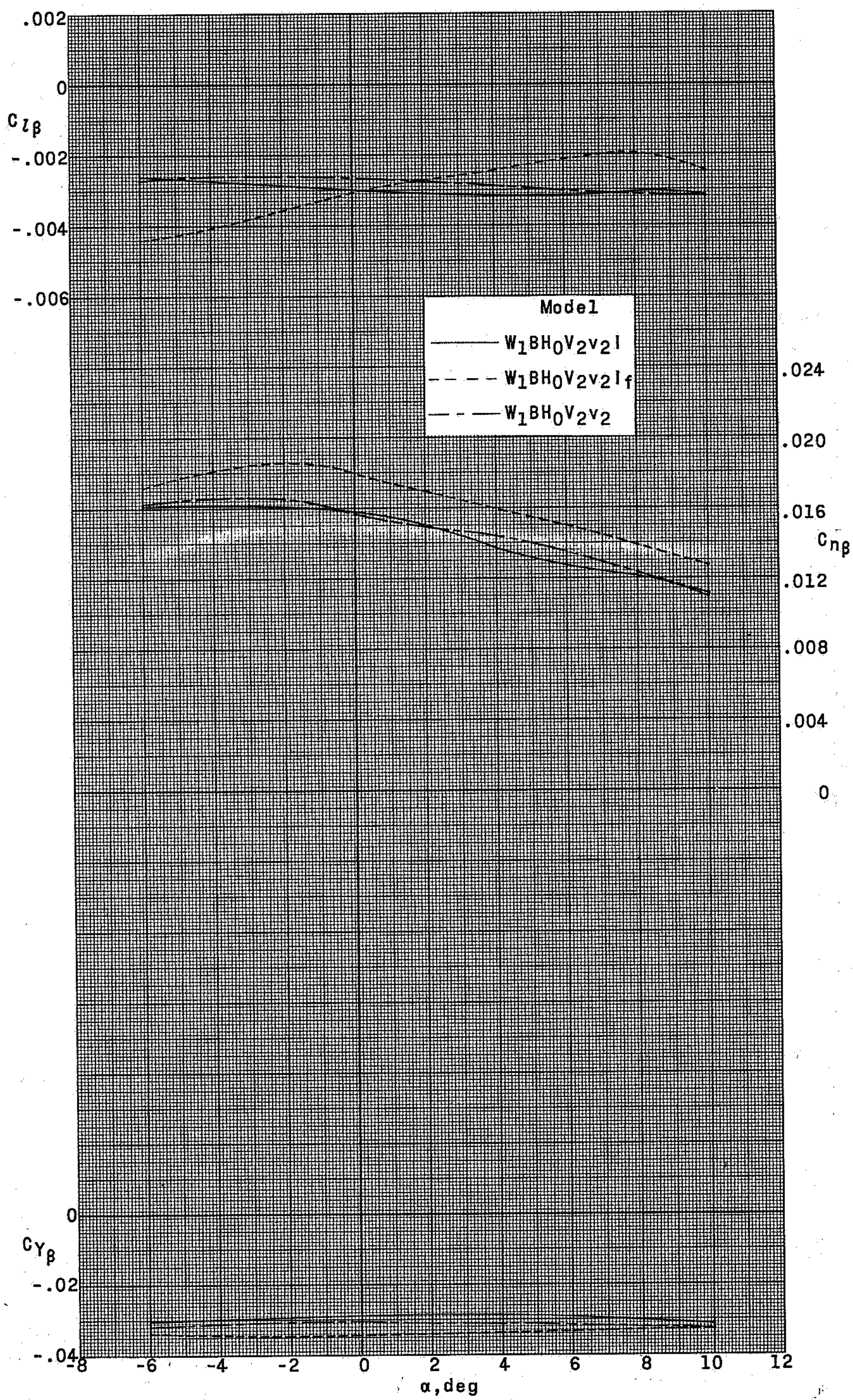

(a) M = 1.57.

Figure 27.- Summary of lateral stability characteristics of a supersonic horizontal-attitude VTOL airplane model as affected by inlet conditions.

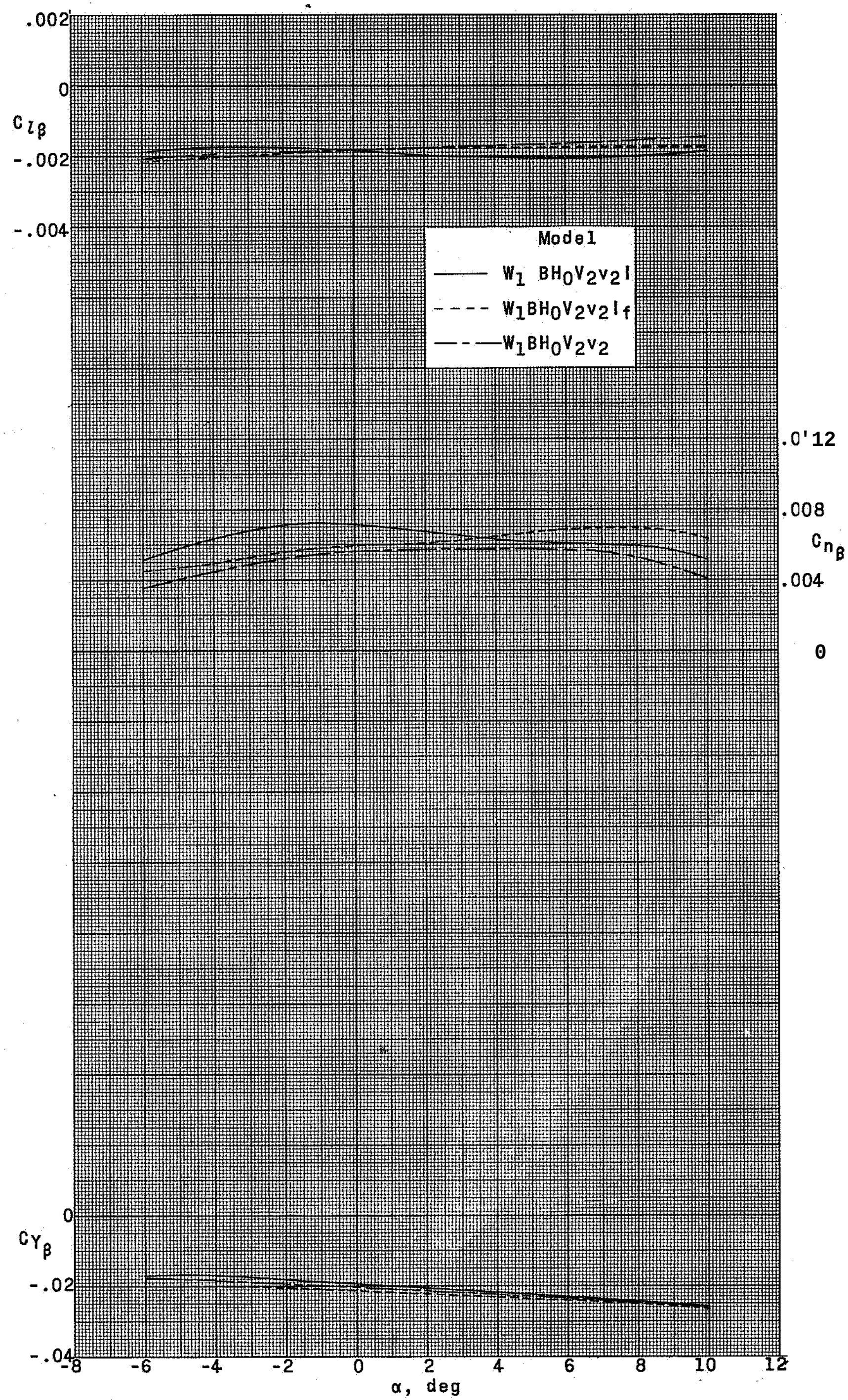

(b) M = 2.14.

Figure 27.- Continued.

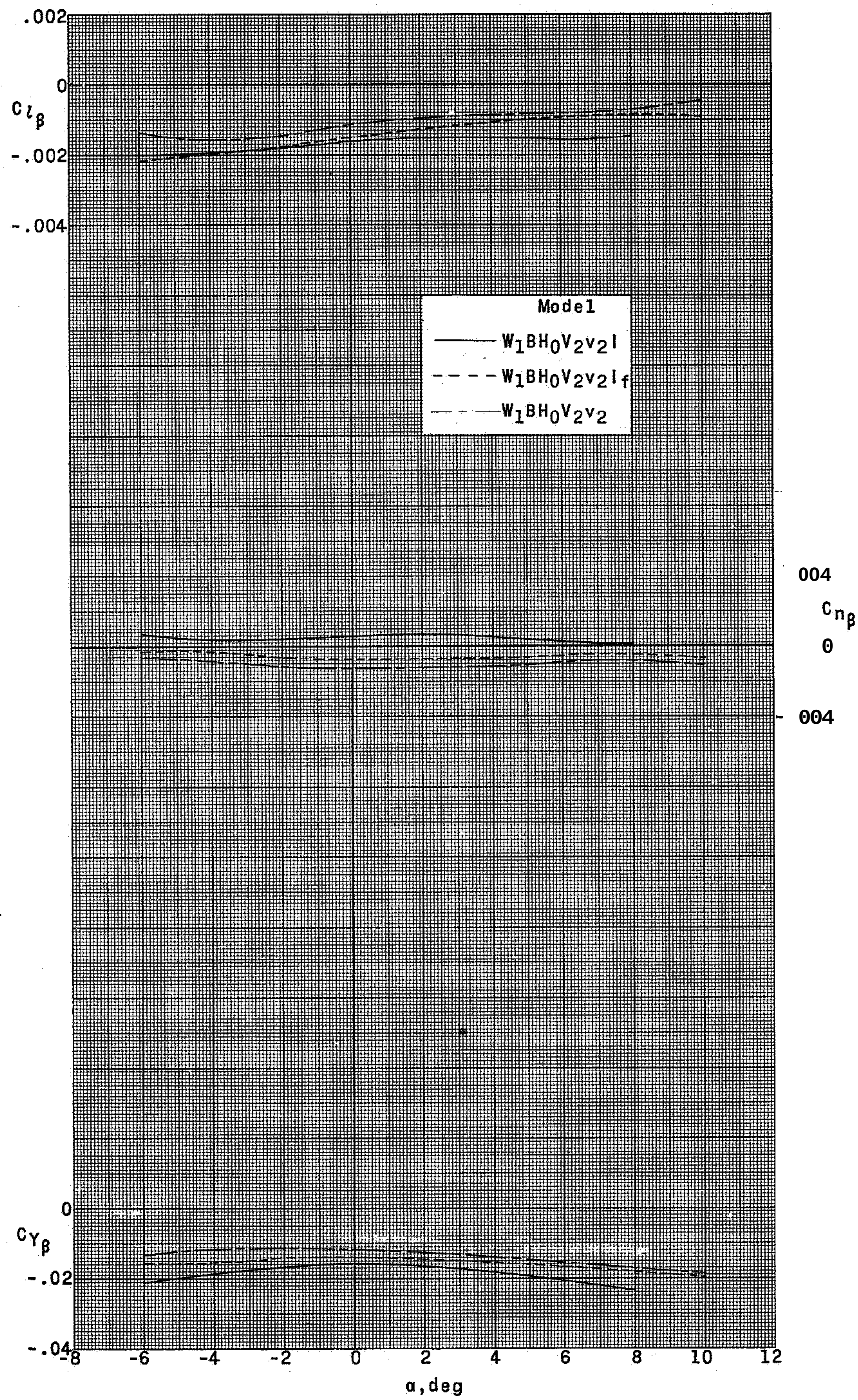

(c) M = 2.54.

Figure 27.- **Continued.**

L-355

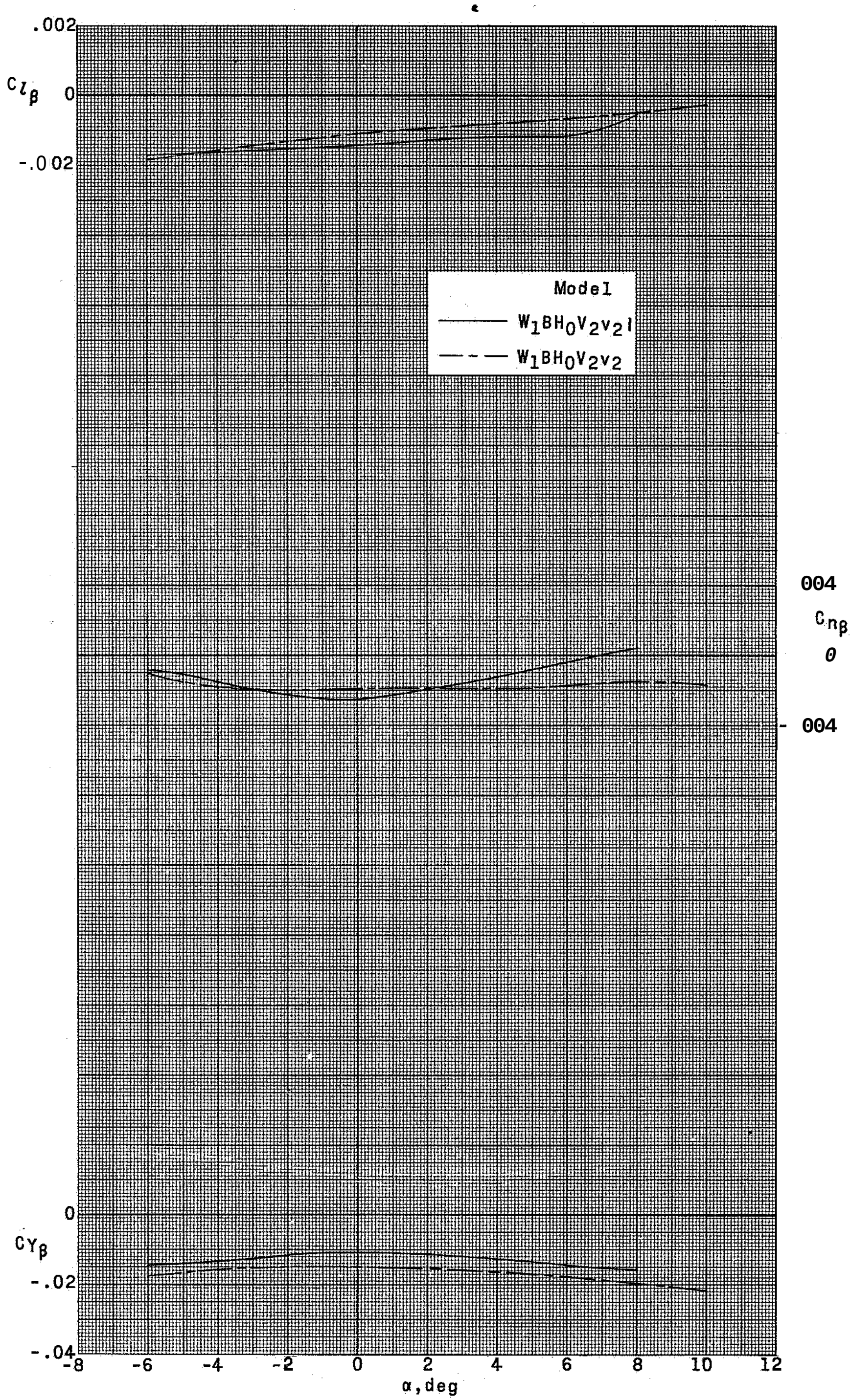

(d) M = 2.87.

Figure 27.- Concluded.

[redacted]

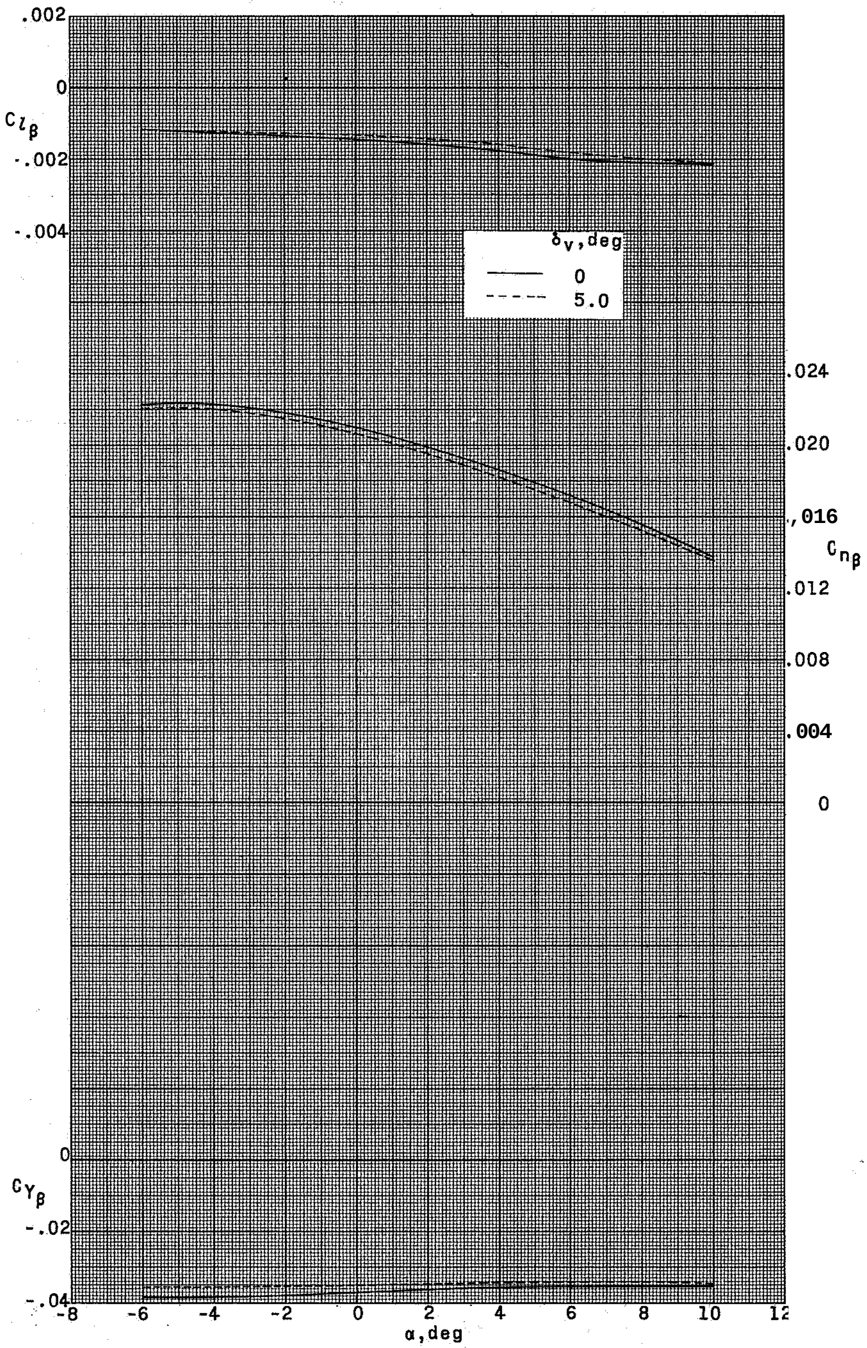

(a) M = 1.57.

Figure 28.- Summary of lateral stability characteristics of a supersonic horizontal-attitude VTOL airplane model as affected by vertical-tail deflection. $W_1BH_{30}V_2v_2$ configuration.

L-355

L-355

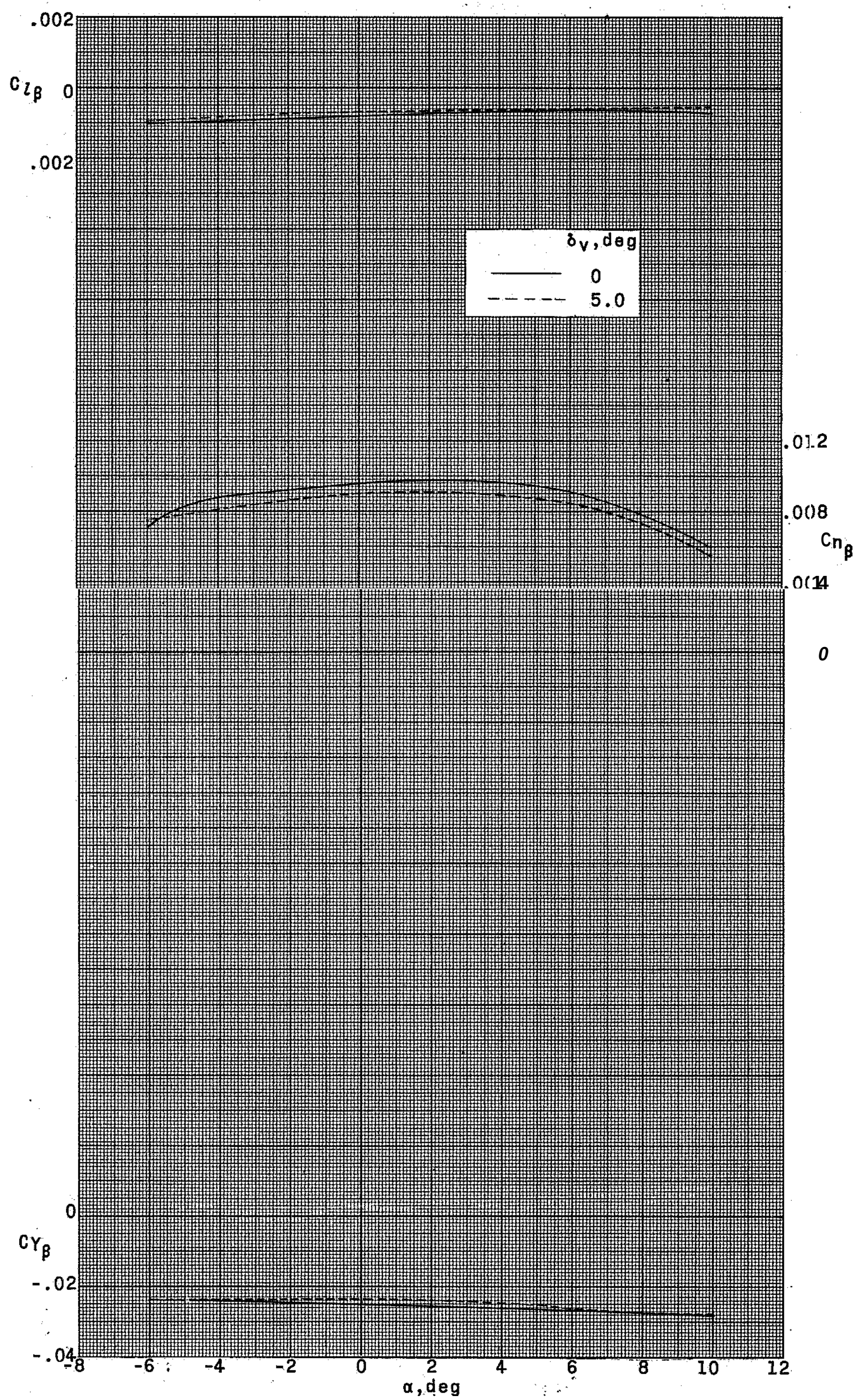

(b) M = 2.14.

Figure 28.- Continued.

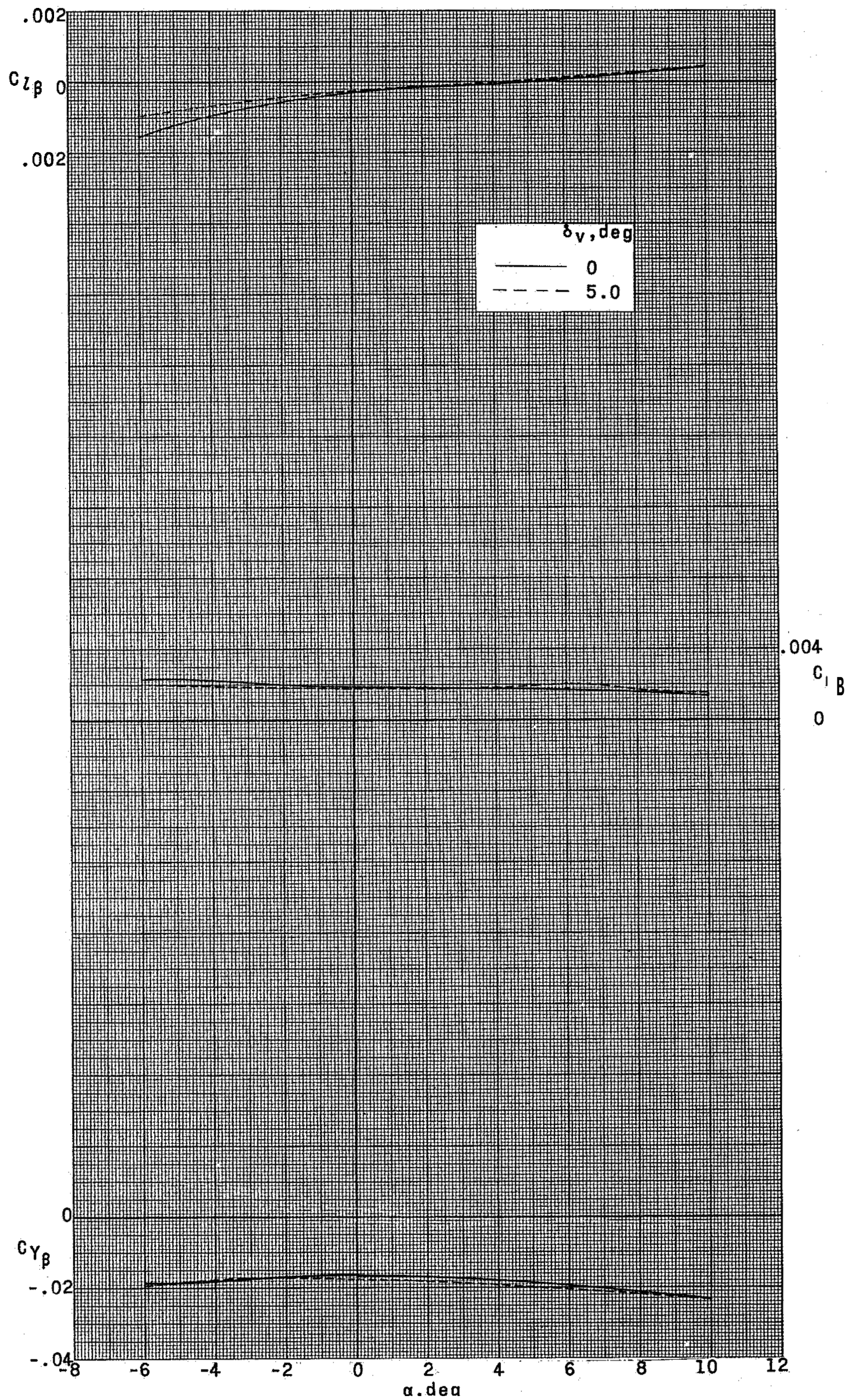

(c) M = 2.54.

Figure 28.- Concluded.

L-355

L-355

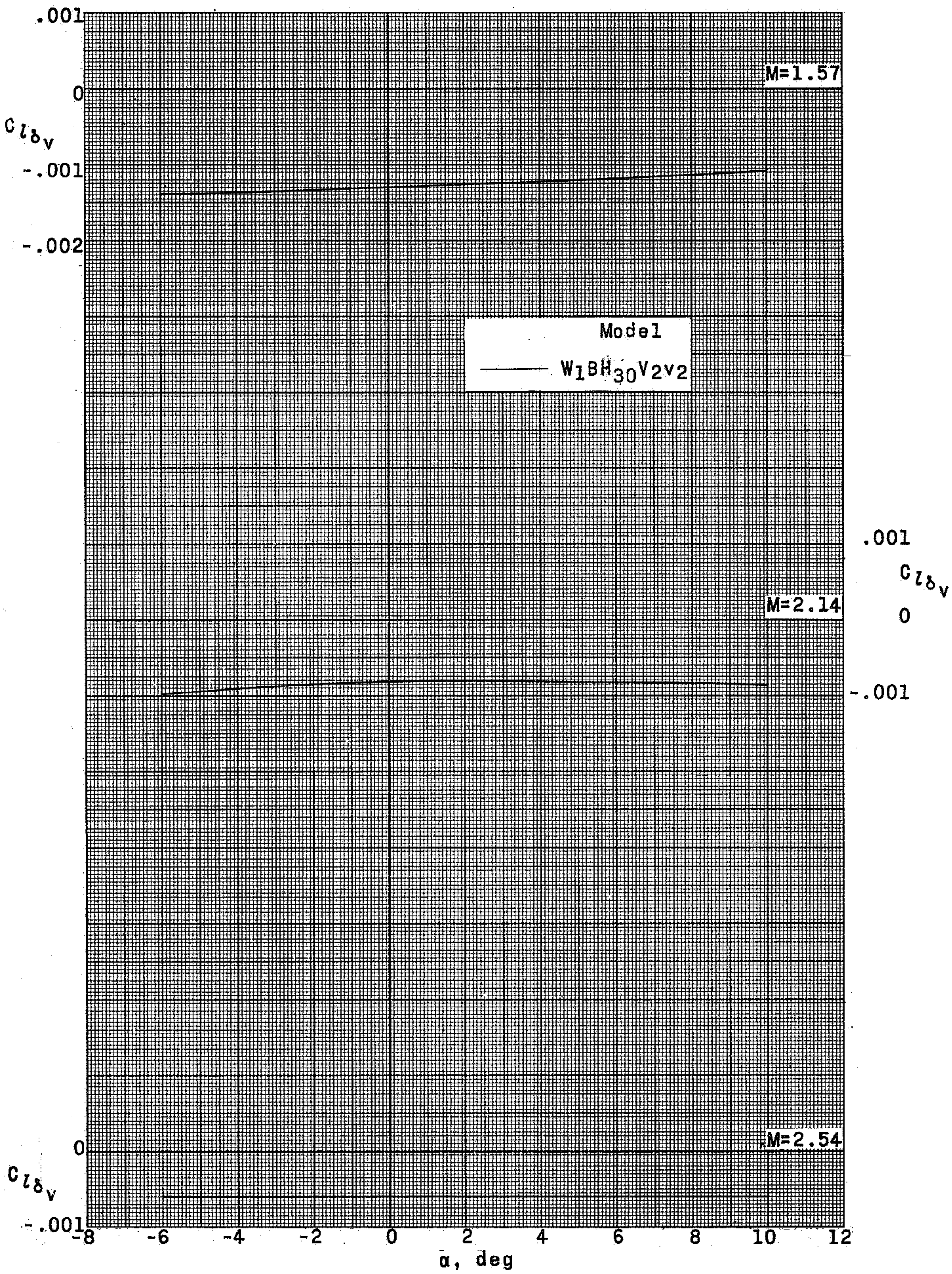

Figure 29.- Summary of vertical-tail control characteristics of a supersonic horizontal-attitude VTOL airplane model.

[redacted]

[redacted]

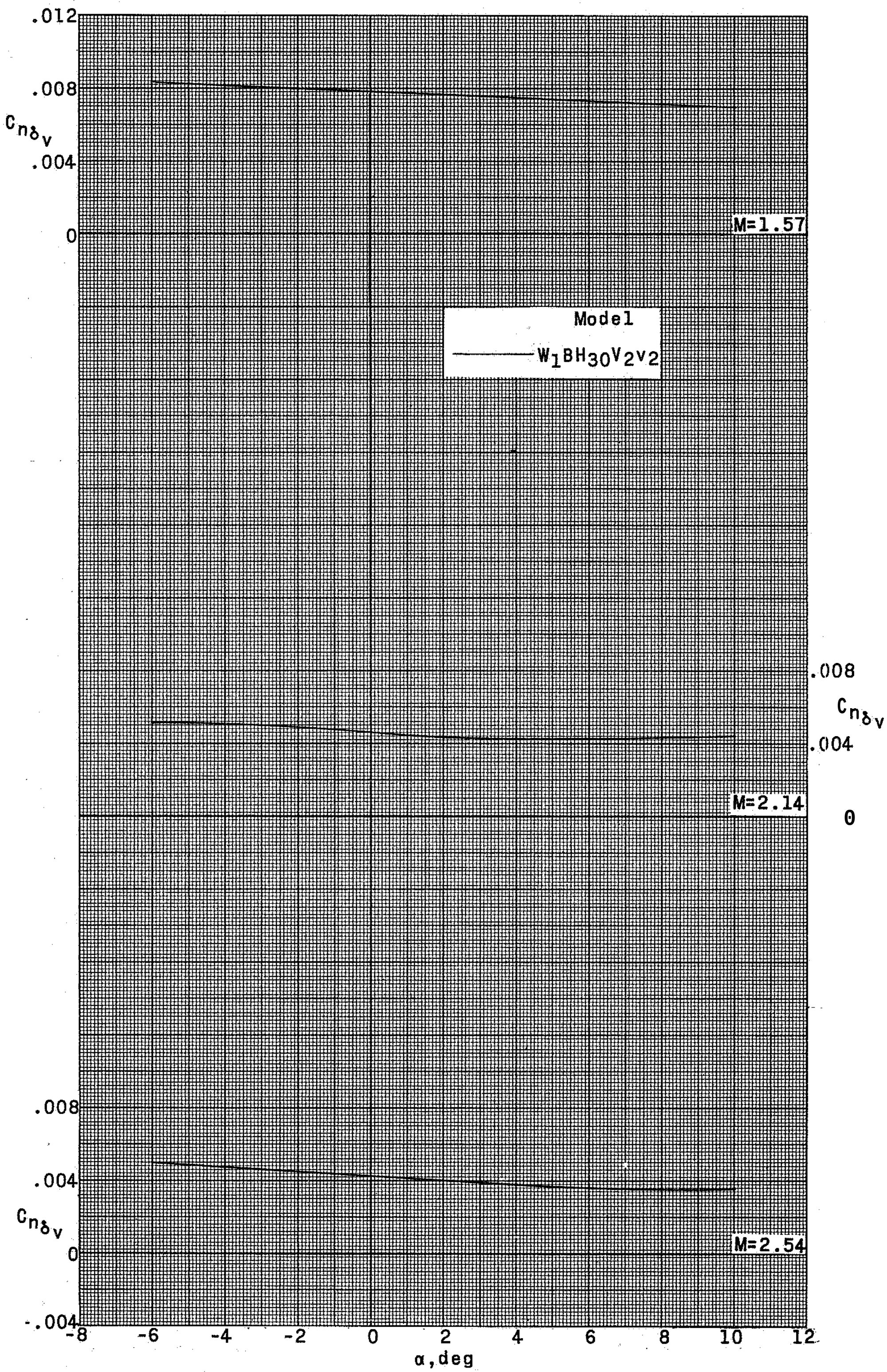

Figure 29.- Concluded.

L-355

[redacted]

L-355

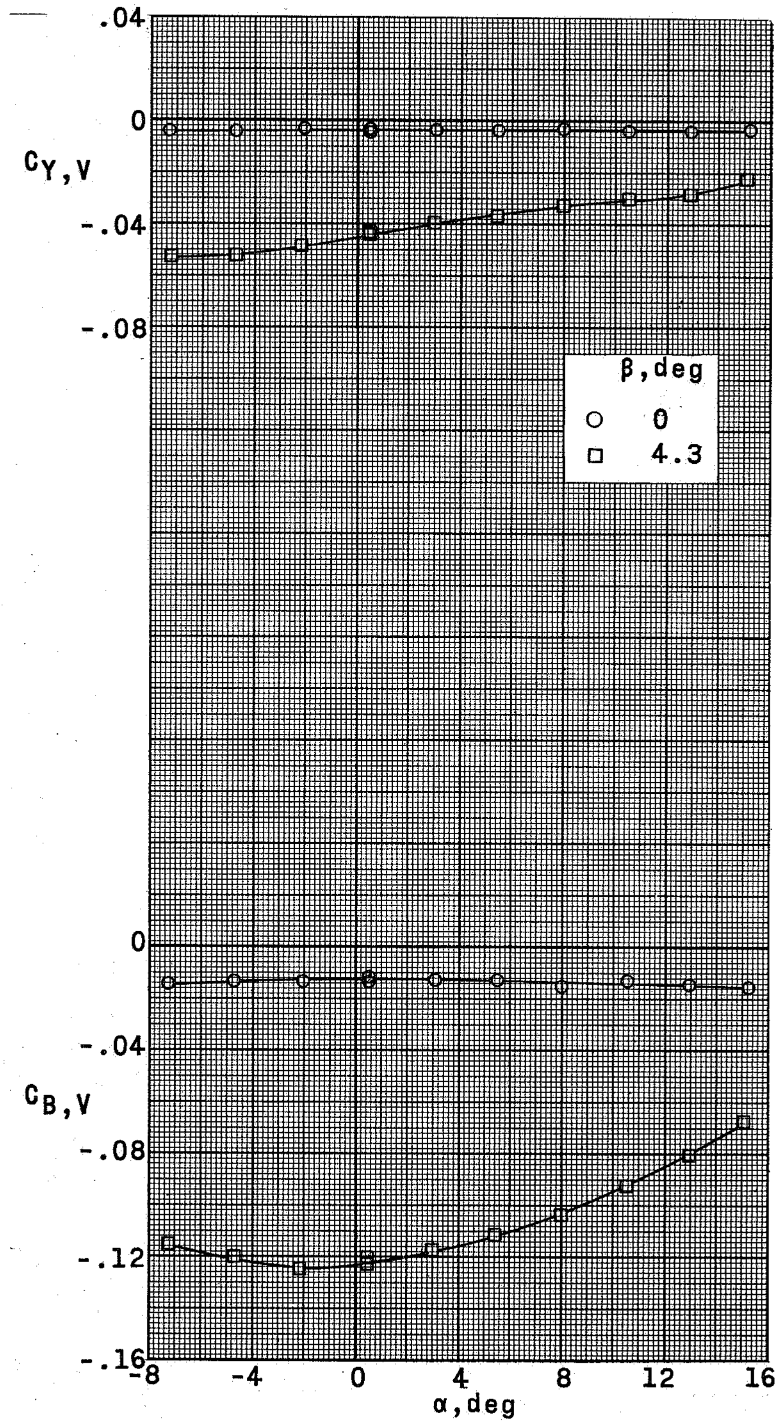

(a) M = 1.57.

Figure 30.- Loading characteristics of the vertical tail of a supersonic horizontal-attitude VTOL airplane model. $W_1BH_0V_2v_2$ configuration; $\delta_V = 0$.

[redacted]

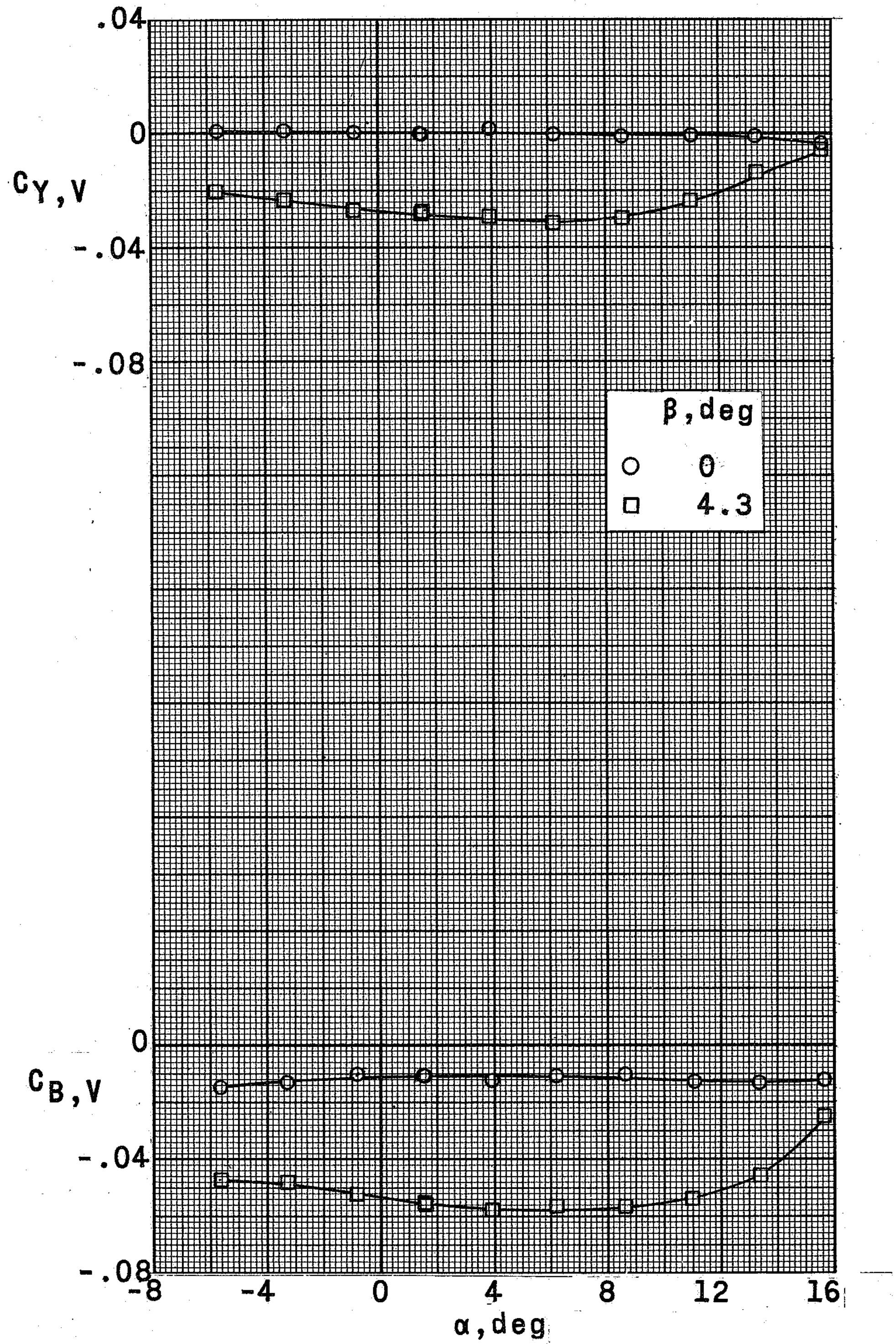

(b) M = 2.14.

Figure 30.- Continued.

L-355

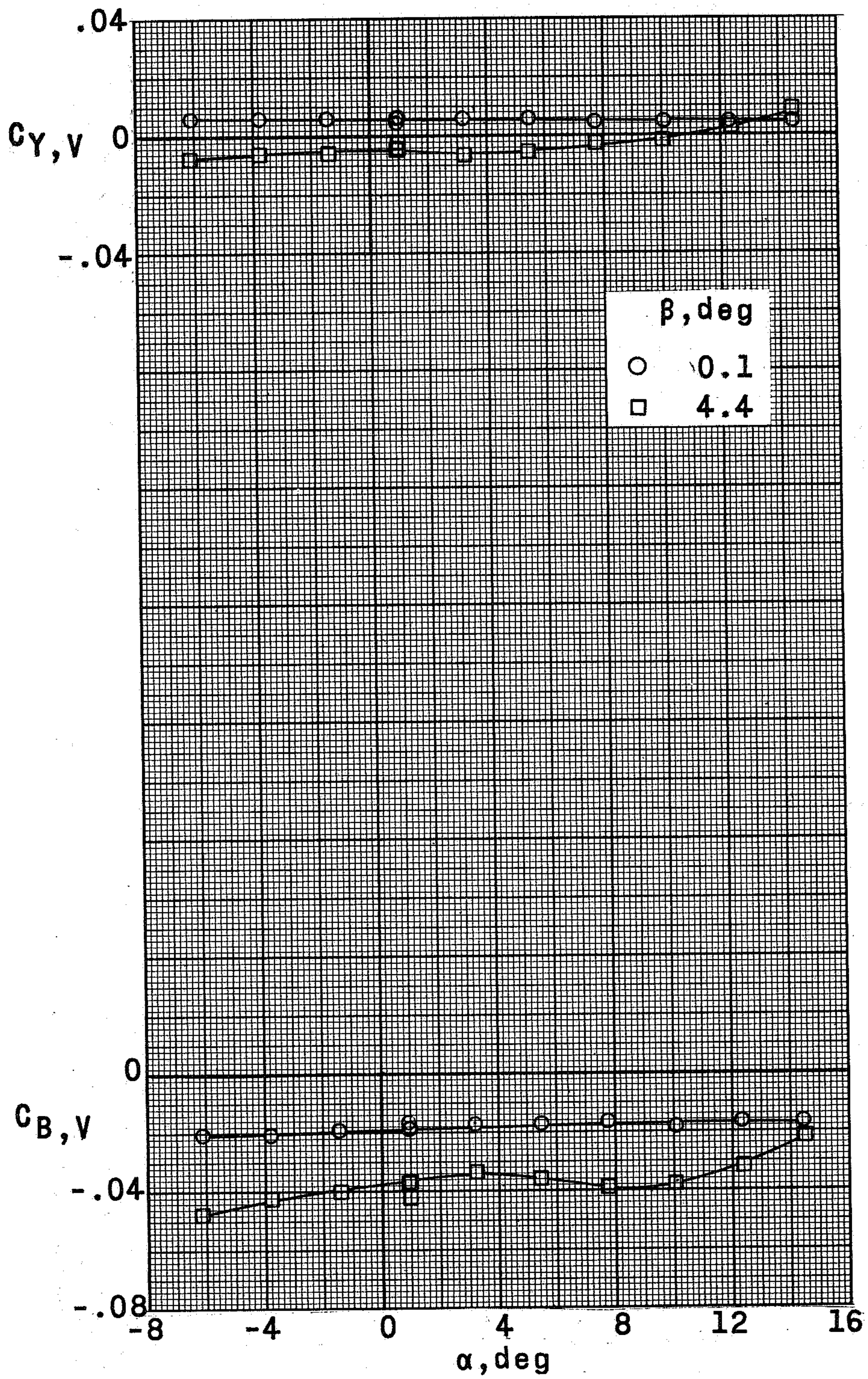

(c) M = 2.54.

Figure 30.- Continued.

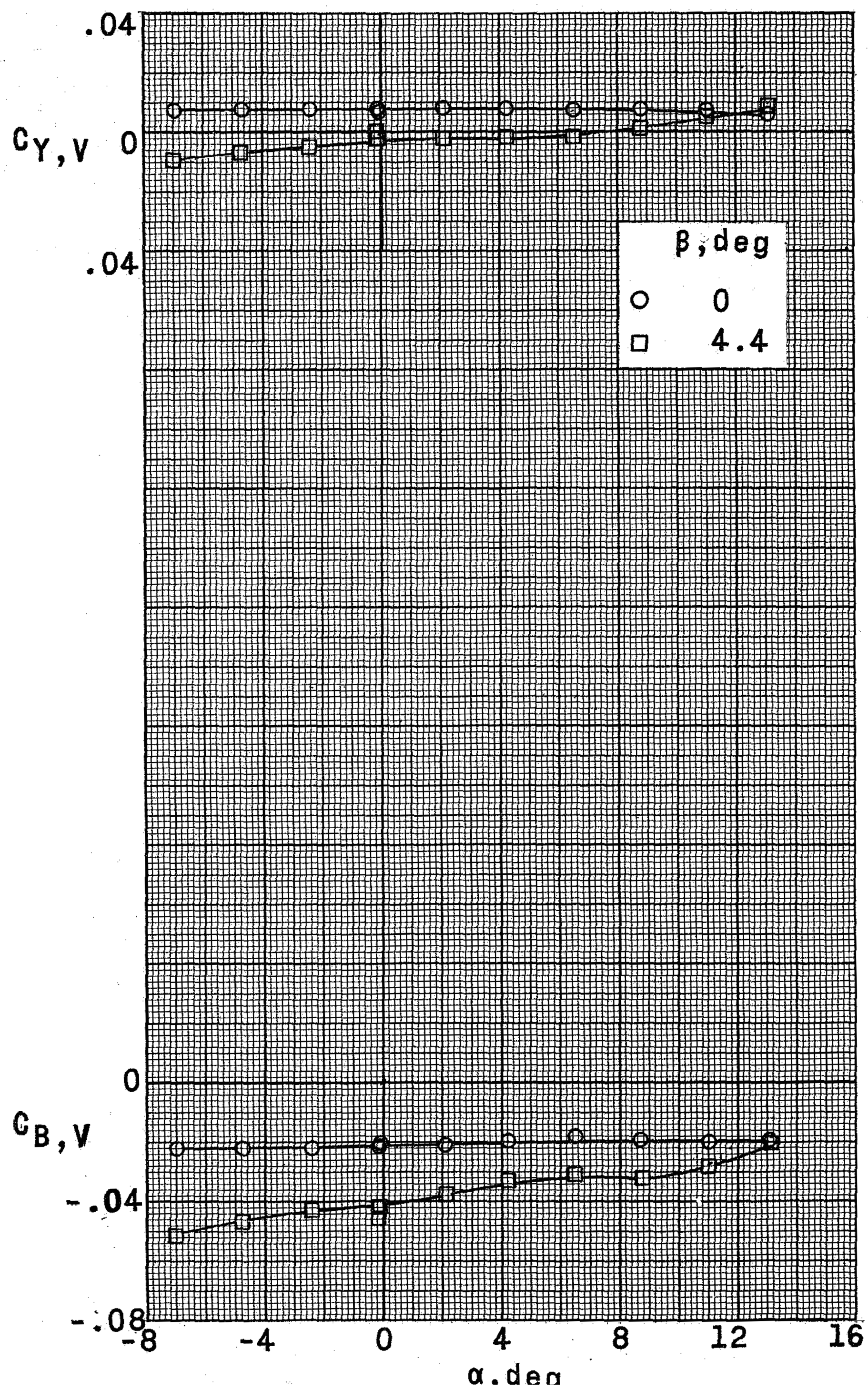

(d) M = 2.87.

Figure 30.- Concluded.

L-355

[redacted]

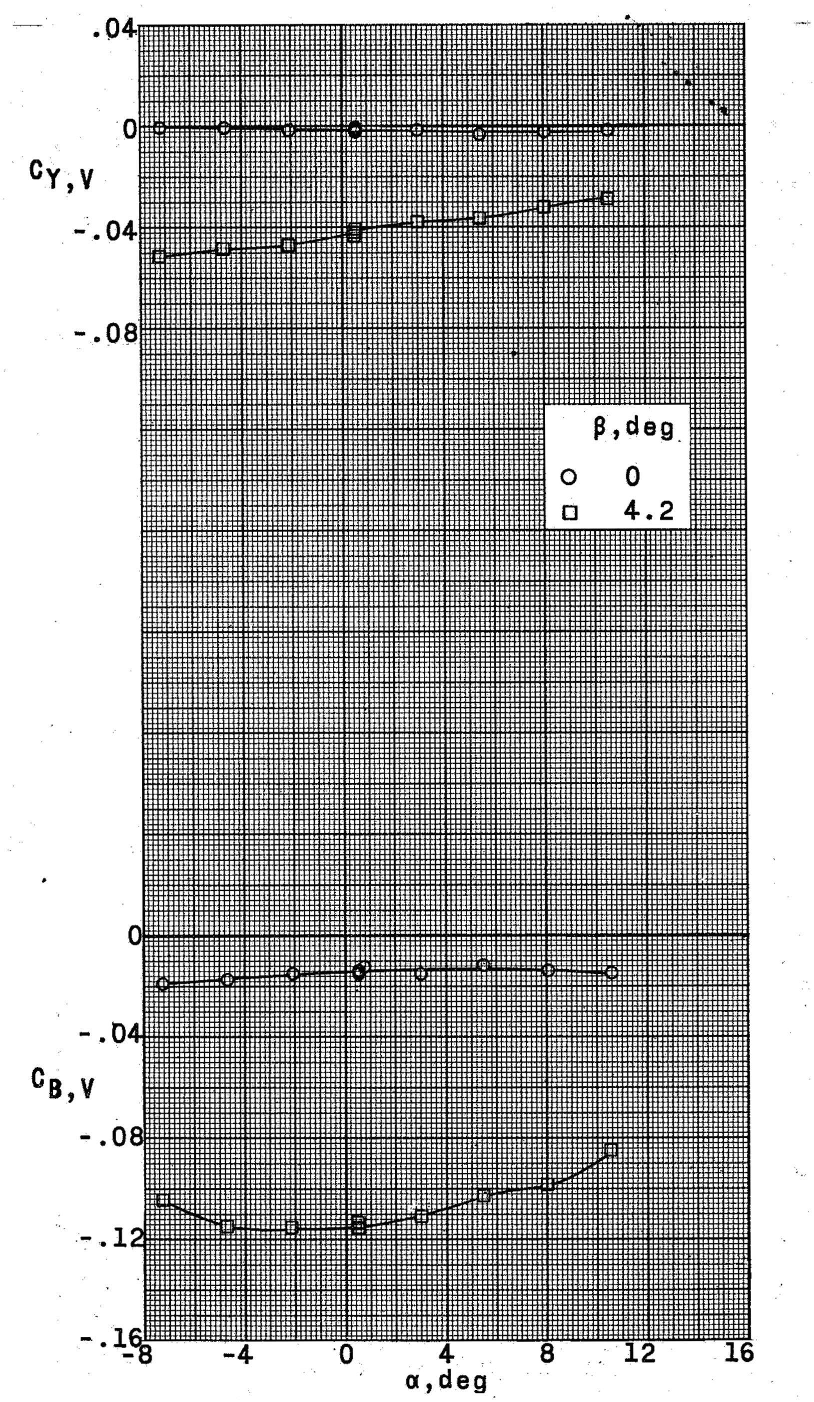

(a) $M = 1.57$.

Figure 31.- Loading characteristics of the vertical tail of a supersonic horizontal-attitude VTOL airplane model. $W_1BH_0V_2$ configuration; $\delta_V = 0$.

[redacted]

[redacted]

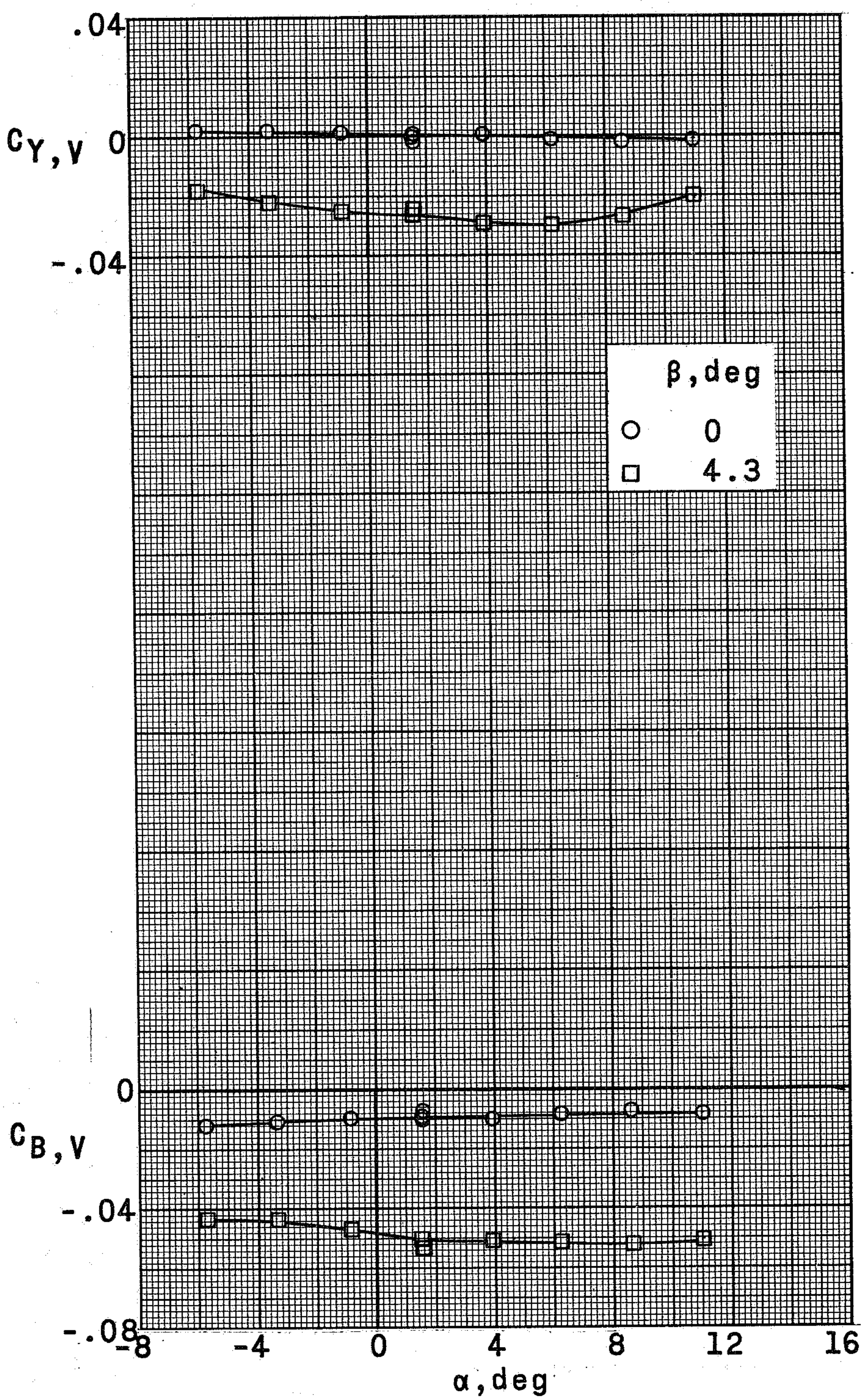

(b) M = 2.14.

Figure 31.- Continued.

[redacted]

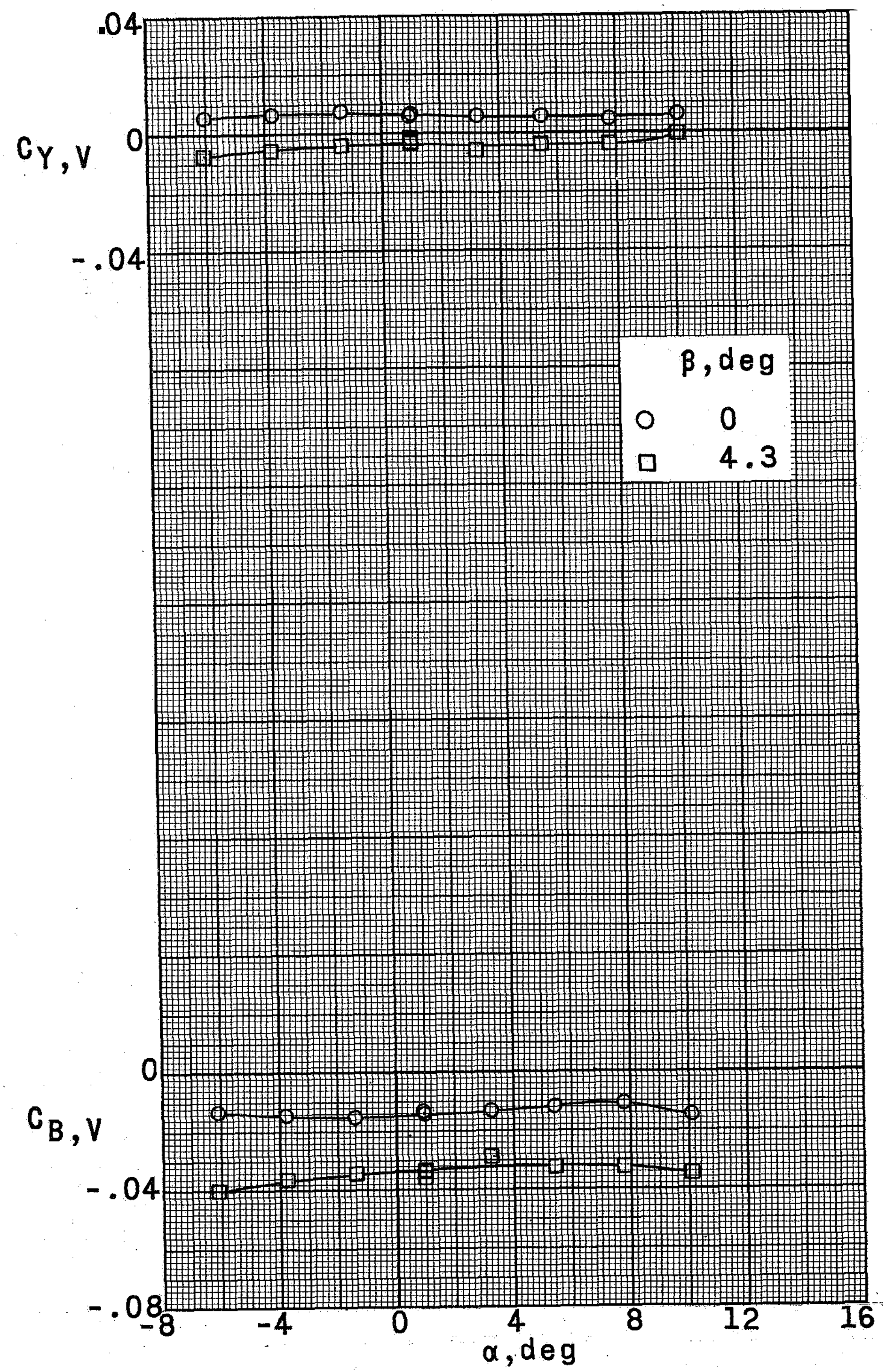

(c) M = 2.54.

Figure 31.- Concluded.

[redacted]

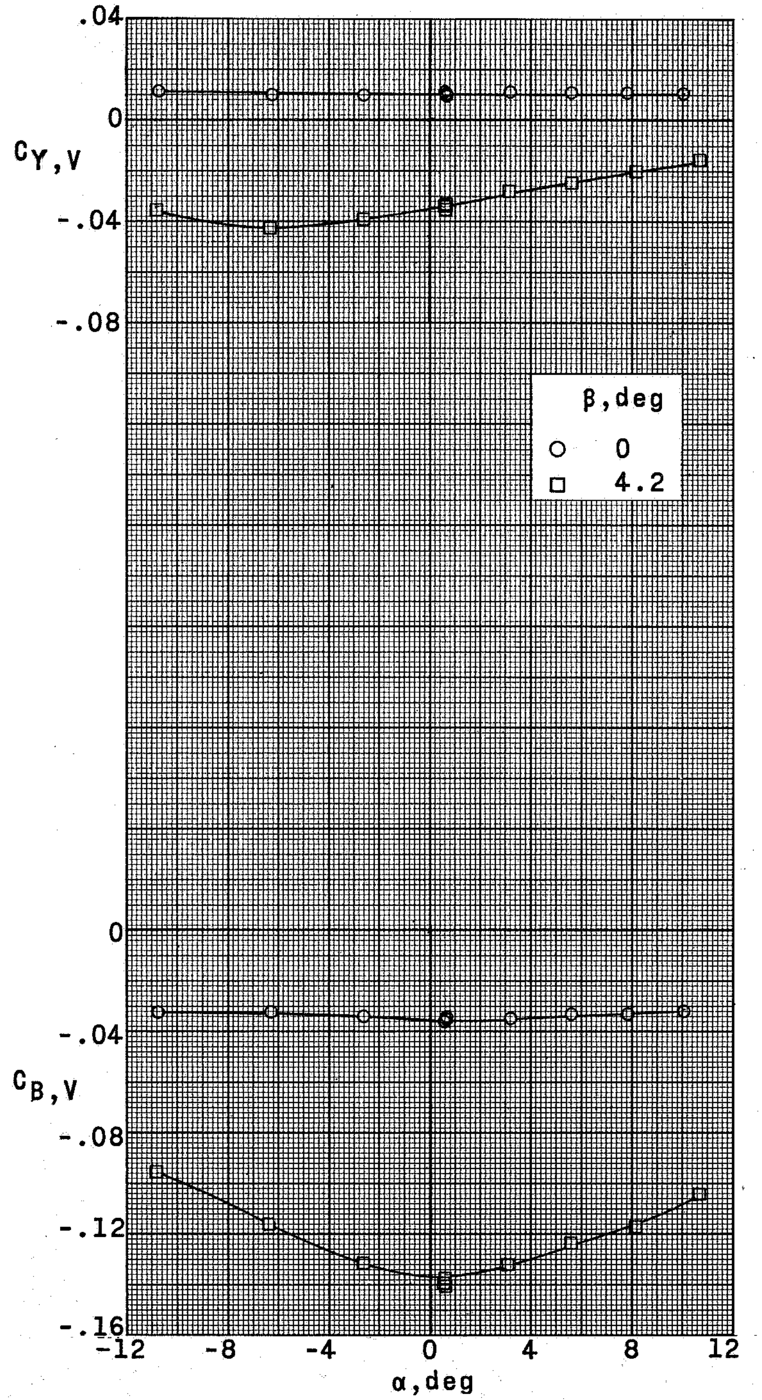

(a) M = 1.57.

Figure 32.- Loading characteristics of the vertical tail of a supersonic horizontal-attitude VTOL airplane model. $W_1BH_0V_2v_2I$ configuration; $\delta_V = 0$.

L-355

[redacted]

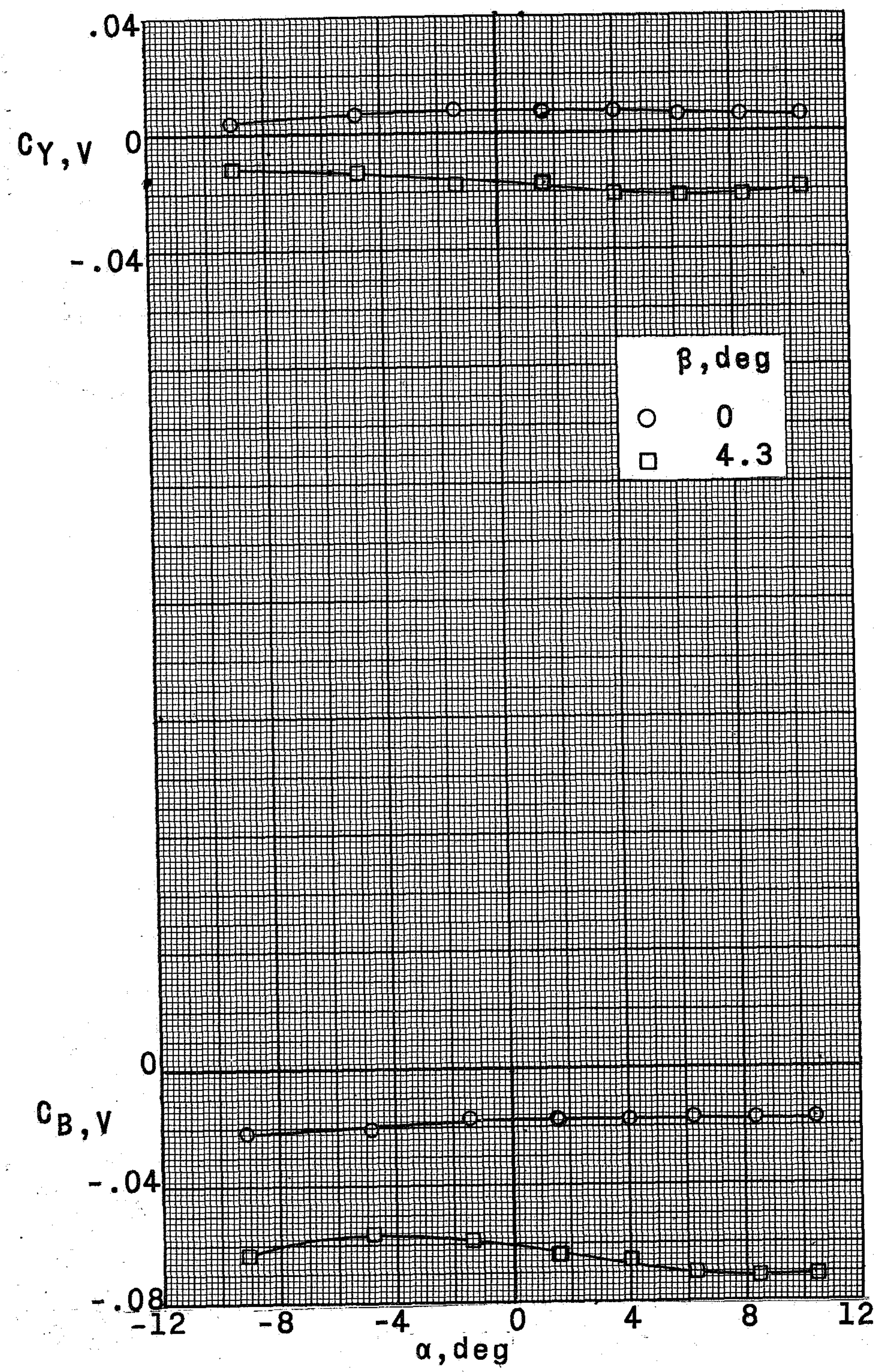

(b) M = 2.14.

Figure 32.- Continued.

[redacted]

[redacted]

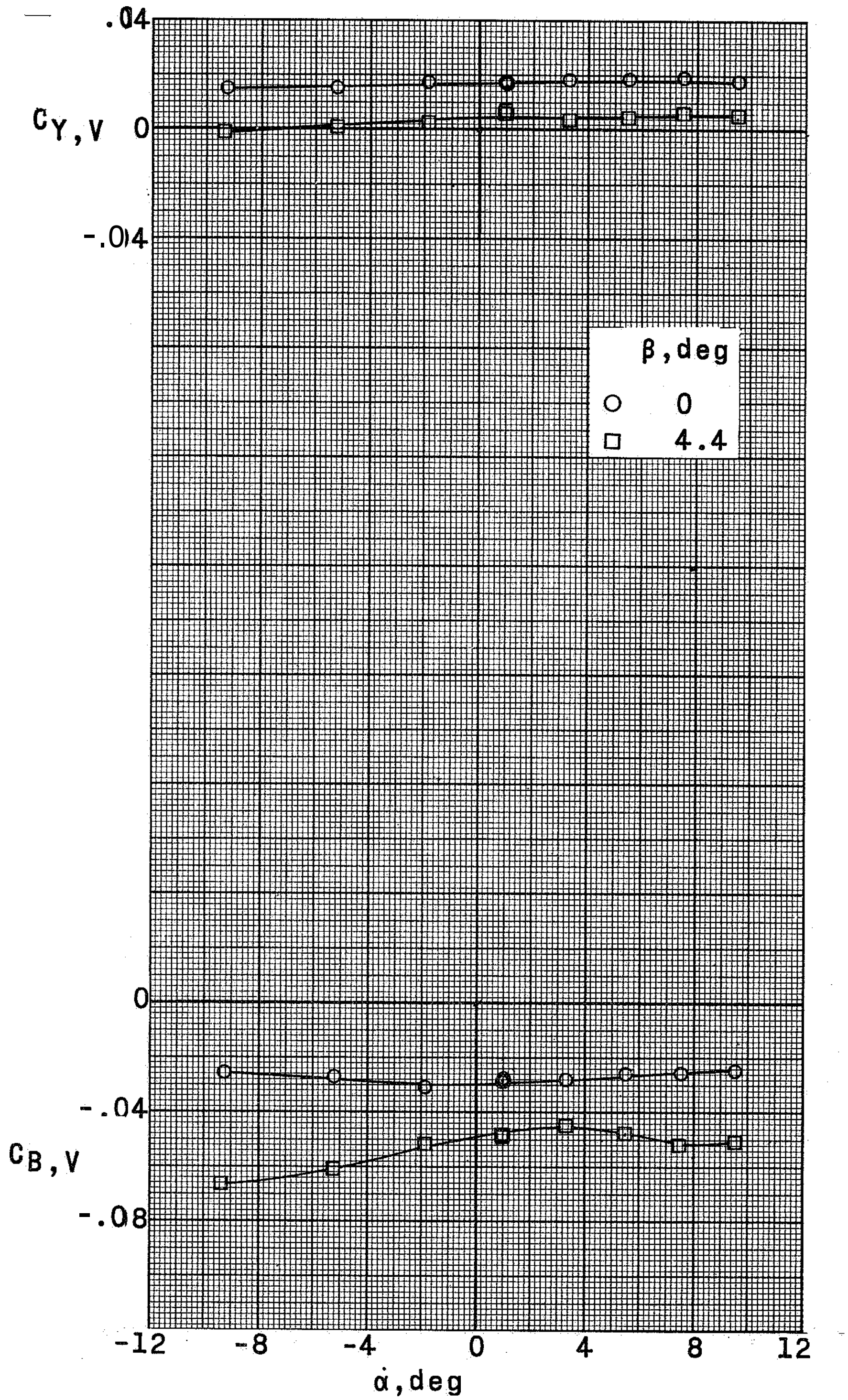

(c) M = 2.54.

Figure 32.- Continued.

[redacted]

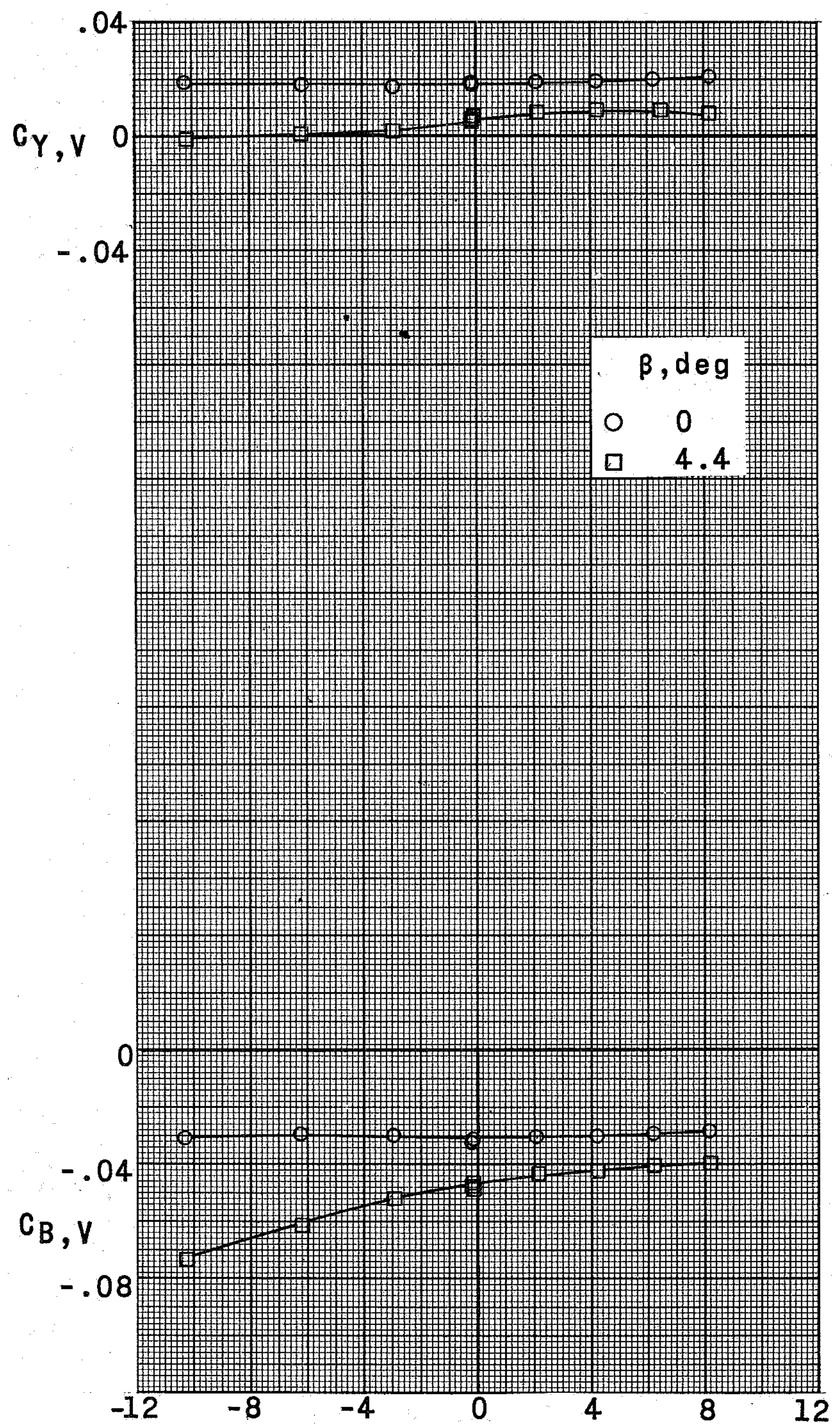

(d) M = 2.87.

Figure 32.- Concluded.

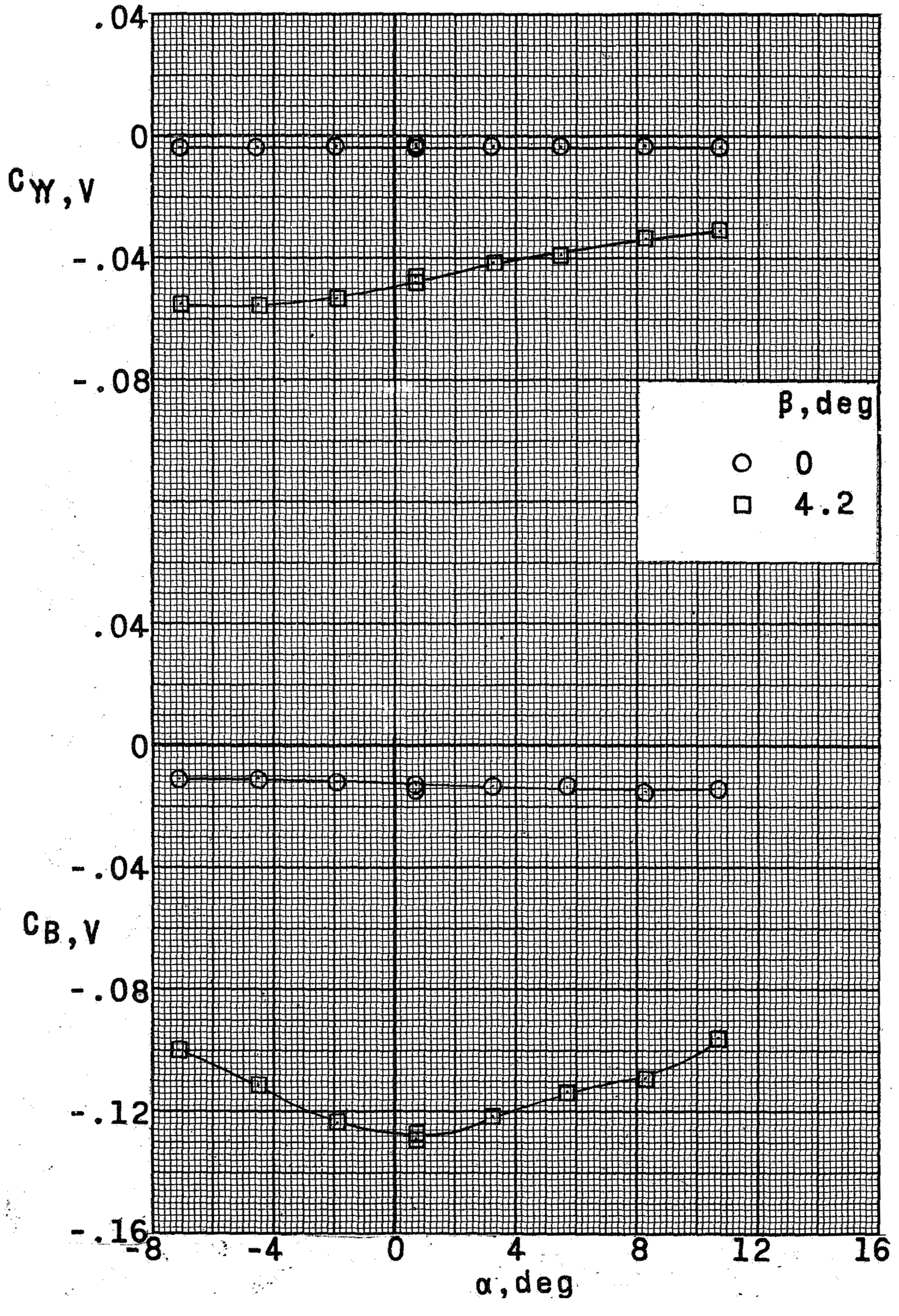

(a) M = 1.57.

L-355

Figure 33.- Loading characteristics of the vertical tail of a supersonic horizontal-attitude VTOL airplane model. $W_1BH_0V_2v_2I_f$ configuration; $\delta_V = 0$.

L-355

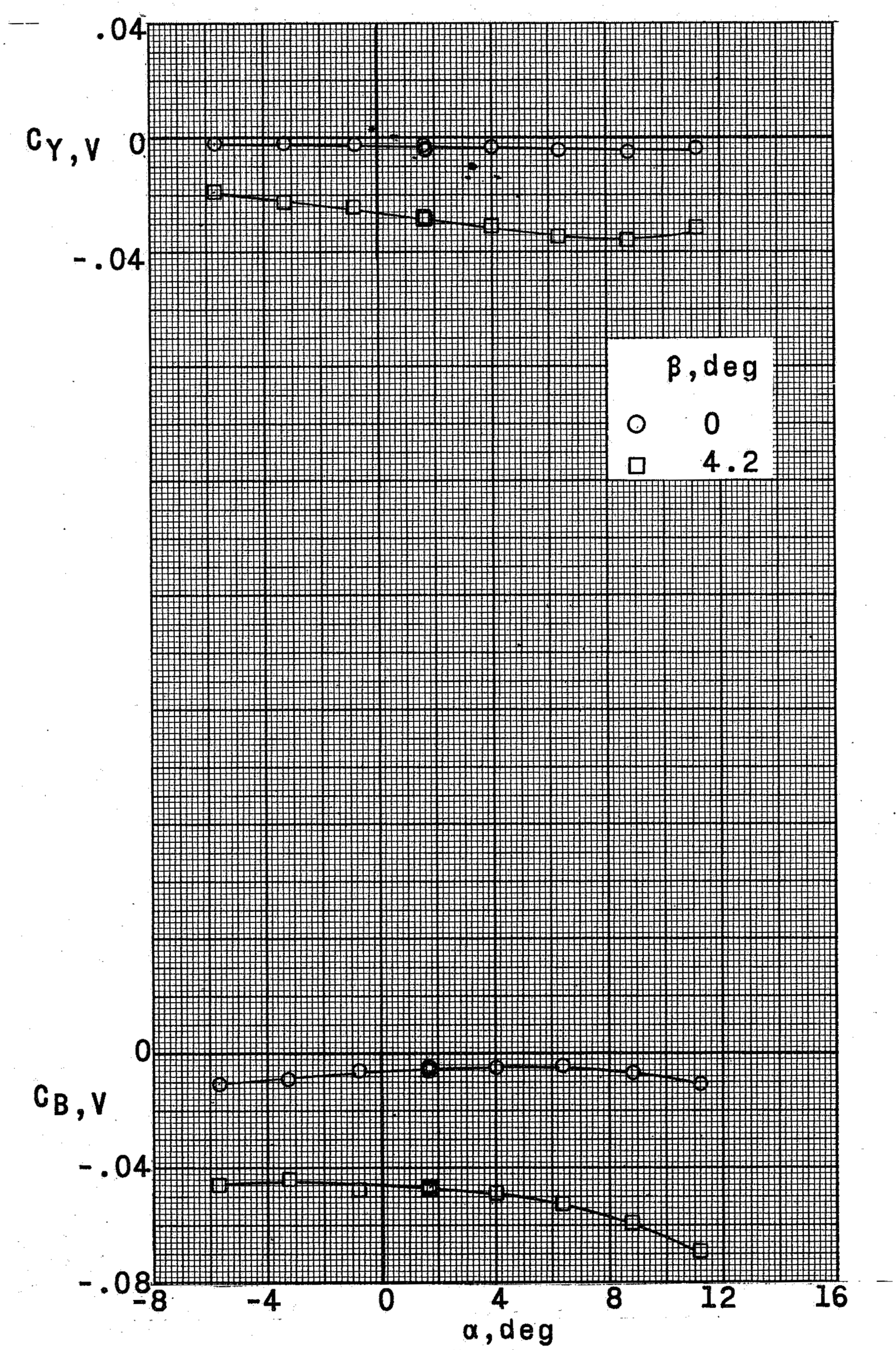

(b) M = 2.14.

Figure 33.- Continued.

[redacted]

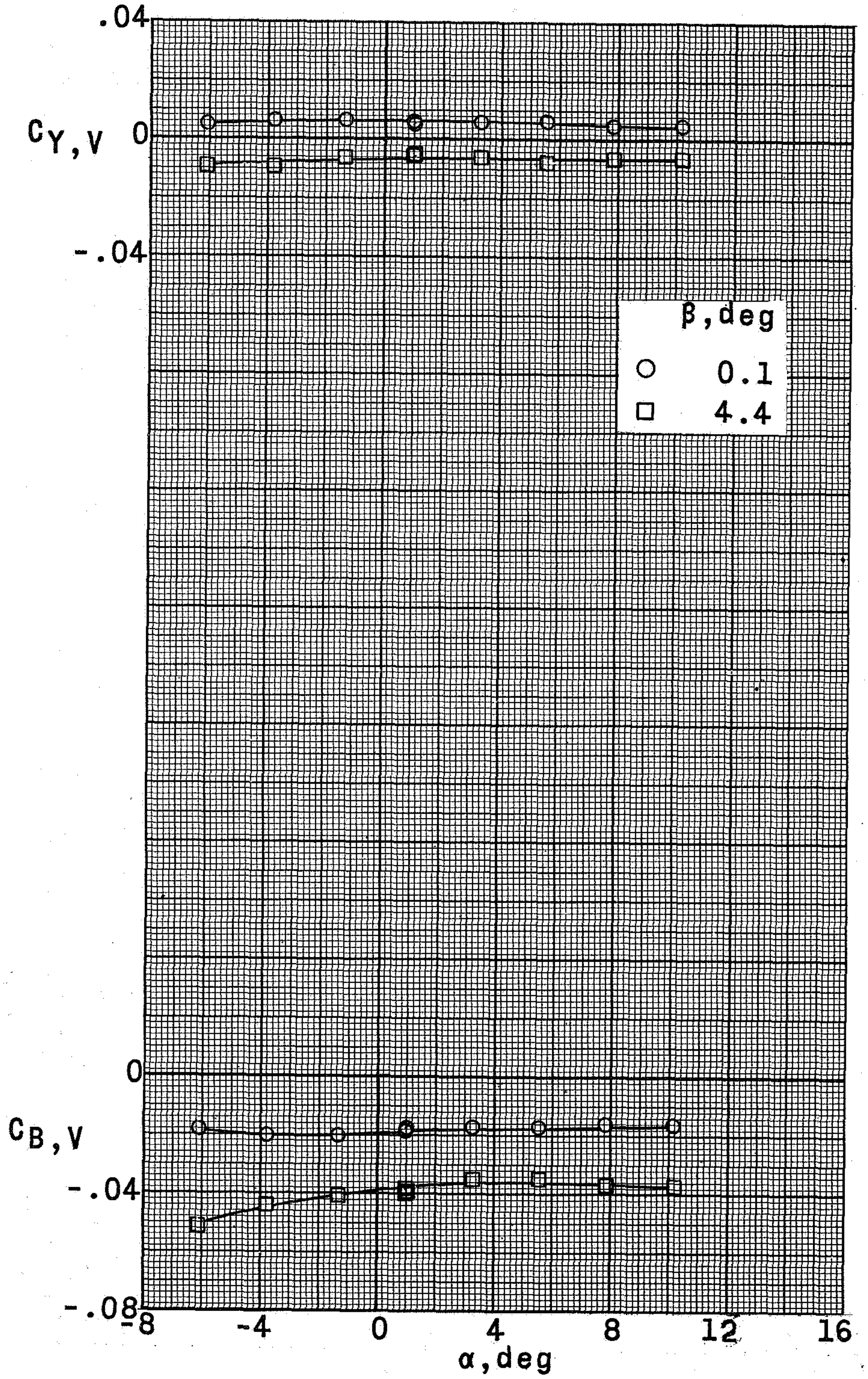

L-355

(c) M = 2.54.

Figure 33.- Concluded.

L-355

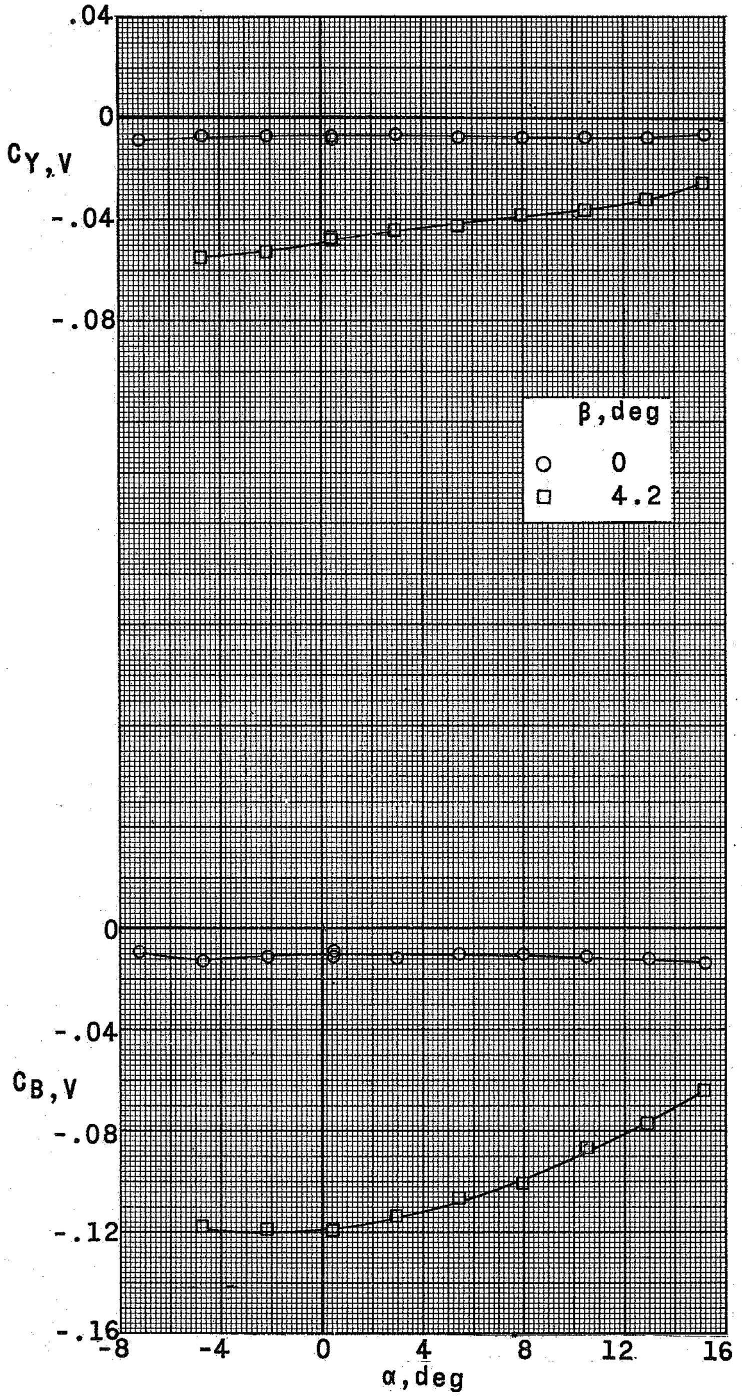

(a) M = 1.57.

Figure 34.- Loading characteristics of the vertical tail of a supersonic horizontal-attitude VTOL airplane model. $W_1BH_{30}V_2v_2$ configuration; $\delta_V = 0$.

[redacted]

[redacted]

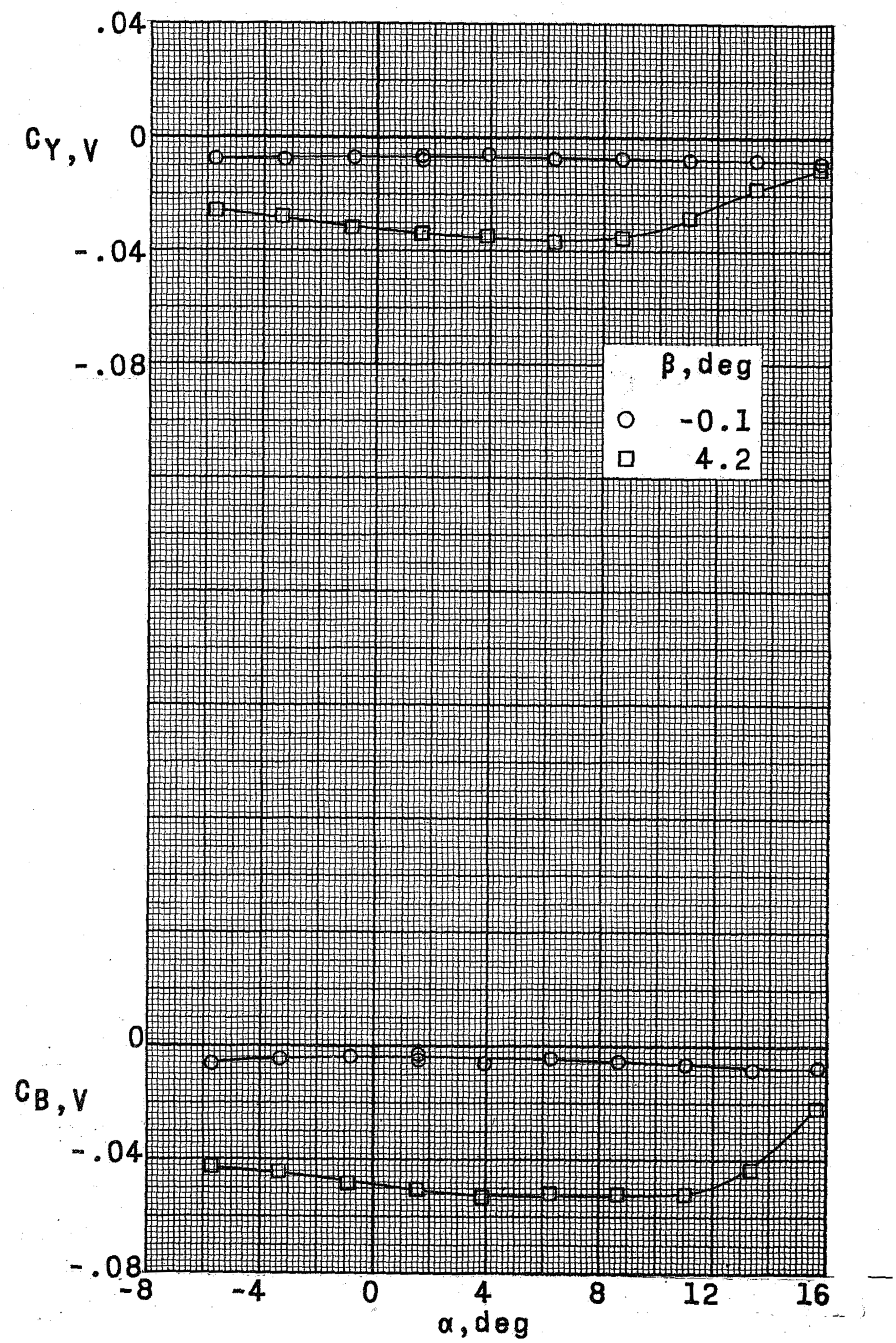

(b) M = 2.14.

Figure 34.- Continued.

L-355

[redacted]

L-355

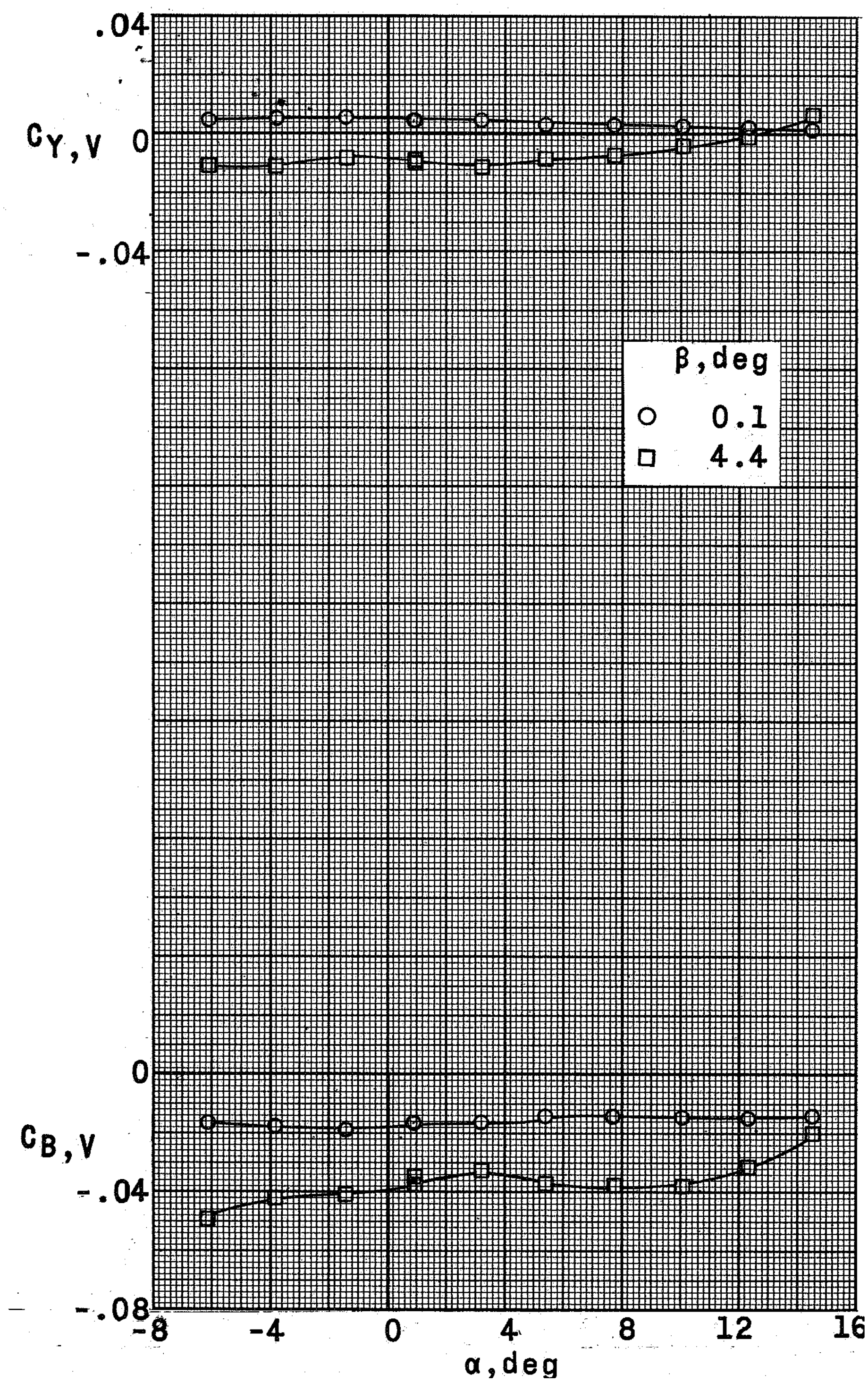

(c) M = 2.54.

Figure 34.- Concluded.

[redacted]

 [redacted]

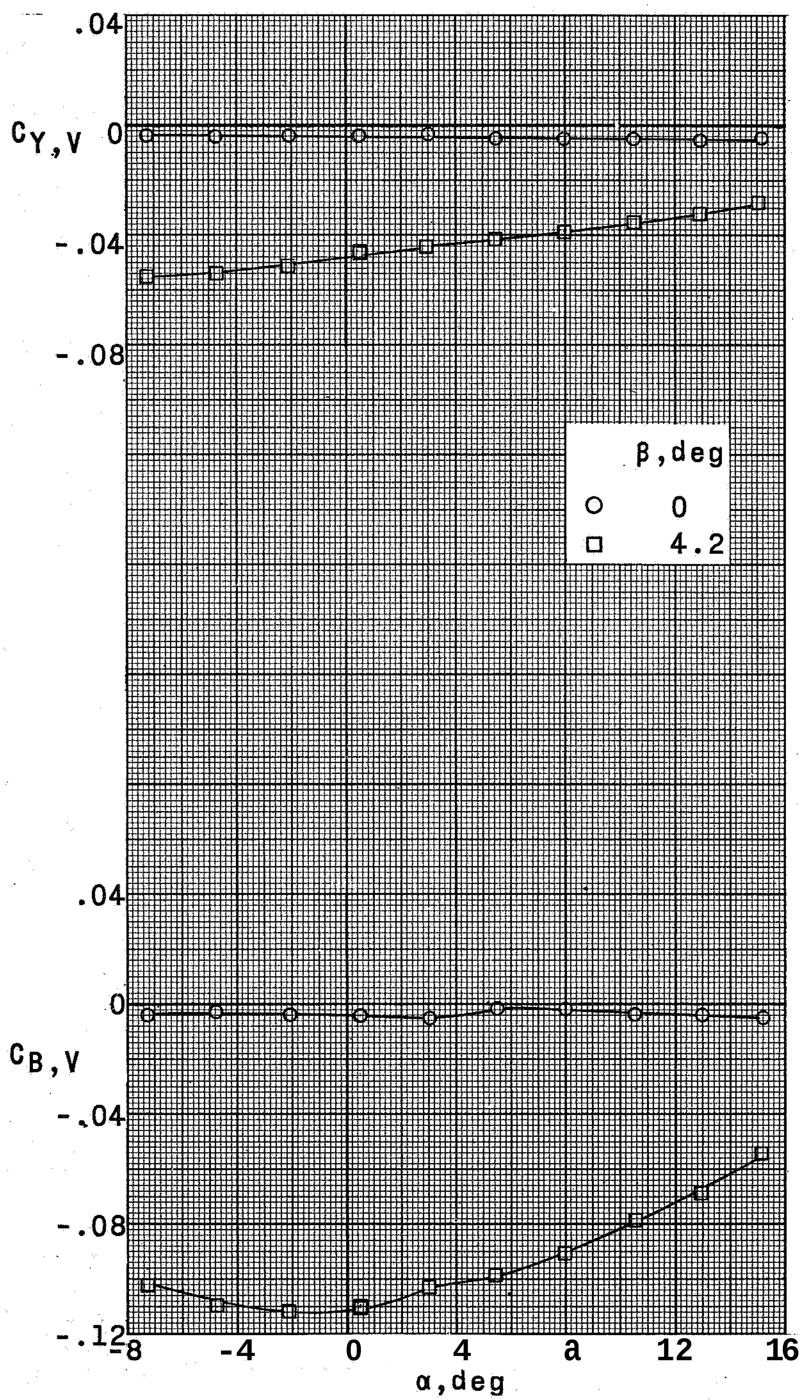

(a) M = 1.57.

Figure 35.- Loading characteristics of the vertical tail of a supersonic horizontal-attitude VTOL airplane model. $W_1BH_{30}V_2$ configuration; $\delta_V = 0$.

I-355

[redacted]

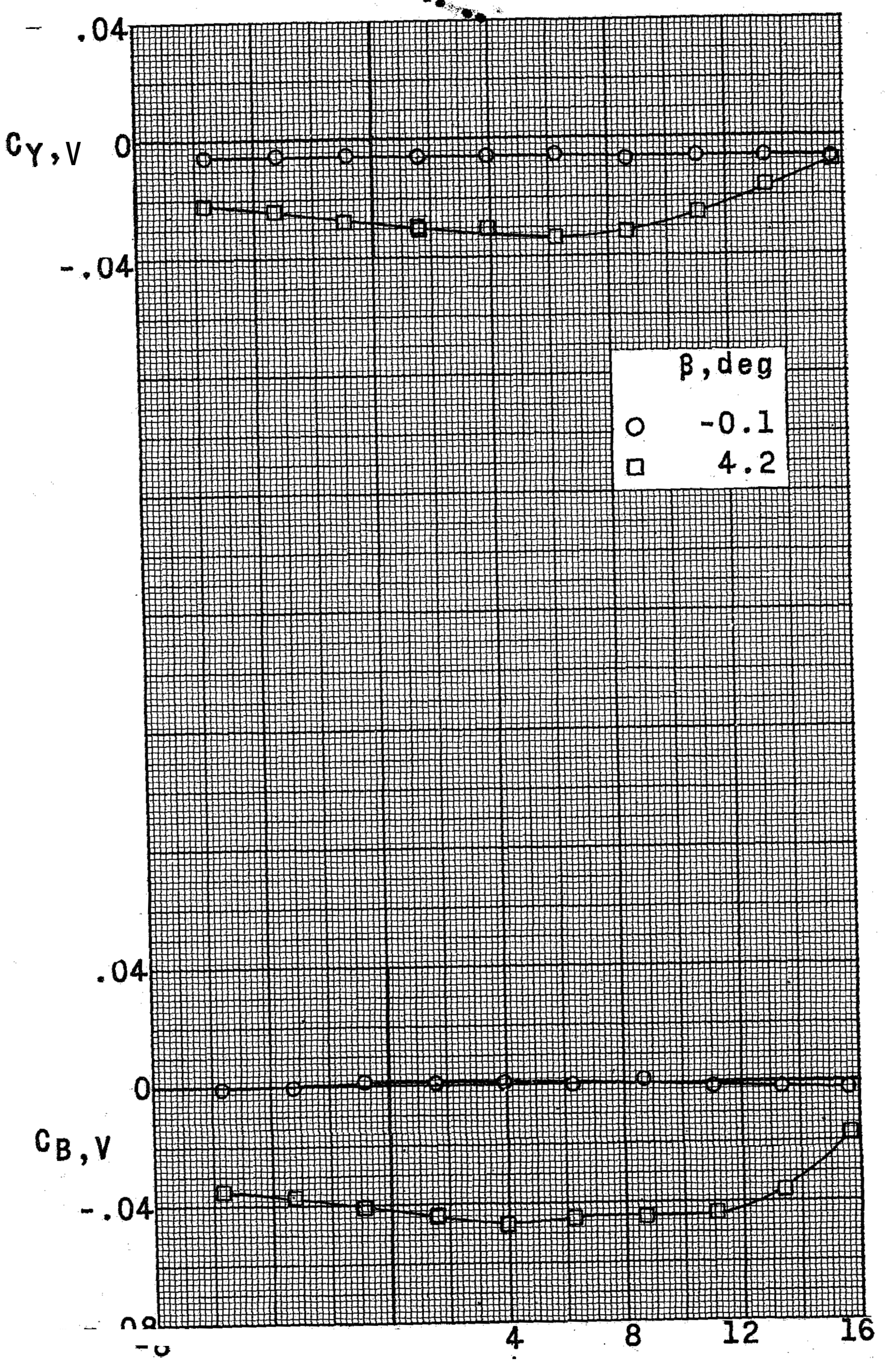

(b) M = 2.14.

Figure 35.- Continued.

[redacted]

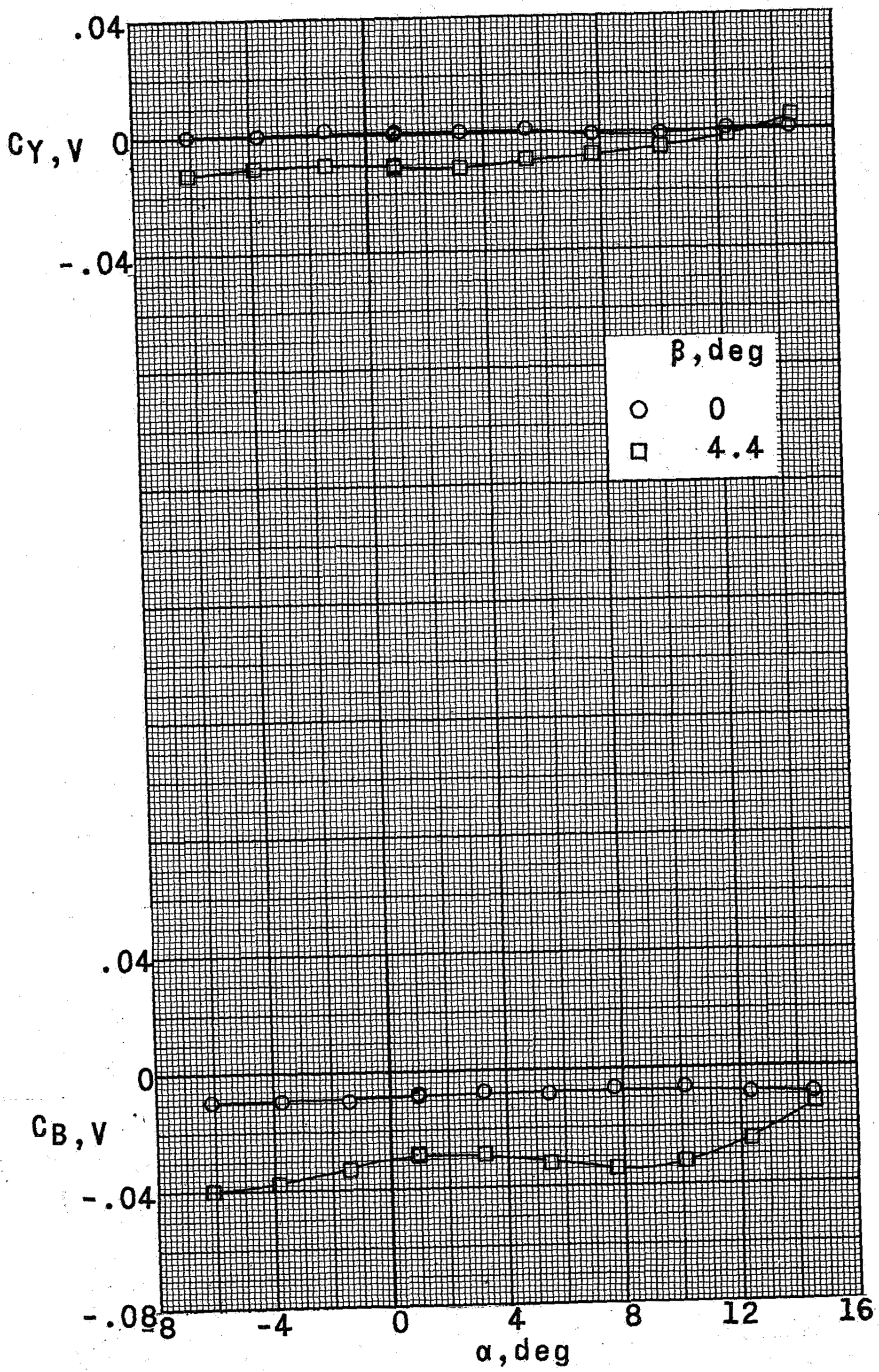

(c) M = 2.54.

Figure 35.- Concluded.

[redacted]

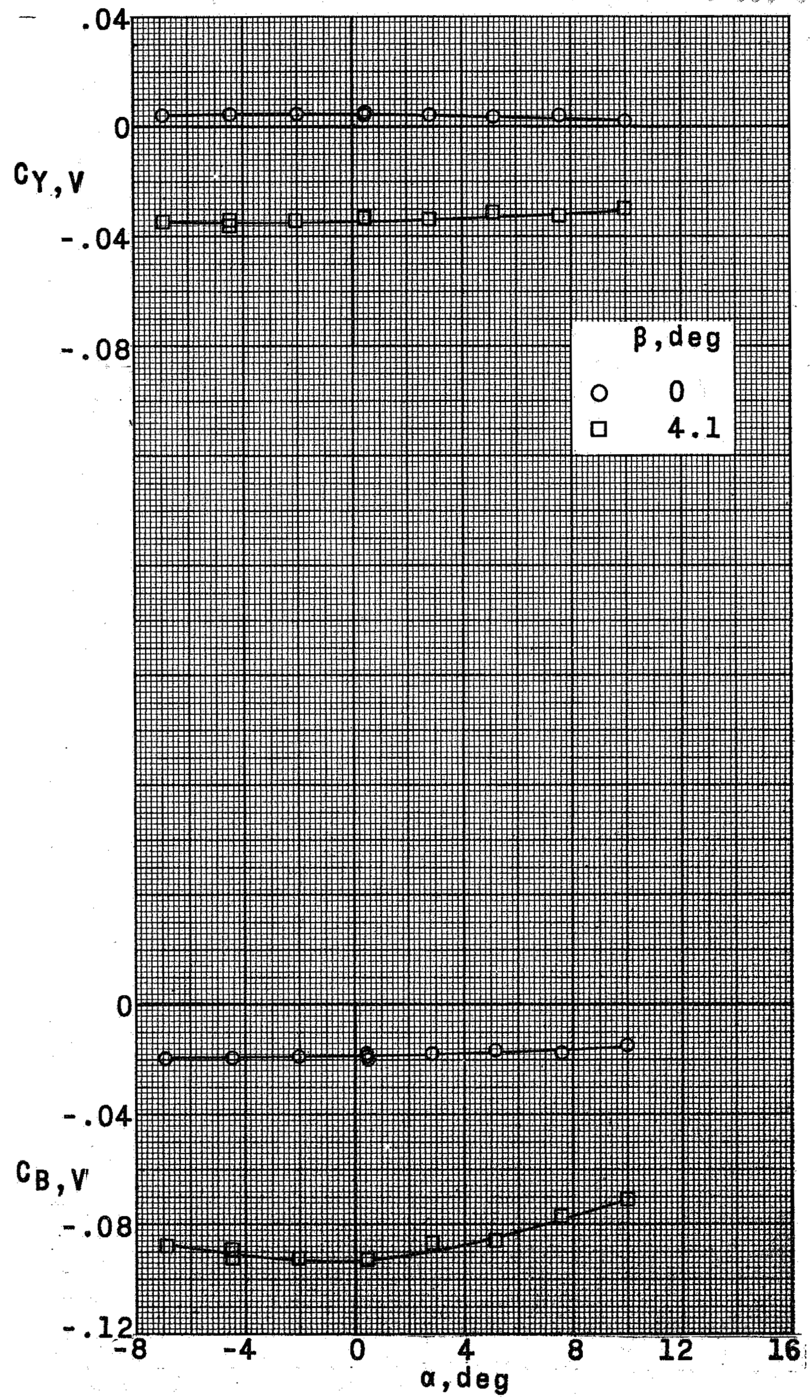

(a) M = 1.57.

Figure 36.- Loading characteristics of the vertical tail of a supersonic horizontal-attitude VTOL airplane model. $W_3BH_{30}V_2v_2$ configuration; $\delta_V = 0$.

[redacted]

[redacted]

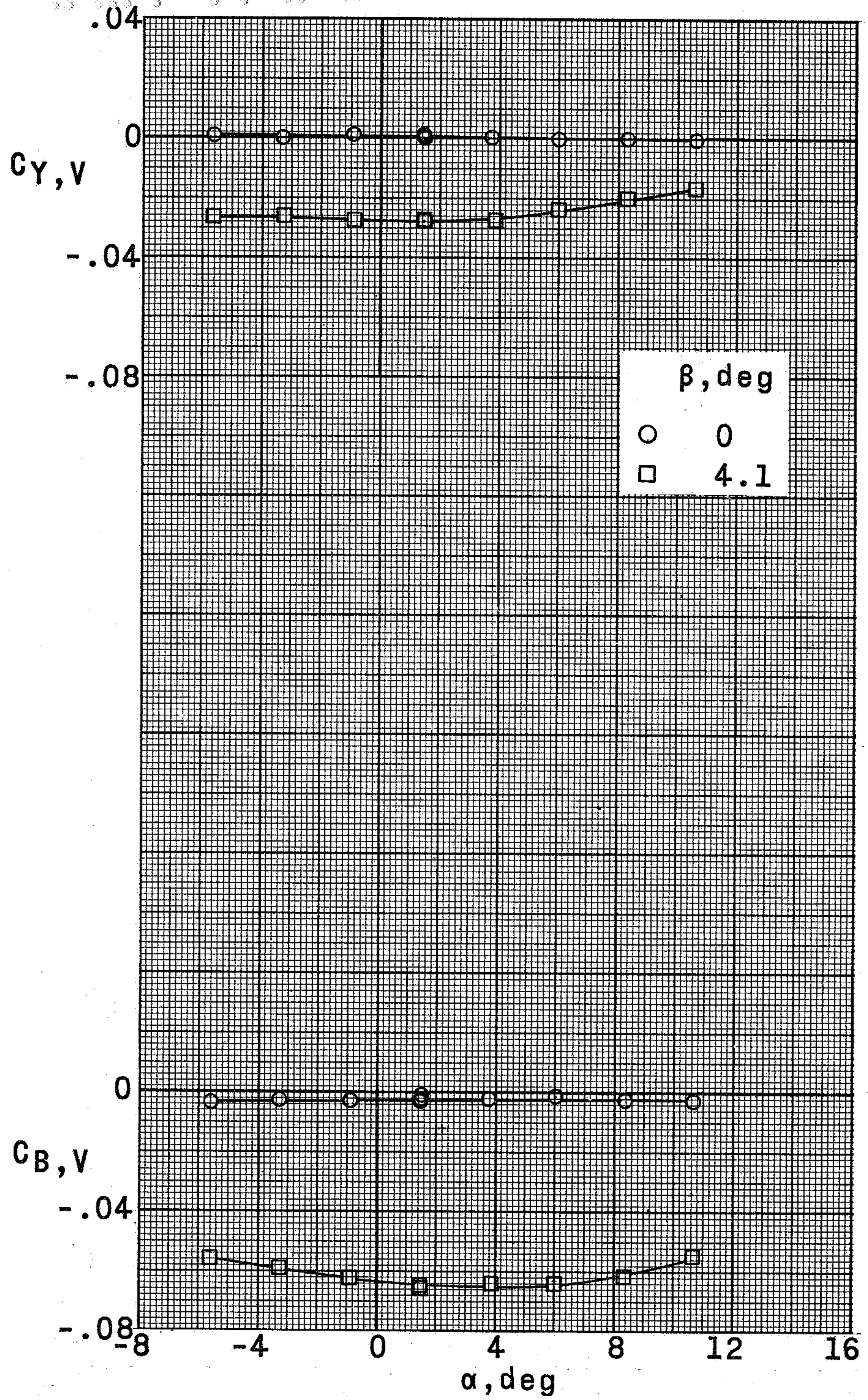

(b) M = 2.14.

Figure 36.- Continued.

[redacted]

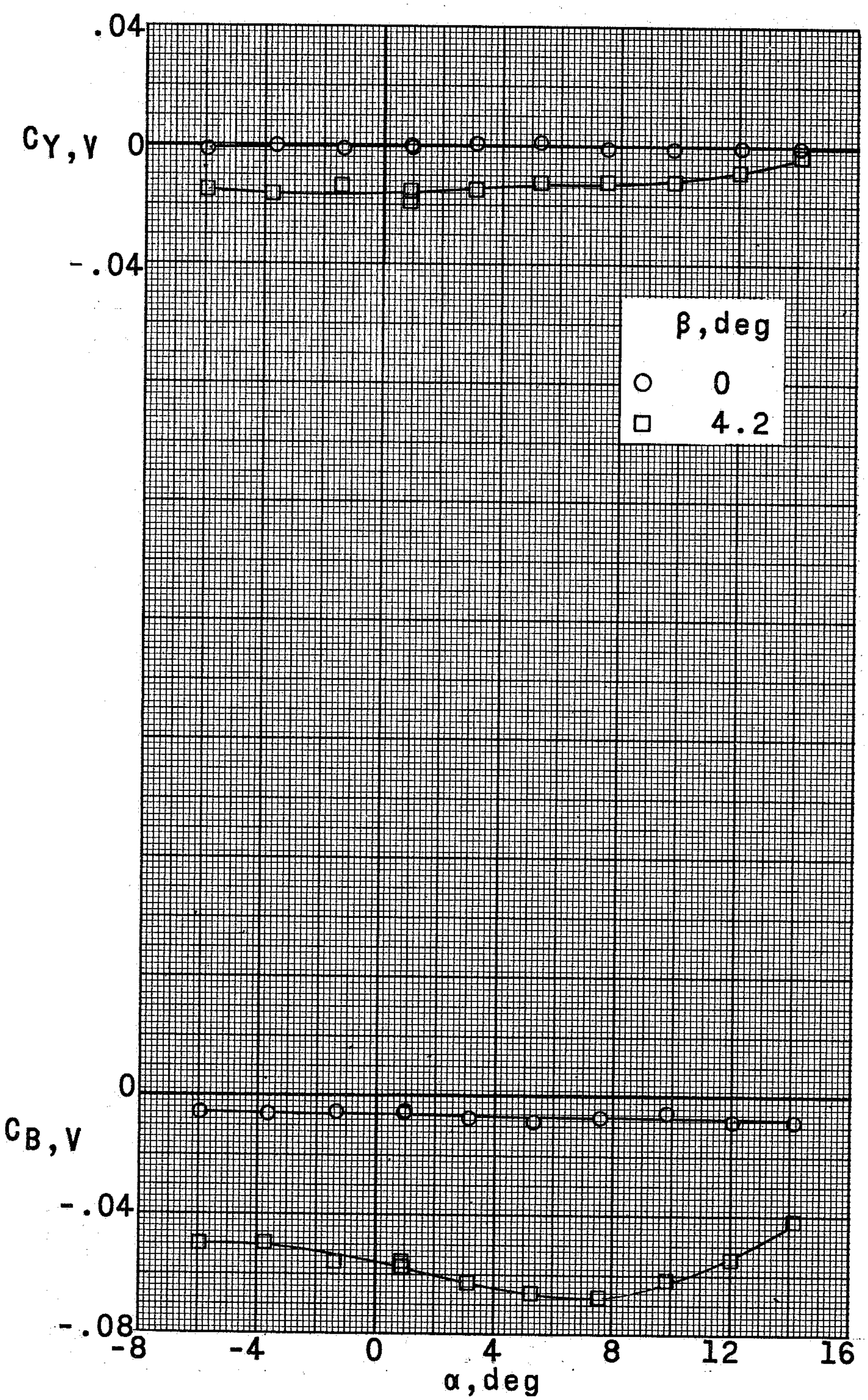

(c) M = 2.54.

Figure 36.- Concluded.

[redacted]

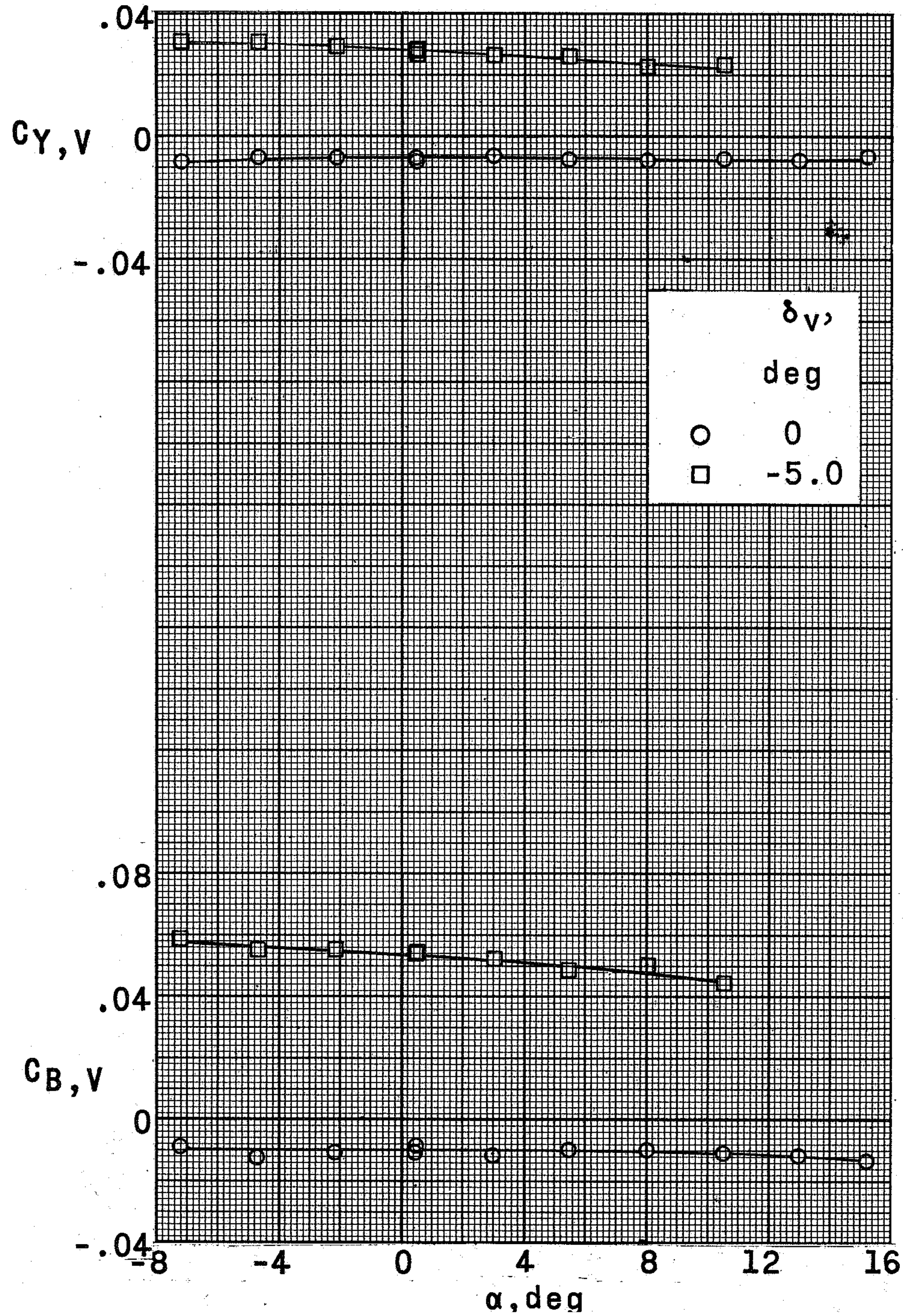

(a) M = 1.57.

Figure 37.- Loading characteristics of the vertical tail of a supersonic horizontal-attitude VTOL airplane model. $W_1BH_{30}V_2v_2$ configuration; β = 0.

[redacted]

[redacted]

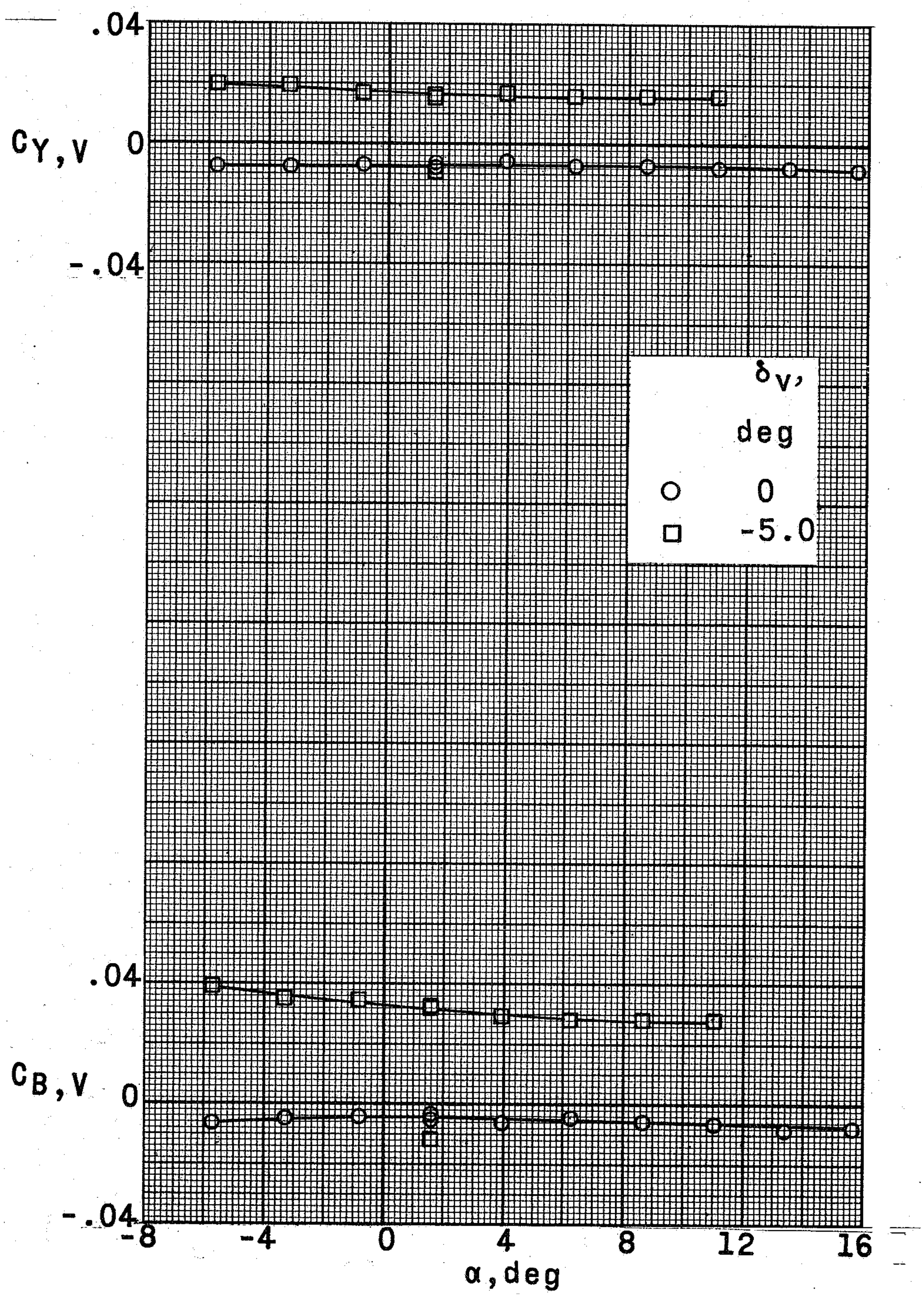

(b) M = 2.14.

Figure 37.- **Continued.**

[redacted]

[redacted]

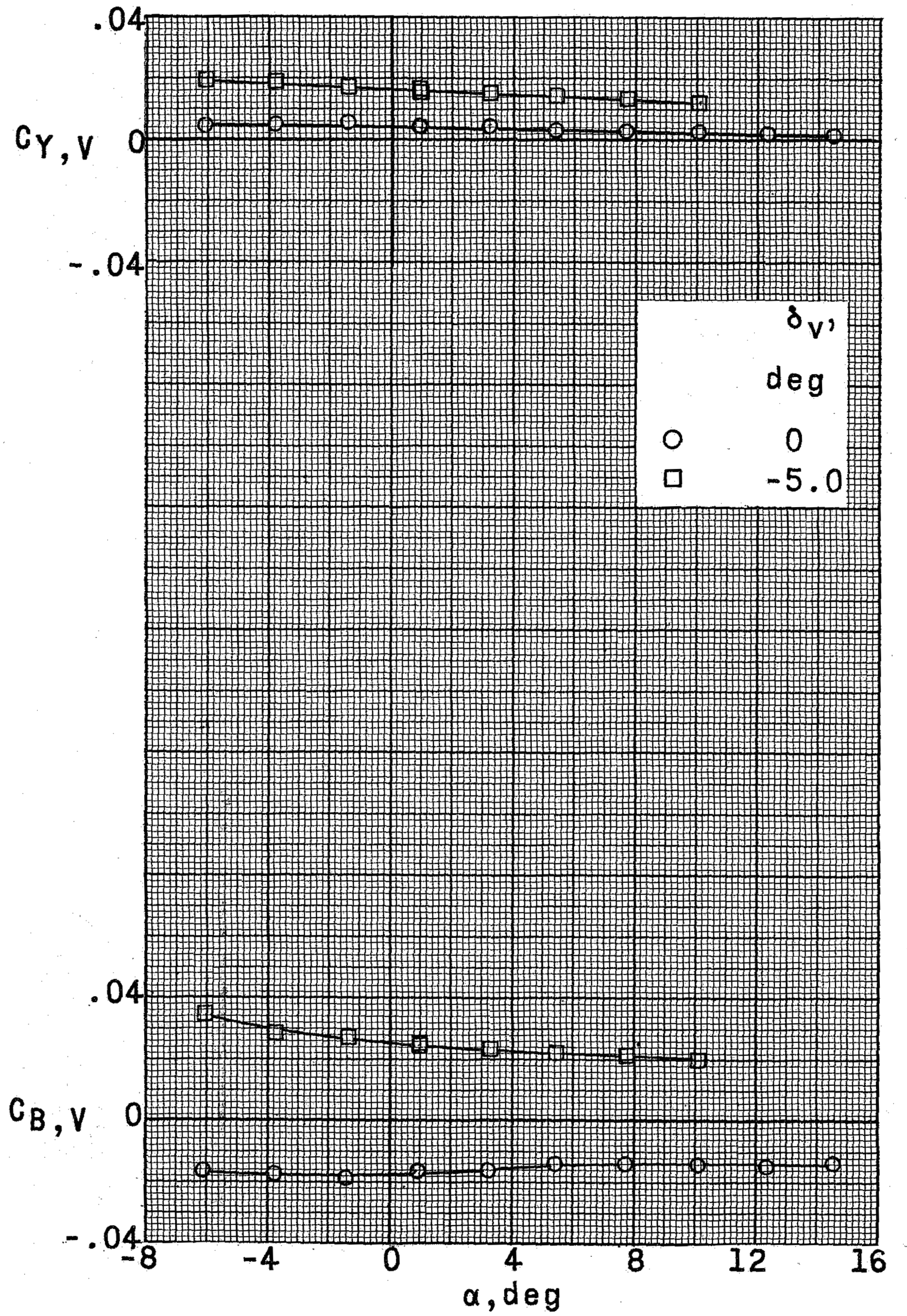

Figure *37.-* Concluded.

[redacted]

L-355

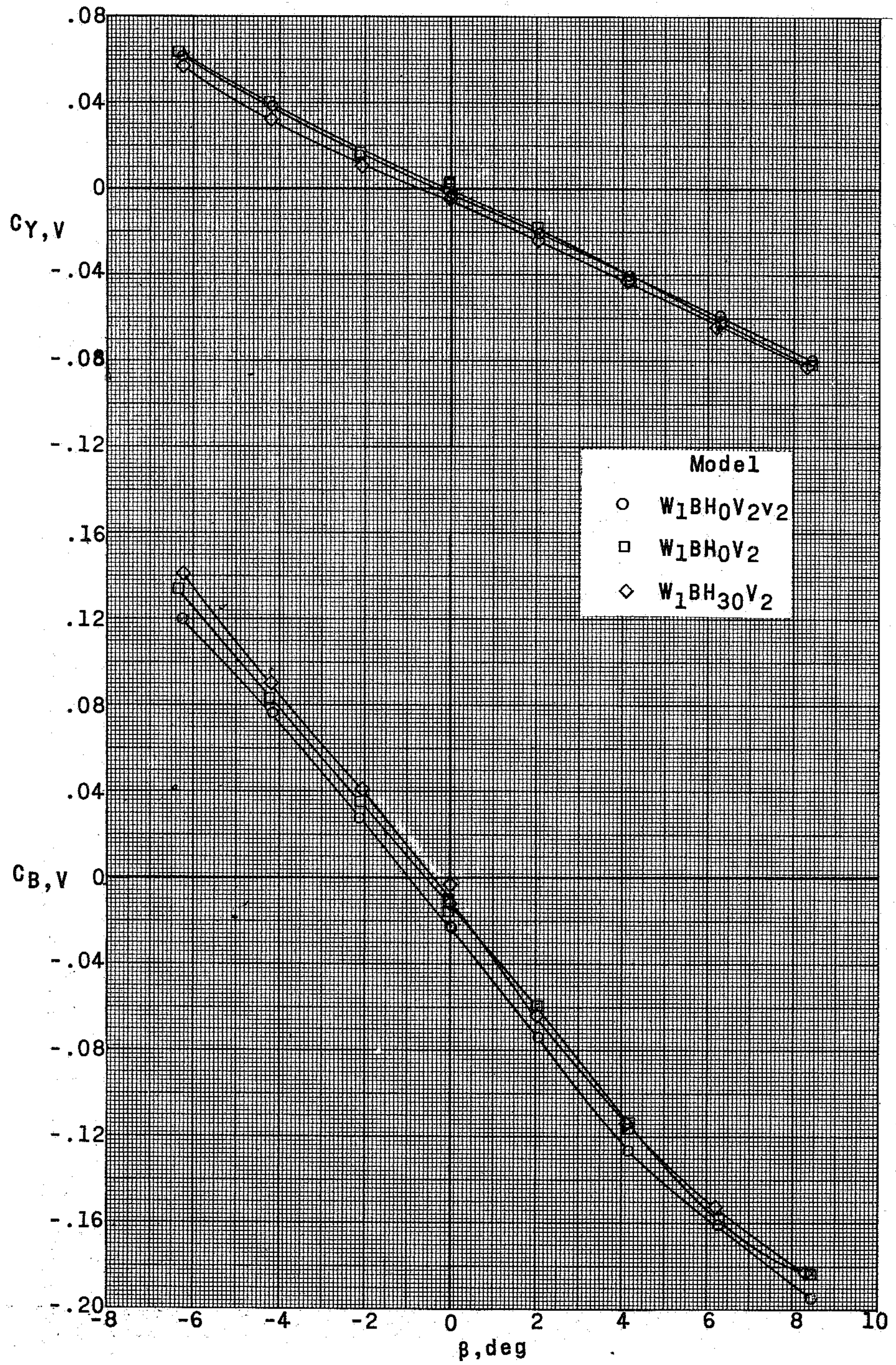

(a) $\alpha = 0.5^{\circ}$.

Figure 38.- Loading characteristics of the vertical tail of a supersonic horizontal-attitude VTOL airplane model. $M = 1.57$; $\delta_V = 0$.

[redacted]

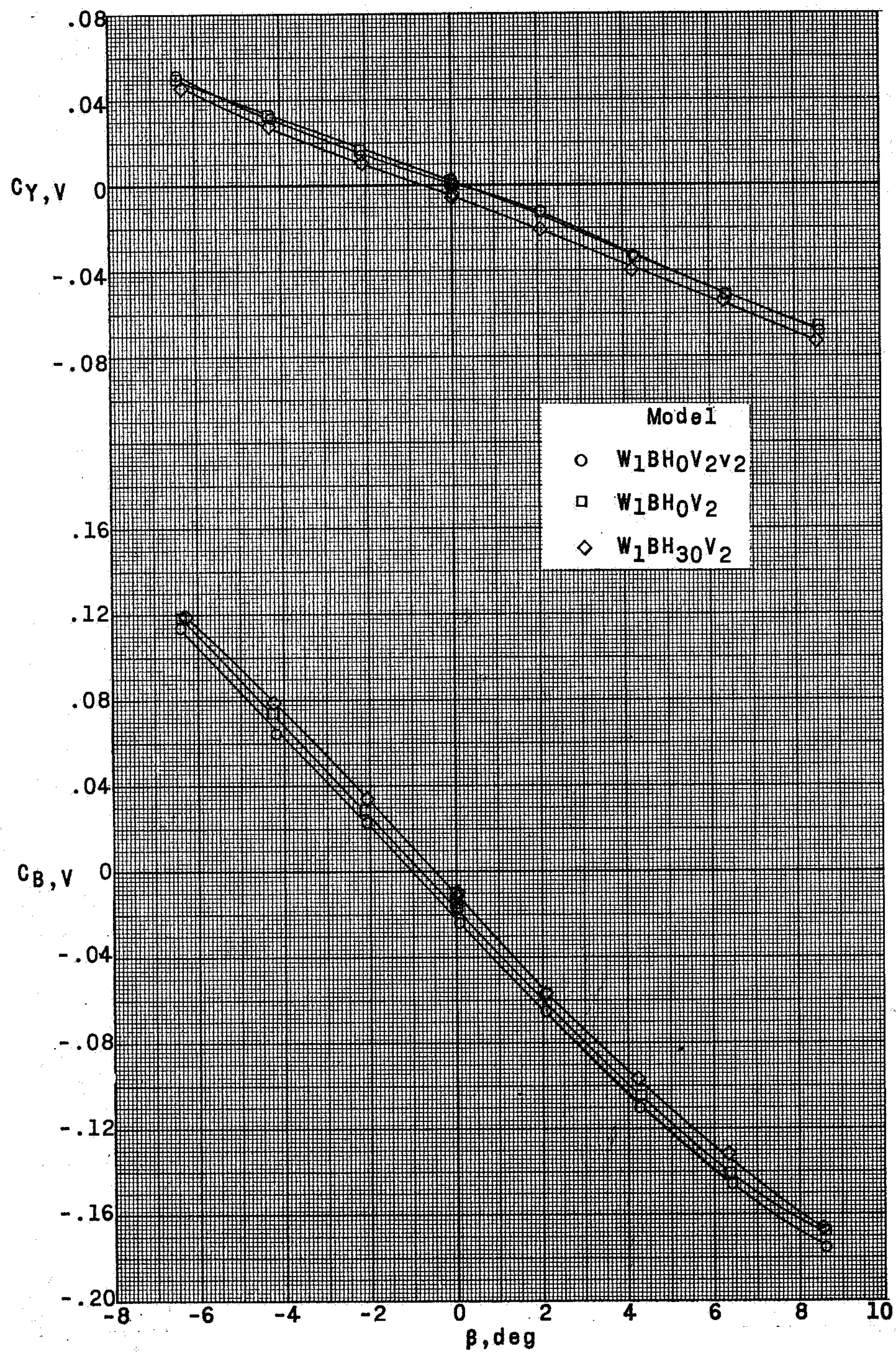

(b) $\alpha = 5.5^{\circ}$.

Figure 38.- Continued.

I-355

[redacted]

L-355

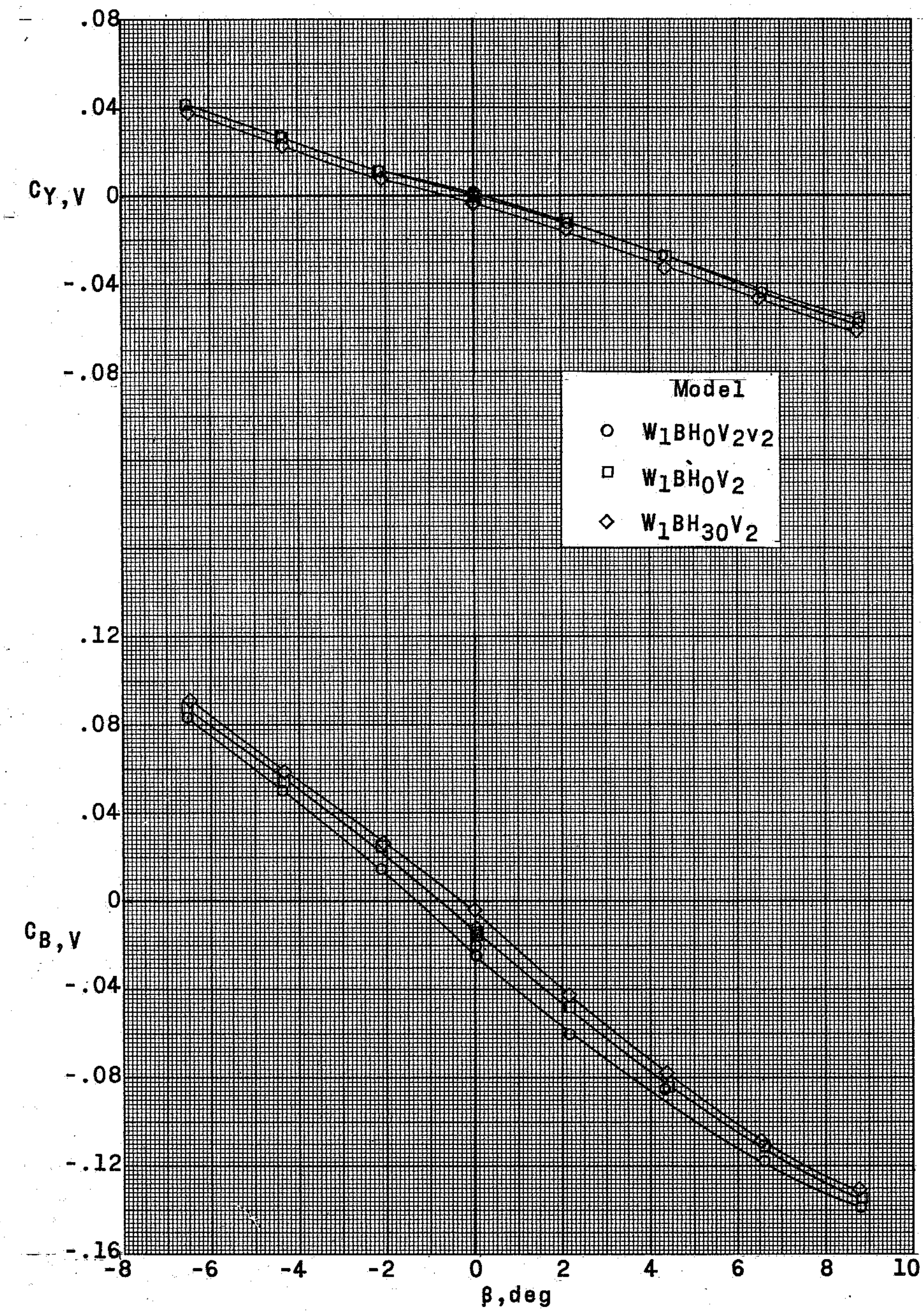

(c) $\alpha = 10.5^{\circ}$.

Figure 38.- Concluded.

[redacted]

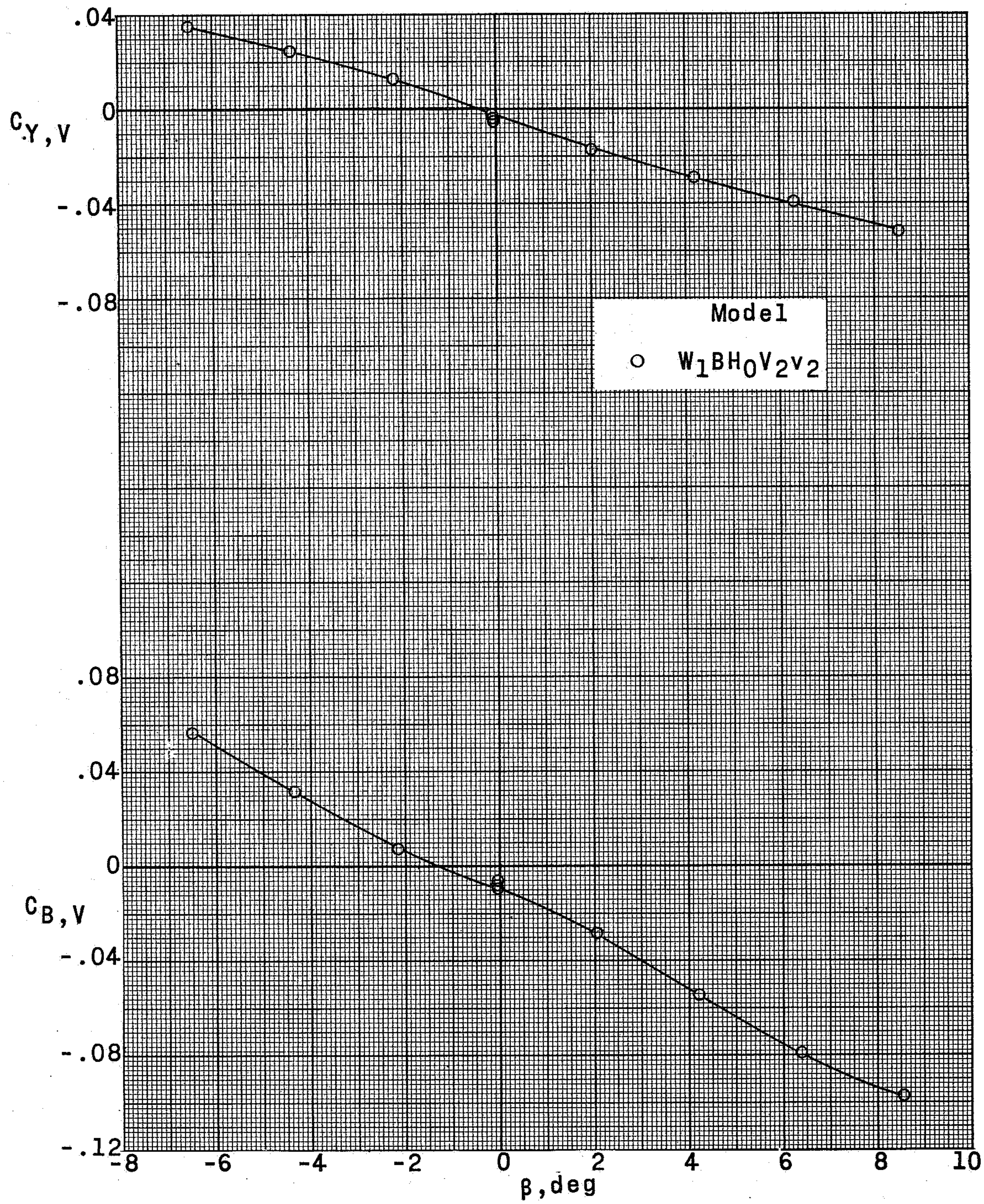

(a) $\alpha = 1.6^\circ$.

Figure 39.- Loading characteristics of the vertical tail of a supersonic horizontal-attitude VTOL airplane model. $M = 2.14$; $\delta_V = 0$.

L-355

[redacted]

L-355

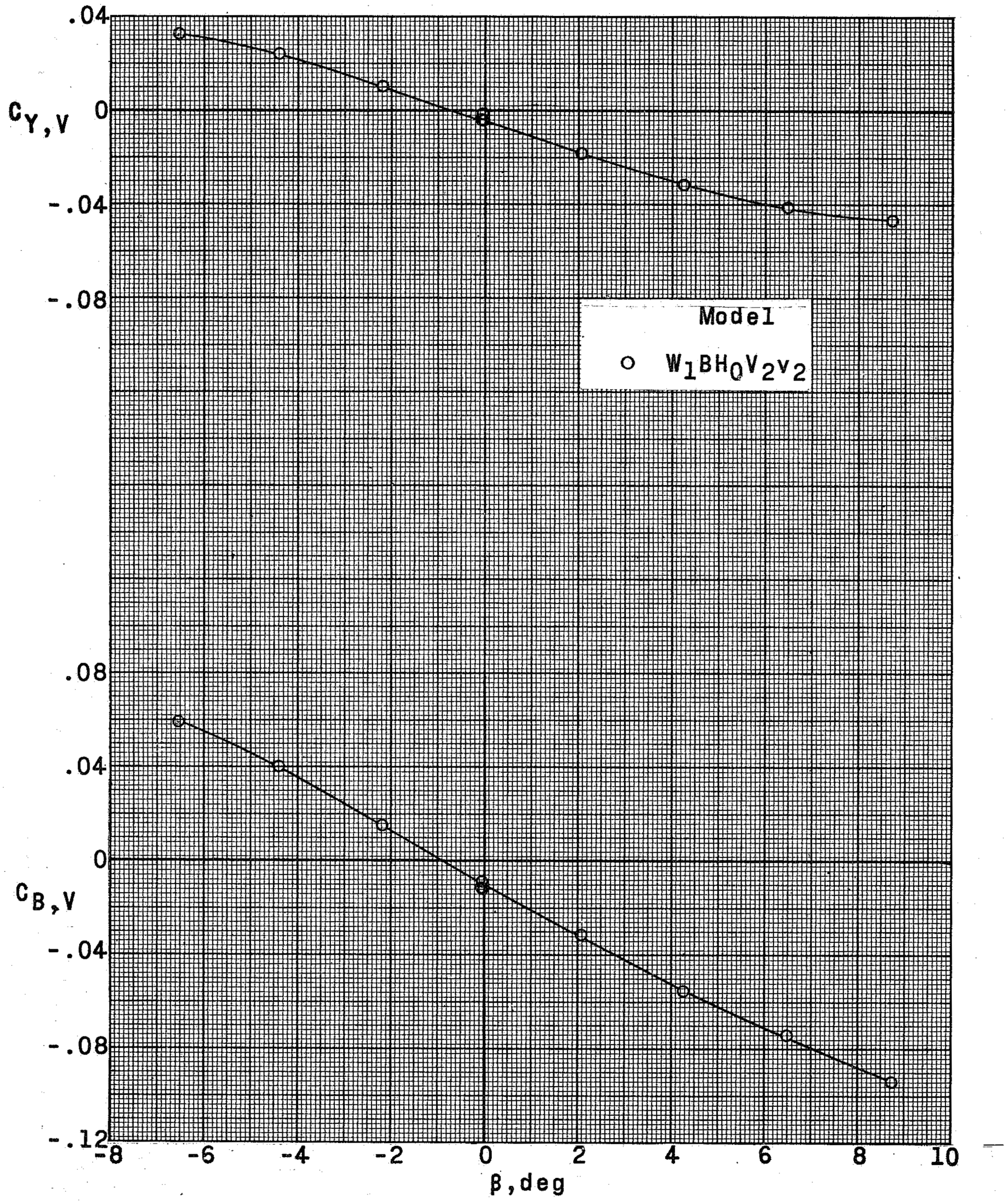

(b) $\alpha = 6.2^{\circ}$.

Figure 39.- Continued.

[redacted]

[redacted]

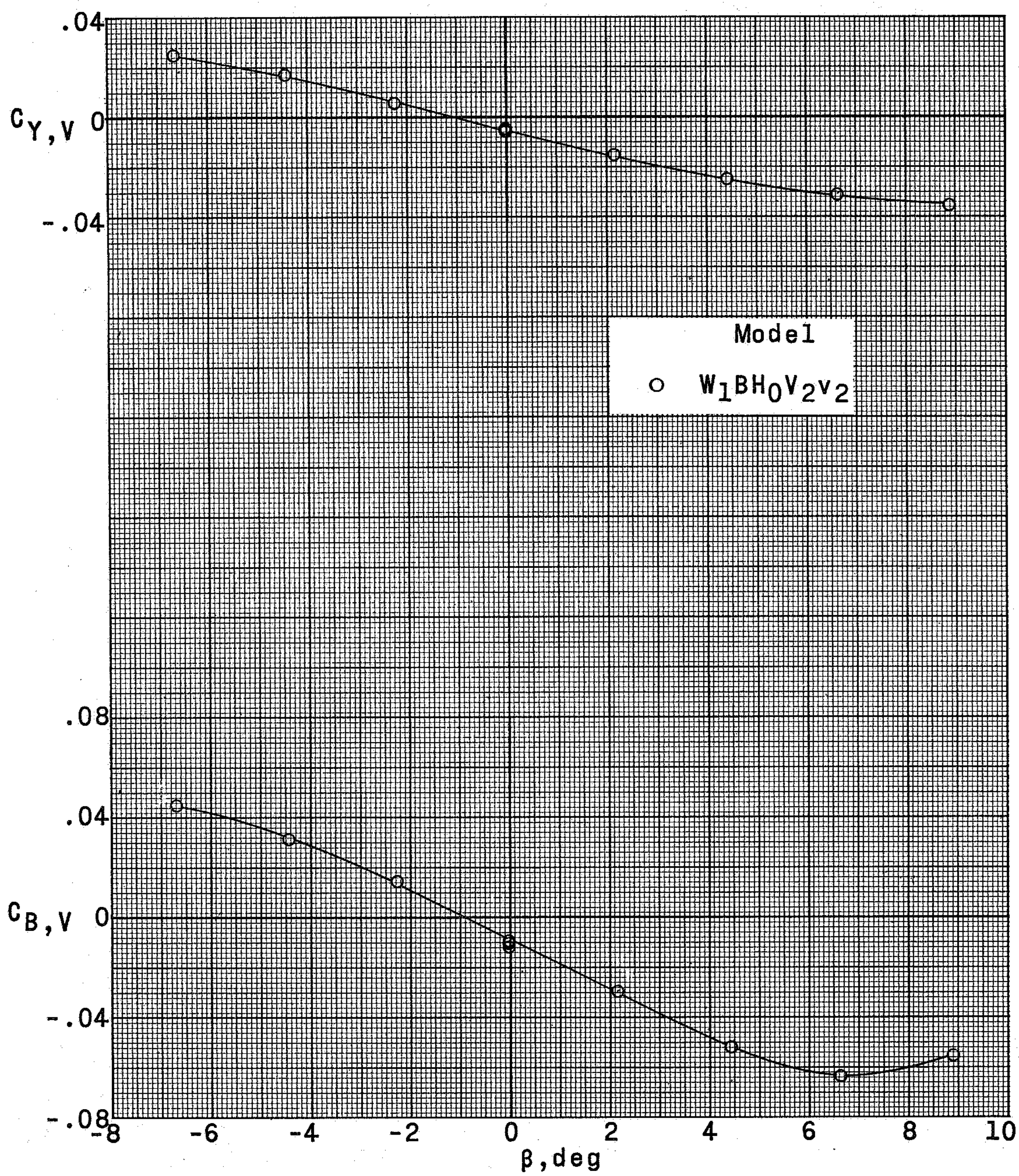

(c) $\alpha = 11.0^{\circ}$.

Figure 39.- Concluded.

L-355

[redacted]

L-355

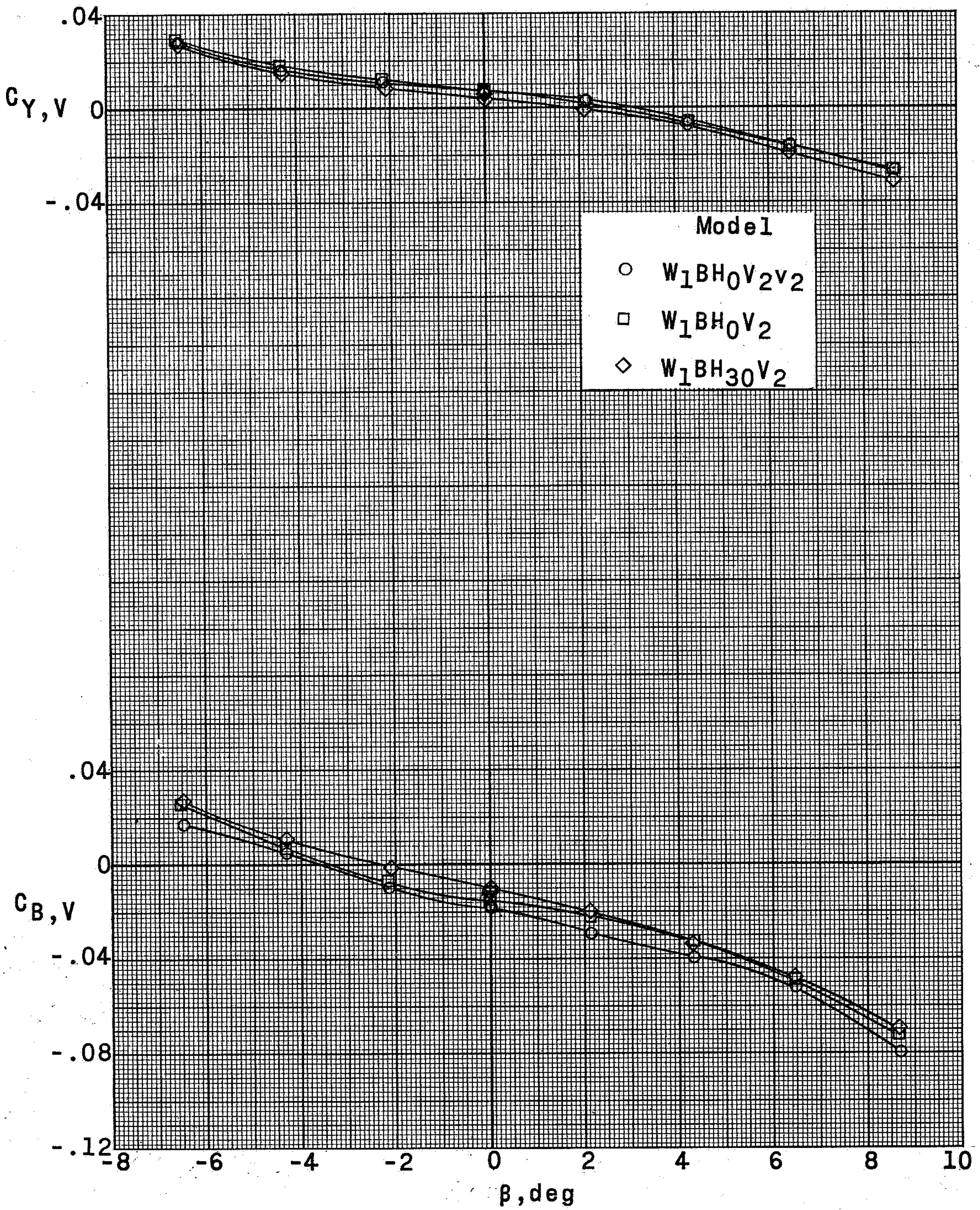

(a) $\alpha = 1.0^{\circ}$.

Figure 40.- Loading characteristics of the vertical tail of a supersonic horizontal-attitude VTOL airplane model with various tail configurations. $M = 2.54$; $\delta_V = 0$.

[redacted]

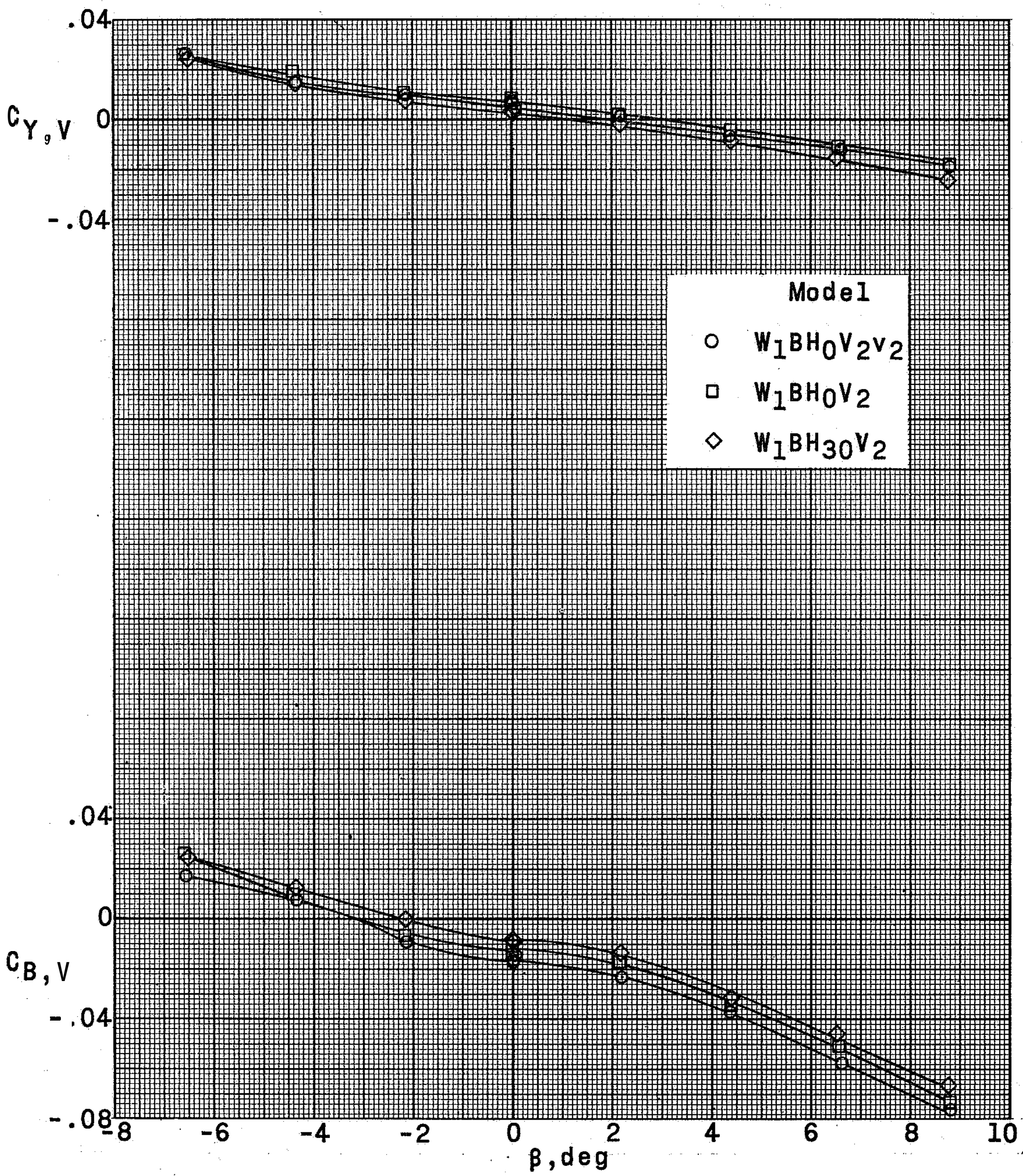

(b) $\alpha = 5.5^{\circ}$.

Figure 40.- Continued.

L-355

[redacted]

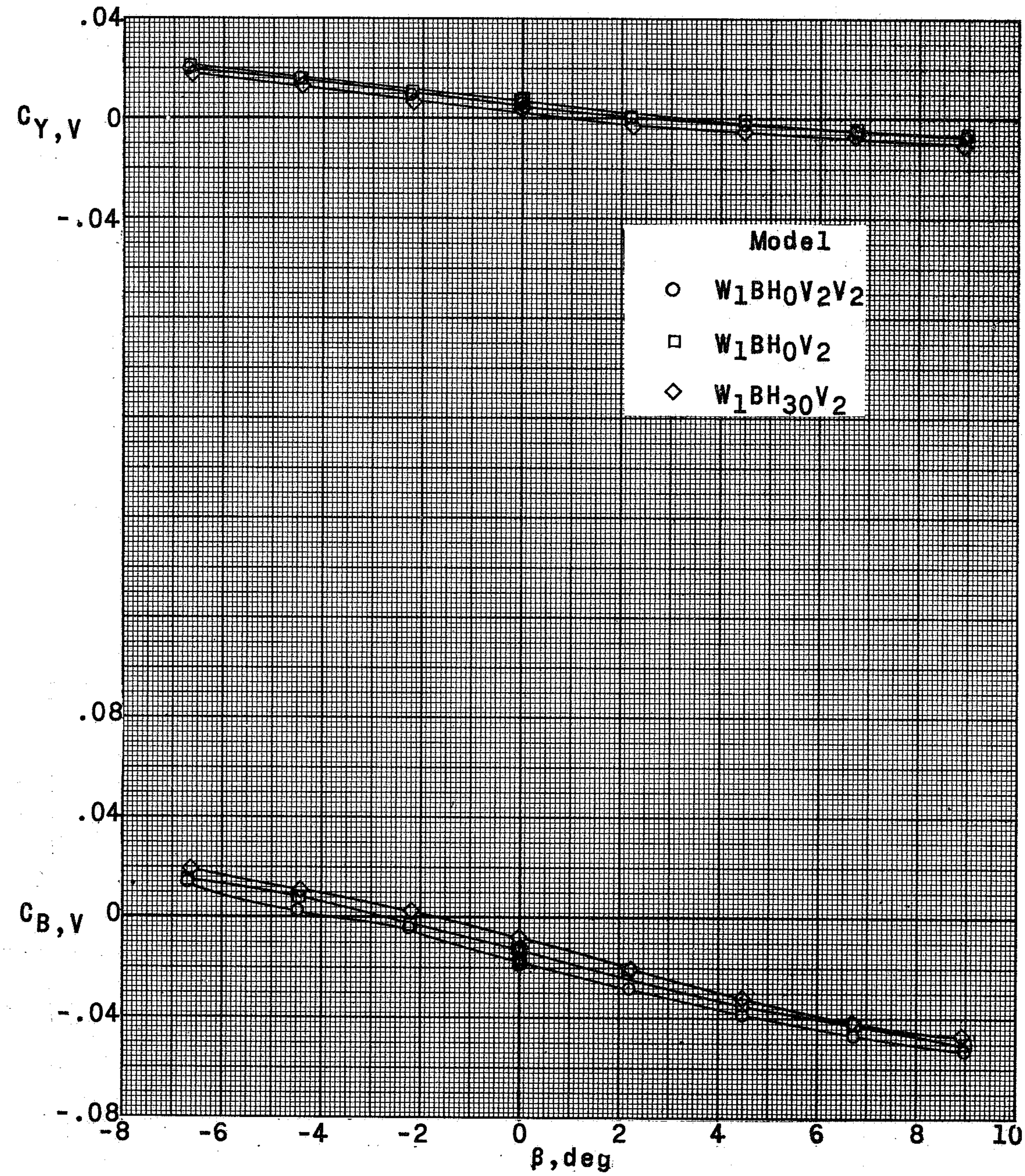

(c) $\alpha = 10.1^{\circ}$.

Figure 40.- Concluded.

[redacted]

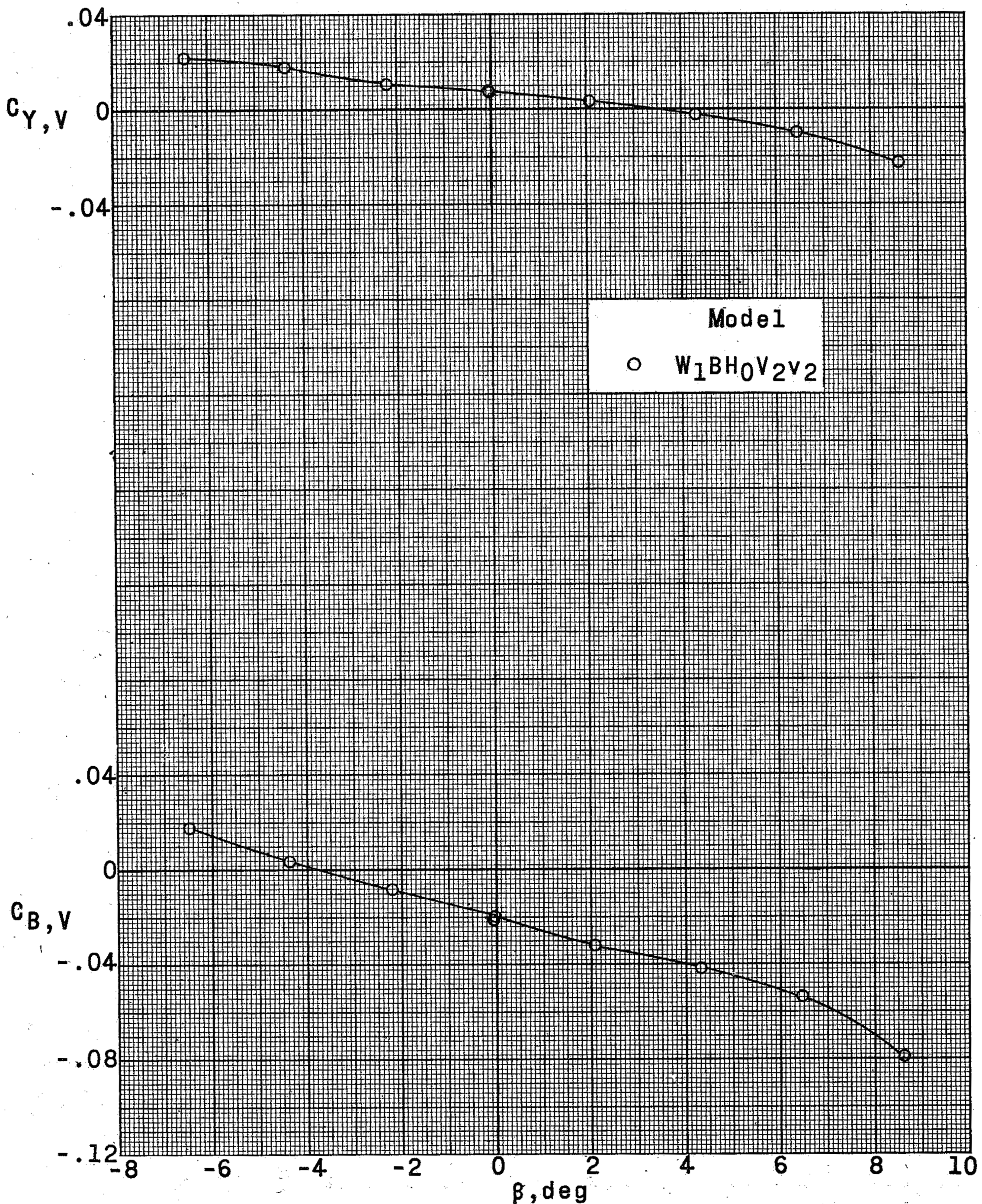

(a) $\alpha = 0.1^{\circ}$.

L-355

Figure 41.- Loading characteristics of the vertical tail of a supersonic horizontal-attitude VTOL airplane model. $M = 2.87$; $\delta_V = 0$.

L-355

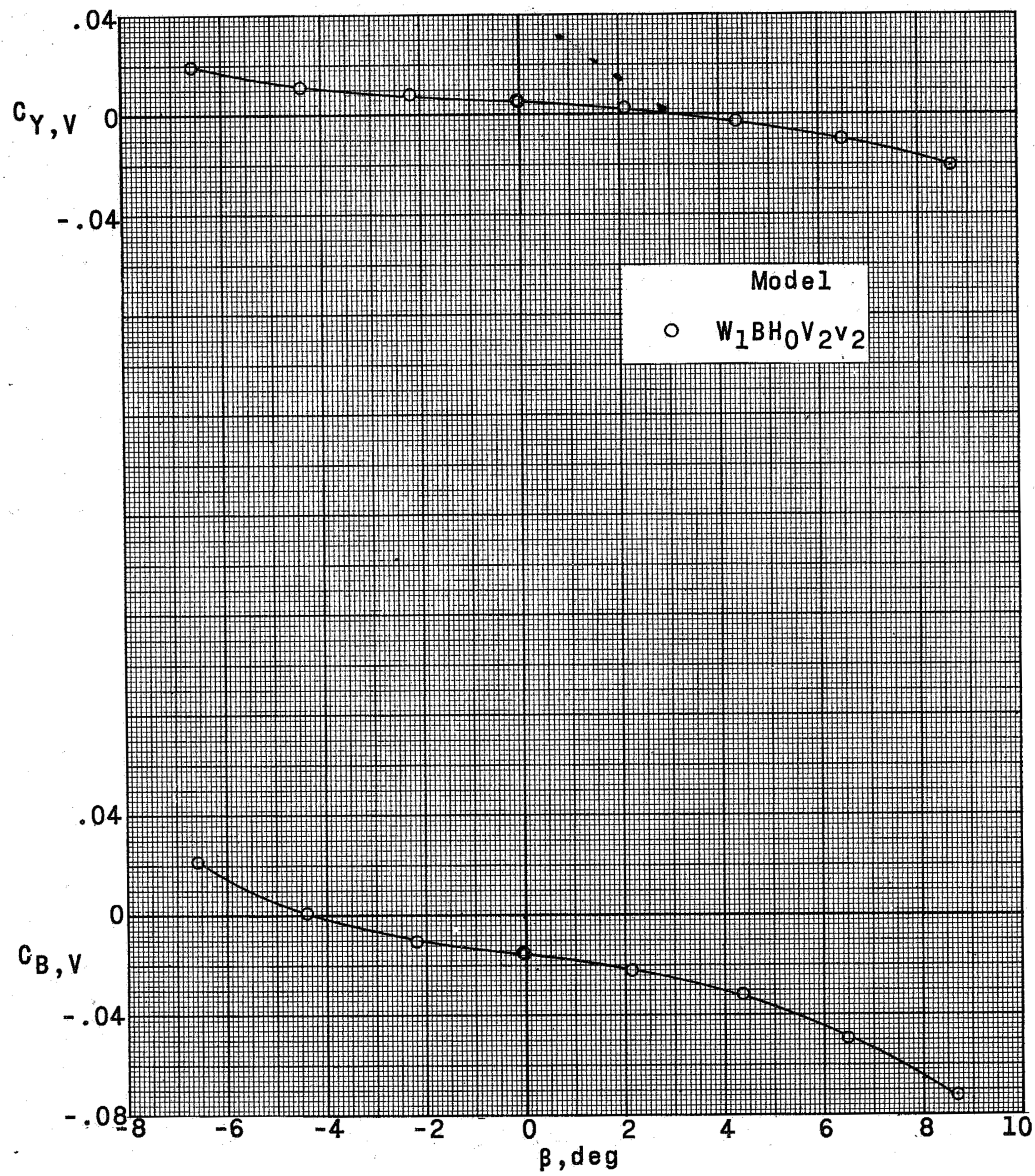

(b) $\alpha = 4.3^{\circ}$.

Figure 41.- Continued.

[redacted]

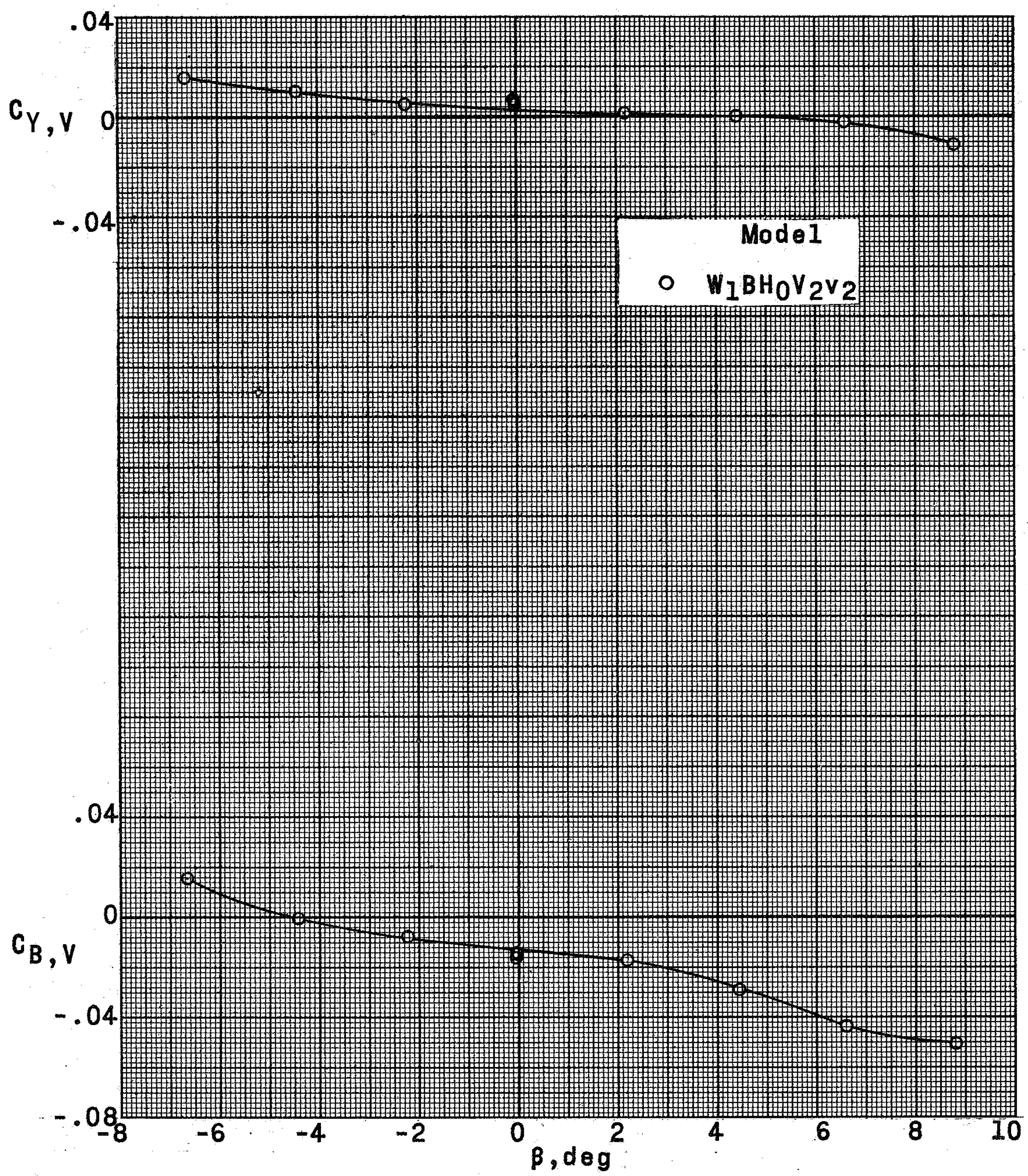

(c) $\alpha = 8.8^{\circ}$.

Figure 41.- Concluded.

L-355

[redacted]

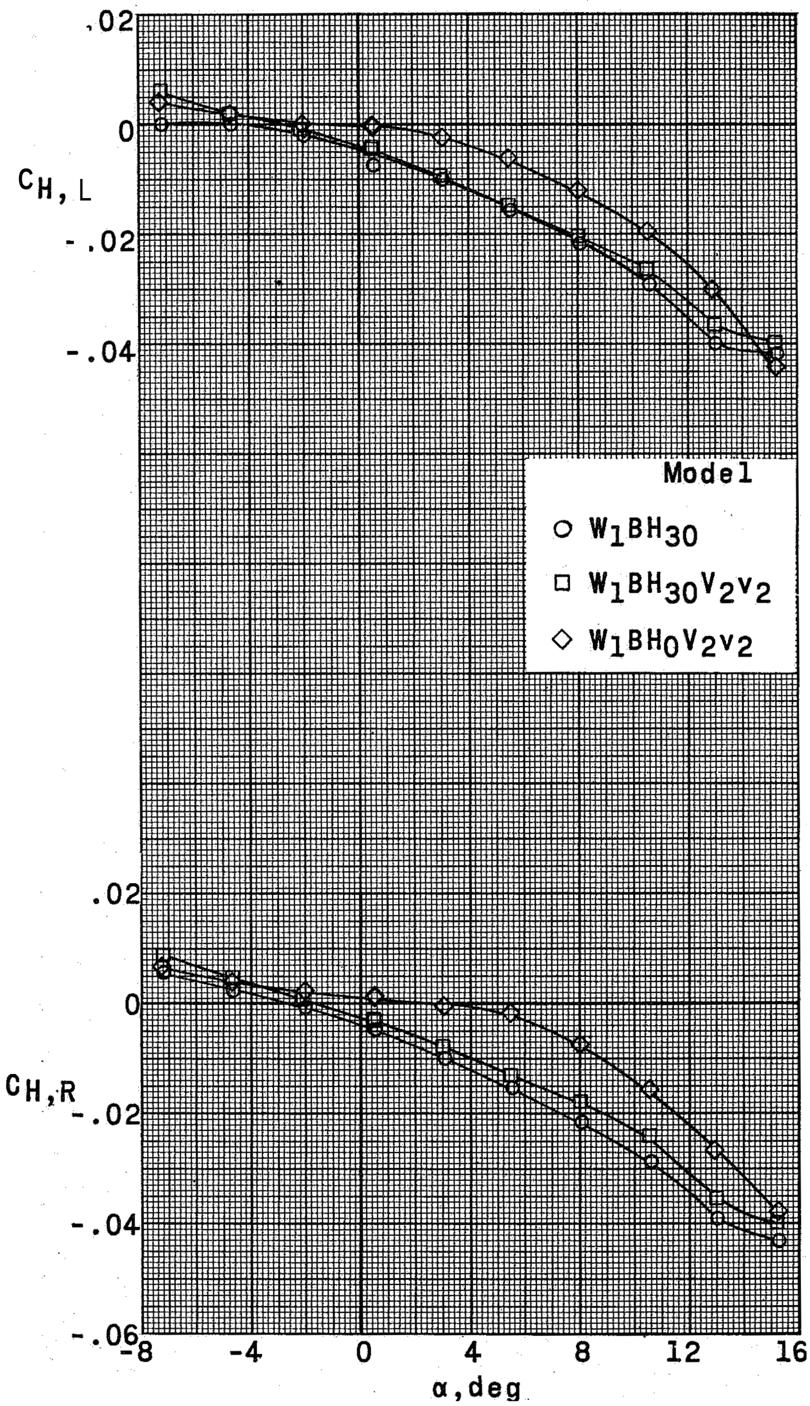

(a) M = 1.57.

Figure 42.- Hinge-moment characteristics of the horizontal-tail panels of a supersonic horizontal-attitude VTOL airplane model with various tail configurations. $\delta_H = 0$.

[redacted]

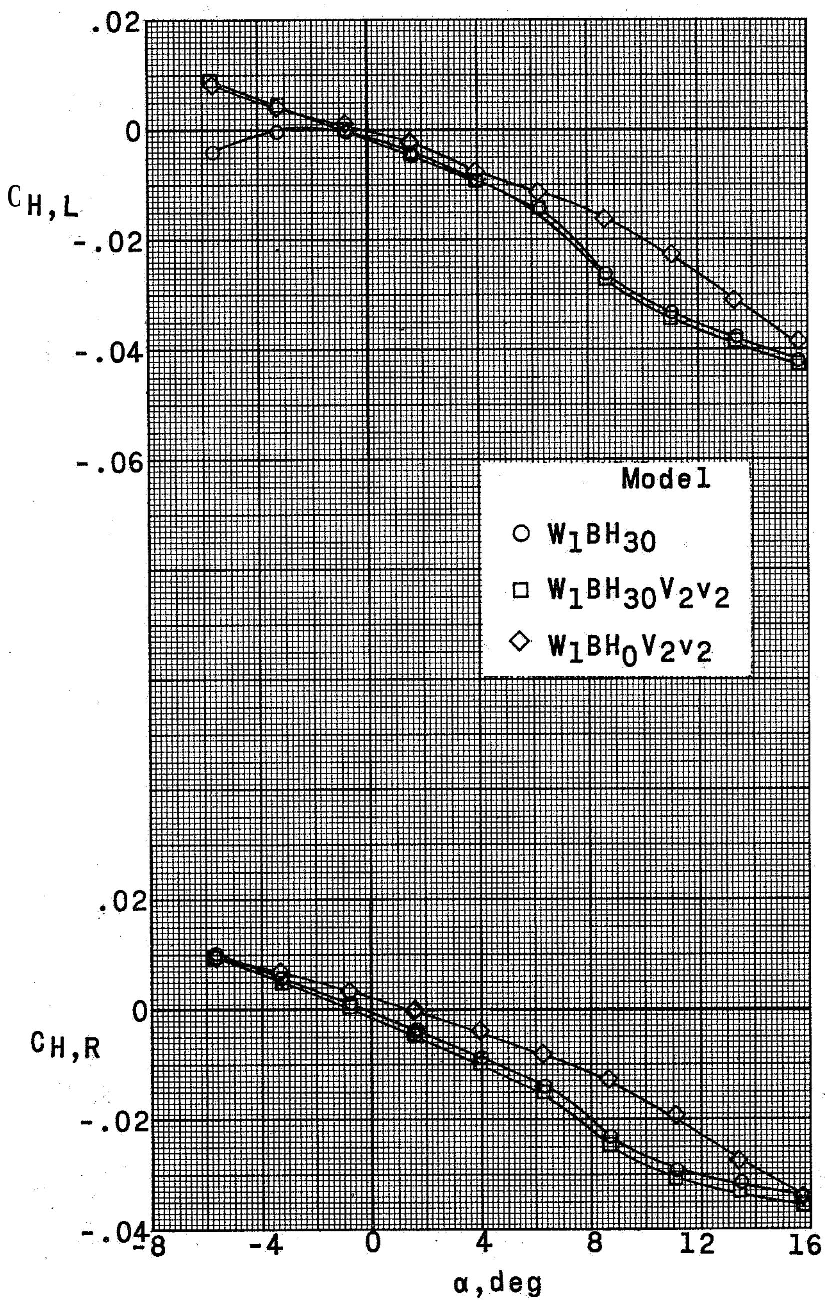

(b) M = 2.14.

Figure 42. - Continued.

[redacted]

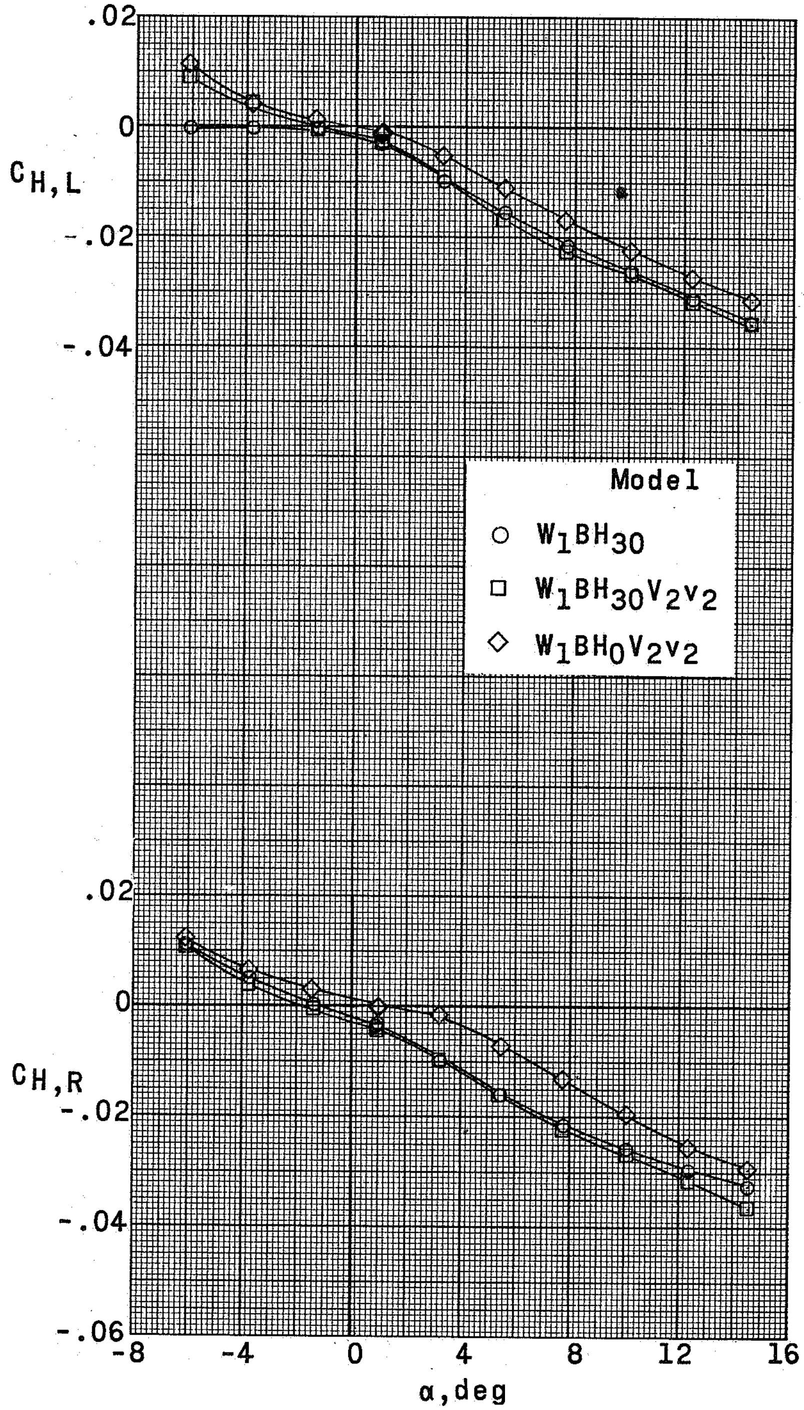

(c) M = 2.54.

Figure 42.- Continued.

[redacted]

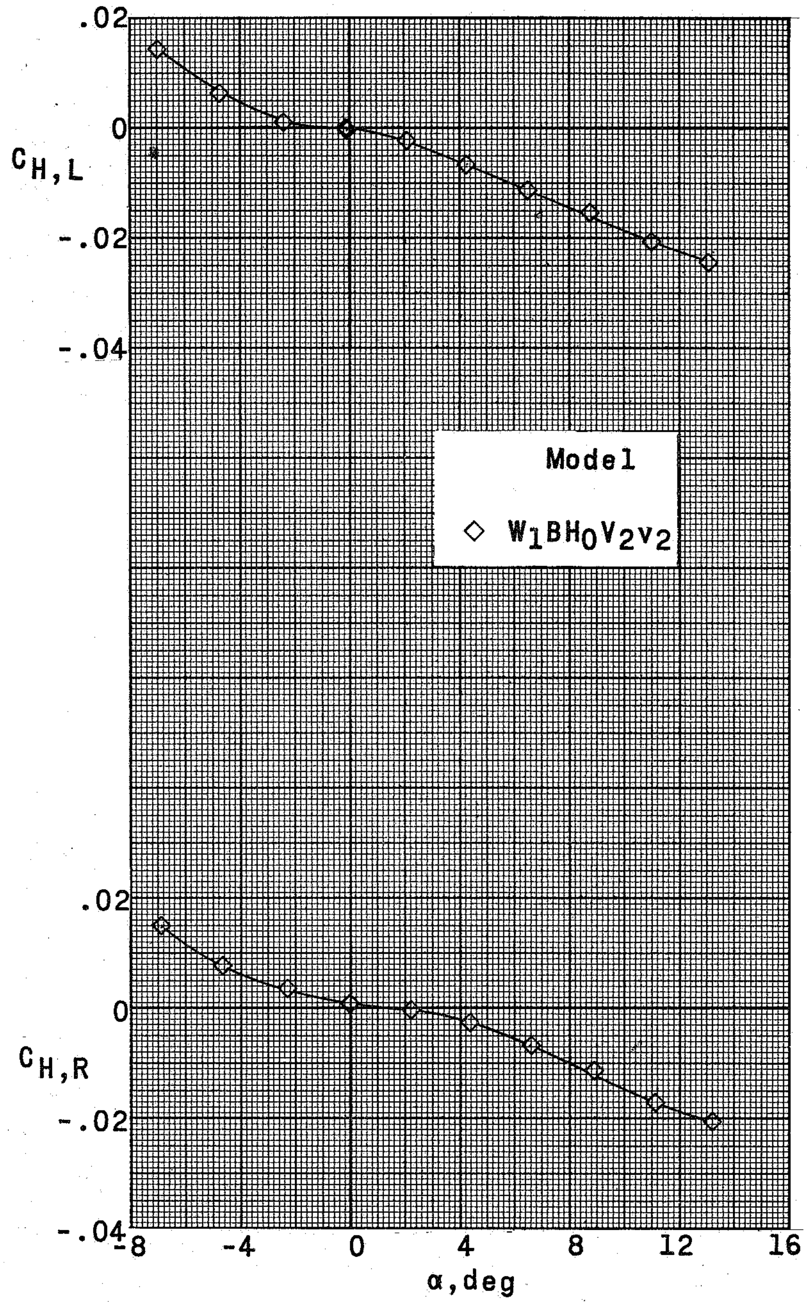

(d) M = 2.87.

Figure 42. - Concluded.

[redacted]

[redacted]L

L-355

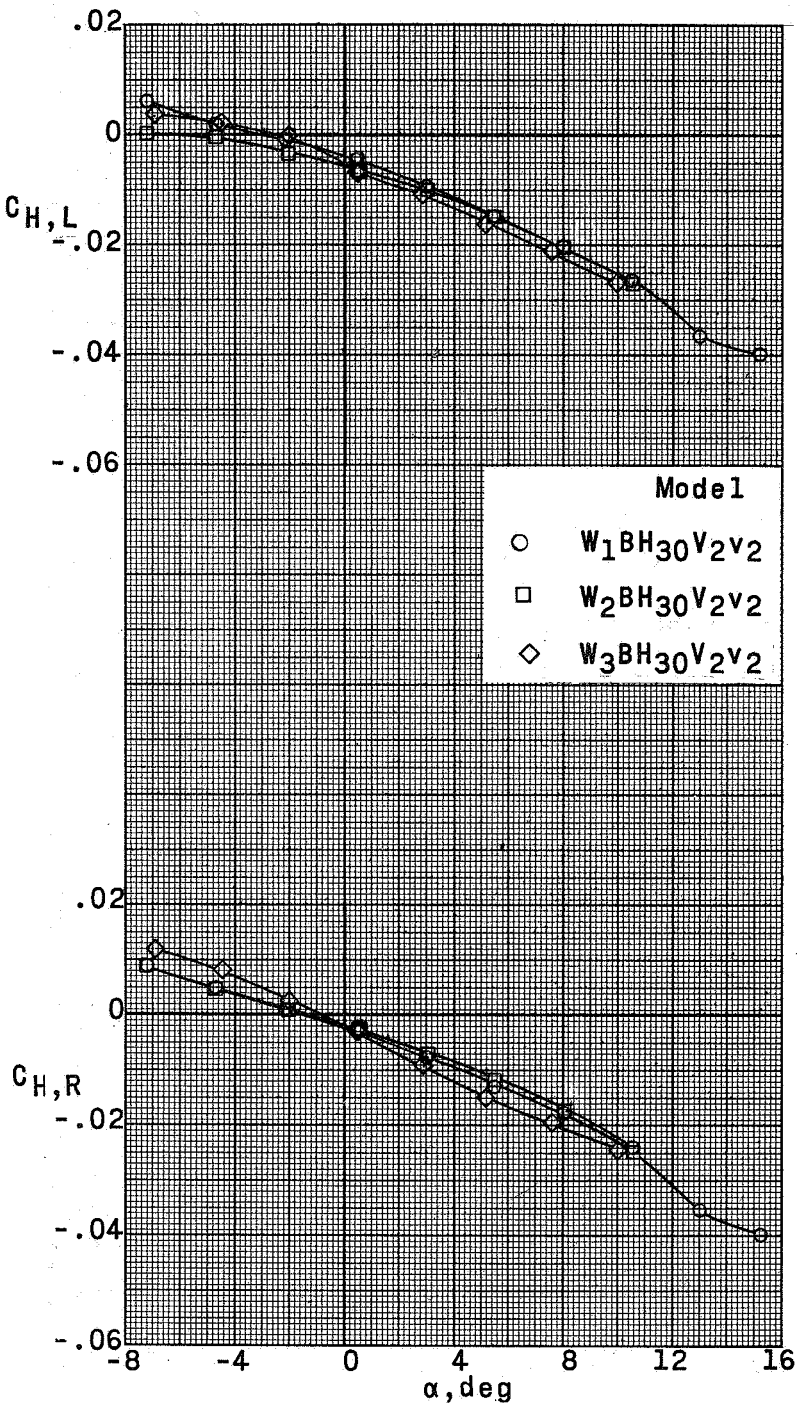

(a) M = 1.57.

Figure 43.- Hinge-moment characteristics of the horizontal-tail panels of a supersonic horizontal-attitude VTOL airplane with various nacelle positions. $\delta_H = 0$.

[redacted]

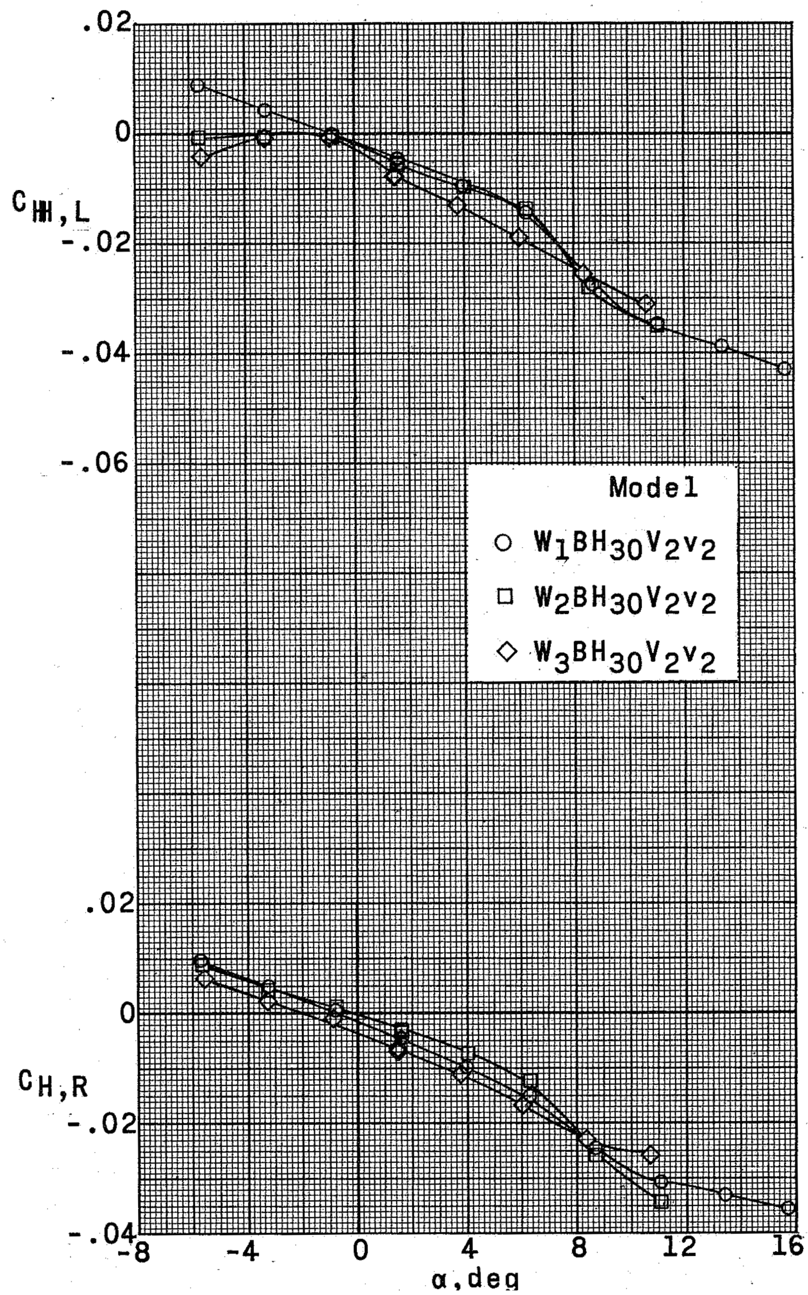

(b) M = 2.14.

Figure 43.- Continued.

L-355

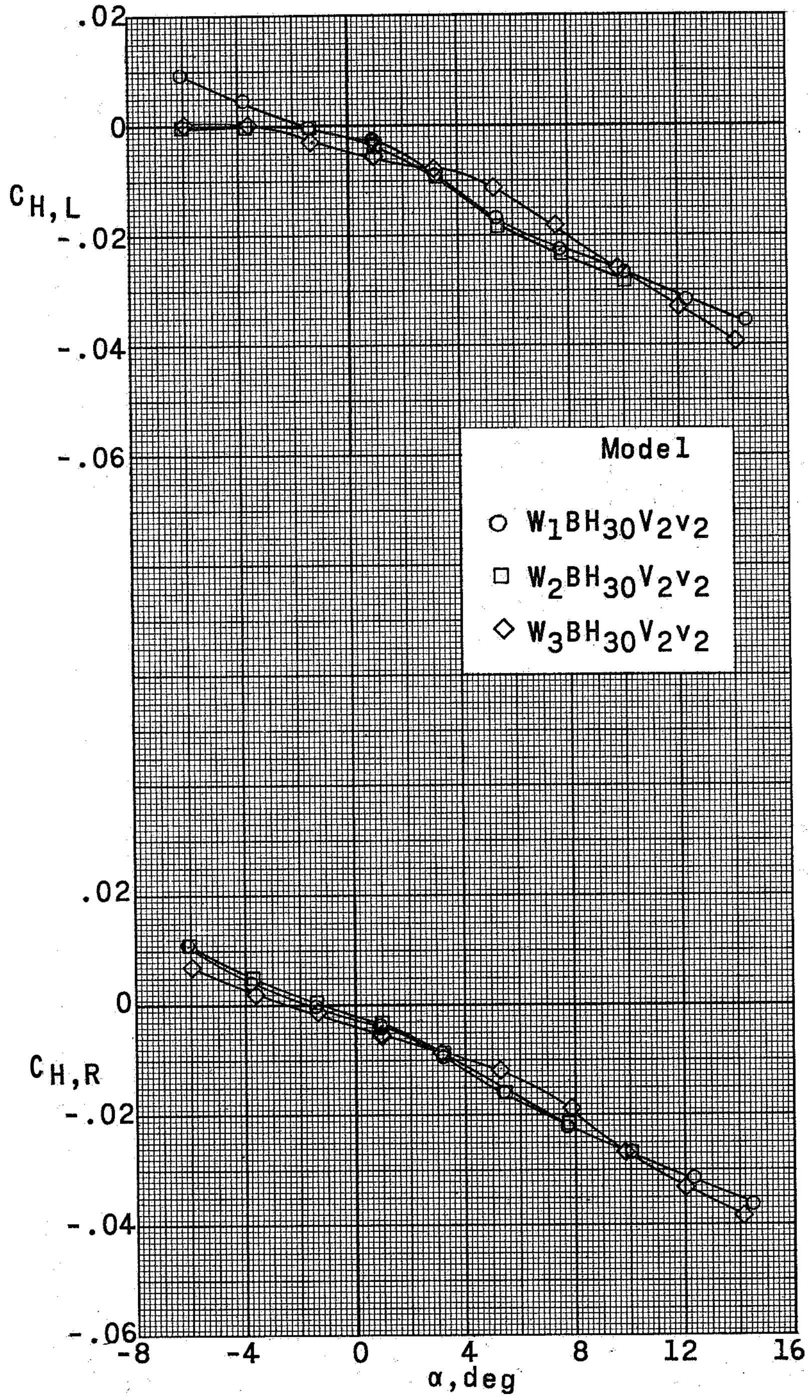

(c) $M = 2.54$.

Figure 43.- Concluded.

[redacted]

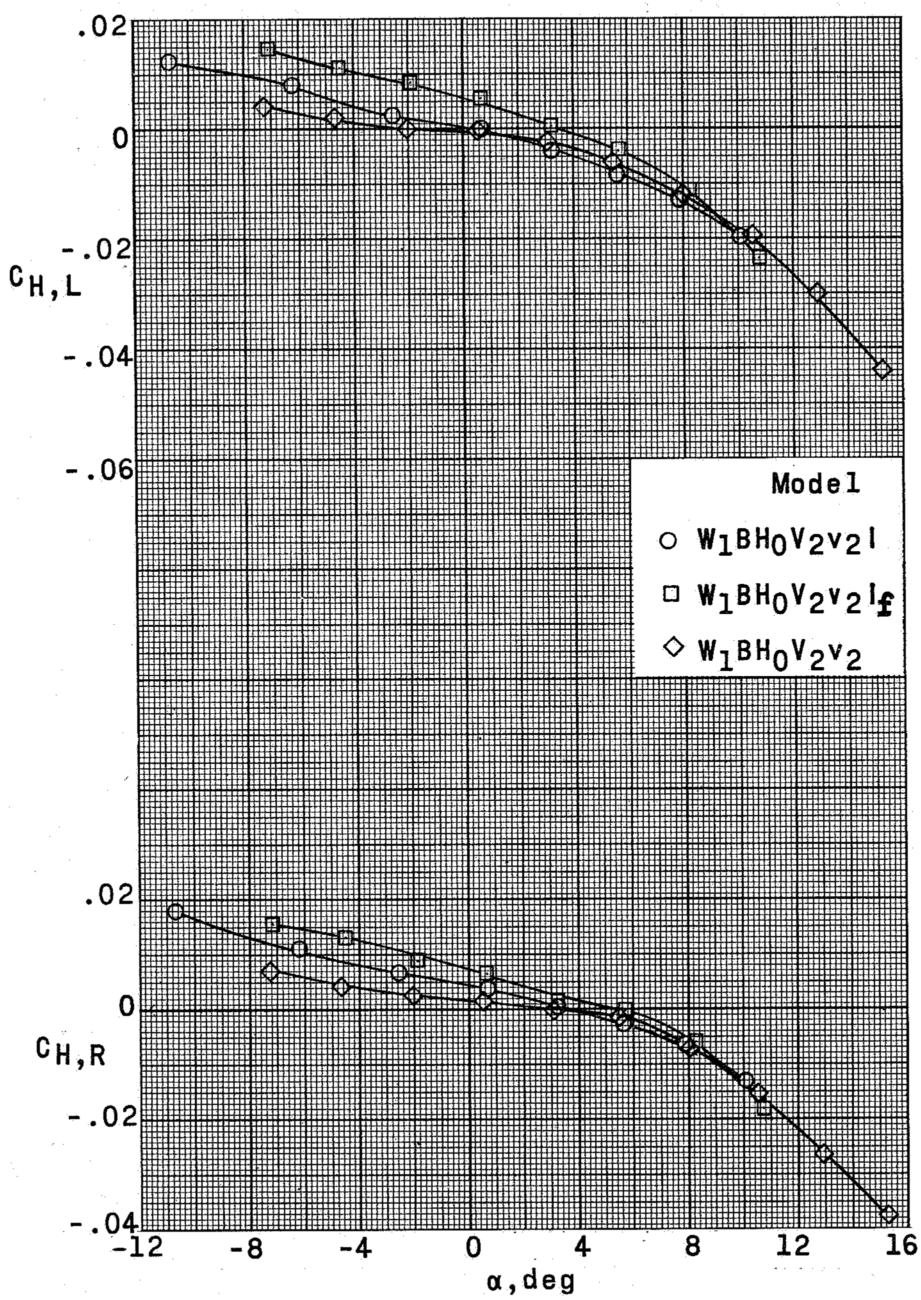

(a) M = 1.57.

Figure 44.- Hinge-moment characteristics of the horizontal-tail panels of a supersonic horizontal-attitude VTOL airplane model with various inlet configurations. $\delta_H = 0$.

L-355

[redacted]

[redacted]

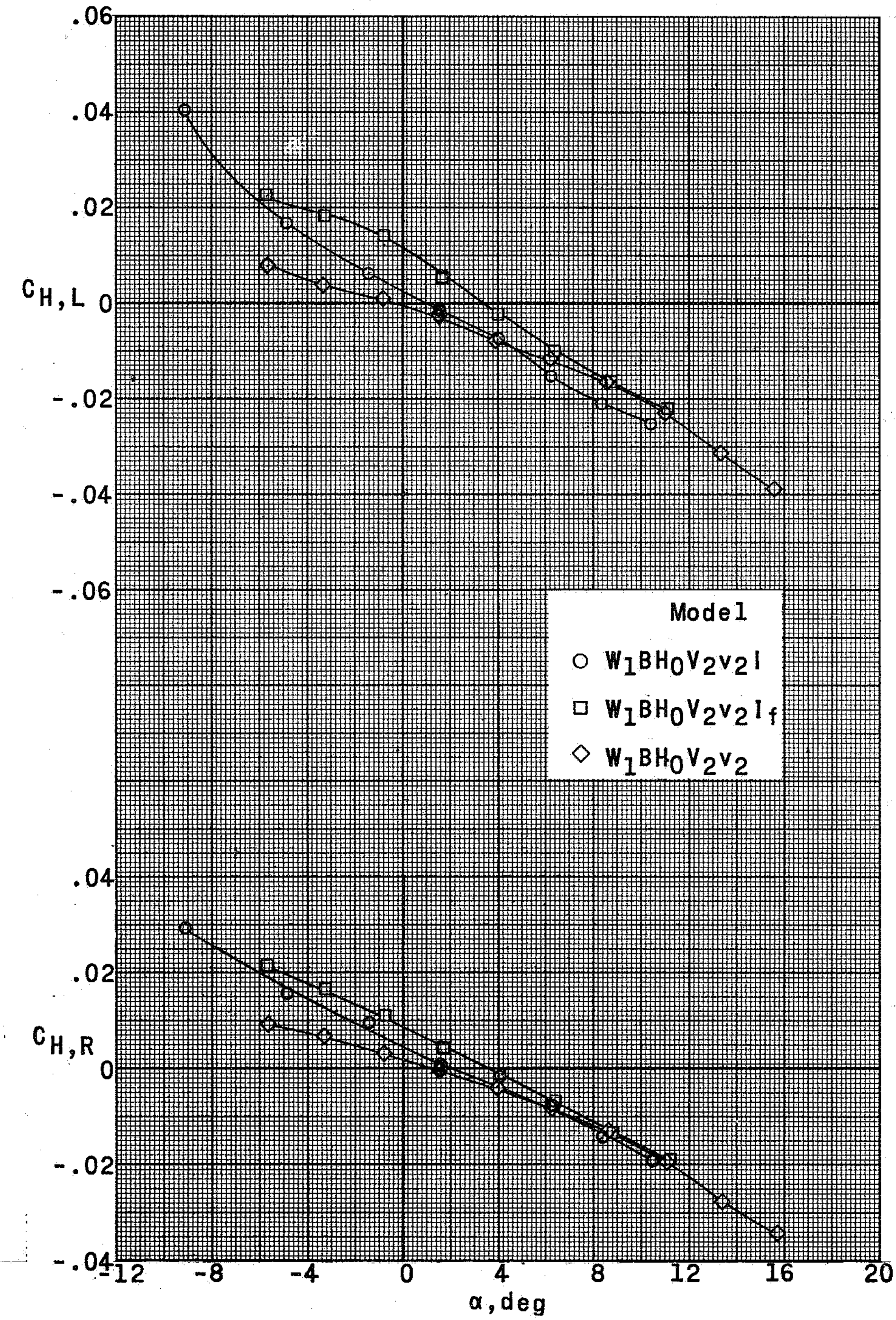

(b) M = 2.14.

Figure 44.- Continued.

[redacted]

[redacted]

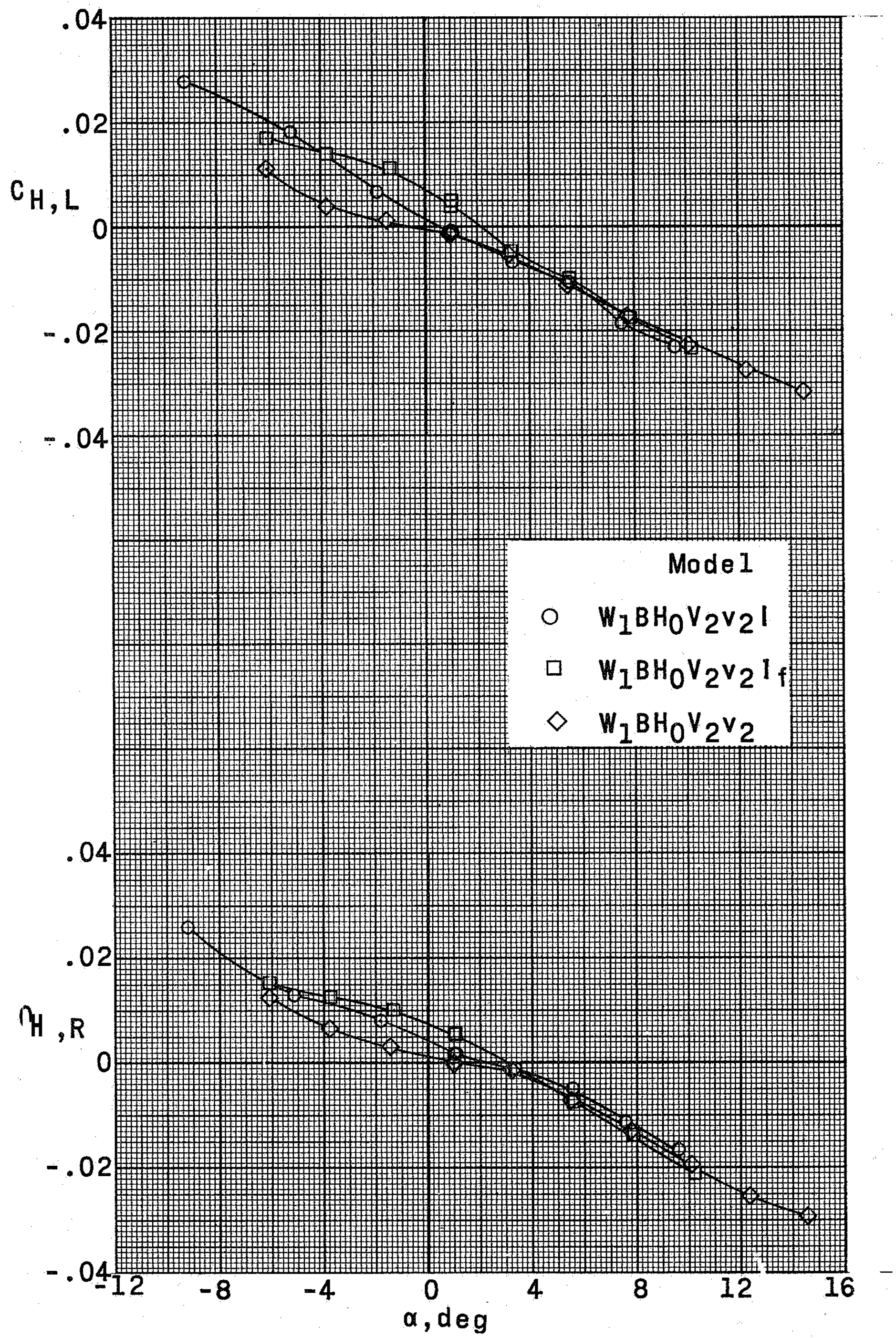

(c) M = 2.54.

Figure 44.- Continued.

L-355

[redacted]

L-355

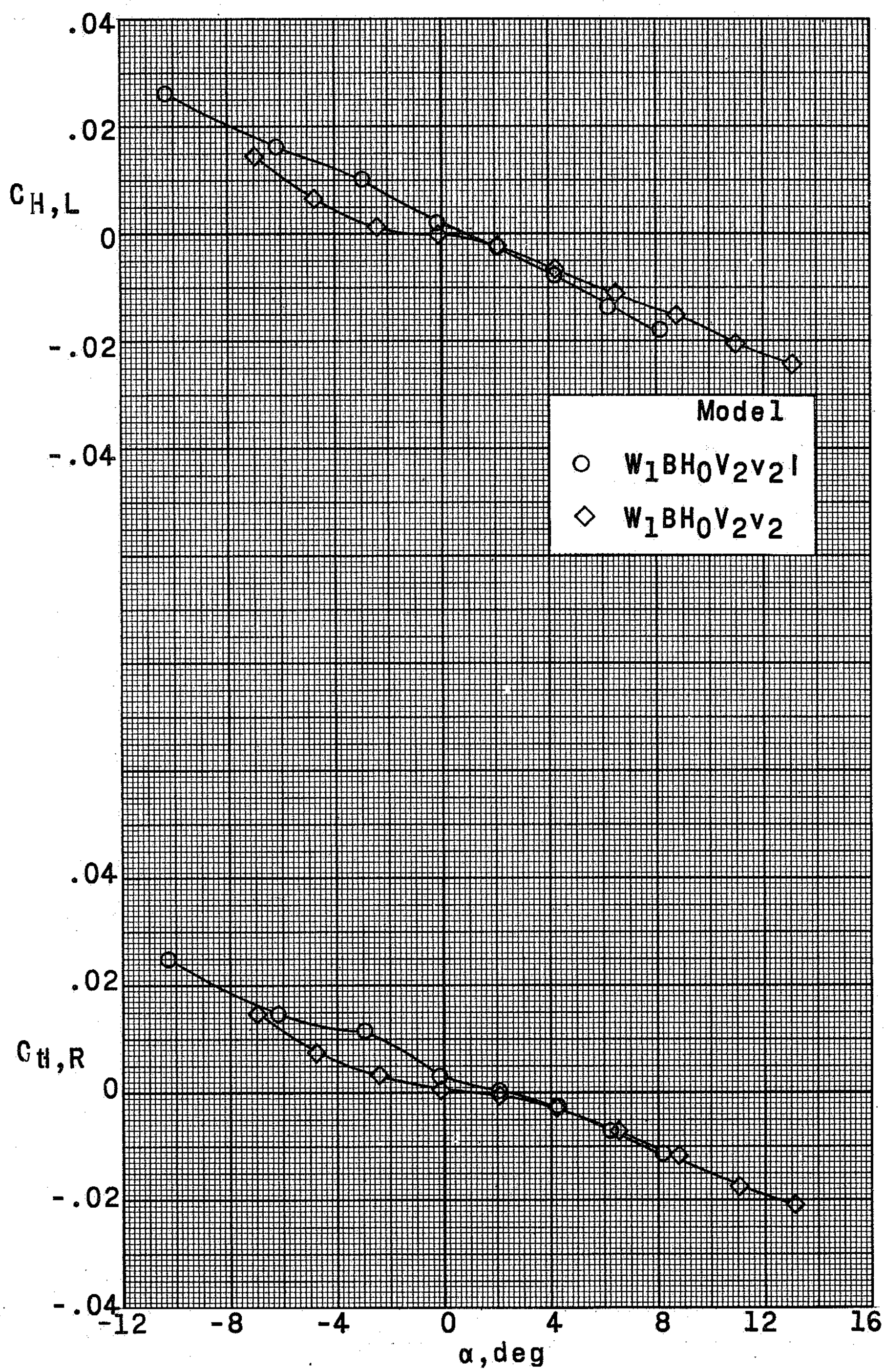

(a) M = 2.87.

Figure 44.- Concluded.

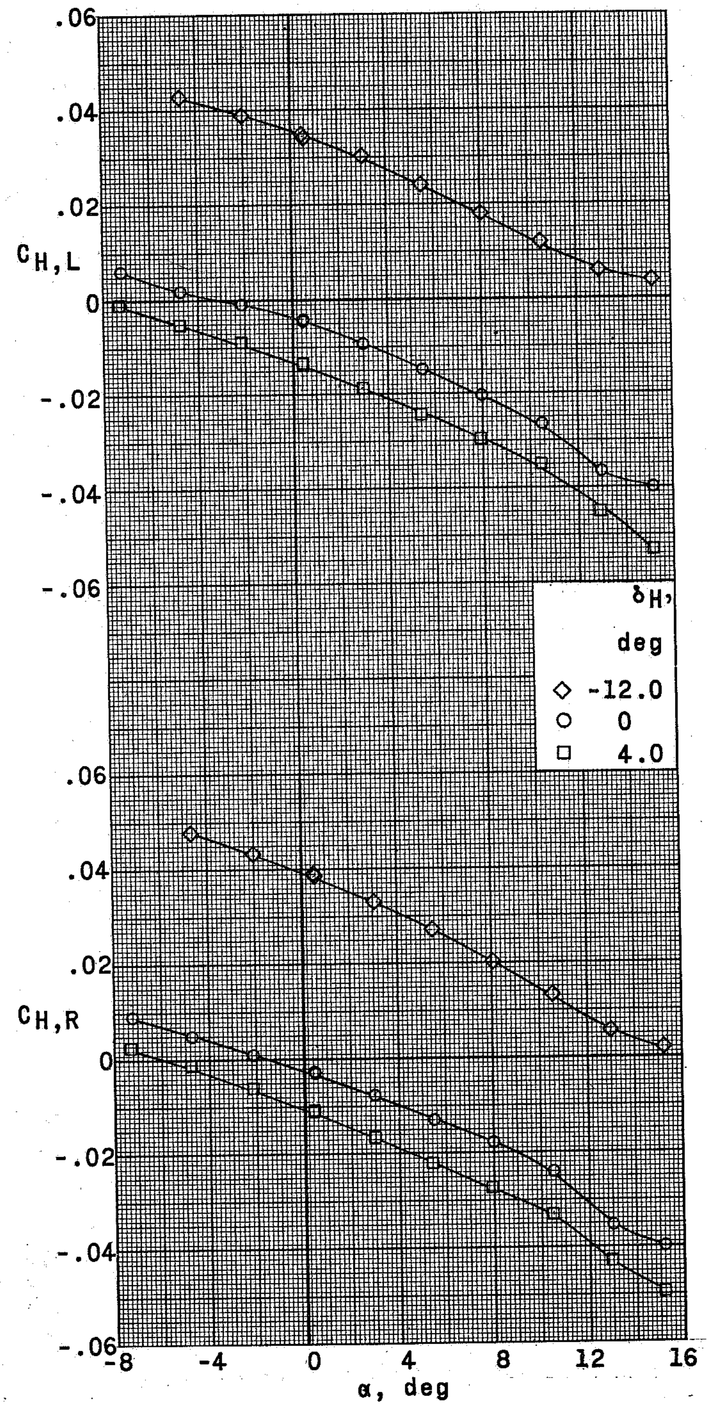

(a) M = 1.57.

Figure 45.- Hinge-moment characteristics of the horizontal-tail panels of a supersonic horizontal-attitude VTOL airplane model as effected by various deflections of the horizontal tail. $\beta = 0$.

L-355

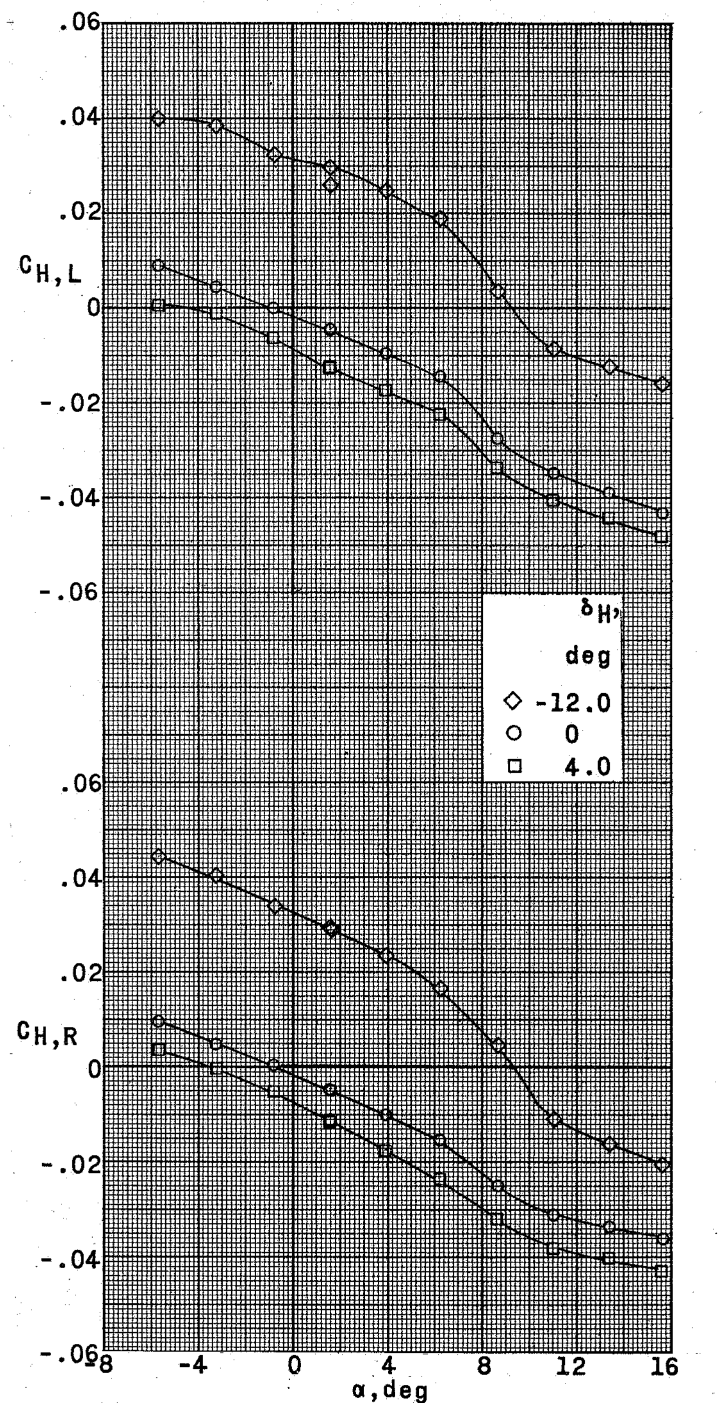

(b) M = 2.14.

Figure 45.- Continued.

[redacted]

3

L-355

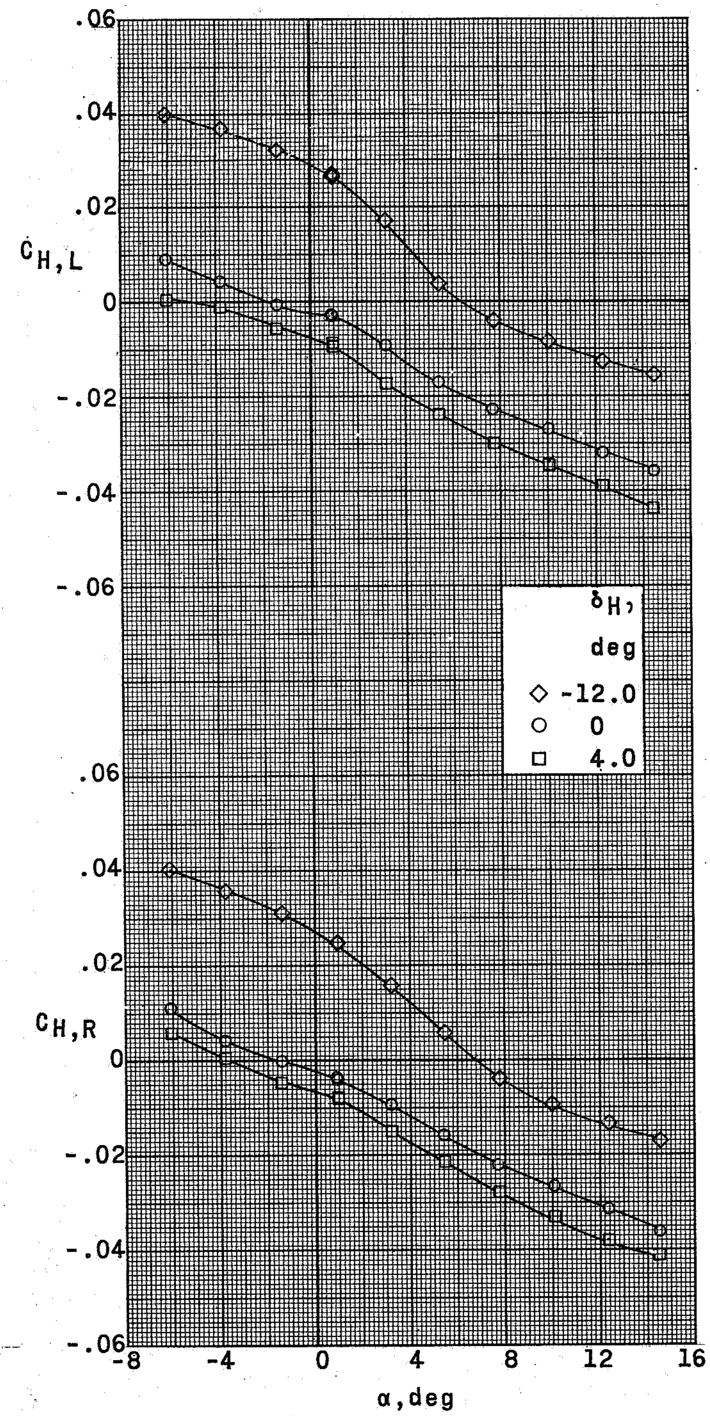

(c) M = 2.54.

Figure 45. - Concluded.

[redacted]

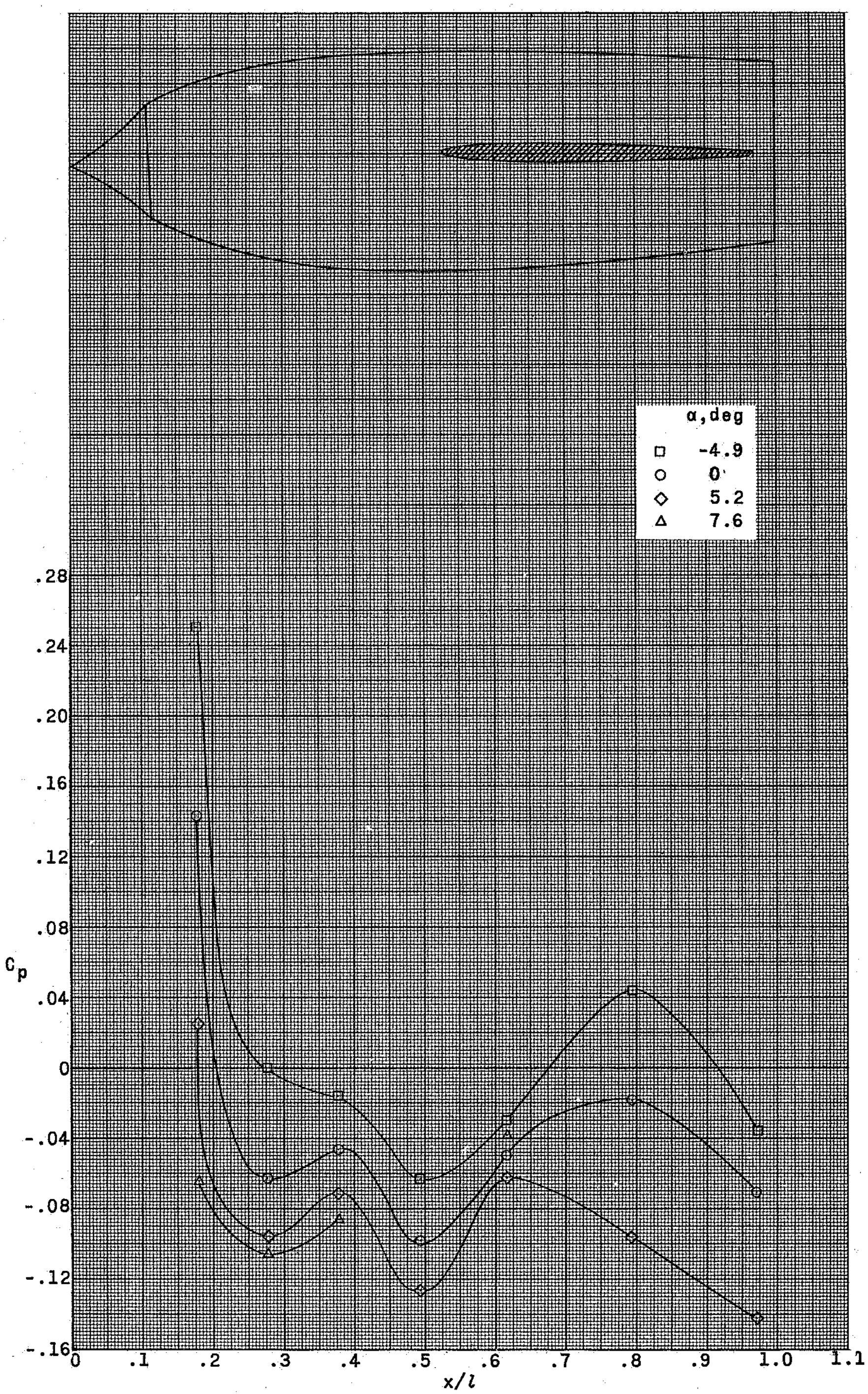

(a) M = 1.57.

Figure 46.- Pressure distribution on the right nacelle of a supersonic horizontal-attitude VTOL airplane model.

[redacted]

L-355

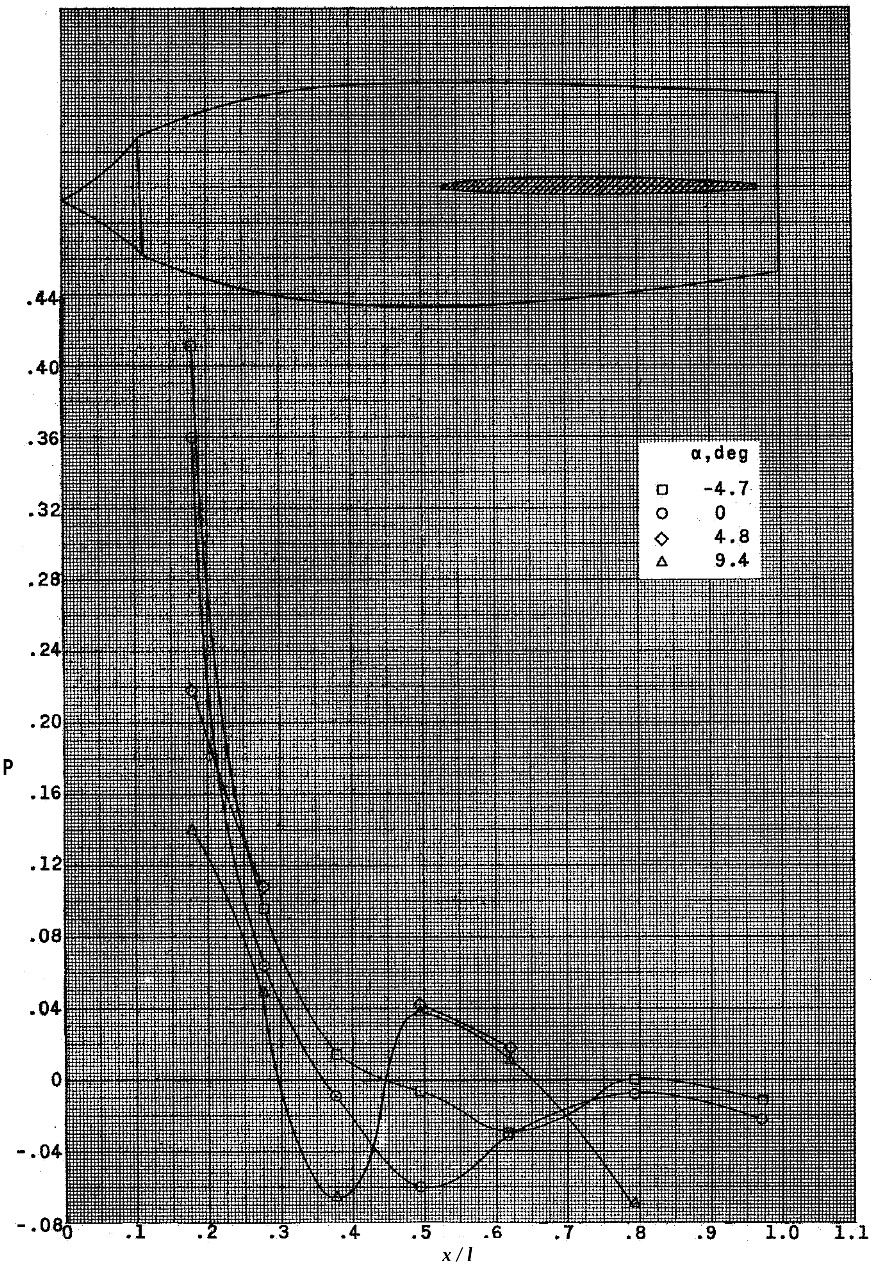

(b) M = 2.14.

Figure 46.- Continued.

[redacted]

L-355

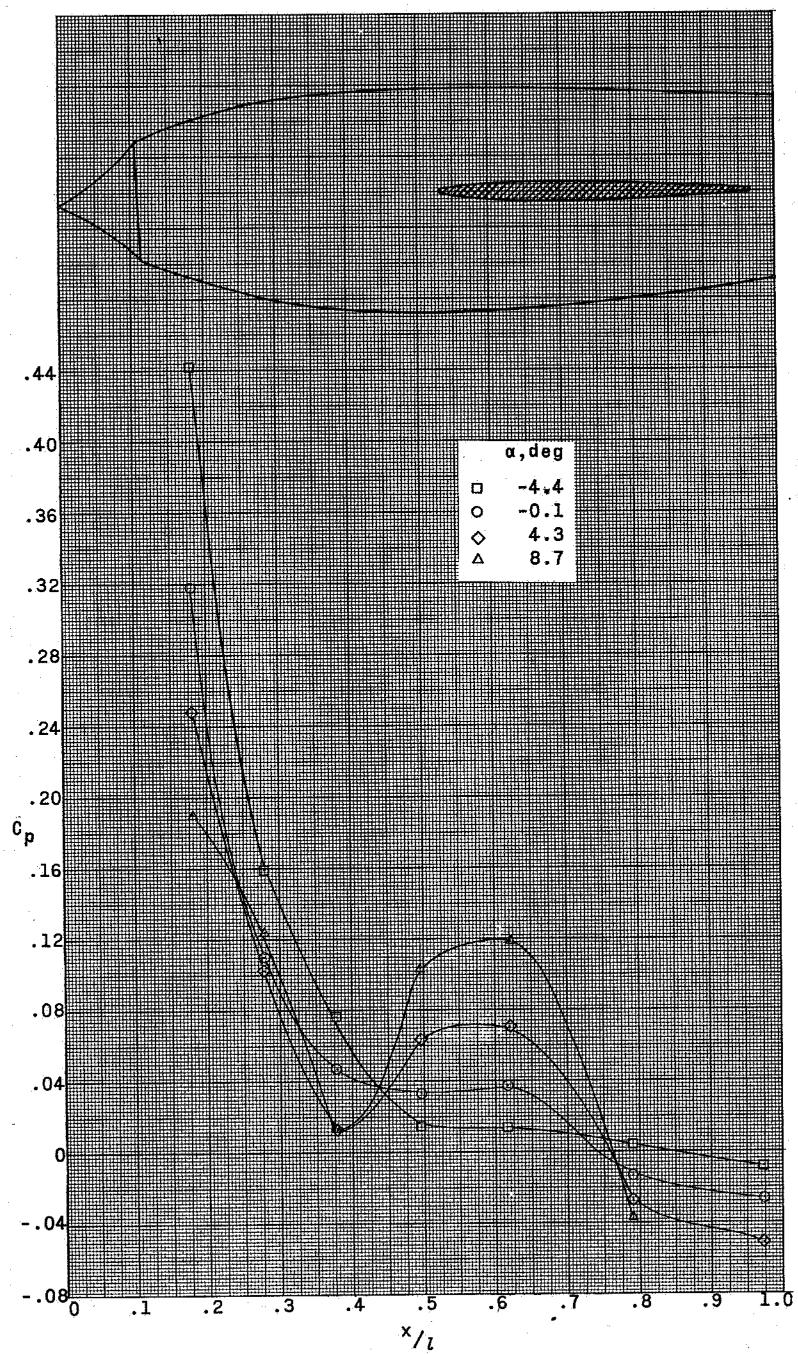

(c) M = 2.54.

Figure 46.- Continued.

[redacted]

[redacted]

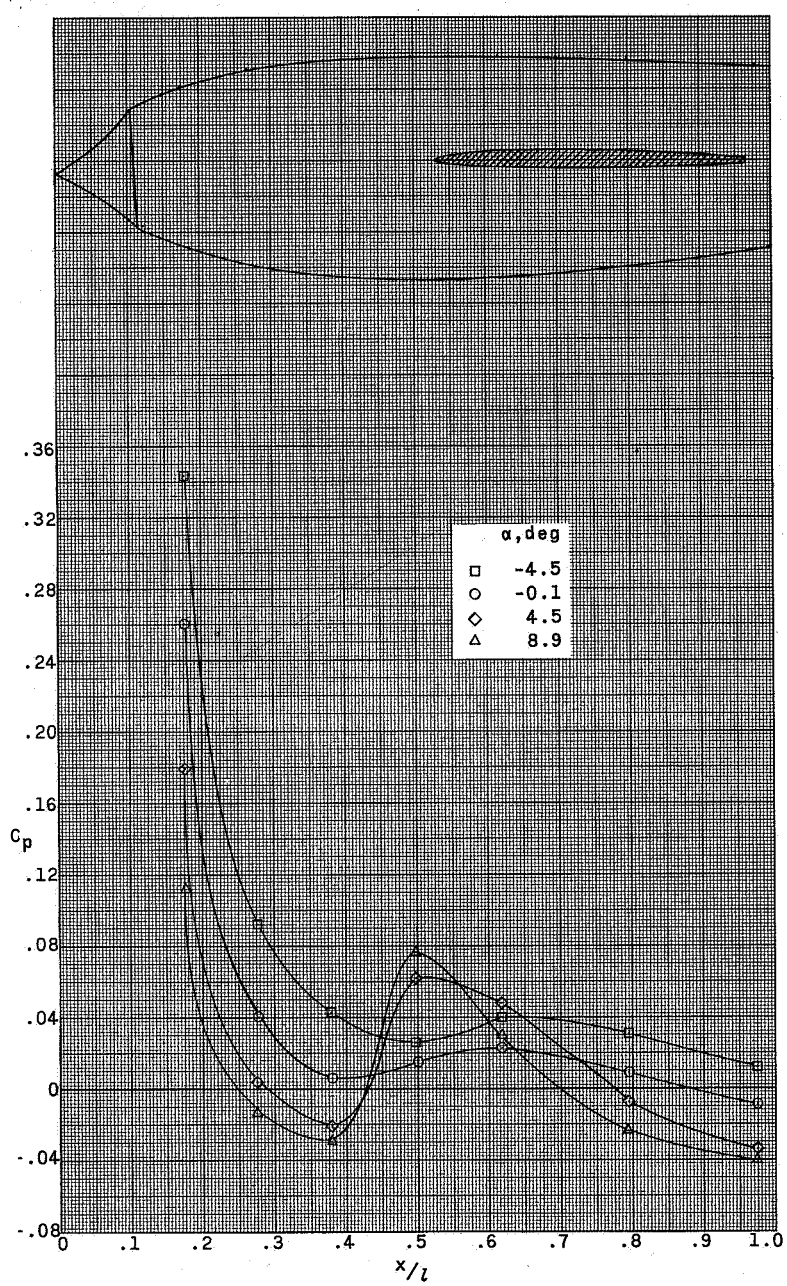

(d) M = 2.87.

Figure 46. - Concluded.

L-355

[redacted]